EPFL

Thèse n° 7818

# Development and applications of hyperpolarized $^{13}C$ and $^{1}H$ MR spectroscopy of cerebral metabolism at ultra-high field

Présentée le 2 juillet 2021

Faculté des sciences de base
Laboratoire Leenaards-Jeantet d'imagerie fonctionnelle et métabolique
Programme doctoral en biotechnologie et génie biologique

pour l'obtention du grade de Docteur ès Sciences

par

**Emmanuelle Ines FLATT**

Acceptée sur proposition du jury

Prof. M. Dal Peraro, président du jury
Prof. R. Gruetter, directeur de thèse
Prof. M. Chaumeil, rapporteuse
Prof. S. R. Williams, rapporteur
Prof. M. Rudin, rapporteur

École
polytechnique
fédérale
de Lausanne

2021

*To my family*

# Abstract

This thesis is composed of four studies centered on investigating cerebral metabolism using magnetic resonance spectroscopy (MRS) of hyperpolarized and non-hyperpolarized compounds at ultra-high field.

In the first two chapters, we studied longitudinally the effects of different treatments for hepatic encephalopathy (HE) on the neurometabolic changes associated with chronic HE using a rat model of type C HE and a multimodal approach including $^{1}H$ MRS. The effects of the antibiotic rifaximin administered at different doses as well as its combination with probiotics were studied in the established model of bile duct ligated (BDL) rats. We showed for the first time the positive effects of the combined rifaximin and the probiotic Vivomixx® on the neurometabolic changes *in vivo* and longitudinally in a rat model of type C HE. The longitudinal changes of some brain metabolites concentration (glutamine, glutamate, creatine), as well as gut bifidobacteria concentration, were significantly less pronounced in the group of rats treated with rifaximin and probiotics compared to non-treated rats. We also showed that rifaximin treatment alone had limited efficacy. When administered at human dose in rats, its effects appeared only at the early stages of the disease, whereas at a higher dose some neurometabolic changes associated with HE were attenuated but the general condition of the rats was worse.

In the third study, we used dissolution dynamic nuclear polarization (DNP) to hyperpolarize [$^{2}H_{7}$, U-$^{13}C_{6}$]-D-glucose, which enabled us to monitor real-time glycolysis in the healthy mouse brain. Given that glucose metabolism is tightly linked to neuronal activity, we first investigated how the change in anesthesia impacts the cerebral metabolism of hyperpolarized glucose. Anesthetics are known to influence brain activity, and in this study we showed for the first time that switching from isoflurane anesthesia to a combination of lower doses of isoflurane and medetomidine had a high impact on cerebral glucose uptake and glycolytic flow, as reflected by the increased labelling of downstream [1-$^{13}C$] lactate. The second part of this study aimed at evaluating the feasibility of quantifying cerebral glucose metabolism kinetics by evaluating two different mathematical models, where kinetic rate constants were determined by fitting the models on $^{13}C$ curves by non-linear regression using the Levenberg-Marquardt algorithm. We showed that a 3-compartment model is more stable and reliable than a 4-compartment model.

Finally, since lithium salts are widely used for treating bipolar disorder but its mechanism of action is still not clearly understood, we evaluated the potential of hyperpolarized $^{6}Li$ injected at pharmacological doses to assess its real-time bio-distribution and pharmacokinetic in the rat brain.

We demonstrated first that hyperpolarized $^{6}Li$ can be detected at pharmacological concentration in the rat head with high signal-to-noise ratio (SNR). We also showed that the transport of lithium through the intact blood-brain barrier brain is a limiting factor and demonstrated a striking difference between apparent $^{6}Li$ $T_1$ values in a brain with normal or disrupted blood-brain barrier.

# Keywords

Brain metabolism, magnetic resonance spectroscopy (MRS), $^{1}H$ MRS, $^{13}C$ MRS, $^{6}Li$ MRS, chronic hepatic encephalopathy (CHE), CHE treatments, bile duct ligation (BDL), dynamic nuclear polarisation (DNP), glucose cerebral metabolism, mathematical modelling

# Résumé

Cette thèse est composée de quatre études du métabolisme cérébral au moyen de la spectroscopie par résonance magnétique (SRM) de composés hyperpolarisés ou non-hyperpolarisés à ultra-haut champ.

Les deux premières parties se consacrent à l'étude longitudinale des effets de différents traitements de l'encéphalopathie hépatique (EH) sur les changements neurométaboliques accompagnant une EH chronique en utilisant un modèle animal d'EH de type C et une approche multimodale incluant la SRM $^{1}H$. Les effets de l'antibiotique rifaximine administré à différentes doses ainsi que sa combinaison avec des probiotiques furent étudiés sur le modèle de rats à voies biliaires ligaturées (VBL). Nous avons montré pour la première fois les effets bénéfiques de la combinaison de la rifaximine et du probiotique Vivomixx® sur les changements neurométaboliques longitudinaux chez le rat VBL. Les variations de la concentration de certains métabolites cérébraux (glutamine, glutamate, créatine) ainsi que la concentration de bifidobactéries dans l'intestin ont été significativement moins prononcés dans le groupe de rats traités comparé aux rats non traités. Nous avons également montré que la rifaximine seule avait une efficacité limitée. Lorsqu'elle est administrée à des rats à dose humaine, ses effets n'apparaissent qu'aux premiers stades de la maladie alors qu'à une dose plus élevée, certains changements neurométaboliques associés à l'EH ont été atténués mais l'état général des rats est moins bon.

Dans la troisième étude, nous avons utilisé la polarisation nucléaire dynamique de dissolution (DNP) pour hyperpolariser le [$^{2}H_{7}$, U-$^{13}C_{6}$]-D-glucose pour mesurer en temps réel la glycolyse dans le cerveau sain de la souris. Comme le métabolisme du glucose est étroitement lié à l'activité neuronale, nous avons d'abord étudié comment le changement d'anesthésie influence le métabolisme cérébral du glucose hyperpolarisé. Les anesthésiants influencent l'activité cérébrale, et nous avons montré pour la première fois que passer d'une anesthésie sous isoflurane à une combinaison d'isoflurane et de médétomidine à plus faible dose avait un fort impact sur l'absorption cérébrale du glucose et le flux glycolytique. La deuxième partie de cette étude visait à évaluer la faisabilité de la quantification de la cinétique du métabolisme cérébral du glucose en évaluant deux modèles mathématiques différents, en déterminant les constantes de vitesse cinétique par régression non linéaire à l'aide de l'algorithme de Levenberg-Marquardt. Nous avons montré qu'un modèle à 3 compartiments est plus stable et fiable qu'un modèle à 4 compartiments.

Enfin, comme le mécanisme d'action du lithium dans le traitement des troubles bipolaire n'est pas encore clairement compris, nous avons évalué le potentiel du $^{6}Li$ hyperpolarisé injecté à des doses

pharmacologiques pour évaluer sa biodistribution et sa pharmacocinétique en temps réel dans le cerveau du rat. Nous avons démontré que le $^{6}$Li hyperpolarisé peut être détecté à concentration pharmacologique dans la tête du rat avec un rapport signal sur bruit (SNR) élevé mais que le transport du lithium à travers la barrière hémato-encéphalique intacte est un facteur limitant. Nous avons mis en évidence une différence frappante entre les valeurs apparentes de $T_1$ du $^{6}$Li dans un cerveau dont la barrière hémato-encéphalique est normale ou perturbée.

# Mots clés

Métabolisme cérébral, spectroscopie par résonance magnétique (SRM), SRM $^{1}$H, SRM $^{13}$C, SRM $^{6}$Li, encéphalopathie hépatique chronique (EHC), voies biliaires ligaturées (VBL), traitements de l'EHC, polarisation nucléaire dynamique (DNP), métabolisme cérébral du glucose, modélisation mathématique.

# Table of Contents

# List of Figures

# List of Tables

# List of Symbols and Abbreviations

| | |
|---|---|
| $\gamma$ | gyromagnetic ratio |
| $\mu$ | magnetic dipole moment |
| $\hbar$ | Planck's constant |
| $\omega_0$ | Larmor frequency |
| $B_0$ | main static magnetic field |
| $B_1$ | radiofrequency magnetic field |
| $B_{eff}$ | effective magnetic field |
| $E$ | energy |
| $F(\omega)$ | Fourier transform |
| $G_x$, $G_y$, $G_z$ | magnetic gradients in x,y,z direction |
| $M_0$ | magnetization at thermal equilibrium |
| $M_{xy}$ | transverse magnetization |
| $M_z$ | longitudinal magnetization |
| $R_1$ | spin-lattice or longitudinal relaxation rate |
| $T_1$ | spin-lattice or longitudinal relaxation time |
| $T_2$ | spin-spin or transverse relaxation time |
| $T_2^*$ | apparent transverse relaxation time (including magnetic field inhomogeneity) |
| Ala | alanine |
| Asc | ascorbate |
| Asp | aspartate |
| ATP | adenosine triphosphate |
| ADP | adenosine 5'-diphosphate |
| BBB | blood-brain barrier |
| BDL | bile-duct ligation/ligated |
| CEST | chemical exchange saturation transfer |
| CHE | chronic hepatic encephalopathy |
| CHESS | chemical-shift selective |
| CLD | chronic liver disease |
| CNS | central nervous system |
| Cr | creatine |
| CRLB | Cramer-Rao lower bounds |
| DMRS | deuterium magnetic resonance spectroscopy |
| dDNP | dissolution dynamic nuclear polarization |
| DNP | dynamic nuclear polarization |
| EEG | electroencephalogram |
| FAD | flavin adenine dinucleotide |
| $FADH_2$ | flavin adenine dinucleotide (fully oxidized) |
| FASTMAP | fast automatic shimming technique by mapping along the projections |
| FDG | fluorodeoxyglucose |

| | |
|---|---|
| FE | fractional enrichment |
| FID | free induction decay |
| FOV | field of view |
| FT | Fourier transformation |
| FWHM | full-width at half maximum |
| GABA | gamma-aminobutyric acid |
| GDP | guanosine diphosphate |
| Glc | glucose |
| Gln | glutamine |
| Glu | glutamate |
| GPC | glycerophosphocholine |
| GS | glutamine synthetase |
| GSH | glutathione |
| GTP | guanosine-5'-triphosphate |
| Hct | hematocrit |
| HE | hepatic encephalopathy |
| Ins | myo-inositol |
| ISIS | image-selected in vivo spectroscopy |
| jMRUI | java based magnetic resonance user interface |
| Lac | lactate |
| LCModel | linear combination of model spectra of metabolites |
| Li | lithium |
| Mac | macromolecules |
| mHE | minimal hepatic encephalopathy |
| MRI | magnetic resonance imaging |
| MRS | magnetic resonance spectroscopy |
| NAA | N-acetyl aspartate |
| NAAG | N-acetylaspartylglutamate |
| NAD+ | nicotinamide adenine dinucleotide (oxidized) |
| NADH | nicotinamide adenine dinucleotide (reduced) |
| NMDA | N-methyl-D-aspartate |
| NMR | nuclear magnetic resonance |
| NOE | nuclear Overhauser effect |
| OVS | outer volume suppression |
| PCho | phosphocholine |
| PCr | phosphocreatine |
| PE | phosphorylethanolamine |
| PET | positron emission tomography |
| ppm | parts per million |
| RF | radiofrequency |
| ROI | region of interest |
| ROS | reactive oxygen species |
| Scyllo | scyllo-inositol |
| SD | standard deviation |
| SNR | signal-to-noise ratio |

| | |
|---|---|
| SPECIAL | spin echo, full intensity aquired localized spectroscopy |
| SSE | sum of squared residuals |
| Tau | taurine |
| TCA | tricarboxylic acid |
| tCho | total choline |
| tCr | total creatine |
| TE | echo time |
| tHb | total hemoglobin |
| TMS | tetramethyl silane |
| tNAA | total N-acetylaspartate |
| TR | repetition time |
| VAPOR | variable pulse power and optimized relaxation delay |
| VOI | volume of interest |
| WS | water suppression |

# Scope of the thesis

## Objectives

Nuclear Magnetic Resonance (NMR) is a phenomenon based on the interaction of magnetic moments of nuclei of different atoms with magnetic field. It is the phenomenon behind magnetic resonance imaging (MRI), a diagnostic tool for obtaining structural images in a non-invasive way and used daily in clinics nowadays. Magnetic resonance spectroscopy (MRS) is also an extremely powerful and non-invasive technique for obtaining detailed information on the structure and physicochemical properties of a system and is a very valuable tool for longitudinal metabolic studies *in vivo*. It is however less used than MRI as a clinical diagnostic tool due to its greater complexity of use. The present thesis exploits the advantages offered by ultra-high field NMR technology for pre-clinical studies of brain metabolic processes. It can be divided into two main parts.

The first part is devoted to the study of hepatic encephalopathy (HE), a serious neuropsychiatric disease present in patients suffering from hepatic dysfunction, and more particularly to its treatment. We studied longitudinally the effects of different treatments for HE currently prescribed in humans, whose mechanisms of action are not yet well understood. The aim was to evaluate in detail the neurometabolic changes associated with chronic HE under different treatments using an animal model of type C HE and a multimodal approach including $^{1}$H MRS at 9.4 T. Because of the physicochemical properties of hydrogen, the high natural abundance of $^{1}$H isotope and the fact that many organic compounds contain hydrogen, $^{1}$H MRS is the most sensitive MRS method. By using an ultra-high field MR scanner and appropriate measurement parameters such as a very short echo time, it is possible to measure and quantify in the brain up to 18 metabolites involved in different metabolic processes.

The second part is dedicated to the development and application of DNP techniques for *in vivo* studies in rodents. Due to the low concentrations of most glycolysis intermediates, it is not possible with current MRS techniques using thermally polarized molecules to detect non-invasively glycolytic intermediates *in vivo* in real-time. Dissolution DNP has significantly improved MR sensitivity by increasing the polarization of nuclear spin, thus enabling the measurement of low-concentrated metabolites and the observation of metabolic processes in real time *in vivo*. Since glucose is the main energy substrate in the brain, our goal was to study the real-time cerebral metabolism of glucose in mice after infusion of $^{13}$C-labelled hyperpolarized glucose. We

subsequently investigated the potential of hyperpolarized lithium to enhance the understanding of the mechanism of action of lithium salts in the treatment of bipolar disorders.

## Outline

**Chapter 1** presents the theoretical background related to the content of the thesis. It presents the basic principles of NMR and MR spectroscopy, as well as dynamic nuclear polarization and its applications. The basics of cerebral metabolism are then introduced and the chapter ends with a description of hepatic encephalopathy including pathogenesis, current therapeutic approaches and animal model of the disease.

**Chapter 2** is devoted to the longitudinal study of the effects of different treatments for chronic hepatic encephalopathy (CHE) on the neurometabolic changes associated with CHE using an animal model of type C HE and a multimodal approach including *in vivo* $^{1}$H MRS at 9.4 T, plasma measurements, microbiota analyses and behavioral tests. The effects of the antibiotic rifaximin and its combination with probiotics in the bile duct ligated (BDL) rat model are discussed. This first study raised the question of the efficacy of the dose used, and we hypothesized that the effect of rifaximin on the neurometabolic profile is dose-related.

To test this hypothesis, **Chapter 3** investigated the effects of a higher dose of rifaximin (6.2x the human dose, resulting from the conversion of the human dose to the rat dose). We used a multimodal approach similar to that of Chapter 2 to assess longitudinally the effect of the antibiotic rifaximin at a higher dose on brain metabolic profile in the hippocampus of BDL rats. Glutamine plays a central role in the pathophysiology of HE, but this disease is also characterized by many brain energetic disorders which are still poorly understood today. Glucose is the main cerebral fuel, but not reliably quantified with $^{1}$H-MRS. Techniques such as FDG-PET, $^{13}$C-MRS and $^{31}$P-MRS have been used, but glucose metabolism, and especially glycolysis, has been only marginally studied in type C HE.

Therefore, the goal of **Chapter 4** was twofold: first, to improve the dDNP protocol for hyperpolarized glucose *in vivo* studies, which could help to better characterize brain energetic deficiencies in diseases such as HE, and second to determine how the change in anesthesia, which affects consciousness and brain activity, impacts the cerebral metabolism of glucose. We first showed that cerebral glucose uptake and glycolytic flux in mice is strongly influenced by the type of anesthesia used. The second part of this chapter assesses the feasibility of quantifying the kinetics of cerebral glucose metabolism by evaluating two different mathematical models.

Finally, since lithium salts are widely used for treating bipolar disorder but its mechanism of action is still not clearly understood, **Chapter 5** explores the potential of hyperpolarized $^{6}$Li injected at pharmacological doses to assess its real-time bio-distribution and pharmacokinetic in the rat brain.

A dedicated coil was designed and built and consisted of a modified Alderman-Grant coil tuned to $^{6}Li$ and a $^{1}H$ surface coil, and the dynamic of hyperpolarized $^{6}Li$ in the rat brain was assessed by performing several different *in vivo* and *ex vivo* experiments in a 9.4 T animal scanner.

**Chapter 6** presents a general conclusion of the thesis and also examines the perspectives of applications of the present work as well as possible improvements.

**Appendix 1** presents a work carried out during this thesis in collaboration with three PhD students from the lab, consisting of the restarting of DNP experiments using a 5 T polarizer connected to a 14 T animal scanner and the optimisation of the protocol.

# Chapter 1 Introduction to MR technology, cerebral metabolism and hepatic encephalopathy

## 1.1 Basis of *in vivo* NMR spectroscopy

Nuclear Magnetic Resonance (NMR) is a phenomenon based on the interaction of magnetic moments of nuclei of different atoms with magnetic field. NMR spectroscopy is an extremely powerful and non-invasive technique for obtaining detailed information on the structure and physicochemical properties of a system. This section summarizes the basic principles of NMR spectroscopy and is based on the books from de Graaf and Hore and Keeler (Graaf 2019; "Understanding NMR Spectroscopy, 2nd Edition | Wiley" n.d.; Hore 1999).

### 1.1.1 Spin physics

Spin angular momentum $\boldsymbol{L}$ or simply "spin" is an intrinsic magnetic property possessed by nuclei and subatomic particles and its amplitude is defined as:

$$L = \frac{h}{2\pi}\sqrt{I(I+1)} \qquad 1.1$$

where $I$ is spin quantum number and $h$ is Plank's constant. Nuclear spin values range from $I$ = 0 to $I$ = 8 in increments of ½-unit and are determined by the spin of neutrons and protons inside the nucleus. Placed in a magnetic field, nuclei have $(2I+1)$ energy levels. This energy difference between the states is known as the nuclear Zeeman effect. $^{1}$H, a nucleus widely used for NMR and MRI, has $I$ = ½, the same spin as the single proton that constitutes it. Only nuclei with a non-zero spin ($I \neq 0$) can absorb and emit electromagnetic radiation and experience "resonance" when they are placed in a magnetic field.

*Table 1.1 NMR properties of some nuclei*

| Isotope | Net spin (I) | Gyromagnetic ratio γ/2π (MHz/T) | Natural abundance (%) |
|---|---|---|---|
| $^{1}$H | 1/2 | 42.58 | 99.985 |
| $^{2}$H | 1 | 6.54 | 0.015 |
| $^{12}$C | 0 | - | 98.9 |
| $^{13}$C | 1/2 | 10.71 | 1.1 |
| $^{31}$P | 1/2 | 17.25 | 100 |
| $^{6}$Li | 1 | 6.27 | 7.59 |

Nuclei also possess a magnetic moment **μ** that is related to the spin angular momentum $\boldsymbol{L}$:

$$\vec{\mu} = \gamma \vec{L} \qquad 1.2$$

where $\gamma$ is a constant specific to a particular nucleus possessing a spin, called gyromagnetic ratio. When there is no magnetic field, the angular momentum $\boldsymbol{L}$ of the nuclei is randomly oriented. When these spins are exposed to an external magnetic field, their magnetic dipole moments will tend to align with the field in either state, with a tendency to take the lower energy orientation. In reality, at room temperature, this orientation is disturbed by thermal energy. Thus, the orientation of nuclear moments in space is almost random, with a slightly higher probability that they are oriented in the direction of the magnetic field, i.e. with lower energy (Hanson 2008).

The occurrence of quantum-field interaction allows the separate states to be measured. For a nucleus with a spin $I$ = ½, such as $^{1}$H, and placed in a magnetic field $\mathbf{B_0}$, two possible energy levels exist:

$$E = \pm \mu B_0 = \pm \frac{1}{2} \gamma \frac{h}{2\pi} B_0 \qquad 1.3$$

These two spin states are often called "spin-up" (low energy state) and "spin-down" (high energy state). The energy difference ($\Delta E$) between two nuclear spin states is directly proportional to the magnetic field strength (Figure 1.1) and is given by the Zeeman equation:

$$\Delta E = \gamma \frac{h}{2\pi} B_0 \qquad 1.4$$

Combining this last equation with the Planck equation for energy of electromagnetic radiation ($\Delta E = h\omega_0$), one gets the famous Larmor equation:

$$\omega_0 = \frac{\gamma}{2\pi} B_0 \qquad 1.5$$

The angular frequency $\omega_0$ is also referred to as the Larmor frequency and defines the resonance frequency for the transition from one energy state to the other. This equation shows that NMR resonance frequency of the nuclear spin $\omega_0$ is simply the gyromagnetic ratio ($\gamma$) times the static magnetic field strength ($\mathbf{B_0}$) experienced by the nucleus.

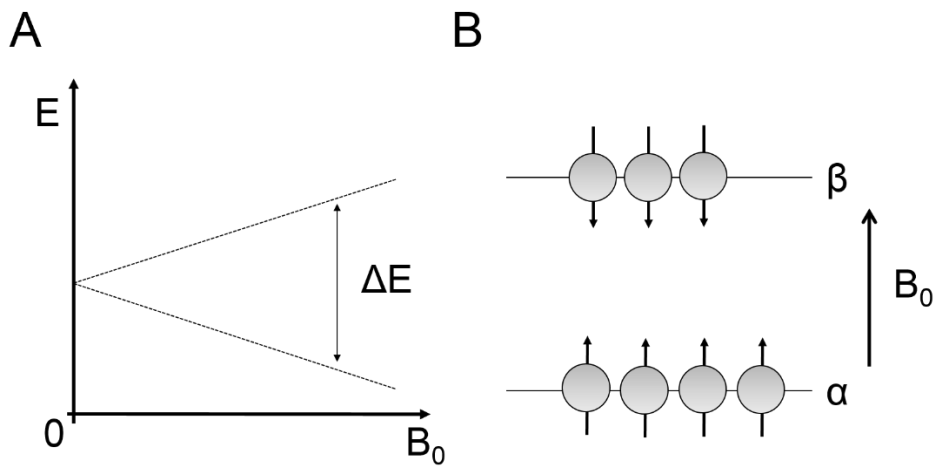


*Figure 1.1 (A) The nuclear spin energy E for nuclei with a spin quantum number of 1/2 as a function of the magnetic field strength $B_0$. (B) Spins in the lower energy level α correspond to magnetic moments parallel with $B_0$, while those of the higher energy level β have are aligned antiparallel to $B_0$.*

### 1.1.2 Macroscopic magnetization

As seen in the previous section, there are two possible energy levels for a nucleus with a spin $I$ = ½ and placed in a magnetic field $\mathbf{B_0}$. It is important to note here that quantum mechanics does not require that a spin exclusively resides in either of its principal states α or β; the only requirement is that the spin exists in a linear combination of the two states. In a static magnetic field and at thermal equilibrium, the probability of measuring these spins in the energy state α or in the energy state β is given by the Boltzmann distribution:

$$P(E_i) = \frac{e^{-E_i/kT}}{\sum_j e^{-E_j/kT}} \qquad 1.6$$

where T is the absolute temperature (in K) and k is Boltzmann constant. Since at room temperature

$$E = \pm\frac{1}{2}\gamma\frac{h}{2\pi}B_0 \ll kT \qquad 1.7$$

the probabilities of being in the energy state α or β can be approximated as:

$$P(E_\alpha) \cong \frac{1}{2} + \frac{\gamma\frac{h}{2\pi}B_0}{4kT} \qquad 1.8$$

$$P(E_\beta) \cong \frac{1}{2} - \frac{\gamma\frac{h}{2\pi}B_0}{4kT} \qquad 1.9$$

And one can derive then the difference between spin populations in the two states α and β:

$$(n_\alpha - n_\beta) = nP(E_\alpha) - nP(E_\beta) = \frac{\gamma\frac{h}{2\pi}B_0}{2kT}n \qquad 1.10$$

Where $n_\alpha$ is the number of spins in the α (low energy) state, $n_\beta$ is the number of spins in the β (high energy) state, and n is the total number of spins in the sample. The net magnetic moment $\mathbf{M_0}$ (also called macroscopic magnetization) of a macroscopic sample is the result of the sum of all individual magnetic moments μ. Since these are not in phase but there is a population difference between the two energy states, the net component of $\mathbf{M_0}$ is only along the z-axis, parallel to $\mathbf{B_0}$ and defined as:

$$M_0 = \sum_{i=1}^{n} \mu_{i,z} = n_\alpha \mu_{z,\alpha} + n_\beta \mu_{z,\beta} = \gamma \left(\frac{h}{4\pi}\right)(n_\alpha - n_\beta) \qquad 1.11$$

The amplitude of the macroscopic magnetization vector $M_0$ can thus be expressed as:

$$M_0 = \left(\frac{\gamma h}{2\pi}\right)^2 \frac{B_0}{4kT} n \qquad 1.12$$

One can identify from the equation 1.12 different factors influencing the sensitivity of NMR experiments. An important practical conclusion that can be deduced from this equation is that $\mathbf{M_0}$ is directly proportional to both the intensity of the magnetic field $\mathbf{B_0}$ and the spin density. The importance of the Larmor frequency of the nuclei is also deduced from the quadratic dependence of $\mathbf{M_0}$ on the gyromagnetic ratio γ. The larger the latter is, the more intense the NMR signals are. Finally, temperature also influences the signal amplitude and sensitivity can be enhanced at low sample temperature.

### 1.1.3 Resonance

The detection of the NMR signal is based on the measurement of the precessional motion of the magnetization vector. Magnetization is a vectorial quantity that obeys the rules of classical electrodynamics (Hoult 1989; Hanson 2008). Therefore, the interaction of magnetization with the magnetic field can be described by classical physics. Conventionally, the main magnetic field $B_0$ is in the direction of +z axis. At thermal equilibrium, there is no phase coherence among the spins and the net longitudinal magnetization $\mathbf{M_0}$ is a static vector along z-axis:

$$\frac{d\boldsymbol{M_z}(t)}{dt} = 0 \qquad 1.13$$

Nuclear magnetization can only be measured in the transverse plane, i.e. perpendicular to the main magnetic field $\mathbf{B_0}$. Thus, $\mathbf{M_0}$ must be tilted in the transverse plane. This is achieved by the transient application of a second magnetic field, $\mathbf{B_1}$, oscillating in the xy plane at the Larmor frequency of the system:

$$\overrightarrow{B_1}(t) = B_1 \cos(\omega t) + B_1 \sin(\omega t) \qquad 1.14$$

Its frequency corresponds to the Larmor frequency of the nuclei of interest and is in the MHz range, from which $B_1$ is called a radio frequency pulse (RF pulse). During the application of the $\mathbf{B_1}$ field, $\mathbf{M_0}$ will precess around both $\mathbf{B_0}$ and $\mathbf{B_1}$, resulting in a relatively complex motion of $\mathbf{M_0}$ and a tilting of $\mathbf{M_0}$ from the z-axis to the transverse xy plane:

$$\frac{d\overrightarrow{\boldsymbol{M}}(t)}{dt} = \gamma\overrightarrow{\boldsymbol{M}}(t) \times (\overrightarrow{\boldsymbol{B_0}} + \overrightarrow{\boldsymbol{B_1}}) \qquad 1.15$$

Depending on the duration and amplitude of the applied field $\mathbf{B_1}$, $\mathbf{M_0}$ can for example be completely tilted on the transverse plane (90° excitation) or reversed with respect to the z-axis (180° excitation).

For a strong, rectangular RF pulse of constant magnitude ($\mathbf{B_1}$) and duration (t), the flip angle α is approximately:

$$\alpha = \gamma B_1 t \qquad 1.16$$

The duration t of the RF pulse is relatively short, usually between 100 µs and a few ms. After application of the RF pulse, $\mathbf{M_0}$ is only exposed to the main magnetic field $\mathbf{B_0}$. $\mathbf{M_0}$ will precede around it with the Larmor frequency and gradually returns to its equilibrium state (i.e. parallel to the z axis). The process of return of magnetization to its thermal equilibrium is called relaxation.

### 1.1.4 Relaxation of the magnetization

After the RF pulse excitation, the magnetization vector can be decomposed into two components: the transverse magnetization $M_{xy}$ which rotates around the z-axis and the longitudinal magnetization $M_z$. It is the oscillation of the magnetization $M_{xy}$ that generates the measured signal in NMR, as explained in more detail in the following section. Following the RF pulse, the net magnetization $\mathbf{M_0}$ returns to its thermal equilibrium state during the relaxation process. This results from several interactions and an exchange and loss of excitation energy and there are many mechanisms underlying the relaxation, among which dipole-dipole interactions, chemical exchange, J-coupling, quadrupolar coupling and chemical shift anisotropy. $M_z$ and $M_{xy}$ return to thermal equilibrium in an exponential manner with different time constants, $T_1$ and $T_2$ respectively. The relaxation process can be written as:

$$\frac{dM_z(t)}{dt} = -\frac{M_z(t) - M_0}{T_1} \qquad 1.17$$

$$\frac{dM_{xy}(t)}{dt} = -\frac{M_{xy}(t)}{T_2} \qquad 1.18$$

with $T_1$ being the longitudinal relaxation time constant and $T_2$ the transversal relaxation time constant. $T_1$ relaxation, also called spin-lattice relaxation or longitudinal relaxation, describes how fast the spin ensemble dissipates energy to its surrounding and comes back to thermal equilibrium. This is due to the transfer of energy from the spins to the surrounding 'lattice'. It results in an increase of the longitudinal magnetization.

Evolution of $M_z$ as function of time is therefore described as:

$$M_z(t) = M_z(0)e^{-\frac{t}{T_1}} + M_0\,(1 - e^{-\frac{t}{T_1}}) \qquad 1.19$$

$T_2$ relaxation, also called spin-spin relaxation or transversal relaxation, describes how fast individual spins become out-of-phase, giving rise to a loss of coherence of the spin ensemble. Transverse relaxation is due to spin dephasing: the loss of phase synchronisation is linked to spin-spin interactions that create field heterogeneities, and thus differences in precession frequency. It results in a decrease of the transverse magnetization.

Evolution of $M_{xy}$ as function of time is therefore described as:

$$M_{xy}(t) = M_{xy}(0)e^{-\frac{t}{T_2}} \qquad 1.20$$

In practice, the main magnetic field $B_0$ is not perfectly homogeneous. This leads to a variation of Larmor frequencies within a sample and an even faster transverse dephasing of the spins, described by the relaxation constant $T_2^*$. As mentionned previously, $T_2$ includes spin-spin interactions only whereas the $T_2^*$ time constant takes into account an additional term considering the loss of phase coherence due to inhomogeneities in the $B_0$ field and magnetic susceptibility effects. The relation between $T_2$ and $T_2^*$ is given by:

$$\frac{1}{T_2^*} = \frac{1}{T_2} + \gamma \Delta B_0 \qquad 1.21$$

Where $\Delta B_0$ represents inhomogeneties of local magnetic field.

### 1.1.5 Free induction decay, signal detection and Fourier transform

The NMR signal is measured after excitation, during the relaxation process. As seen previously, when an RF pulse is used to tilt the magnetization in the transverse plane, the spin system is rotated so that the net magnetization $\mathbf{M_0}$, initially aligned with the main magnetic field $\mathbf{B_0}$, now precesses around the $\mathbf{B_0}$ direction and develops transverse components ($M_{xy}$). After the RF pulse is turned off, this transverse magnetization continues to freely rotate at the Larmor frequency around the main magnetic field $\mathbf{B_0}$. This oscillating magnetization in the transverse plan induces

electromotive force in a receiver coil according to Lenz-Faraday's induction principle. This receiver coil is placed perpendicular to $\mathbf{B_0}$. It can be the same coil as the one used for the RF excitation or a separate coil specifically used for signal reception. The loss of phase coherence of the spins due to both magnetic field inhomogeneities and intrinsic $T_2$ mechanisms results in a decrease of the $\mathbf{M_{xy}}$ vector, characterized by the relaxation time constant $T_2^*$. The measured decay and oscillation signal is therefore called free induction decay (FID):

$$S(t) \propto M_{xy}(t) = M_{xy}(0)e^{-\frac{t}{T_2^*}} e^{i(\omega-\omega_0)t+\varphi} \qquad 1.22$$

Where $M_{xy}(0)$ is the transverse magnetization directly after the RF excitation pulse and depends on the flip angle used. The free induction decay S(t) is detected as complex motion of transverse magnetization ($M_{xy} = M_x + iM_y$) where x and y components are usually detected as both real ($M_x(t)$) and imaginary ($M_y(t)$) FIDs:

$$M_x(t) = M_{xy}(max)\cos[(\omega-\omega_0)+\varphi]\, e^{-\frac{t}{T_2^*}} \qquad 1.23$$

$$M_y(t) = M_{xy}(max)\sin[(\omega-\omega_0)+\varphi]\, e^{-\frac{t}{T_2^*}} \qquad 1.24$$

where φ stands for the phase at t = 0.

Time domain data (i.e. FIDs) contain all relevant information about nuclear spins, but are rarely used directly. Instead, FIDs are converted into frequency domain (i.e. spectrum) data by a Fourier transform, expressed as:

$$F(\omega) = \int_{-\infty}^{+\infty} f(t)e^{-i\omega t}dt \qquad 1.25$$

Fourier transform is performed on S(t):

$$S(\omega) \propto M_{xy}(0)\int_0^{\infty} e^{-\frac{t}{T_2^*}} e^{-i(\omega_0-\omega)t+\varphi} e^{-i\omega t}dt = R(\omega) + iI(\omega) \qquad 1.26$$

Real and imaginary signals of the frequency domain (i.e. the spectrum) are given by the Fourier transform of time domain signals and are expressed as:

$$R(\omega) = A(\omega)cos\varphi - D(\omega)sin\varphi \qquad 1.27$$

$$I(\omega) = A(\omega)sin\varphi + D(\omega)cos\varphi \quad 1.28$$

With

$$A(\omega) = \frac{M_0 T_2^*}{1 + (\omega_0 - \omega)^2 T_2^{*2}} \quad 1.29$$

$$D(\omega) = \frac{M_0(\omega_0 - \omega)T_2^*}{1 + (\omega_0 - \omega)^2 T_2^{*2}} \quad 1.30$$

Where $A(\omega)$ and $D(\omega)$ represent the absorption and dispersion components of Lorentzian lineshape, respectively. The full width at half maximum (FWHM) of the absorption component equals $1/\pi T_2^*$ while the dispersion component is broader. Thus, to obtain the best separation of several lines in an NMR spectrum, spectra displayed in absorption mode are usually prefered. However, when $\varphi \neq 0$ the measured signals contain a mixture of absorption and dispersion components. Spectra in pure absorption mode can be obtained by 'phasing' the two spectra $R(\omega)$ and $I(\omega)$ according to:

$$A(\omega) = R(\omega)cos\varphi_c + I(\omega)sin\varphi_c \quad 1.31$$

$$D(\omega) = I(\omega)cos\varphi_c - R(\omega)cos\varphi_c \quad 1.32$$

Absorption mode spectra are obtained when $\varphi_c = \varphi$. On the majority of NMR spectrometers, the phase correction is done according to:

$$\varphi_c = \varphi_0 + (\omega_0 - \omega)\varphi_1 \quad 1.33$$

With $\varphi_0$ and $\varphi_1$ being the zero order correction and first order correction, respectively.
The absolute value (or magnitude mode) of the signal is defined as:

$$M(\omega) = \sqrt{R(\omega)^2 + I(\omega)^2} \quad 1.34$$

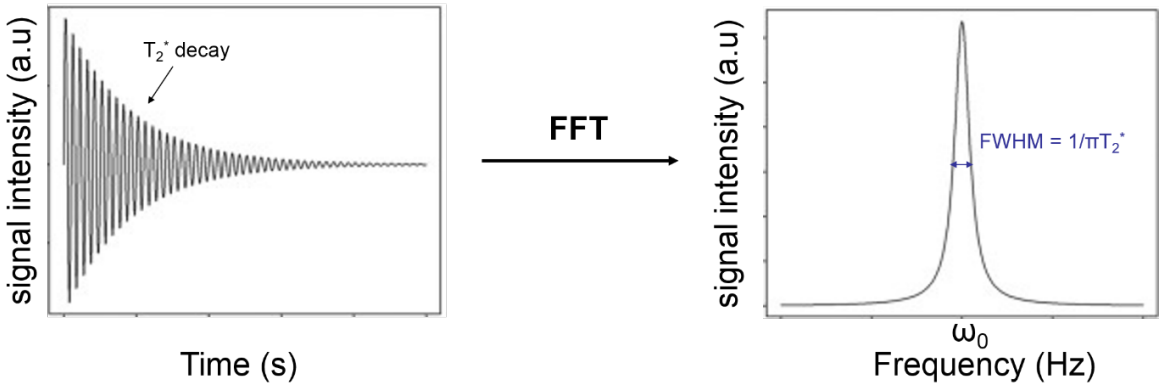


*Figure 1.2 On the left, the FID oscillating at the larmor frequency $\omega_0$. By applying a fast Fourier transform (FFT) on the time domain signal, the frequency domain signal is obtained, as depicted on the right. The full width at half maximum (FWHM) of the absorption component is $1/\pi T_2^*$.*

### 1.1.6 Chemical shift

Chemical shift describes the slight difference in resonance frequency between two identical nuclei residing in different molecular environments. When inside a $\mathbf{B_0}$ magnetic field, currents are induced in the electronic environment of the nucleus, creating another magnetic field and thereby slightly changing the magnetic field at the nucleus position. The effective magnetic field 'felt' by the nucleus is thus not $\mathbf{B_0}$ but $\mathbf{B_{eff}}$:

$$B_{eff} = B_0(1-\sigma) \qquad 1.35$$

where σ is shielding constant which depends on the density of the electron cloud close to the nuclei of interest. The resonance frequency of these shielded nuclei of interest is therefore expressed as:

$$\omega_{eff} = \gamma B_0(1-\sigma) \qquad 1.36$$

Thus, all nuclei do not resonate at exactly the same frequency: the latter depends both on the molecule where the nucleus resides as well as its specific position on that molecule (Figure 1.3). These differences in local field experienced by the nucleus at the atomic level give a specific spectral signature to the molecules and its different groups. This phenomenon is crucial in NMR spectroscopy because it allows to discriminate the signal from the nuclei of different molecules as well as within the same molecule. The chemical shift is not defined in Hz but in parts per million (ppm), independent of $\mathbf{B_0}$:

$$\delta = \frac{(\omega - \omega_{ref})}{\omega_{ref}} \times 10^6 \; [ppm] \qquad 1.37$$

where $\omega$ and $\omega_{ref}$ are resonance frequencies of nuclei of interest and of nuclei in a reference compound, respectively. For proton NMR, the reference is generally TMS (tetramethylsilane), whose shielding constant is very strong for the proton. The lower the shielding constant, the further away it is from the reference. In other words, the more the electron cloud is around the proton of interest, the closer its resonance is to TMS, whose chemical shift is arbitrarily set to 0. Very few molecules are more shielded than TMS. A single proton ($H^+$) would resonate at about 40 ppm. Water protons resonate at 4.8 ppm.

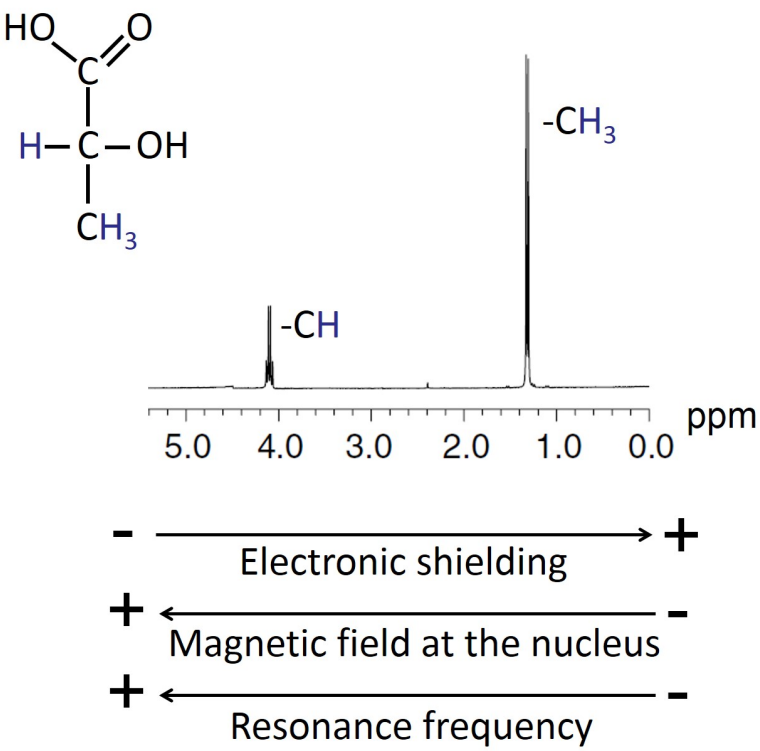


*Figure 1.3 A lactate molecule and its corresponding NMR spectrum. The methine proton (-CH) is closer to the electronegative oxygen atoms than the three methyl protons (-$CH_3$) , resulting in less shielding, and therefore a higher Larmor frequency and a higher chemical shift.*

### 1.1.7 Localization methods (ISIS, SPECIAL, OVS) and water suppression

#### *1.1.7.1 Spatial encoding*

The principle of localization consists in extracting information from a specific location within a tissue. The spatial localization of a volume of interest (VOI) is obtained by modifying the main magnetic field as a function of location, thus making Larmor frequencies spatially dependent. This is achieved by applying magnetic field gradients (G) that add or subtract from the main magnetic field $\mathbf{B_0}$ in the three orthogonal directions (x, y, z). The intensity of these gradients depends linearly on the position:

$$G(x,y,z) = G_x \cdot x + G_y \cdot y + G_z \cdot z \qquad 1.38$$

Therefore, the resonance frequency of spins $\omega_0$ (Larmor frequency) depend on their specific location:

$$\omega_0(x,y,z) = \gamma B(x,y,z) = \gamma[B_0 + G(x,y,z)] \qquad 1.39$$

Since the intensity of the gradients can be modified and the RF excitation can be adjusted to excite a particular range of frequencies, in the presence of gradients it is possible to specifically excite the magnetization in a particular location in the sample (i.e slice) and thus obtain only the signal from that part of the sample. This is also known as "slice-selective excitation".

#### *1.1.7.2 Image-Selected In vivo Spectroscopy – ISIS*

The ISIS localization method, first described by Ordidge et al. (Ordidge, Connelly, and Lohman 1986), provides a complete 3D localization in eight scans using a slice intersection strategy for voxel localization. The spectrum is not acquired in a single acquisition, but is derived using data from 8 separate RF pulse cycles which are combined (added or subtracted) to obtain the signal from the the VOI. The sequence consists of three slice selective 180°-inversion pulses and gradients in three orthogonal directions (Figure 1.4). The eight successive acquisitions necessary to obtain the final ISIS spectrum result from the $2^3 = 8$ permutations of the 180°-inversion pulses (ON or OFF). Each spectrum consists of positive or negative signal from different volumes of the sample. By adding and subtracting these spectra appropriately, one obtain the spectrum from the VOI only. The FID of each cycle is generated using a non-selective 90° excitation pulse which excites the entire volume under the coil.

*In vivo* MRS measurements are often performed with surface coils because they have an increased sensitivity. However, the inhomogeneity of the $B_1$ magnetic field associated with surface coils can impair the performance of the pulses. Thus, to improve $B_1$ magnetic field homogeneity and avoid contamination from unwanted signals, the RF-pulses used in this sequence are typically adiabatic (adiabatic pulses yield a uniform flip angle if their RF amplitude reaches a certain threshold). The main limitation of the ISIS sequence comes from its sensitivity to sample motion during the 8 successive acquisitions, resulting in subtraction errors.

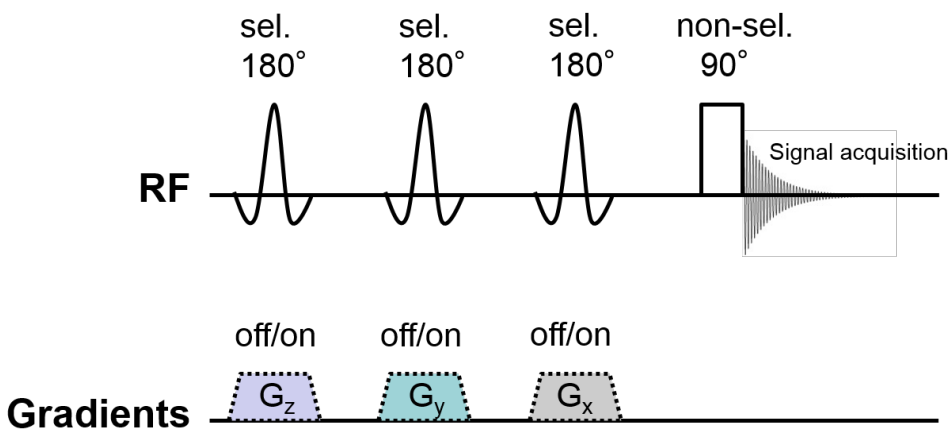


*Figure 1.4 Simplified pulse-timing diagram of the ISIS sequence*

#### *1.1.7.3 Spin Echo, full Intensity Acquired Localized Spectroscopy - SPECIAL*

This 3D localization sequence associates the ISIS 1D with a double slice selective spin-echo sequence (Mlynárik et al. 2006) and enables a very short echo time (the echo time represents the time between the first exciting pulse and the echo production). A slice selective full-passage adiabatic pulse is used as a 1D ISIS module in one of the two acquisitions, which is followed by asymmetric 90° and 180° slice-selective spin-echo pulses for the other two directions (Figure 1.5). The echo time can be shortened while preserving the full magnetization of the VOI by using a single 180° pulse to manipulate the transverse magnetization, combined with a 90° asymmetric pulse. Its sensitivity to motion is reduced compared to the eight modules of the 3D ISIS because there is only one addition-subtraction module. As in the ISIS sequence, adiabatic pulses are employed because of their insensitivity to $B_1$ inhomogeneity.

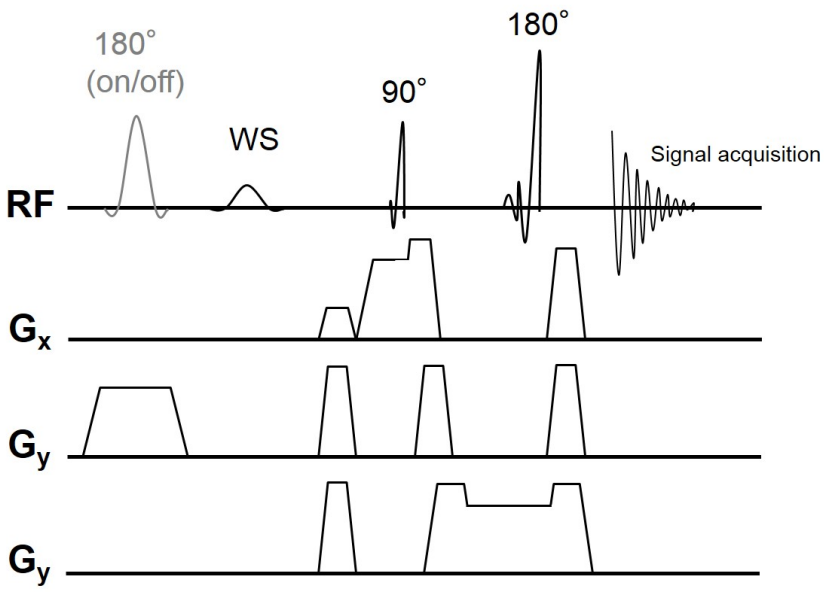


*Figure 1.5 Pulse timing diagram of the SPECIAL sequence. The first 180° adiabatic pulse is applied in alternate scans. WS represents an additional water suppression pulse.*

#### *1.1.7.4 Outer volume suppression (OVS)*

Outer volume suppression (OVS) can be used as a localization method or as a complement to another localization sequence in order to remove possible contamination from outside the VOI and improve localization. The principle of this technique consists in getting rid of the signal of the spins outside the VOI during a preparation time before the excitation. The spins outside the VOI are selectively dephased through a combination of selective RF pulses and dephasing gradients, resulting in zero net magnetization around the VOI while the VOI signal remains intact. This is repeated several times to ensure good suppression of the external volume. Then, the delay between the OVS and the excitation pulse should be as short as possible to limit the influence of the spins outside the VOI, which undergo $T_1$ relaxation.

#### *1.1.7.5 Water suppression*

In *in vivo* $^1$H MRS, good water suppression is crucial. The concentration of water in tissues is about $10^4$ times higher than that of the metabolites of interest. Thus, an MR spectrum without water suppression would be dominated by a large water peak whereas small organic molecules would be practically undetectable above the background. In addition to the overlap of its important signal with metabolites whose resonances are close to that of water (4.8 ppm), baseline distortion and other artifacts may occur if the water peak is not properly suppressed.

Usually a water suppression module is placed upstream of the spectroscopy sequence. The VAPOR (VAriable Pulse power and Optimized Relaxation delays (I. Tkác et al. 1999)) water suppression module is generally very efficient and is the one used in this thesis. It is composed of seven CHESS (chemical shift selective) pulses applied on water resonance with variable power and separation delays and 3 OVS (Outer Volume Suppression) modules. A CHESS pulse (Haase et al. 1985) is a 90° pulse that flips the magnetization over a small range of chemical shifts, followed by a dephasing gradient that dephases the magnetization and thus suppresses the corresponding signal. The advantage of the VAPOR module is its low sensitivity to $B_1$ field inhomogeneities and this method is therefore suitable when a surface coil is used for transmission.

## 1.2 Hyperpolarization

Hyperpolarization is the increase of the polarization of the nuclear spin well beyond the polarization achieved at thermal equilibrium conditions. In the past decades various hyperpolarization techniques aiming to enhance MR spectroscopy and MR imaging sensitivity have been developed, including the "brute force" approach, optical pumping of noble gases, parahydrogen induced polarization (PHIP) and dynamic nuclear polarization (DNP) (Abraham, McCausland, and Robinson 1959). These techniques are more and more used for *in vivo* applications and open perspectives for a wide range of new applications which are unfeasible with thermally polarized molecules. Dissolution DNP is arguably the most versatile technique and is the one used during the studies conducted in this thesis.

### 1.2.1 Polarization

As detailed in the previous section (Chapter 1.1), at thermal equilibrium and in the presence of an external magnetic field $\mathbf{B_0}$, there is a slightly greater number of spins in the lower energy state $(E_\alpha)$, i.e parallel to the field. The polarization *P* is defined as the fraction of spins parallel to $\mathbf{B_0}$. Since at usual magnetic field and temperature there is $\gamma \frac{h}{2\pi} B_0 \ll kT$, the polarization P for a nucleus with a spin $I$ = ½ can be approximated as:

$$P = \frac{(n_\alpha - n_\beta)}{n} \cong \left(\frac{h}{2\pi}\right)\frac{\gamma B_0}{2kT} \qquad 1.40$$

where $n_\alpha$ is the number of spins in the α (low energy) state, $n_\beta$ is the number of spins in the β (high energy) state, and n is the total number of spins in the sample, as defined in the previous section. For example, at 7 T and room temperature, the polarization of the proton is $P \cong 2.4 \cdot 10^{-5}$. The lower the magnetic field strength, the weaker the polarization. It is also weaker for almost all the other nuclei observable in NMR, the gyromagnetic ratios of the other nuclei being almost all lower than that of the proton. The difference in population between the possible energy states for a spin nuclei can be modified by several orders of magnitude and this non-equilibrium state of the spin populations is the hyperpolarized state.

### 1.2.2 Dynamic nuclear polarization (DNP)

DNP process is based on polarization transfer from electron spin to nuclear spin. The process itself takes place at extremely low temperatures (≈1 K) and inside a magnetic field (3.35 T – 7 T) on frozen glassy samples which contain the target molecules and a low quantity of radical, the latter being the source of paramagnetic centers (polarizing agents). At these conditions the electron

spins are almost fully polarized (Figure 1.6). The unpaired electron spins of stable radicals are continuously irradiated by microwave close to the Larmor frequency of the electron spins $\omega_e$ (typically a few hundreds of GHz) and result in the saturation of the electron spin resonance (ESR) line. The electron polarization is then transferred to its neighboring nuclear spins by dipolar-dipolar hyperfine coupling. This interaction generally involves one or more electron spins and one nuclear spin. Then, the polarization of one nuclear spin is transferred to its neighboring nuclear spins by a mechanism called "spin-diffusion". The polarization will increase but is also in competition with nuclear $T_1$ relaxation. The polarization will therefore increase as long as the nuclear relaxation time $T_1$ allows it (i.e until the steady state is reached).

In DNP, it is the electron spins that polarize the nuclear spins, but at the same time they also induce a faster relaxation. There is a competition between the two and it is therefore important to optimize the ratio between the density of the nuclear spins and that of the electron spins. It is for this reason that in the frozen glassy solution containing the labeled substrates, the concentration of paramagnetic centers is typically kept much lower than the nuclear population, generally a few tens of mM.

To date, two main families of mechanisms for polarization transfer are identified: the first one comprises the nuclear Overhauser effect (NOE) and the solid effect and the second one includes the thermal mixing and the cross effect. In DNP, there is an interplay of these mechanisms, and one or the other can be favored depending on experimental conditions such as the radical used and its concentration, the temperature and the magnetic field.

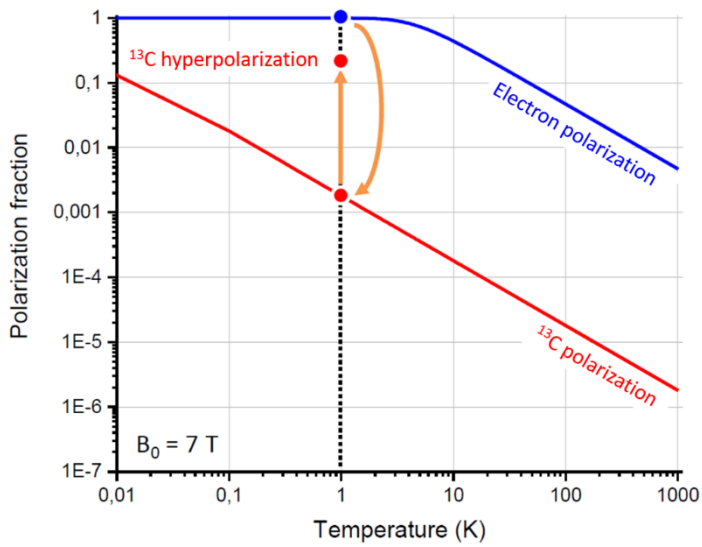


*Figure 1.6 Spin polarization fraction for $^{13}$C and unpaired electrons as a function of temperature at a magnetic field of $B_0$ = 7 T. DNP process is based on the transfer of electron spin polarization to nuclear spin polarization.*

### 1.2.3 Dissolution DNP

Due to the need to work at low temperature, the DNP process itself is performed on a frozen sample and thus had limited applicability for *in vivo* NMR applications until 2003, when DNP techniques based on the rapid dissolution of highly-polarized small molecules were developed (hence the name dissolution DNP). Using this technique one can improve the signal to noise ratio (SNR) by several orders of magnitude, up to 10 000-fold (Ardenkjær-Larsen et al. 2003), thus enabling to benefit from the DNP signal improvement for *in vivo* applications (Golman, Zandt, and Thaning 2006). Once the nuclear spin reached its maximal polarization, the sample is rapidly dissolved using superheated water or phosphate buffer (typically 5 mL). In the setup used in our experiments, immediately after dissolution, the solution is transferred to a separator/infusion pump and automatically injected 3 [s] after dissolution into the subject (Cheng et al. 2013), as shown in Figure 1.7.

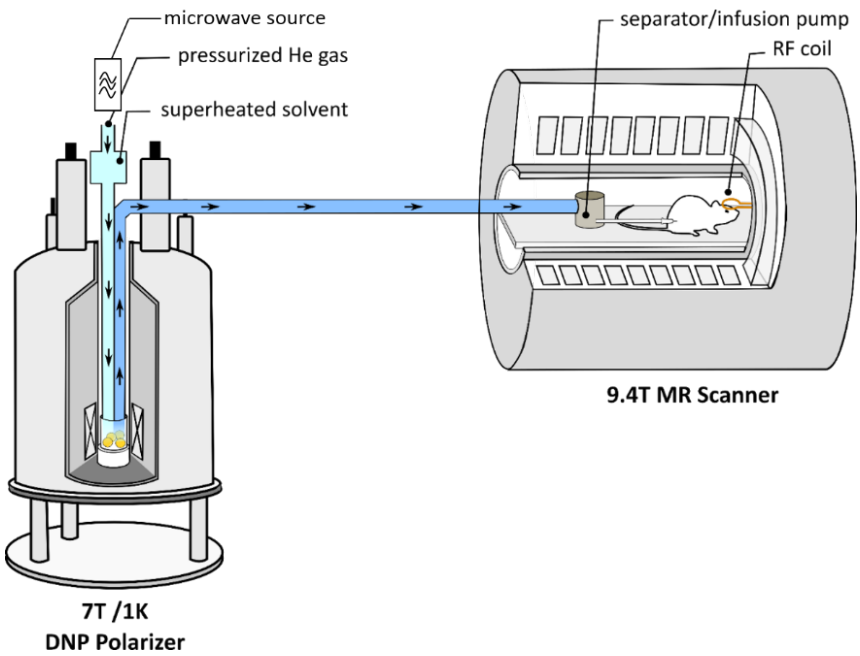


*Figure 1.7 Scheme of* in vivo *DNP experimental setup [courtesy of Emine Can]. The sample is dynamically hyperpolarized in a 7 T polarizer. The hyperpolarized substrate is then quickly dissolved with superheated buffer and automatically transferred to a separator/infusion pump and injected 3 s after dissolution into the subject.*

Thanks to the great improvement in sensitivity, this technique enables the detection of important low concentrated metabolic intermediates that cannot be easily detected by other MR methods. In addition, it provides new and unique information about fast metabolic processes in real-time *in vivo* (Golman and Petersson 2006). However, hyperpolarization always has two major drawbacks, due to the "out of equilibrium" state:

(1) First, the lifetime of the hyperpolarized spin state is short: the relaxation processes rebalance the spin populations at thermal equilibrium with the time constant $T_1$, which limits the measurement time. Longitudinal relaxation time $T_1$ of $^{13}C$-labelled metabolites typically range between 15 to 60 s. The lifetime of the polarization is one of the main challenge with hyperpolarized molecules, which can be very short for some molecules such as for example $^{13}C$-labelled glucose.

(2) Secondly, the loss of hyperpolarization due to each RF pulse: for the measurement, part of the hyperpolarized magnetization is excited and moved to the transverse plane. But it then comes back to its thermal equilibrium and not to its initial hyperpolarized level. The measurement of a part of the hyperpolarized magnetization thus results in a loss of polarization.

The signal decay due to the effect of RF pulses and $T_1$ relaxation can be described as:

$$S(t) = S(0)e^{-\frac{t}{T_1}}\cos^{n-1}(\alpha) \qquad 1.41$$

These two processes render the loss of hyperpolarization irreversible. It is therefore essential to take these specificities into account in experimental design and acquisition strategies. For instance, if several acquisitions are performed during an experiment, small flip angles are preferentially chosen after injection of the hyperpolarized sample.

## 1.3 Cerebral metabolism

### 1.3.1 Glycolysis and oxidative metabolism

The brain represents only 2 % of the total weight of the human body but consumes a quarter of the body's total energy, mainly in the form of glucose. Brain function is characterized by high metabolic activity and requires a continuous supply of oxygen and nutrients from the blood stream. Brain metabolism involves complex intercellular trafficking of metabolites and many processes are compartmentalized. It is well established that the mammalian brain is primarily sustained by glucose as a fuel to supply its high metabolic demand (Mergenthaler et al. 2013), consuming up to 25 % of circulating glucose under normal conditions (L. Pellerin 2010). In normal conditions, glucose crosses the endothelial cells of the blood-brain barrier via GLUT1, the most abundant glucose transporter found in red blood cells, endothelial cells, astrocytes and microglia. In neurons, GLUT3 is the major glucose transporter (Patching 2017). Inside the brain, glucose from the extracellular space is rapidly taken up by different types of brain cells among which astrocytes, microglia and neurons. Glucose then undergoes several metabolic reactions including two of the main metabolic pathways: glycolysis, which occurs in the cytosol, and the tricarboxylic acid (TCA) cycle and oxidative phosphorylation, which takes place into the mitochondrial matrix.

**Glycolysis**

Glycolysis is the metabolic pathway taking place in the cytosol that converts glucose into pyruvate. The production of cerebral pyruvate from glucose is the result of 11 steps including glucose transport and 10 enzymatic steps of glycolysis. During glycolysis, four ATPs molecules are formed but two ATPs are consumed as well, resulting in the net production of two molecules of ATP per glucose molecule. Glycolysis is also linked to other metabolic pathways. For example, glucose-6-phosphate (Glc6P) is the product of the first step of glycolysis and is thus at the beginning of two major metabolic pathways: glycolysis and the pentose phosphate pathway. In addition, Glc6P can also be utilized for the storage of glucose in the form of glycogen (in astrocytes only).

Glycolysis is regulated at different stages (Figure 1.8). Hexokinase regulates the phosphorylation of glucose and is inhibited by glucose-6-phosphate. Then, the reaction catalysed by the phosphofructokinase is a key step in glycolysis, both in its rate (it is the limiting step in terms of the rate of glycolysis) and in its regulation; phosphofructokinase being regulated allosterically by ATP and its products, as well as citrate. The last reaction, catalyzed by pyruvate kinase, is also a control point for glycolysis. Its activity is also regulated by the levels of high-energy phosphates, as

well as acetyl-CoA. Finally, pyruvate, via lactate dehydrogenase, is in dynamic equilibrium with lactate.

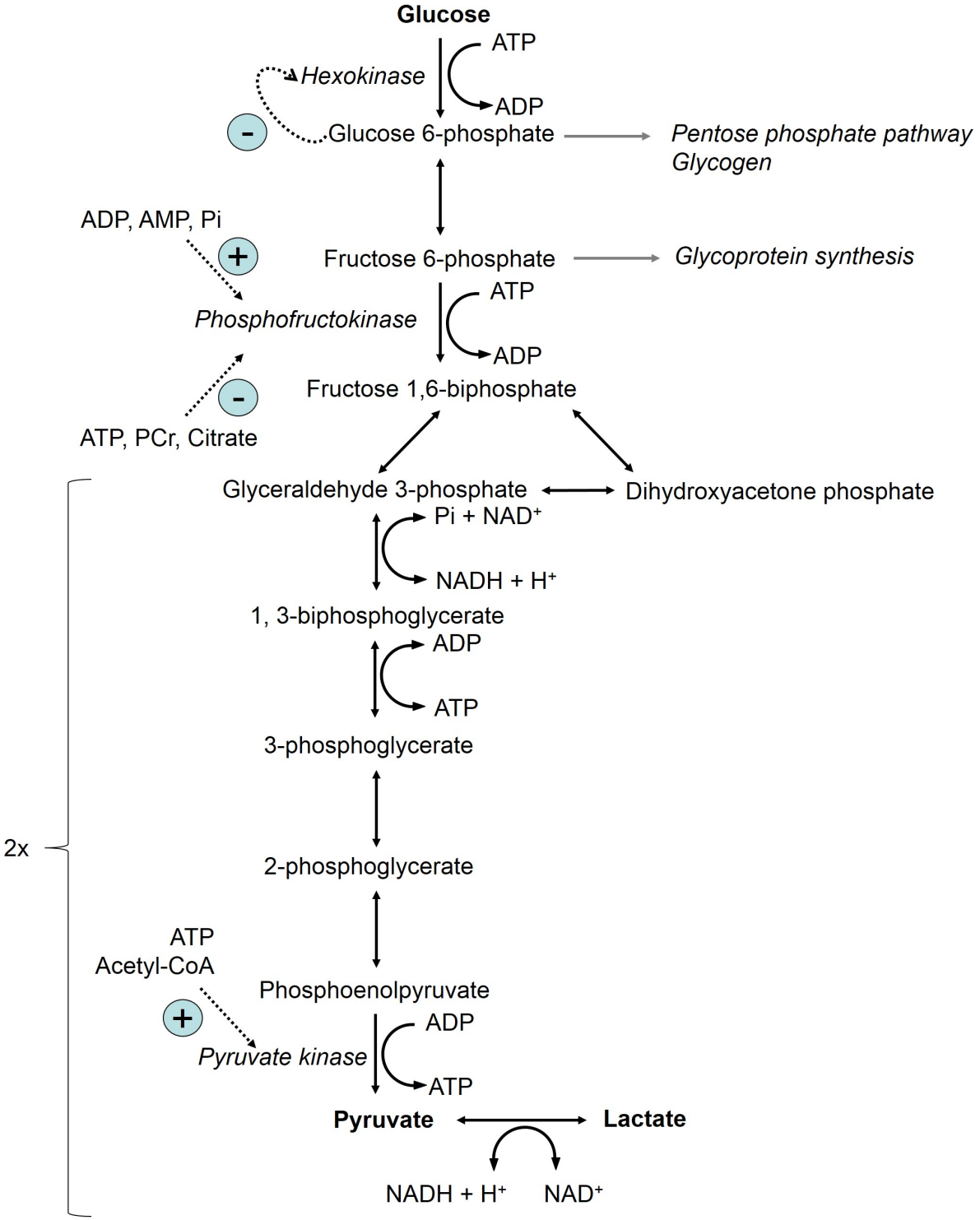


*Figure 1.8 Biochemical reactions and regulation steps of glycolysis and its associated pathways. Overall, glycolysis consumed two ATPs during the first phase and produced 4 ATPs during the second phase, resulting in a net gain of two ATPs.*

**Oxidative metabolism**

Once glucose is converted to pyruvate, it enters the mitochondria. It is transformed into acetylcoenzyme A (CoA) and then enters the TCA cycle (Dienel, 2014). The TCA cycle, or Krebs cycle, is a fundamental biochemical process where several major metabolic pathways converge. This metabolic pathway produces energy substrates that provide the majority of the cell's energy needs. The TCA cycle is a complex series of biochemical reactions present in all aerobic organisms whose primary function is the common terminal oxidation of glucose, lipids, glycogen and amino acids. Overall, the Krebs cycle converts pyruvate into carbon dioxide, GTP and ATP molecules, and reduced coenzymes (NADH and $FADH_2$), coenzymes whose electrons contain most of the chemical energy of the degraded molecules. NADH and $FADH_2$ are then used by the electron transport chain to further generate ATP as part of oxidative phosphorylation.

In greater detail, this aerobic catabolism takes place in the presence of oxygen in diatomic free form ($O_2$) in the mitochondrial matrix of eukaryotic cells. The TCA cycle is based on the modification of a citrate molecule by enzymes and co-factors. The cycle thus generates eight different molecules, including a new citrate at the end of the cycle. Pyruvate is first oxidatively decarboxylated to form acetyl-CoA in a reaction catalyzed by the enzyme pyruvate dehydrogenase (PDH). Isocitrate, 2-oxoglutarate, succinyl-CoA, succinate, fumarate, malate, oxaloacetate and finally regenerated citrate are then successively produced (Figure 1.9). NADH and $FADH_2$ transfer their electrons to molecular $O_2$ via the electron transport chain in the mitochondria to produce ATP in the oxidative phosphorylation process. A total of 32 ATP is generated by the oxidative metabolism process for one glucose and 6 $O_2$ (Papa, Petruzzella, and Scacco 2007). The main function of the TCA cycle is the production of energy for the cells, but it is also an important source of biosynthetic precursors for synthesis of different molecules such as amino acids, nucleotide bases, cholesterol and porphyrin. For example, in the brain, the TCA cycle intermediate 2-oxoglutarate is a precursor of glutamate, an important neurotransmitter.

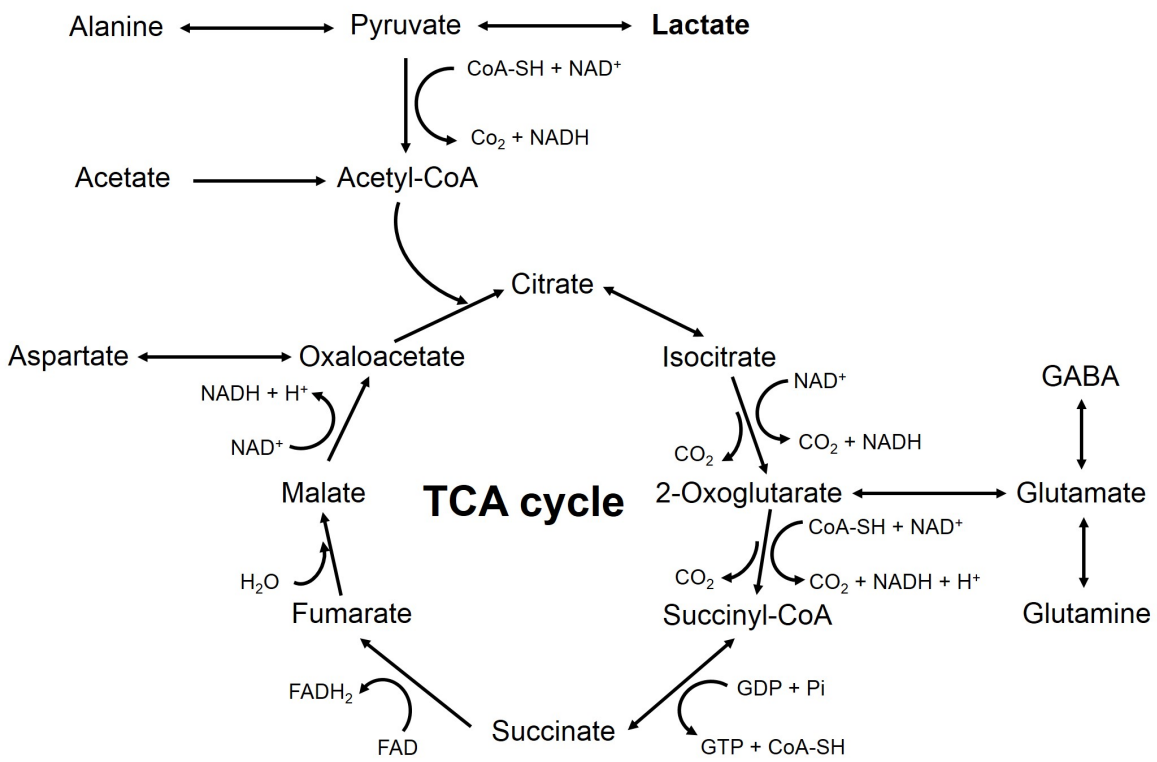


*Figure 1.9 Biochemical reactions of tricarboxylic acid cycle (TCA cycle) and related metabolites. The TCA cycle takes place in the mitochondrial matrix and yields a total of 32 ATP per glucose molecule.*

An important question is related to the main energy substrate supporting cell activity. Glucose is the primary energy substrate delivered to the brain in normal circumstances, but the roles of glycolysis and oxidative phosphorylation in the energy metabolism of neurons and astrocytes during brain activation are not fully elucidated. It has been postulated that lactate is the main fuel of neurons during their activity (Luc Pellerin and Magistretti 2012), but this fact and the corresponding neuron-astrocyte interactions are still debated (Dienel 2012), studies having demonstrated in particular that both astrocytes and neurons metabolize glucose through the glycolysis (Ivanov et al. 2014).

### 1.3.2 Commonly measured major brain metabolites using $^{1}$H MRS

Ultra-high magnetic field combined with ultra-short TE allow to detect and quantify by *in vivo* $^{1}$H MRS 18 metabolites involved in osmoregulation, neurotransmission, energy or antioxidant metabolism: alanine (Ala), ascorbate (Asc), aspartate (Asp), glycerophosphocholine (GPC), phosphocholine (PCho), creatine (Cr), phosphocreatine (PCr), γ-aminobutyric acid (GABA), glucose (Glc), glutamine (Gln), glutamate (Glu), glutathione (GSH), myo-inositol (Ins), lactate (Lac), N-acetylaspartate (NAA), N-acetylaspartylglutamate (NAAG), phosphoethanolamine (PE), and taurine (Tau). In this part, we give an overview of the function and properties of these metabolites.

**Myo-inositol (Ins):** Myo-inositol is a metabolite found mainly in astrocytes and is an important osmotic agent regulator for cell volume. Due to its relatively high concentration (4-8 mM) (Pouwels and Frahm 1998; Kreis 1997), myo-inositol is easily detectable in short-TE $^{1}$H NMR spectra of the brain. The six NMR detectable protons of myo-inositol result in four groups of resonances: a doublet-of-doublets centered at 3.52 ppm, a triplet at 3.61 ppm and one at 4.05 ppm. A smaller triplet is found at 3.27 ppm and is generally masked by the larger resonances of total choline.

**Glutamine (Gln):** Glutamine plays an important role in intermediary metabolism and is involved in neurotransmission and osmoregulation. It is generally considered to be primarly located in astroglia (Martinez-Hernandez, Bell, and Norenberg 1977) at a concentration of 2-4 mM. Glutamine is a glutamate precursor. Glutamine synthetase, the enzyme that synthesizes glutamine from glutamate, is located exclusively in astrocytes. In addition to its role in the glutamate-glutamine neurotransmitter cycle, one of the main roles of glutamine is the detoxification of ammonia. Glutamine concentration increases substantially during hyperammonemia and plays a central role in the pathogenesis of hepatic encephalopathy. The glutamine spectra is composed of a triplet resonating at 3.76 ppm, of multiplets grouped between 2.12 ppm and 2.46 ppm and two NMR-detectable protons downfield from water (6.82 and 7.73 ppm).

**Taurine (Tau):** Taurine is an important component of osmoregulation (Solís et al. 1988; Taylor et al. 1995) and may play a role in neurotransmission as a modulator of neurotransmission action, although this is not clearly established. The concentration of taurine in the adult rat brain is typically between 6–8 mM (Ivan Tkác et al. 2003). The taurine spectra is composed of two triplets centered at 3.25 and 3.42 ppm.

**Choline-containing compounds (tCho):** Choline-containing compounds (tCho) are composed of free choline (Cho), phosphocholine (PCho), and glycerophosphocholine (GPC). They are part of cell membranes constituent and are involved in phospholipid synthesis and degradation pathways, thereby representing membrane turnover. The methyl protons of choline-containing compounds is at 3.2 ppm, which is one of the most important resonance in $^{1}$H NMR spectra from brain. An increase in choline signaling is reported in some diseases such as Alzheimer's disease (Firbank, Harrison, and O'Brien 2002) or multiple sclerosis (Narayana 2005; Gonzalez-Toledo, Kelley, and Minagar 2006), while a decrease in choline levels is related to liver disease and stroke (Malisza, Kozlowski, and Peeling 1998). Yet, the multiple contributions to the measured total choline resonance complicate the interpretation of variations in total choline signal.

**Lactate (Lac):** Lactate is the end product of anaerobic glycolysis and is also an important alternative energy source for the brain (Schurr et al. 1999; Luc Pellerin and Magistretti 2004, 200). It has been postulated that lactate links astroglial glucose uptake and metabolism to the metabolism and cycling of neuronal neurotransmitters (Magistretti et al. 1993; L. Pellerin et al. 1998), but this hypothesis remains debated in the scientific community (Chih and Roberts 2003). Lactate is generally found at a low concentration of about 0.5 mM in the brain, but is still clearly observable in $^{1}$H NMR spectra with short echo time. Lactate spectra is composed of a doublet resonance at 1.31 ppm and a quartet at 4.10 ppm.

**Creatine (Cr) and phosphorylated creatine (PCr):** In the brain, creatine and phosphorylated creatine are present in both glial and neuronal cells. Creatine and phosphorylated creatine, together with ATP, are central to the energy metabolism of tissues (Wallimann et al. 1992). In addition to this, it has been shown that creatine is also an important osmolyte in the brain and may also act as a possible neuromodulator/neurotransmitter. Creatine has also been described as a potential antioxidant molecule (Sestili et al. 2006). The $^{1}$H NMR spectra of creatine and phosphorylated creatine are very similar. Their methyl and methylene protons give rise to resonances at 3.03 ppm and 3.93 ppm. At ultra-high magnetic field (>7.0 T) the creatine (3.913 ppm) and phosphorylated creatine (3.930 ppm) methylene resonances become separable and quantifiable. However, the difference between their two methyl resonances (3.027 ppm and 3.029 ppm) is too low to enable an accurate separation *in vivo*. The concentrations for phosphorylated creatine in human brain is around 4.0-5.5 mM for Cr and 4.5-6.0 mM for PCr (Graaf 2019). The sum of both is referred to as 'total creatine' (tCr).

**Glucose (Glc):** Glucose is central to the brain's energy metabolism. The mammalian brain is mainly supported by glucose as fuel to meet its high metabolic demand (Mergenthaler et al. 2013), consuming up to 25 % of circulating glucose under normal conditions (L. Pellerin 2010). Glucose is also the precursor of many compounds. Under normal circumstances, its concentration is about 1.0 mM in the brain (Gruetter et al. 1992). The resonance of one glucose proton at 4.63 ppm is usually eliminated during water suppression and the glucose spectrum is mainly composed of resonances of the other six nonexchangeable protons between 3.2 ppm and 3.9 ppm; the spin system being strongly coupled. However, the large spectral overlap restricts the reliability of detection.

**Glutamate (Glu):** Glutamate is an important amino acid involved in the neurotransmission process; it is the main excitatory neurotransmitter released by neurons (Erecińska and Silver 1990). It also

plays other roles *in vivo* by being the direct precursor of the inhibitory neurotransmitter GABA and is also involved in the synthesis of other small metabolites such as glutathione. Glutamate is converted to glutamine by the addition of ammonia by the enzyme glutamine synthetase which is uniquely found in astrocytes in the brain. Glutamate is present in all cell types at a concentration between 6–12.5 mM, with the largest pool located in glutamatergic neurons. The glutamate spectra is composed of a doublet-of-doublets resonating at 3.75 ppm (signal from the single $^{2}$CH proton), and of multiplets between 2.04 ppm and 2.35 ppm (resonances of the other four protons). At low magnetic field, glutamate and glutamine are virtually impossible to separate. At ultra-high magnetic field (>7.0 T), the glutamate and glutamine multiplets resonances between 2.04 ppm and 2.46 ppm become separable and quantifiable.

**γ-aminobutyric acid (GABA):** GABA is the major inhibitory neurotransmitter in the mammalian brain and has a brain concentration of approximately 1 mM. Altered concentrations of GABA are implicated in different neurological and psychiatric conditions, including depression, epilepsy and schizophrenia. The detection and reliable quantification of GABA by $^{1}$H MRS is challenging because the resonances of GABA (triplet resonances at 3.01 ppm and 2.28 ppm, and a quintet centered at 1.89 ppm) are overlapped by those of other more concentrated metabolites. Spectral editing methods are thus often used for GABA detection.

**Aspartate (Asp**): Aspartate is a non-essential amino acid that plays a role as an excitatory neurotransmitter. It is found in the brain at a concentration of approximately 1-2 mM (Pfeuffer et al. 1999; Govindaraju, Young, and Maudsley 2000) and is synthesized from glucose and possibly other precursors. Together with glutamate, aspartate also plays a key role in the malate-aspartate shuttle. Aspartate spectra is composed of a doublet-of-doublets at 3.89 ppm and a pair of doublet-of-doublets at 2.65 ppm and 2.80 ppm.

**Ascorbate (Asc):** Ascorbate (vitamin C) is physiologically present in the form of the ascorbate anion with an average concentration of ascorbate in the brain is about 1.0 mM. Ascorbate levels in the brain are tightly controlled, but despite an enormous amount of work, the exact role of ascorbate remains unclear. It has neuroprotective properties and is part of the intracellular antioxidant network, but it is also apparently involved in neuromodulation and may be a specific extracellular antioxidant. Ascorbate spectra is composed of a doublet at 4.49 ppm and multiplet resonances at 4.00 ppm and 3.73 ppm (Graaf 2019).

**Glutathione (GSH):** Glutathione is an antioxidant mainly located in astrocytes that protects the cell against reactive oxygen compounds in particular. It is fundamental for the synthesis and degradation of proteins and the formation of DNA precursors and is also a cofactor in several reactions (Cooper and Kristal 1997). Its concentration in the brain is between 1-3 mM (Trabesinger et al. 1999). Neurodegenerative diseases such as Parkinson's disease can alter altered GSH levels (Sian et al. 1994). Glutathione spectra is composed of a singlet at 3.77 ppm, two separate multiplets at around 2.15 and 2.55 ppm and three doublet-of-doublets at 2.93, 2.98 and 4.56 ppm. *In vivo* measurement of glutathione is difficult because of the large overlap of resonances with the stronger signal of other metabolites (Glu, Gln, Cr, NAA) but it can be detected directly by combining short-TE spectra with spectral fitting at ultra-high magnetic fields.

***N*-Acetylaspartate (NAA):** *N*-acetylaspartate (NAA) is one of the most concentrated free amino acids in the brain, its concentration reaching up to 8-11 mM in gray matter (Pouwels and Frahm 1998; Wang and Li 1998; Pan, Twieg, and Hetherington 1998). Despite many years of investigation, the exact function of *N*-acetylaspartate is not currently known, but it is often considered to be a neuronal marker, particularly as a marker of neuronal density and viability. It is also a known osmolyte, but various other roles have been suggested for *N*-acetylaspartate, including its function in the synthesis of fatty acids and myelin (D'Adamo and Yatsu 1966; D'Adamo, Gidez, and Yatsu 1968). Its resonance at 2.02 ppm is the highest peak in the normal spectrum. Smaller resonances are seen as doublet-of-doublets at 2.49 ppm, 2.67 ppm and 4.38 ppm.

***N*-Acetylaspartylglutamate (NAAG):** *N*-acetylaspartylglutamate is a dipeptide of aspartate and N-substituted glutamate with a concentration varying between different regions of the brain, ranging from 0.6 to 3.0 mM (Koller, Zaczek, and Coyle 1984; Pouwels and Frahm 1997). Although its exact function is uncertain, *N*-acetylaspartylglutamate is thought to be implicated in excitatory neurotransmission and is also a source of glutamate. Its largest resonance is found at 2.04 ppm. It is very close to the main resonance of *N*-acetylaspartate at 2.01 ppm, requiring ultra-high field and very good magnetic field homogeneity to be able to separate them. The spectral overlap with more concentrated metabolites combined with a relatively low concentration results in other resonances not generally being observed directly.

**Alanine (Ala):** Alanine is a non-essential amino acid whose concentration does not exceed 0.5 mM in the brain. It has been proposed by several studies that alanine is an important carrier for ammonia transfer (Bröer et al. 2007) and an increase in alanine concentration has been measured following ischemia (Brulatout et al. 1996) and in meningioma (Poptani et al. 1995). The doublet of

alanine is often observable at 1.4 ppm in $^{1}H$ NMR spectra from rat brain acquired at high magnetic field.

**Phosphorylethanolamine (PE):** Phosphorylethanolamine is considered to be an intermediate in the phospholipid metabolism, but its precise physiological role remains poorly understood. Phosphorylethanolamine spectra is composed of two multiplets resonances of its four NMR-observable protons at circa 3.1-3.2 ppm and 3.8-4.0 ppm. Phosphorylethanolamine has been measured at a concentration of 0.5-1.0 mM in the human brain (Blüml, Seymour, and Ross 1999) while it is slightly higher in rats (2-2.5 mM). Increased concentrations have been reported during seizures (Lehmann et al. 1985).

## 1.4 Hepatic encephalopathy

Hepatic encephalopathy (HE) is defined as a reversible neuropsychiatric syndrome caused by an acute or chronic liver dysfunction such as chronic liver disease (CLD). It is a very common complication of cirrhosis and is characterized by a wide range of neurological or psychiatric abnormalities. Patients with HE suffer from intellectual impairment, personality changes, motor disturbances as well as depressed level of consciousness. In the worst cases, the patients may fall into a coma. Despite an enormous effort to characterize the physiopathology of HE, it has not been fully elucidated and the exact molecular mechanisms and their chronology remain unclear (Swaminathan, Ellul, and Cross 2018).

### 1.4.1 Classification of HE

There are three types of hepatic encephalopathy:

(1) Type A is associated with acute liver failure.

(2) Type B is associated with port-systemic shunt without the presence of liver disease.

(3) Type C is associated with cirrhosis and portal hypertension.

Symptoms and signs of HE vary from mild to severe and neurological disorders of varying intensity may be observed. The most typical are those related to altered state of consciousness. Episodes of encephalopathy can be classified according to their intensity and recurrence. Five stages are determined by the West-Haven classification (Blei, Córdoba, and Practice Parameters Committee of the American College of Gastroenterology 2001). Grade 0 (or minimal HE) is characterized by the absence of clinical abnormalities and causes only subtle cognitive abnormalities and symptoms are only detectable by psychometric or neurophysiological tests (Abdo 2006). Grade I is characterized by moderate attention deficit disorder, grade II by disorientation, apathy or lethargy, grade III by confusion or drowsiness, and grade IV by coma. The main limitation of this classification is that the identification of moderate impairment of consciousness is based on subjective assessment and is subject to considerable inter- and intra-observer variability. In addition, grade 0 is heterogeneous as it includes patients without encephalopathy and others with a degree of encephalopathy that is not clinically detectable. Conversely, the distinction between stages I and II is easier and is based mainly on the existence of disorientation or asterixis.

### 1.4.2 Pathogenesis

For several years, it has been accepted that HE results from a multifactorial pathophysiological process in which hyperammonemia and inflammation play a central role. There are several hypotheses about the mechanisms of ammonia toxicity, but despite the considerable work carried out in the field of HE, the precise pathophysiological mechanisms remain incompletely elucidated (Prakash and Mullen 2010), explaining in particular the lack of very effective therapeutic solutions (Rose et al. 2020).

**Ammonia**

Ammonia is recognized as an important factor in the pathogenesis of hepatic encephalopathy. It is a by-product of nitrogen metabolism, primarily produced in the intestines from nitrogenous substances from the diet, the deamination of glutamine by glutaminase, and the metabolism of nitrogenous compounds by colonic flora. Under normal physiological conditions, most ammonia is detoxified in the liver where it is metabolized to urea, thus maintaining blood ammonia levels below 50 $\mu$M.

Ammonium in solution is present both as a gaseous component, the weak base $NH_3$ (ammonia), and in ionic form, the weak acid $NH_4^+$ (ammonium). Their relative ratio depends on the pH, defined by the Henderson-Hasselbach equation. In blood, under normal physiological conditions (pH = 7.4), more than 98 % is in the form of $NH_4^+$ ions (Bromberg, Robin, and Forkner 1960). Both are capable of crossing plasma membranes by diffusion ($NH_3$) and transport channel ($NH_4^+$) mechanisms and therefore have a direct effect on intracellular and extracellular pH. The deleterious effects of of ammonia are multiple and involve various pathways such as cellular swelling, oxidative stress, mitochondrial dysfunction and disruption of cellular bioenergetics (Bosoi and Rose 2009). As ammonia is also a product and a substrate for various biochemical reactions, an increase in cerebral ammonia leads to disturbances in brain metabolism by influencing the activities of many enzymes, signaling transduction pathways, the alternation of protein phosphorylation and the state of different other ion channels and transporters (Busa and Nuccitelli 1984; Norenberg 1998).

When the liver function is altered, it causes a rise in blood ammonium and a high ammonium delivery to the brain, and consequently neurotoxicity induced through different cellular pathways and mechanisms. Cerebral ammonium removal leads to the formation of glutamine by glutamine synthetase: the major CNS pathway of $NH_4^+$ removal involves the astrocytic enzyme glutamine synthetase which catalyzes the formation of glutamine from $NH_4^+$ and glutamate (Braissant 2010). Important enzymes such as glutaminase, glutamine synthetase and glutamate dehydrogenase are

affected and altered in their regulatory function by increased concentrations of ammonium in the brain (Bosoi and Rose 2009). In addition, increased glutamine in the brain disrupts astrocyte metabolism and causes osmotic stress that is only partially compensated by the gradual release of other brain metabolites (myo-inositol, taurine, total choline and creatine) to prevent the occurrence of cytotoxic edema (Häussinger 2006; Braissant et al. 2019).

Ammonia plays an irrefutable and key role in the pathogenesis of HE, but additional factors such as gut flora modifications, systemic inflammation, neuroinflammation and oxidative stress play an important role and exacerbate the neurological effects of HE, which are critical factors in the precipitation of HE, leading to a multifactorial disease (Coltart, Tranah, and Shawcross 2013; Azhari and Swain 2018).

**Inflammation**

A synergistic effect of inflammation with ammonia is hypothesized (Shawcross et al. 2004) and even mild infection is often a trigger for HE in cirrhotic patients (Merli et al. 2013). Circulating immune cells are suspected to have an abnormally activated phenotype in cirrhotic patients and several pro-inflammatory cytokines such as TNF-α are generally found at high concentrations in plasma. Alterations in the intestinal microbiota and increased permeability of the intestinal barrier are believed to be responsible for bacterial translocation and facilitated endotoxin passage, and are associated with increased production of inflammatory mediators in patients with cirrhosis (Bajaj et al. 2012). Systemic inflammation appears to strengthen the neurotoxic effects of ammonium (Shawcross et al. 2004) and ammonium-induced brain inflammation also contributes to the evolution of HE (Butterworth et al. 2009). This neuroinflammation is characterized by microglial activation and the local production and release by the brain of interleukins (IL-1β and IL-6) and pro-inflammatory cytokines, likely by both astrocytes and microglia (Bémeur and Butterworth 2013; Wright et al. 2007).

**Increased permeability of the blood-brain barrier**

It appears that the brain accumulation of toxic substances, particularly ammonia, combined with systemic inflammation leads to a functional and structural alteration of the blood-brain barrier (BBB), which would favour a change in neurotransmitter levels (mainly glutamate and GABA, as discussed in the following section) (Weiss, Jalan, and Thabut 2018).

Ammonium affects the transport of amino acids. Intracerebral accumulation of glutamine acts directly on amino acid transporters at the BBB and leads to increased passage of aromatic amino

acids, impairing intracerebral synthesis of serotonin and dopamine. Transporters of small to medium-sized molecules located in the BBB are also affected, altering the transcellular passage of these molecules.

Also, structural abnormalities such as alteration of the BBB tight junction proteins have been suggested in both acute hepatocellular failure and cirrhosis (Nguyen et al. 2006), suggesting an increase in BBB permeability (Abdo 2006). It is believed that these different alterations render the patient suffering from cirrhosis more susceptible to endogenous (hyperammonia or inflammation) or exogenous (accumulation of drugs, for example) cerebral aggression.

**Neurotransmission alterations and energy metabolism disturbances**

Structural changes in astrocytes directly alter synaptic transmission. In addition, the brain metabolism of ammonium appears to have an effect on neurotransmission through different mechanisms: $NH_4^+$ increases synaptic glutamate release and also has a strong effect on inhibitory neurotransmission (GABA-ergic) by decreasing the absorption and increasing the release of glial GABA, which raises extracellular levels of GABA (Bender and Norenberg 2000). Also, $NH_4^+$ increases the affinity of GABA receptors for GABA (Takahashi et al. 1993) and stimulates astrocytic benzodiazepine receptors, thereby increasing the synthesis and release of the neurosteroid agonist complex GABA-a agonist complex (Palomero-Gallagher and Zilles 2013).

In addition to these neurotransmission effects, it has long been suspected that HE induces alterations in the brain's energy metabolism (primarily in acute HE), although the precise underlying mechanisms are not yet elucidated. Studies on the effect of ammonia on energy metabolism have yielded conflicting results (Schousboe et al. 2014) and the hypothesis that altered brain energy may explain the pathogenesis of HE remains to be proven.

It is likely that the efficiency of the TCA cycle and thus the production of ATP can be disrupted, either by inhibition of α-ketoglutarate dehydrogenase (Lai and Cooper 1986), or by ammonia-induced decreases in levels of α-ketoglutarate (Bessman and Bessman 1955), resulting in reduced oxidative metabolism. However, a recent study using $^{31}P$ MRS and $^{1}H$ MRS showed that in a rat model of type C HE, the ATP concentration tended to decrease only at week 8, at the end of the disease. The authors therefore proposed that energy metabolism was not a major cause of early symptoms of HE in the established model of type C HE (Rackayova et al. 2016).

Thus, it is possible that reduced ATP production is not a major factor in the pathogenesis of HE and that the reduction in brain glucose utilization observed by $^{18}F$-FDG PET (Lockwood et al. 2002) may

be due to reduced glucose requirements (Butterworth 2003). Future studies are needed to clarify these points.

### 1.4.3 Clinical manifestations and diagnosis

HE is characterized by impaired alertness ranging from moderate confusion to a deep coma, and the various neurological manifestations render the diagnosis of HE challenging for hepatologists. While its importance is widely recognised, there is little consensus on how optimally to diagnose and monitor HE. There are currently no specific clinical and/or paraclinical tests available and the diagnosis is thus first made by excluding other causes of disturbances in the state of consciousness. The first diagnostic approach is based on questioning the patient and his family and on the clinical examination. One of the usual electrophysiological tests for the diagnosis of hepatic encephalopathy is the classical electroencephalogram (EEG), where the changes typically associated with HE are high amplitude low frequency and triphasic waves (Amodio et al. 2001; Cash et al. 2010). These tests are used to diagnose hepatic encephalopathy, but they are easily performed only in hospitalized patients. Brain imaging may also be useful, in particular magnetic resonance imaging (MRI) with detection of low-grade cerebral edema (Prakash and Mullen 2010) or the detection of specific signs of accumulation of substances usually metabolized by the liver, such as a hyper signal from the central grey nuclei which is attributed to manganese excess (Pujol et al. 1993). However, they are poorly correlated with neurological status and the use of MRI as a diagnostic tool for HE remains limited (Fukuzawa et al. 2006; Hermann et al. 2018). Magnetic resonance spectroscopy (MRS) is also promising in providing evidence of a metabolic profile of HE such as elevated glutamate-glutamine peak, decreased choline and decreased myo-inositol (Chavarria and Cordoba 2015), although this method is not commonly used clinically for the diagnosis of HE (Rose et al. 2020). Furthermore, as mentioned previously, stage 0 (minimal HE) is extremely difficult to detect since changes in memory, concentration and confusion are not always obvious to diagnose for a health care provider. Also, other sensitive tests can diagnose minimal HE. The most commonly used are psychometric tests and automated tests such as Inhibitory Control Test and Critical Flicker Frequency (Bajaj et al. 2008). These are tests of symbol connection, attention and accuracy that assess psychomotor impairment, attention deficit and impairment of executive functions (Weissenborn et al. 2001). The results are expressed as the number of standard deviations from a population matched on age and education level. In practice, these tests are not always easy to carry out because of the time they require (at least 30 minutes).

### 1.4.4 Treatments

Currently, the only curative treatment for patients with liver failure or disease is liver transplantation. Since more patients need a liver transplantation compared to the number of available livers, managing liver diseases complications remains the primary challenge. Moreover, there is no universally accepted standards for treatment and the challenge of finding the right treatment to reduce HE symptoms remains to be met. Most treatments are validated in the prevention of recurrence of HE episodes after an initial episode. There are fewer data available for the treatment of chronic HE to the acute phase or for the treatment of minimal HE. Therapeutic approaches for partially treating HE have focused a lot on reducing plasma ammonia levels implicated in HE pathogenesis either by decreasing its production or promoting its removal, thereby reducing the neurotoxins reaching the central nervous system.

Such treatments imply the usage of non-absorbable disaccharides such as lactulose, which modify the intestinal microbiota and ammonia production by lowering colonic transit time and increasing fecal excretion and which is nowadays the first line treatment in Europe and USA and has been reported to improve cognitive functions in patients with minimal HE (mHE) (Luo et al. 2011; Prasad et al. 2007). However, there is no significant effect reported on mortality (Sharma et al. 2011; Als-Nielsen, Gluud, and Gluud 2004). Lactulose is an effective therapy as a preventive treatment of mHE and clinic HE (Sharma et al. 2011); however, its use is limited because of the various side-effects of its administration such as bloating, diarrhea and nausea (Gitlin 2011).

Other therapeutic options for HE such as the antibiotic rifaximin or the administration of probiotics are also currently used and evaluated as specific or prophylactic treatment. Rifaximin is a gut-selective non–absorbable antibiotic. It has a broad spectrum of antibacterial activity, acting against Gram-positive and Gram-negative bacteria, both aerobes and anaerobes. The division of colonic bacteria responsible for urea deamination is therefore inhibited, reducing the production of gut ammonia and preventing absorption through the gastrointestinal tract ("Compendium" n.d.). In healthy subjects, systemic absorption appears to be low. It is probably slightly higher in cirrhotic patients with increased intestinal permeability, but few data are available (Hermann et al. 2018). Rifaximin is very well tolerated over the long term, and in combination with lactulose, rifaximin is effective in preventing the recurrence of clinical HE episodes and is associated with a decrease in the number and duration of HE hospitalizations, as well as a decrease in mortality and improved quality of life (Bass et al. 2010; Mullen et al. 2014).

More recently, treatments aiming to increase the outside brain ammonium detoxification, such as glycerol phenylbutyrate or L-ornithine-L-aspartate, have been proposed. Glycerol phenylbutyrate has been shown to be effective in secondary prevention in a randomized, placebo-controlled trial (Rockey et al. 2014). In addition, fecal transplantation recently showed encouraging results (Kao et al. 2016; Bajaj et al. 2017), and several additional studies are already planned.

### 1.4.5 Bile duct ligated rat, an animal model of chronic HE

Animal models of type C HE are necessary to improve the understanding of the mechanisms underlying HE and to better characterize the effects of the different treatments. Although an optimal animal model of type C HE does not currently exist, the bile duct-ligated (BDL) rat model is one of the few chronic HE models validated by the International Society for Hepatic Encephalopathy and Nitrogen Metabolism (ISHEN) (Butterworth et al. 2009). These rats undergo abdominal surgery where common bile duct is clipped in the middle between liver and duodenum. The bile is pushed back to the liver and its toxicity results in death or dysfunction of the liver cells, inducing a reproducible model of biliary cirrhosis in rats. It mimics the metabolic changes associated with cholestatic liver disease and related fibrosis: animals develop jaunice, hyperamonemia, portal hypertension, bacterial translocation and immune system dysfunction (Butterworth et al. 2009). BDL rats develop memory difficulties and decreased locomotor activities, showing low-grade encephalopathy (Chan et al. 2004).

# Chapter 2 Treatments in a rat model of type C HE: synergistic effect of probiotic Vivomixx® and antibiotic rifaximin

## Abstract

Chronic hepatic encephalopathy (HE) is a severe complication of chronic liver disease (CLD), and finding the right treatment to reduce HE episodes before liver transplant remains a challenge. Both rifaximin (non-absorbable antibiotic) and probiotics are currently used to reduce HE symptoms, but their precise effect on brain metabolites has never been studied. In the present study, our aims were to assess *in vivo* and longitudinally the effect of rifaximin alone and the combination of probiotics and rifaximin on bile duct ligated (BDL) rats in different brain regions; and to compare these results with non-treated BDL rats. *In vivo* $^{1}$H MRS at 9.4T combined with biochemical tests (plasma $NH_4^+$, bilirubin), microbiota analysis and behavioral test (open field) were performed on adult Wistar rats before BDL (week 0) and at weeks 2, 4, 6 and 8 after surgery. Evolution of metabolites was studied in the hippocampus and cerebellum. All rats displayed the characteristic rise in plasma bilirubin, regardless of treatment group, as well as a similar ammonium increase. However, the combination of probiotics and rifaximin was beneficial: the longitudinal changes of some brain metabolites concentration (Gln, Cr, Glu) were significantly less pronounced in the group of rats treated with rifaximin and probiotics compared to the two other groups. Also, bifidobacteria concentration was higher in the group treated with both probiotics and rifaximin group at week 8. Overall, we showed that the administration of rifaximin associated with this probiotic had more positive effects than rifaximin alone, as such both could be used to maintain a balanced microbiota and may provide opportunities for reducing the spread of antibiotic resistances.

This chapter was partially adapted from:

**E.Flatt**, V.A. McLin, O.Braissant, P.Mastromarino, R.Gruetter and C.Cudalbu, Do probiotics combined with rifaximin influence the neurometabolic changes in a rat model of type C HE?, Clinical and Translational Gastroenterology, submitted.

I contributed to the design of this study, data collection and processing, results interpretation and writing of the paper. Gut microbiota analysis were done in collaboration with Prof. Paola Mastromarino and the ammonium measurements in plasma samples were done in collaboration with Dr. Olivier Braissant.

## 2.1 Introduction

Chronic hepatic encephalopathy (CHE) is a neuropsychiatric disease affecting the brain caused by hepatic dysfunction secondary to chronic liver disease (CLD). Patients with hepatic encephalopathy (HE) suffer from intellectual impairment, personality changes, motor disturbances as well as depressed level of consciousness. Despite an enormous work aiming at characterizing the physiopathology of HE, the exact molecular mechanisms and their chronology remain unclear (Swaminathan, Ellul, and Cross 2018). CHE is characterized by neurometabolic changes, in particular an increase in brain glutamine due to cerebral ammonium removal by glutamine synthetase, causing osmotic stress and secondary disruption in astrocyte metabolism (Brusilow et al. 2010). It appears that this is only partially compensated by the gradual release of other brain metabolites (myo-inositol, taurine, total choline and creatine) from the cell (Braissant, McLin, and Cudalbu 2013; Häussinger 2006; Braissant et al. 2019) . While ammonium plays an indisputable and central role in the pathogenesis of HE, additional factors are known to contribute such as gut flora modifications, systemic inflammation, neuroinflammation and oxidative stress, all of which may precipitate the onset of HE (Shawcross et al. 2004; Ochoa-Sanchez and Rose 2018; Coltart, Tranah, and Shawcross 2013; Azhari and Swain 2018). Management of HE remains an important challenge because treatment options are limited. Therapeutic approaches for treating HE have focused on reducing plasma ammonium levels either by decreasing its production or promoting its removal.

In patients, such treatments imply the usage of non-absorbable disaccharides such as lactulose, which is accepted to improve cognitive function in patients with minimal HE (mHE), the covert premise of CHE (Luo et al. 2011; Prasad et al. 2007). While lactulose is an effective therapy for hepatic encephalopathy, it comes with side-effects including bloating, diarrhea and nausea, which limit its use (Gitlin 2011). Other therapeutic options currently being evaluated include the non-absorbable antibiotic rifaximin or the administration of probiotics. These therapies act on the modulation of gut flora, in line with the current evidence that gut flora is a major contributor to HE.

**Rifaximin** is a broad-spectrum non–absorbable antibiotic, commonly used to treat HE. It has a broad spectrum of antibacterial activity, acting against Gram-positive and Gram-negative bacteria, both aerobes and anaerobes. The division of colonic bacteria responsible for urea deamination is thereby inhibited, reducing the production of gut ammonium and preventing absorption through the gastrointestinal tract ("Compendium" n.d.). However, different mechanisms of action have been proposed to underlie the effects of rifaximin. Rifaximin may affect gut microbiota and

modulate inflammatory signals in one of three ways: either by promoting anti-inflammatory cytokines such as IL-10 (Jasmohan S. Bajaj et al. 2011), by reducing pro-inflammatory mediators (IL-6, TNF-α) (Kalambokis et al. 2012) or by reducing systemic endotoxin levels (Kalambokis and Tsianos 2012)—none of these clearly contribute to lowering ammonia absorption from the gastrointestinal tract. Nonetheless, rifaximin has been shown to improve cognition in patients with mHE (Jasmohan S. Bajaj 2018) and has been shown to prevent hospitalizations and the recurrence of overt HE episodes if combined with lactulose (Bass et al. 2010; Gitlin 2011). However, the combined administration of rifaximin with lactulose in many of these studies is an important limitation to assess the efficacy of the rifaximin alone (Hadjihambi et al. 2017) and the benefit of rifaximin could not be demonstrated for the most serious encephalopathies (Sogni, n.d.).

Animal models of CHE are necessary to improve the understanding of the effects of these treatments. Until now, very few studies evaluating the effect of rifaximin and/or probiotics have been performed in animal models of type C HE (Thabut et al. 2015). One recent study suggested that rifaximin (50mg/kg/day) did not reduce inflammation (TNF-α levels) and fibrosis in bile duct ligated (BDL) rats (Shin et al. 2017), but there is a lack of knowledge about how rifaximin administration impacts changes in brain metabolites concentration, which are frequently present in HE. Therefore, further studies are needed to characterize further the potential role and mechanisms of action of rifaximin in the setting type C HE (J. S. Bajaj 2016).

**Probiotics** modulate the gut bacterial flora by altering the microbial population and promoting non-ammoniogenic bacteria (Rowland et al. 2010). A probiotic formulation containing a mixture of eight strains (Vivomixx® in EU, Visbiome in USA®) has been recently shown to improve cognitive function and inflammatory response in patients with cirrhosis (Román et al. 2019). This probiotic formulation has also been associated with significant improvement in minimal HE symptoms in humans (Mittal et al. 2011), decreasing hospitalization rates and preventing HE episodes in patients with cirrhosis (Lunia et al. 2014). While the effect of probiotics was often similar to lactulose (Saab et al. 2016; Ding, Zhang, and Wang 2014; Pratap Mouli et al. 2015) they were better tolerated clinically. Further, it is important to emphasize that there is high variability among published studies in the strains of probiotics, daily dose or the duration of the administration of the probiotics, all of which might influence treatment efficacy. Regarding animal studies, D'Mello et al. reported that probiotics (formulation sold as VSL#3 until 2016, but now exclusively available under the brands Vivomixx® and Visbiome®) improved inflammation-associated sickness behavior in a mouse model of liver inflammation (D'Mello et al. 2015), while Lactobacillus rhamnosus GG

reduced liver fibrosis and hepatic gene expression of IL-6 in BDL rats (Hammes et al. 2017). However, to date, there are very few reports in animal models of type C HE.

Both the antibiotic rifaximin and probiotics have been evaluated through neurological testing in humans. They are currently used to reduce the symptoms of HE, but longitudinal studies assessing their effects on brain metabolism are lacking while the molecular mechanisms underpinning their effects are not fully understood (Swaminathan, Ellul, and Cross 2018). Therefore, we aimed to use the advantages of highly resolved $^{1}$H MRS to analyze longitudinally in an established model of type C HE the effect of the antibiotic rifaximin alone or in combination with the probiotic Vivomixx® on the brain metabolic profile in the hippocampus and cerebellum, as they are key regions involved in HE (Manto et al. 2012; Bahceci et al. 2005). We hypothesized that a lesser increase in brain glutamine would be measured in the treated animals compared to the non-treated ones, followed by a milder decrease in osmolytes and neurotransmitters. We also expected that probiotics and rifaximin would act synergistically to induce better outcomes than rifaximin alone. The present study evaluates for the first time the effect the antibiotic rifaximin and its use associated with a specific probiotic formulation on the neurometabolic changes both *in vivo* and longitudinally in a rat model of type C HE.

## 2.2 Material and methods

### 2.2.1 Study design

Adult male Wistar rats (150–175 g, Charles River Laboratories, L'Arbresle, France) underwent bile duct ligation (BDL), a model of type C chronic liver disease induced HE (Butterworth et al. 2009). Two groups of BDL rats were used. The first group was treated with rifaximin at human pharmacological doses ('rifaximin', n = 12, 15.7mg/kg/day). It was administered orally twice daily in the morning (8am) and in the evening (6pm) starting 2 weeks after BDL-surgery ('week 2'). The second group was treated with the same dose of rifaximin combined with the multi-strain probiotics mixture Vivomixx® (n = 9, 'rifaximin + probiotics', Vivomixx® in EU, Visbiome® in USA, 60 billion bacteria/kg of rat). Vivomixx® contains 8 lyophilized, highly viable bacterial strains: 4 lactobacilli (*Lactobacillus acidophilus* DSM24735®, *L. plantarum* DSM24730®, *L. paracasei* DSM24733®, *L. bulgaricus* DSM24734®), 3 bifidobacteria (*Bifidobacterium infantis* DSM24737®, *B. longum* DSM24736®, *B. breve* DSM24732®) and *Streptococcus thermophilus* DSM24731®). Probiotics administration started two weeks before BDL-surgery until the end of the study. In this group, rifaximin was administrated orally at 8 am and 3 pm, and probiotics was administered orally daily at 7 pm.

Starting from week 0 (before BDL surgery) and every two weeks thereafter, all rats underwent $^{1}$H MRS scan, blood sampling (sublingually), and feces collection for microbiology studies. Behavioral tests (open field test) were performed to evaluate motor activity as previously described (Braissant et al. 2019). The study design is summarized in Table 2.1.

Each animal served as its own control for all measurements. The treated groups were compared to our previously published groups of BDL non-treated rats (n = 29) and sham-operated rats (n = 18) (Braissant et al. 2019) for comparison of open field test and $^{1}$H MRS measurements in the hippocampus region. The treated groups were compared to another group of our BDL non-treated rats (n = 15) for comparison of $^{1}$H MRS measurements in the cerebellum region. Of note, as the groups of non-treated rats were composed of males only, male rats were used in this study in order to ensure comparable groups and the potential influence of sex on the results was not evaluated in the present study.

*Table 2.1 Longitudinal study design. The number of rats (n) measured in every group are indicated for each week and each type of measures: 'H' stands for MRS scan in the hippocampus and 'C' for MRS scan in the cerebellum, 'B' for the rats whose bifidobacteria in the feces were analysed, and 'O-F' for the rats who undergone open field test. Of note for blood sampling we used the same number of rats as for the MRS scan (data not included in the Table for readability).*

| Week -2 | Week 0 | Week 2 | Week 4 | Week 6 | Week 8 |
|---|---|---|---|---|---|
| • Stool collection<br>• Start of probiotics administration | • Blood sampling<br>• Stool collection<br>• MRS scan<br>• BDL surgery | • Blood sampling<br>• Stool collection<br>• MRS scan<br>• Start of Rifaximin administration | • Blood sampling<br>• Stool collection<br>• MRS scan<br>• Open field | • Blood sampling<br>• Stool collection<br>• MRS scan<br>• Open field | • Blood sampling<br>• Stool collection<br>• MRS scan<br>• Open field<br>• Sacrifice and organ collection |
| $n_{non\text{-}treated}$ | H:29 / C:15 / B:9 | H:10 / C:15 | H:26 / C:15 / B:9<br>O-F: 26 | H:22 / C:14<br>O-F:22 | H:22 / C:9 / B:4<br>O-F:5 |
| $n_{probiotics+rifaximin}$ | H:9 / C:9 / B:6 | H:9 / C:9 | H:9 / C:9 / B:6<br>O-F:9 | H:9 / C:9<br>O-F: 9 | H:8 / C:8 / B:5<br>O-F:7 |
| $n_{rifaximin}$ | H:12 / C:12 / B:10 | H:12 / C:12 | H:12 / C:12 / B:10<br>O-F:11 | H:11 / C:11<br>O-F:11 | H:8 / C:8 / B:8<br>O-F:8 |

### 2.2.2 Biological and clinical characteristics of the BDL rats

Plasma measurements of ammonium and total bilirubin (sub-lingual blood collection) were performed on a COBAS8000© analyzer (Roche, Switzerland). In order to test whether the fine motor deficits are present (characteristic of chronic HE), locomotor activity was assessed in the open field test as described previously (Braissant et al. 2019) at week 4, 6 and 8, before MRS scan. This test analyzes the rodent's exploratory behavior in a confined space and is mainly used to measure its motor functions. Open field test was performed at week 4, 6 and 8 after BDL surgery. The rat was placed in an open circular arena divided into three concentric virtual part of different

light intensities. Its behavior was recorded during 10 minutes. Different parameters were evaluated with the video tracking system (Noldus Ethovision software 11.5) such as distance moved (cm) and velocity. These parameters were calculated for the 10 minutes of the test.

### 2.2.3 *In vivo* $^{1}$H Magnetic Resonance Spectroscopy ($^{1}$H MRS)

*In vivo* $^{1}$H MRS was performed on a 9.4T MRI system (Varian/Magnex Scientific, Oxford, UK) interfaced to a Varian Direct Drive console (Palo Alto, CA, USA) using an inhouse-built 14 mm diameter quadrature $^{1}$H coil as a transceiver, as previously described (Braissant et al. 2019). Brain metabolites longitudinal evolution was studied in the hippocampus in a voxel of interest (VOI) of 2x2.8x2mm$^{3}$, implicated in cognitive deficits observed in chronic HE (Bahceci et al. 2005) and in cerebellum in a VOI of 2.5x2.5x2.5mm$^{3}$, for its important role in motor control (Manto et al. 2012) which is affected in chronic HE (Kharbanda, Saraswat, and Dhiman 2003), using the SPECIAL (Mlynárik et al. 2006) sequence (TE = 2.8ms, TR = 4000ms, 160 averages). Metabolite concentrations were estimated using LCModel combined with an in vitro metabolite basis set of metabolites and the spectrum of macromolecules measured *in vivo* (Cudalbu 2013). Unsuppressed water signal from the same VOI was used as internal reference for absolute metabolites quantification. The ultra-high magnetic field and ultra-short TE allow to detect and quantify *in vivo* 18 metabolites involved in osmoregulation, neurotransmission, energy or antioxidant metabolism: alanine (Ala), ascorbate (Asc), aspartate (Asp), glycerophosphocholine (GPC), phosphocholine (PCho), creatine (Cr), phosphocreatine (PCr), γ-aminobutyric acid (GABA), glucose (Glc), glutamine (Gln), glutamate (Glu), glutathione (GSH), myo-inositol (Ins), lactate (Lac), N-acetylaspartate (NAA), N-acetylaspartylglutamate (NAAG), phosphoethanolamine (PE), and taurine (Tau). Cramer-Rao lower bounds (CRLB) calculated from the LCModel were used as a reliability measure for the metabolite concentration estimate. Only metabolites with CRLB lower than 30 % were considered for further analysis.

During all the MRS/MRI procedures and biochemical measurements, animals were anesthetized using 1.5–2 % of isoflurane in 50 % air / 50 % oxygen. Respiration rate was maintained at 60–70 breaths/min and body temperature at 37.5–38.5 °C. Animals had unrestricted access to standard rat food and water for the duration of study. All procedures were approved by the Committee on Animal Experimentation for the canton of Vaud, Switzerland (authorization 2812).

### 2.2.4 Bifidobacteria measurements

Feces were collected at week 0, 4 and 8 to measure bifidobacteria concentration. Real-time PCR was used to quantify bifidobacteria and lactobacilli using genus-specific primers as described previously (Mastromarino et al. 2014). These measurements were performed in collaboration with Prof. Mastromarino.

### 2.2.5 Statistical analysis

All results are presented as mean ± SD and % increase/decrease compared to week 0. One-way ANOVA (Prism 5.03, Graphpad, La Jolla CA USA) with respect to each metabolite in the neurochemical profile followed by Bonferroni's multi-comparisons post-test was used within a single group.

Two-way ANOVA (Prism 5.03, Graphpad, La Jolla CA USA) followed by the Bonferroni's multi comparisons post-test was used to assess significance ($p<0.05$) in bifidobacteria, distance moved, brain and plasma metabolite's changes between the groups ('treatment' factor). As variations in metabolite concentrations between groups may appear as early as week 0, our analysis is based on the results of the two-way ANOVA on metabolites changes both in absolute value and relative to week 0. All tests were 2-tailed. In addition, for metabolites with a significant difference between groups ('treatment' factor) both in absolute concentration and relative to week 0, additional two-way ANOVA tests were performed by comparing the 'non-treated' group and each of these two groups individually. This was done to eliminate the potential influence of the differences between the 'rifaximin' group and the 'rifaximin + probiotics' group.

Pearson correlation analysis was performed on longitudinally acquired data to test for correlations between brain metabolites and plasma values.

### 2.2.6 Sample size calculation

Our study consists of evaluating a continuous response variable (metabolite concentration) from independent controls (non-treated) and experimental (treated) subjects. In our first preliminary study, the SD was ≈ 1.2 mmol/kg ww for Gln concentration at week 8, a key metabolite in HE. To be able to detect a difference in brain Gln concentration of 20 % at week 8 between the groups, which is what we expected considering our preliminary study (Flatt et al. 2017), we needed to include at least n = 8 treated and n = 13 non-treated rats to be able to reject the null hypothesis that the population means of the treated and non-treated groups are equal with probability

(power) of 0.8 ("PowerSampleSize < Main < Vanderbilt Biostatistics Wiki" n.d.). The type I error associated with this test of null hypothesis is 0.05. The number of BDL rats in each group were chosen accordingly.

## 2.3 Results

To characterize the biological and clinical features of the BDL rats we measured plasma bilirubin levels, whose increase was present in the three groups of rats without significant difference between groups, confirming the presence of CLD-induced HE (Figure 2.1A). All rats displayed a similar ammonium increase regardless of the group (Figure 2.1B). During the open field test, the distance traveled decreased from week 4 to week 8 in all groups of BDL rats and was significantly shorter than the sham-operated animals. No significant differences were observed between the three BDL groups throughout of the study (Figure 2.1D). Regarding the time spent in the wall-zone, centre-zone and inter-zone, and latency to enter centre-zone, we found no difference between the groups, suggesting animal anxiety was not a variable.

There were significant differences in the longitudinal evolution of the amount of bifidobacteria in feces between the three groups ($p = 0.03$, Figure 2.1C). The difference was particularly pronounced at week 8 where the amount of bifidobacteria in the 'rifaximin + probiotics' group was on average twelve times higher compared to 'non-treated' group.

We further noted that the general condition of the rats in the 'rifaximin + probiotics' group was overall better than in the 'rifaximin' group, as reflected by the fact that only one rat reached the humane endpoint (euthanasia) in this group before the eight weeks of the study compared to four rats in the 'rifaximin' group (Figure 2.1E). Of note, the 'non-treated' BDL rats come from a previously published study (Braissant et al. 2019) where no such assessment was performed since some of the rats were sacrificed before reaching the humane endpoint for additional measures.

To assess the neurometabolic consequences of BDL we performed in vivo $^{1}$H Magnetic Resonance Spectroscopy ($^{1}$H MRS) at 9.4 Tesla. The high quality of the spectra throughout the study allowed the separation of Gln from Glu and thus quantification of 16 brain metabolites (Figure 2.2). All the groups exhibited a significant increase of brain Gln due to ammonia detoxification, and a subsequent reduction of other brain osmolytes (Ins, Tau, tCho), as well as antioxidants and neurotransmitters.

Brain Gln significantly increased in all three groups both in the hippocampus and the cerebellum (Figure 2.3). However, $^{1}$H MRS revealed significant differences in longitudinal Gln changes between

the ‘rifaximin + probiotics’, the ‘rifaximin’ and the ‘non-treated’ rats: Gln increase was significantly lower in the ‘rifaximin + probiotics’ group at week 2, 4, 6, and 8 in the hippocampus compared to the ‘non-treated’ group, both in absolute value and relative to week 0 (+99 % in the ‘rifaximin + probiotics’ group vs +136 % in the ‘non treated’ group at week 8, Figure 2.3A and Table 2.2). Similarly, in the cerebellum region, the ‘rifaximin + probiotics’ rats showed a lower rise in brain Gln at early stage of HE compared to ‘non-treated’ rats (+26 % in the ‘rifaximin + probiotics’ group vs +66 % in the ‘non treated’ group at week 4, Figure 2.3B) with the differences observed between groups being significant both in absolute value and relative to week 0 (Table 2.2). However, no significant differences were observed between ‘rifaximin’ rats and the ‘non-treated’ rats.

Furthermore, brain Gln in the hippocampus correlated positively with blood ammonium in the ‘rifaximin + probiotics’ group ($r = 0.85$, $p<10^{-3}$, Figure 2.3C) while the correlation did not reach significance in the ‘rifaximin’ group ($r = 0.27$, $p = 0.056$, Figure 2.3C). The correlations between cerebellar Gln and ammonium measured were similar to those observed in the hippocampus ($r = 0.83$, $p<10^{-3}$ in the ‘rifaximin + probiotics’ group; $r = 0.26$, $p = 0.081$ in the ‘rifaximin’ group). Interestingly, in both treated groups the distance moved in the open field test correlated negatively with Gln in the cerebellum, an important region implicated in motor control ($r = -0.51$, $p = 0.009$ in the ‘rifaximin + probiotics’ group; $r = -0.65$, $p = 0.0001$ in the ‘rifaximin’ group, Figure 2.6).

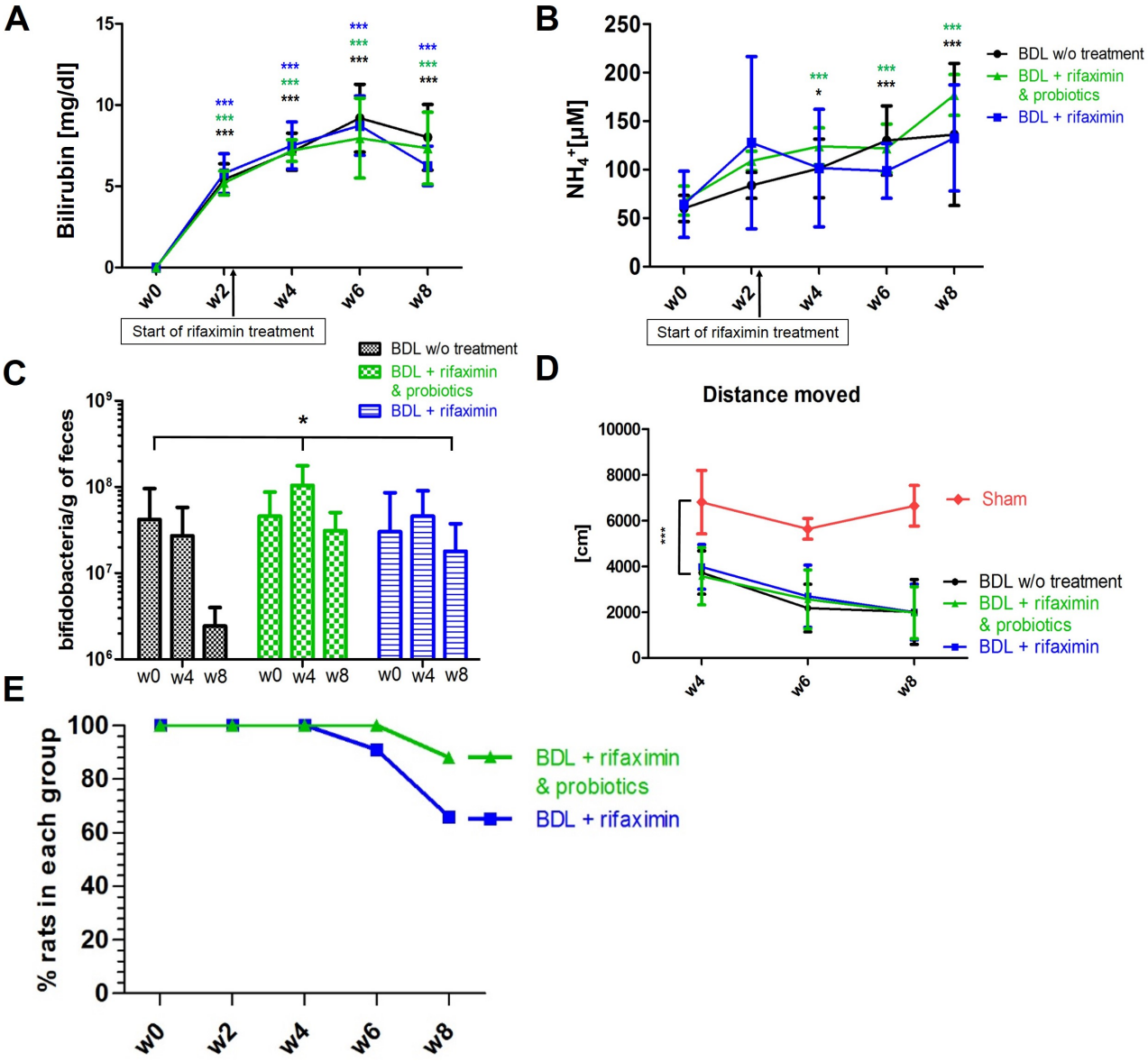


*Figure 2.1 Longitudinal changes in plasma total bilirubin (A) and $NH_4^+$ (B) in the three groups. (C) Bifidobacteria concentration in feces in the three BDL groups. (D) Distance traveled by the three groups of BDL and sham-operated rats. (E) Percentage of BDL rats at each week in the 'rifaximin + probiotics' group and in the 'rifaximin' group. One-way ANOVA was used to assess the significance intra-group (A,B) and two-way ANOVA to assess significance between-groups ('treatment' factor; C,D). Statistical significance: * $p < 0.05$; ** $p < 0.01$; *** $p < 0.001$.*

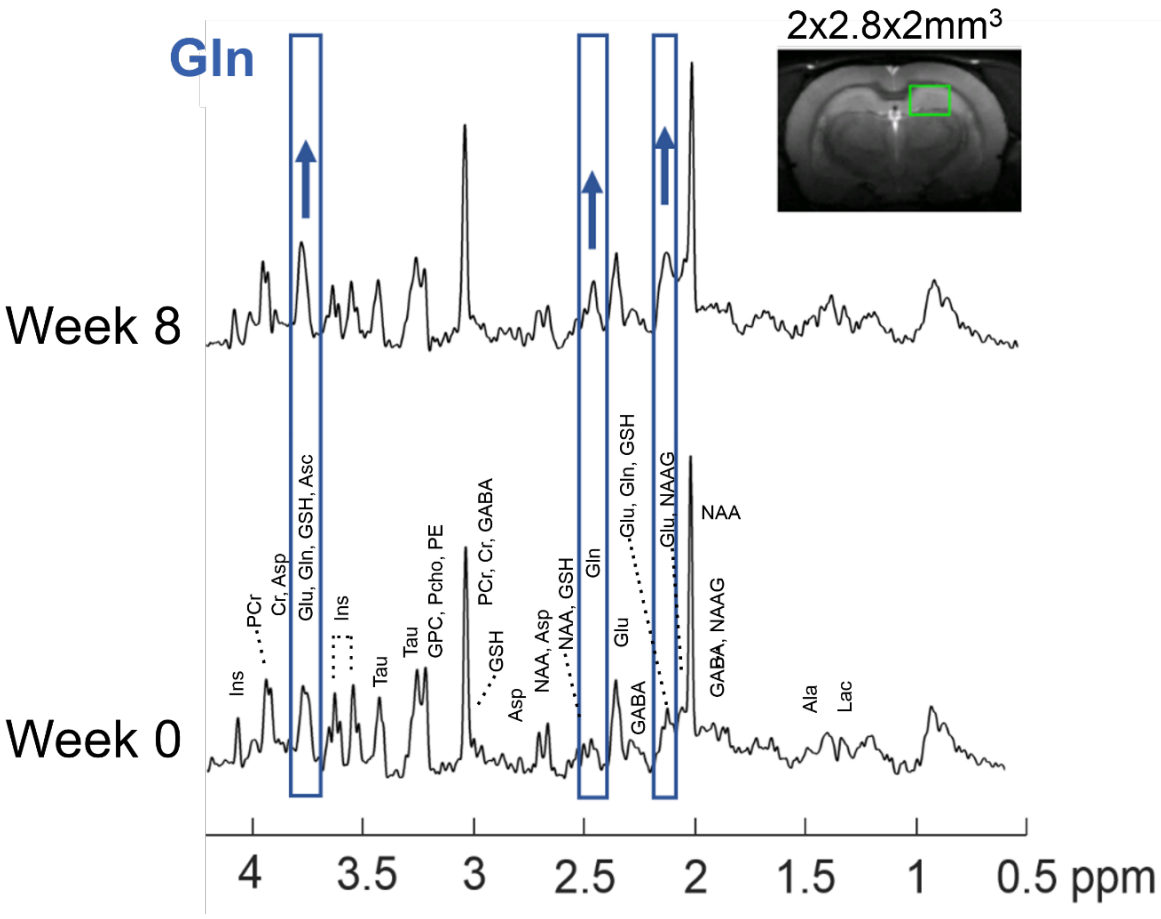


*Figure 2.2 Representative $^{1}H$ MRS spectra in the hippocampus of a 'BDL + rifaximin & probiotics' rat at week 0 and week 8 after BDL. Part of the spectra corresponding to Gln are shown in blue, which visibly increased from week 0 to week 8. The green rectangle shows the region considered in the hippocampus on the $T_2$ weighted axial image of the rat brain.*

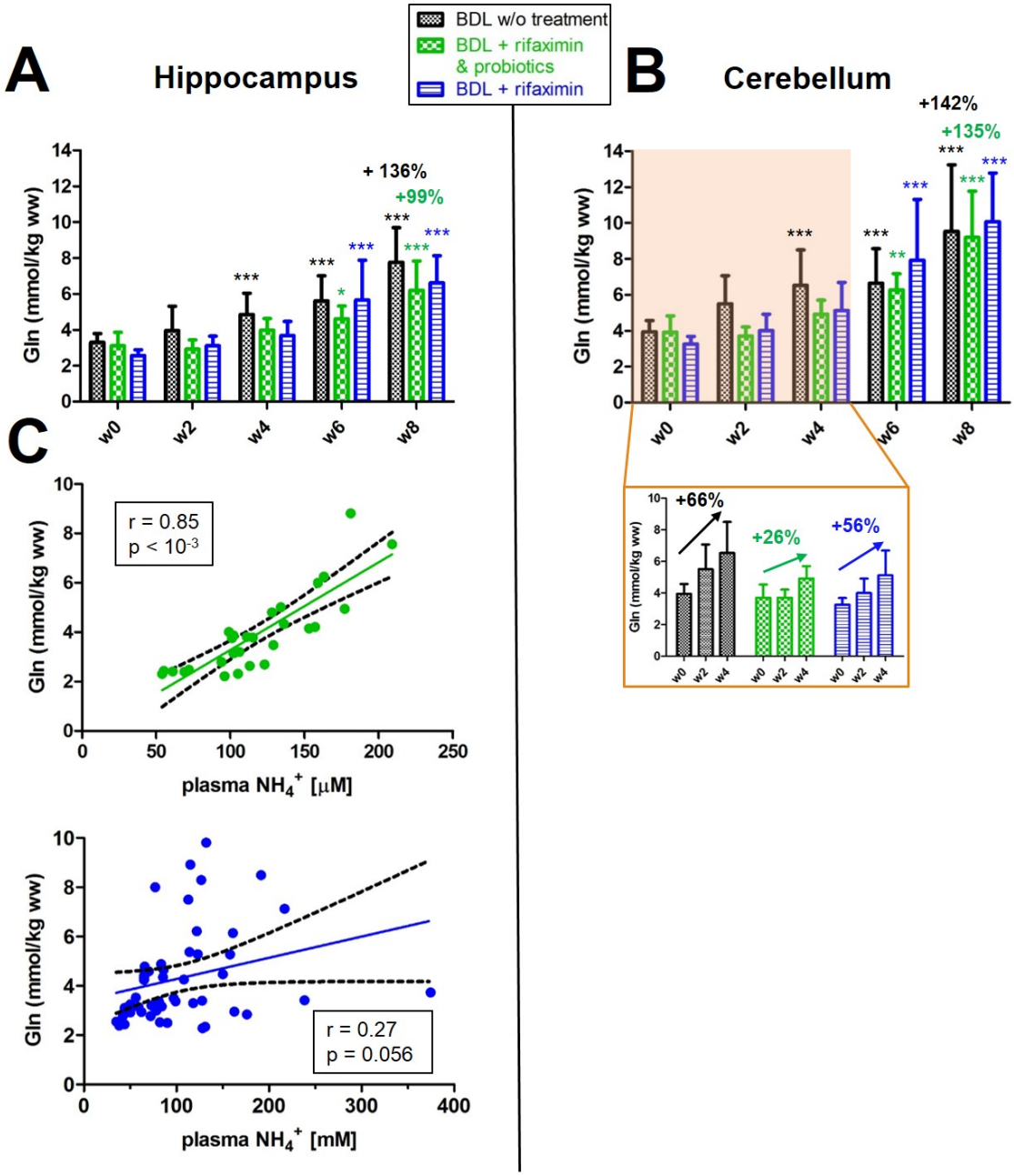


*Figure 2.3 Brain Gln evolution in the hippocampus (A) and in the cerebellum (B) from week 0 to week 8 in the three groups. Statistical significance intra-group reported: one-way ANOVA (* p < 0.05; ** p < 0.01; *** p < 0.001). The relative increases shown are relative to week 0. (C) Correlation between brain Gln in the hippocampus and plasma ammonium in rats treated with the combination of rifaximin and probiotics (green) and in rats treated with rifaximin only (blue).*

The decrease of the osmolyte Ins was significant in all groups in both hippocampus and in cerebellum but was less marked in the 'rifaximin + probiotics' group compared to two the other groups at week 6 and at week 8, both in absolute value and relative to week 0 (-10 % in the 'rifaximin + probiotics' group vs -15 % in the 'non treated' group at week 6, Figure 2.4).

Among the other brain organic osmolytes, no significant differences were observed between the groups in the decrease of Tau, an important osmolyte preferentially concentrated in neurons (Brand, Richter-Landsberg, and Leibfritz 1993), neither in the hippocampus nor in the cerebellum. Similarly, no difference was found in cerebral tCho decrease between groups (Figure 2.4 & Figure 2.5).

Cr, a metabolite known for its role in energy metabolism and reported to be involved in neuroprotection and osmoregulation (Rae 2014; Braissant 2010) showed a decrease in the hippocampus in the three groups without any significant difference between groups. However, in the cerebellum, Cr concentration was nearly stable over time in the 'probiotics + rifaximin' group (-4 % at week 8, Figure 2.5) while its decrease was stronger in the two other groups (-11 % in the 'rifaximin' group vs -15 % in the 'non-treated' group at week 8, Figure 2.5). These differences between the groups were significant both in absolute and relative value (Figure 2.5 and Table 2.2). Although not reaching significance, there was a trend toward lesser reduction of tCr in the 'rifaximin + probiotics' group compared to the 'non-treated' group both in the hippocampus (-2 % vs -6 % at week 6) and in cerebellum (-4 % vs -10 % at week 6).

Among the neurotransmitter-related metabolites, Glu decrease was less marked in the 'rifaximin + probiotics' group and in the 'rifaximin' groups compared to the 'non-treated' group in both hippocampus (-4 % in the 'rifaximin + probiotics' group vs -8 % in the 'non-treated' group at week 6, Figure 2.4) and cerebellum (-2 % in the 'rifaximin + probiotics' group vs -15 % in the 'non-treated' group at week 6, Figure 2.5). Interestingly, these differences between groups were significant only in the cerebellum (Table 2.2). Asp decreased similarly between groups without reaching significance (Figure 2.4).

When considering antioxidants measurable by $^{1}$H MRS, the Asc decrease was slightly less marked in the two treated groups while no significant changes were observed for GSH. Lac, a metabolite involved in CNS energy metabolism, exhibited a slight tendency to increase in the three groups in the hippocampus, but none of these changes reached significance. In the cerebellum, however, the Lac increase was more substantial and significant at week 8 in all groups (+80 %, +109 %, + 92 % at week 8 in the 'non-treated', 'rifaximin + probiotics', 'rifaximin' groups respectively) but did not significantly vary between the groups (Figure 2.4, Figure 2.5 and Table 2.2). GABA, PE, NAA, NAAG nor tNAA did not change significantly during the course of the study in any of the groups or brain region.

We also measured the correlations between Gln, for its central role in the development of HE, and other neurometabolites to assess inter-metabolite dependencies in treated BDL rats. Overall, with each of the two treatments, the hippocampal Gln increase was strongly correlated with the decrease in Ins ($p<0.001$ for both groups) and with the decrease in tCho ($p<0.001$ for both groups). We found also a negative correlation between Gln and Glu, which was more marked in the 'rifaximin + probiotics' group ($r = -0.36$, $p = 0.017$) compared to the 'rifaximin' group ($r = -0.29$, $p = 0.027$). In the cerebellum region, in both treated groups Gln also correlated negatively with Ins ($p<0.001$ in both groups), tCho ($p<0.01$ in both groups). Gln correlated negatively with Glu in the 'probiotics + rifaximin' group only ($p<0.01$). Unlike the hippocampal region, a strong correlation was measured with Tau ($p<0.001$ in both groups).

Furthermore, for metabolites with a significant difference between groups ('treatment' factor) both in absolute concentration and relative to week 0 (Gln, Cr, Glu, Table 2.2) as well as for bifidobacteria (Figure 2.1C), we performed an additional two-way ANOVA test to compare only the 'non-treated' group and the 'rifaximin + probiotics' group. The differences between the groups were all significant: Gln hippocampus, $p < 0.001$; Gln cerebellum, $p < 0.05$; Glu cerebellum, $p < 0.05$; Cr cerebellum, $p < 0.01$; bifidobacteria, $p < 0.05$.

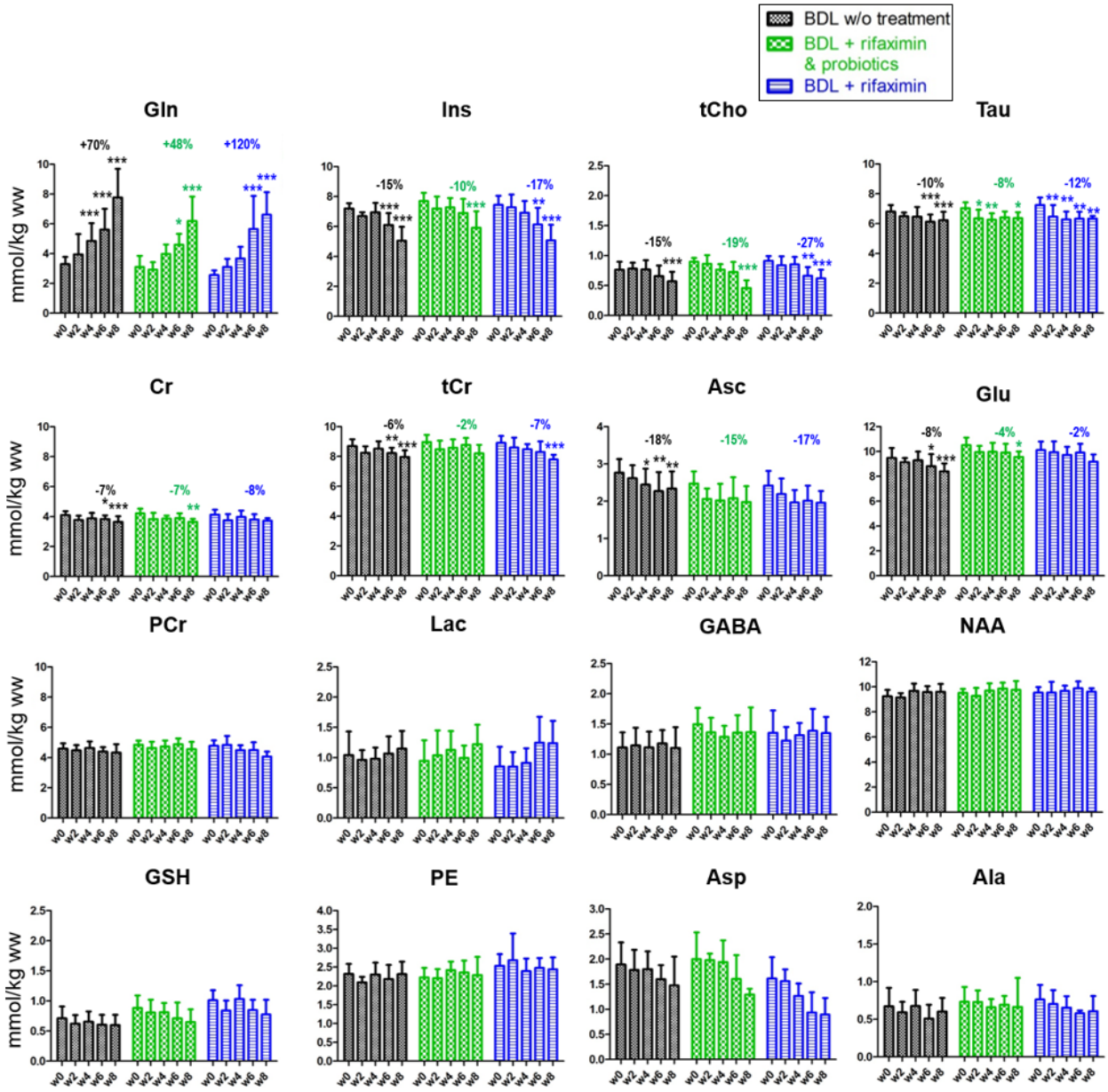


*Figure 2.4 Longitudinal $^{1}H$ MRS data of brain metabolites in the hippocampus region of the 'rifaximin' treated group, the 'rifaximin + probiotics' treated group and the group without treatment. Relative changes indicated in the graph at week 6 are calculated relative to week 0 and are indicated for metabolites whose concentrations significantly varied over time. Statistical significance: one-way ANOVA (* $p < 0.05$; ** $p < 0.01$; *** $p < 0.001$).*

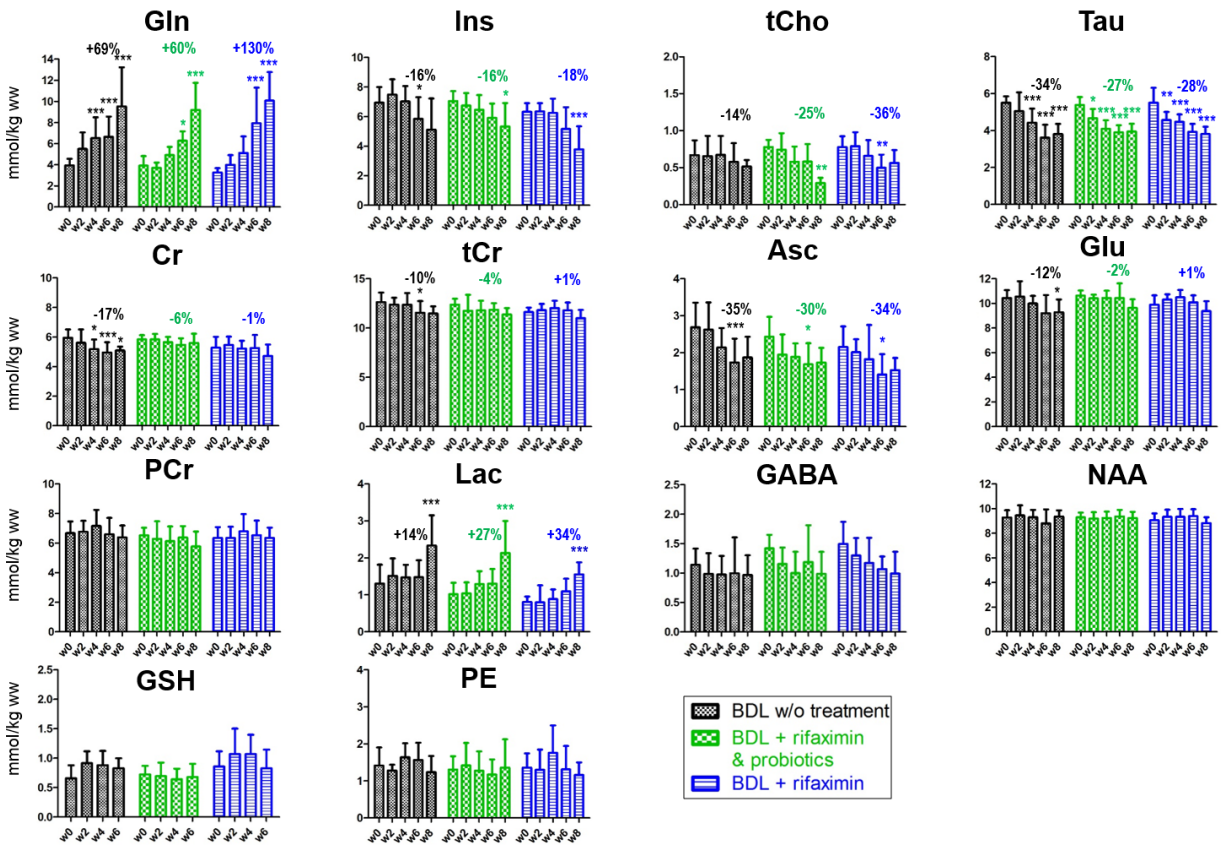


*Figure 2.5 Longitudinal $^{1}H$ MRS data of the brain metabolites in the cerebellum region of the 'rifaximin' treated group, the 'rifaximin + probiotics' treated group and the group without treatment. Relative changes indicated in the graph at week 6 are calculated relative to week 0 and are indicated for metabolites whose concentrations significantly varied over time. Statistical significance: one-way ANOVA (* $p < 0.05$; ** $p < 0.01$; *** $p < 0.001$).*

*Note that in the cerebellum many concentrations estimated with LCModel of Asp and Ala were excluded due to their unreliability. As this made difficult to interpret the variations of these metabolites, their evolutions are not shown. GSH at week 8 is not shown for the same reason.*

*Table 2.2 Summary of statistical significance of the two-way ANOVA for 'treatment' factor (i.e 'rifaximin', 'rifaximin + probiotics', 'non-treated') for each metabolites whose concentrations significantly varied over time, both in absolute concentrations and relative to week 0 in hippocampus and cerebellum. Metabolites which significantly differ between the groups both in absolute and relative values are highlighted in red. Of note, the interaction was not significant for any of the metabolites. The relative increase reported are relative to week 0. Statistical significance:* p < 0.05; ** p < 0.01; *** p < 0.001.*

| Two way ANOVA - significance for 'treatment' factor | Hippocampus | | Cerebellum | |
|---|---|---|---|---|
| | Absolute concentrations | Relative to week 0 | Absolute concentrations | Relative to week 0 |
| Gln | *** | ** | * | * |
| Ins | *** | ns | *** | ns |
| tCho | * | ns | ns | ns |
| Tau | ns | ns | ns | ns |
| Cr | ns | ns | ** | * |
| tCr | * | ns | ns | ns |
| Lac | ns | ns | *** | ns |
| Glu | *** | ns | * | ** |
| Asc | *** | ns | ns | ns |

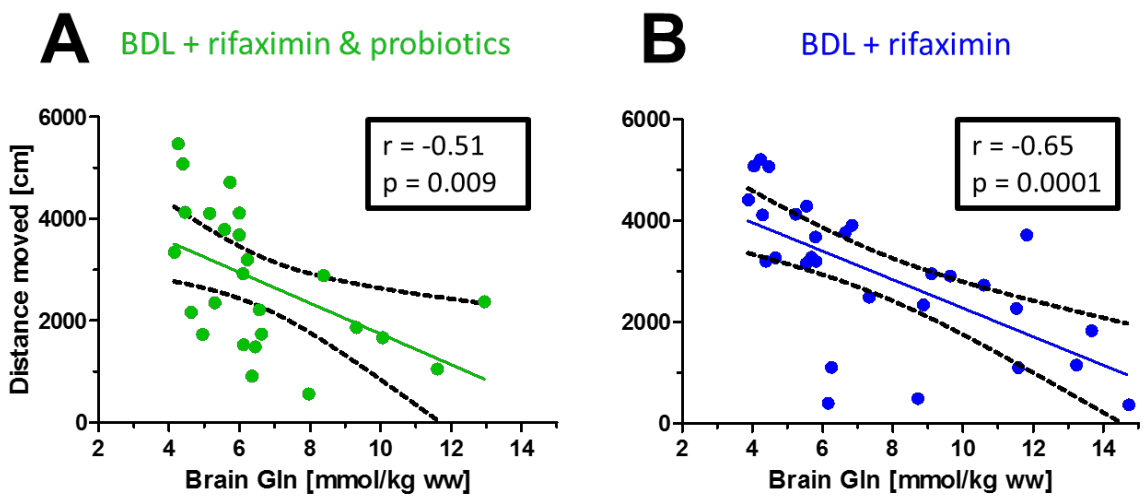


*Figure 2.6 Correlation between brain Gln in the cerebellum and the distance moved in the open field test in BDL rats treated with the combination of rifaximin and probiotics (A) and in BDL rats treated with rifaximin only (B).*

## 2.4 Discussion

The present study reports for the first time the positive effect of combined rifaximin and the probiotic Vivomixx® on the neurometabolic changes *in vivo* and longitudinally in a rat model of type C HE. The characteristic longitudinal increase of Gln and decrease of Glu, known to characterize HE, and the recently reported decreased in Cr, were significantly less pronounced in rats treated with rifaximin and probiotics compared to the two other groups.

In each group, the pattern characteristic of chronic HE was observed by $^{1}$H MRS longitudinal measurements and was also noticeable from the spectra (Figure 2.2). We measured in all three groups a gradual increase of brain Gln followed by a gradual decrease in Ins and other osmolytes, such as Tau and Cr. These observations are in agreement with previously published studies in BDL rats and CLD patients (Córdoba et al. 2001; Rackayova et al. 2016; Braissant et al. 2019) and confirm the already well-known partial compensatory effect to maintain osmotic balance in the presence of Gln accumulation.

The measured plasma bilirubin values as well as the lack of significant changes in treated animals are in agreement with a recently published study on BDL rats treated with probiotics (Hammes et al. 2017). We observed a significant increase in plasma ammonium in all groups to a level similar to that reported in other studies using BDL rats (Aamann et al. 2019), with a high intra-group variability. No significant differences were observed between groups, despite the administration of rifaximin combined with probiotics or rifaximin alone, whose purported role is to reduce the production of gut ammonium. However, the effect of rifaximin on plasma ammonium levels is still disputed, and some studies reported that its use had no significant effect on plasma ammonium levels either in BDL rats (Thabut et al. 2015) or in humans (Jasmohan S. Bajaj et al. 2011). In contrast, some studies reported a reduction in blood ammonium after the treatment (Pedretti et al. 1991; Festi et al. 1993; Paik et al. 2005), but it is now generally considered that despite the irrefutable and central role of ammonium in the pathogenesis of HE, its plasma levels display large inter-individual variability and are not always useful to predict the severity of HE or to assess the response to therapy, especially in chronic HE (Nicolao et al. 2003; Felipo and Butterworth 2002; Aldridge, Tranah, and Shawcross 2015; Mallet et al. 2018). Given these aforementioned elements and the challenges related with the ammonium measurements, additional multi-modal methods must be used and combined to accurately assess the effect of different therapeutic options in chronic HE, as put forth in the present study.

The Gln increase was significantly less pronounced in the 'rifaximin + probiotics' group at weeks 4, 6 and 8 compared to the two other groups. Therefore the significantly lower decrease of brain Glu in the 'rifaximin + probiotics' group suggests that the reduction in brain Glu is mainly the result of ammonium detoxification through glutamine synthetase, which catalyzes the formation of glutamine from ammonium and glutamate in astrocytes (Cooper and Plum 1987). The significant correlation between Gln and Glu (in all of the three groups) is consistent with this hypothesis. In addition, the correlations found between hippocampal Gln, Ins, Tau and plasma $NH_4^+$ are in agreement with the previously published results in non-treated BDL rats (Braissant et al. 2019).

While Glu showed a significantly less pronounced decrease in the 'rifaximin + probiotics' group, Asp, a selective NMDA receptor agonist, showed a similar trend of decreasing concentration in all groups, although not significant (Figure 2.4). Even if the role of Asp as an excitatory neurotransmitter is still debated, its decrease might be linked to alteration in the neurotransmission system, which is known to play an essential role in the pathophysiology of HE even though the precise mechanisms are not yet fully identified (Felipo 2013). In addition, no significant changes in the inhibitory neurotransmitter GABA concentrations were observed in all groups, consistent with our previous studies in non-treated BDL rats (Braissant et al. 2019).

A smaller decrease of Cr, tCr and Ins was measured in the 'rifaximin + probiotics' group, consistent with the fact that following the osmotic imbalance created by the increased Gln, the decreases of these different osmolytes are compensatory mechanisms to maintain osmotic balance. These smaller variations of Cr and tCr, metabolites also involved in energy metabolism, suggest a lower osmotic imbalance and possibly improvement of the energy metabolism in the 'rifaximin + probiotics' group.

Regarding microbiota, rifaximin alone did not significantly alter bifidobacteria concentration in feces. This is in keeping with previous findings reporting no significant change in microbial composition after rifaximin administration in humans (DuPont et al. 2005; Ridlon et al. 2013) and stating that the potential positive effects of the treatment result most likely from a beneficial modulation of the gut microbiota metabolic profile rather than from a significant rearrangement of the intestinal microbial community (Ponziani et al. 2015; Jasmohan S. Bajaj et al. 2013). The probiotics used in our study resulted in a significantly higher bifidobacteria concentration at week 4 and week 8 in the intestines of rats treated with rifaximin combined with probiotics compared to the two other groups. These modifications may have decreased the production and absorption of ammonium, as reported in various studies in humans (Sharma et al. 2008; Pratap Mouli et al. 2015; Pereg et al. 2011) and might explain the lower brain Gln measured in this group. These

results are consistent with a previous preliminary study showing an increase of bifidobacteria in gut microbiota in BDL rats treated with probiotics only (Rackayova et al. 2017). Nonetheless, further investigation is warranted as only three time points were assessed (weeks 0, 4 and 8) and only a limited number of samples were analyzed in the present study.

Alterations in gut microbiota composition and function in CLD contribute to the systemic inflammation and accumulation of gut-derived toxins. As both rifaximin and probiotics influence systemic inflammation (J. S. Bajaj 2016; Stadlbauer et al. 2008), the longitudinal assessment of inflammatory markers in the blood (TNF-α, CRP, WBC counts) and markers of neuroinflammation remains to be performed.

Of note, different elements motivated the design of this study: first, various studies suggested that probiotics improve antibiotic therapy as they possess immunomodulatory properties, promote the recovery of commensal microbiota and increase treatment tolerability (Reid 2006; Boyanova and Mitov 2012). To date, the evidence is unclear as to the best time to take probiotics. For now, patients are advised to take probiotics before, at the same time as, or even after taking antibiotics. Second, one purpose of the present study was to have two comparable groups. Therefore, modulation of the gut flora started two weeks before BDL surgery in the 'rifaximin + probiotics' group and rifaximin was administered at the same dosage per day in both treated groups ('rifaximin' and 'rifaximin + probiotics'). In the 'rifaximin + probiotics' group, the timing of administration was chosen in order to minimize the direct interaction between the two treatments in the gastrointestinal tract. These strategies used in our experimental design may have affected the magnitude of the results and evaluating the effect of rifaximin and probiotics administered under a different protocol remains to be further investigated.

Overall, while rifaximin alone at this specific dose appeared to induce no significant effect on the neurometabolic profile compared to non-treated BDL rats, its association with probiotics resulted in more attenuated neurometabolic alterations in BDL rats followed longitudinally. Our results on rifaximin alone are consistent with a recent study that explored the effects of rifaximin in BDL rats, where the authors concluded that rifaximin at this specific dose did not show efficacy in the treatment of HE (Petrazzo 2020). These observations leads us to consider that the positive effects observed are mainly due to this specific probiotic formulation, which has shown to help to recover intestinal barrier, decrease inflammation (Nava and Stappenbeck 2011) and decrease the production of bacterial toxins in humans (Rowland et al. 2010). Our results are consistent with our findings showing a beneficial effect of probiotics alone in BDL rats (Rackayova et al. 2017).

We conclude that in BDL rats rifaximin treatment combined with probiotics administration can be associated with positive effects on brain Gln, Glu and Cr levels in a model of type C HE. The clinical implications of these findings are essential given that both rifaximin and some probiotics are used in the treatment of HE.

# Chapter 3 Antibiotic rifaximin at different doses for treatment of chronic liver disease-induced HE: a longitudinal *in vivo* $^{1}$H MRS study of brain metabolism in bile duct-ligated rat model

## Abstract

Rifaximin is a commonly-used antibiotic to treat hepatic encephalopathy (HE), a complex neuropsychiatric syndrome caused by hepatic dysfunction. Rifaximin aims at reducing the production of gut ammonia, an important toxin in HE pathogenesis. In Chapter 2, we showed that rifaximin at the recommended human dose induced overall no significant effect on the neurometabolic profile compared to non-treated BDL rats, and that it may help reduce brain Gln levels only in early stages of HE. These findings raised the question of the efficacy of the dose used, therefore we hypothesized that the effect of rifaximin on neurometabolic profile is dose-related. To test this hypothesis, the effects of a higher dose of rifaximin (6.2x human dose, resulting from the conversion from human dose to rat (Nair and Jacob 2016)) were assessed. We used the advantages of highly resolved $^{1}$H MRS at 9.4 T combined with plasma measurements ($NH_4^+$, bilirubin) and behavioral test (open field) to analyze longitudinally the effect of the antibiotic rifaximin at a higher dose on the brain metabolic profile in the hippocampus in BDL rats. Results were compared with non-treated rats and human-dose treated rats (15.7 mg/kg/day). While rifaximin at human dose appeared to have an effect only at the early stages of the disease, a higher dose resulted in lesser alterations in the concentrations of some brain metabolites (Gln, Glu, tCr). However, and importantly, BDL rats treated with a higher dose of rifaximin moved significantly less than the two other groups. We also noted that the general condition of these rats was overall worse than the rats treated with human dose of rifaximin. It is therefore possible that such a high dose of antibiotics also leads to some undesirable side-effects such as electrolyte abnormalities or inherent drug toxicity.

This chapter was partially adapted from:

**E.Flatt**, V.A. McLin, O.Braissant, R.Gruetter and C.Cudalbu, Antibiotic rifaximin at different doses for treatment of chronic liver disease-induced HE: a longitudinal in vivo $^{1}$H MRS study of brain metabolism in bile duct-ligated rat model, manuscript in preparation.

I contributed to the design of this study, collected and processed the data, interpreted the results and wrote the paper.

## 3.1 Introduction

Hepatic encephalopathy (HE) is a complex neuropsychiatric syndrome caused by hepatic dysfunction. Currently, the only curative treatment for patients with liver failure or disease is liver transplantation. Since more patients need a liver transplantation compared to the number of available livers, managing liver diseases complications remains the primary challenge. Moreover, there is no universally accepted standards for treatment and the challenge of finding the right treatment to reduce HE symptoms remains to be met.

Rifaximin is a gut-selective non–absorbable antibiotic, commonly used to treat HE. It has a broad spectrum of antibacterial activity, acting against Gram-positive and Gram-negative bacteria, both aerobes and anaerobes. As detailed in Chapter 2, the molecular mechanisms behind the effect of rifaximin are still not clear and the lack of placebo group in many of the studies using rifaximin is an important limitation to assess its efficacy alone (Hadjihambi et al. 2017). Studies are needed to characterize further the potential role and mechanisms of action of rifaximin in the setting of cirrhosis and hepatic encephalopathy (J. S. Bajaj 2016).

In Chapter 2, we showed that rifaximin at human dose may help reduce brain Gln levels only in early stages of HE but no difference between treated or non-treated rats was observed from week 6 post-BDL (Flatt et al. 2017; 2019). These findings raised the question of the efficacy of the dose used, therefore we hypothesized that the effect of rifaximin on neurometabolic profile is dose-related. To test this hypothesis, the effects of a higher dose of rifaximin (6.2x human dose) were assessed. This 6.2 factor results from the conversion from human dose to rat and takes into account not only the body weight, but also the body surface area and pharmacokinetics (Nair and Jacob 2016)). We used the advantages of highly resolved $^{1}$H MRS to analyze longitudinally the effect of the antibiotic rifaximin at a higher dose on the brain metabolic profile in the hippocampus in an established rat model of type C HE.

## 3.2 Material and methods

### 3.2.1 Study design

Adult male Wistar rats (150–175 g, Charles River Laboratories, L'Arbresle, France) underwent bile duct ligation (BDL). A group of 8 BDL rats were treated with rifaximin at 6.2x human dose, resulting from the conversion from human dose to rat ('Rifaximin 6x human dose' = 'high-dose rifaximin' = 97.3 mg/kg/day, n = 8) (Nair and Jacob 2016)). $^{1}$H MRS was performed in hippocampus region,

implicated in cognitive deficits observed in chronic HE. Rifaximin was administered orally twice daily at 8 am and 6 pm starting 2 weeks after BDL-surgery ('week 2').

Starting from week 0 (before BDL surgery) and every two weeks thereafter, all rats underwent $^{1}H$ MRS scan and sublingually blood sampling. Behavioral tests were also performed in order to evaluate motor activity at week 4, 6 and 8, before MRS scan. The longitudinal study design is summarized in Table 3.1. Each animal served as its own control for all measurements.

The results were compared to a group of 12 BDL rats treated with rifaximin at human pharmacological doses ('Rifaximin human dose' = 15.7mg/kg/day) presented in Chapter 2, and to a group of BDL non-treated rats (n=17) scanned in the same period of time (Simicic et al. 2019; Braissant et al. 2019). Of note, as the group of non-treated rats is composed of males only, male rats were used in this study in order to get rid of the potential influence of sex on the results.

*Table 3.1 Longitudinal study design. The number of rats (n) measured in every group are indicated for each week and each type of measures: 'MRS' stands for MRS scan in the hippocampus and 'O-F' for the rats who undergone open field test. Of note for blood sampling we used the same number of rats as for the MRS scan (data not included in the Table for readability).*

| | Week 0 | Week 2 | Week 4 | Week 6 | Week 8 |
|---|---|---|---|---|---|
| | • Blood sampling<br>• MRS scan<br>• BDL surgery | • Blood sampling<br>• MRS scan<br>• Start of Rifaximin administration | • Blood sampling<br>• MRS scan<br>• Open field | • Blood sampling<br>• MRS scan<br>• Open field | • Blood sampling<br>• MRS scan<br>• Open field<br>• Sacrifice and organ collection |
| $n_{non\text{-}treated}$ | MRS:17 | MRS:17 | MRS:13 / O-F: 13 | MRS:13 / O-F:13 | MRS:9 / O-F:5 |
| $n_{rifaximin\ 6x\ human\ dose}$ | MRS:8 | MRS:8 | MRS:8 / O-F:8 | MRS:6 / O-F: 6 | MRS:2 / O-F:2 |
| $n_{rifaximin\ human\ dose}$ | MRS:12 | MRS:12 | MRS:12 / O-F:11 | MRS:11 / O-F:11 | MRS:8 / O-F:8 |

### 3.2.2 Biochemical measurements and behavorial test

Plasma measurements of total bilirubin were performed on each rat before BDL surgery (week 0) and at post-operative weeks 2, 4, 6 and 8 on an Integra© or a COBAS8000© analyzers (Roche, Switzerland). As described in Chapter 2, plasma ammonium was measured on the rats in 'rifaximin human dose' group (Integra© analyzer, Roche, Switzerland). In both the non-treated rats and the rats treated with a higher dose of rifaximin ('6x human dose'), blood ammonium was measured using a PocketChem™ BA analyzer. Evolution of the three groups is thus reported in relative value, as ammonium was measured in the plasma for the 'rifaximin human dose' group and in the blood for the two other groups. In order to evaluate motor activity in the different groups, the open field test was used as explained in Chapter 2.

### 3.2.3 *In vivo* $^1$H Magnetic Resonance Spectroscopy ($^1$H MRS)

Brain metabolites longitudinal evolution was studied in the hippocampus in a voxel of interest (VOI) of 2x2.8x2mm$^3$ using a 9.4T MRI system. The details of the procedure used for *in vivo* $^1$H MRS are described in Chapter 2.

### 3.2.4 Statistical analysis

All results are presented as mean ± SD. One-way ANOVA (Prism 5.03, Graphpad, La Jolla CA USA) with respect to each metabolite in the neurochemical profile followed by Bonferroni's multi-comparisons post-test was used within a single group. Two-way ANOVA (Prism 5.03, Graphpad, La Jolla CA USA) followed by the Bonferroni's multi comparisons post-test was used to assess significance ($p<0.05$) in brain and plasma metabolite's changes between the groups ('treatment' factor). Of note, repeated measures ANOVA were not performed on our longitudinal data since in the 'non-treated' group, some of the rats were sacrificed before reaching the humane endpoint for additional measures. Pearson correlation analysis was performed on different longitudinally acquired data to test for correlations between brain metabolites and plasma values.

## 3.3 Results

The increase in plasma bilirubin confirmed the presence of CLD-induced in the three groups of rats (Figure 3.1A). The rats displayed a similar blood ammonium increase in the 'non-treated' and the 'high-dose rifaximin' group (Figure 3.1D) and the relative increase of ammonium (blood or plasma) was less marked in the 'rifaximin human dose' group (Figure 3.1B). During the open field test, the distance travelled significantly decreased from week 4 to week 8 in all groups of BDL rats, indicating the presence of motor deficits, characteristic of chronic HE. Interestingly, BDL rats treated with a higher dose of rifaximin ('BDL + rifaximin 6x human dose') moved significantly less than the two other groups (Figure 3.1C).

The high quality of the spectra throughout the study allowed the separation of Gln from Glu and the reliable quantification of 16 brain metabolites (Figure 3.2).

Brain Gln significantly increased in all of the three groups ($p<0.001$, Figure 3.3) due to ammonia detoxification and showed significant differences between the 'high-dose rifaximin', the 'non-treated' and the 'rifaximin human dose' groups: Gln increase was significantly lower in the 'high-dose rifaximin' group compared to the two other groups. This difference was especially marked at week 6 and at week 8, both in absolute value and relative to week 2 (42 % vs +118 % at week 8, Figure 3.3). Moreover, a trend of decrease of brain Gln was observed between week 4 and week

6 in the 'high-dose rifaximin' group while it was continuously and significantly increasing in the 'non-treated' and the 'rifaximin human dose' groups. Also, brain Gln was positively correlated with blood ammonia in the 'high-dose rifaximin' group (R = 0.61, p<0.001, Figure 3.3C) while the correlation did not reach significance in the 'rifaximin human dose' group (r = 0.27, p = 0.056).

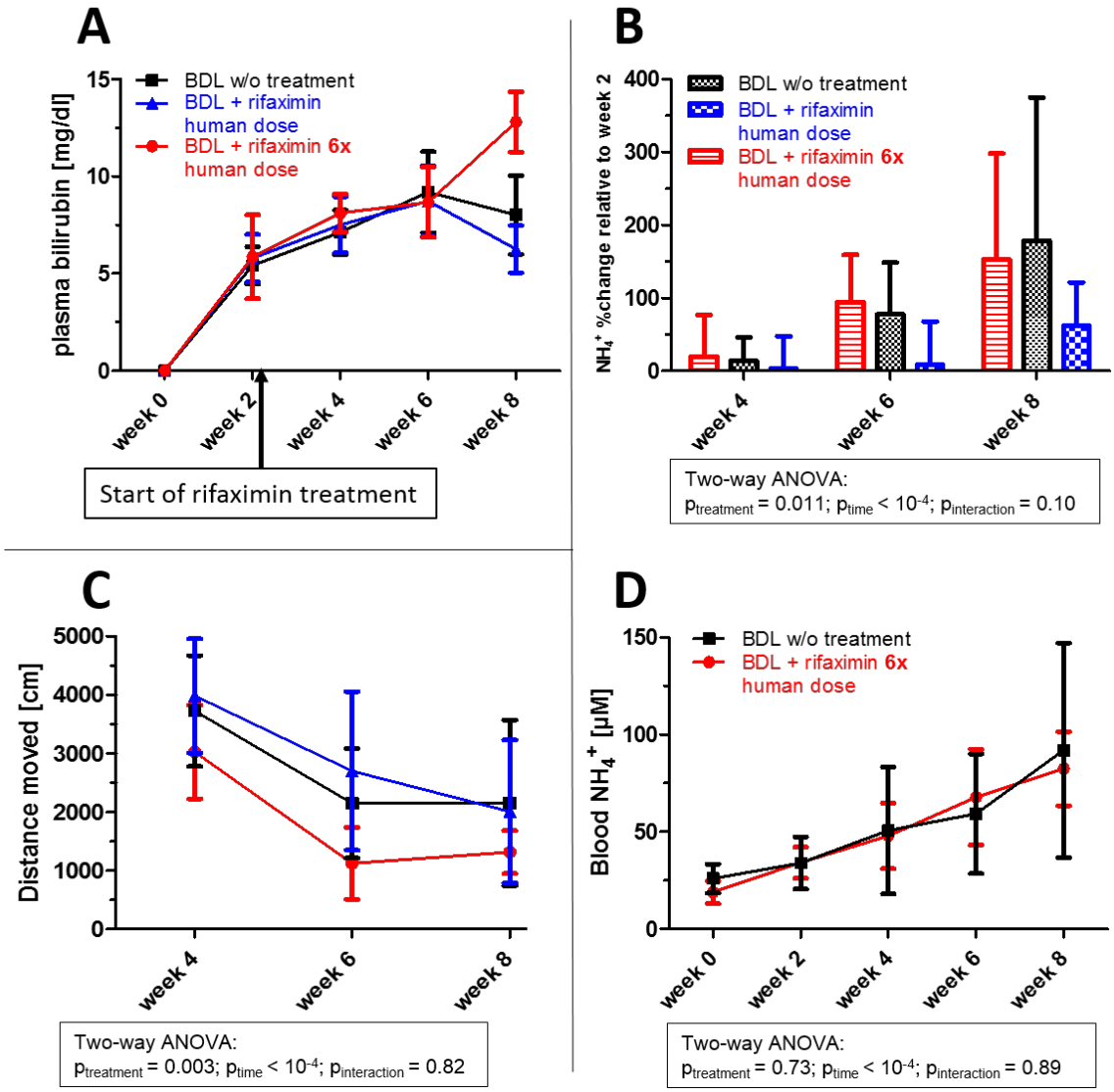


*Figure 3.1 (A) Longitudinal changes in plasma total bilirubin (B) $NH_4^+$ evolution in relative value in the three groups (measured in plasma for the 'rifaximin' group and in blood for the two other groups) and (D) blood $NH_4^+$ in absolute value in 'non-treated' and 'high-dose rifaximin' groups. (C) Distance traveled by the three groups of BDL rats. Two-way ANOVA was used to assess significance between-group ('treatment' factor).*

Gln increase was followed by a subsequent reduction of other brain osmolytes as an osmolatory response. The diminution of Ins was significant in all groups but was less marked in the 'high-dose rifaximin' group (-15 ± 7 % from week 2) compared to the non-treated group (-24 ± 10 %) and the group treated with the human dose of rifaximin (-28 ± 16 %). Among the other brain organic osmolytes, Tau concentration decreased in all of the three groups and there was no significant

difference between the groups. The decrease was highly pronounced between week 0 and 2 in the two treated groups with no significant variations thereafter while in the non-treated group, Tau concentration decreased linearly from week 0 to week 8 (Figure 4). PCho, another brain osmolyte, showed no significant difference in its decrease between the groups (Table 3.2).

Cr, a metabolite recognized for its role in energy metabolism and reported to be involved in osmoregulation and neuroprotection (Rae 2014; Braissant 2010) showed a stronger decrease in the 'rifaximin human dose' group and in the 'non-treated' group (significant at week 8, $p<0.01$) while a less marked and non-significant change was observed in the 'high-dose rifaximin' group. Similarly, tCr decreased significantly over the course of the study in the 'non-treated' group ($p<0.05$) and the 'rifaximin human dose' group ($p<0.01$) while no significant decrease was observed in the 'high-dose rifaximin' group (Figure 3.4).

Among the neurotransmitter, Glu showed no significant decrease in the 'high-dose rifaximin' treated group, whereas it reached -11 ± 6 % at week 8 compared to week 2 in the non-treated group ($p<0.001$) and -9 ± 10 % in the 'human-dose rifaximin' group ($p<0.05$, Figure 3.4). Asp decreased similarly between the groups without reaching significance.

Regarding antioxidants, the Asc decrease was slightly less marked in the 'high-dose rifaximin' group without reaching significance in any of the groups. No significant changes were observed for GSH. In addition, Lac, a metabolite involved in CNS energy metabolism, exhibited a small tendency to increase in each of the treated groups, but no variation were significant. No significant changes were observed in GABA, PE, NAA, NAAG nor tNAA during the course of the disease in any of the groups.

However, and importantly, we noted that the general condition of the rats in the 'high-dose rifaximin' group was overall worse than in the 'rifaximin human dose' group, as reflected by the fact that six out of eight rats reached the humane endpoint (euthanasia) in this group before the eight weeks of the study compared to four out of twelve rats in the 'rifaximin' group. The number of rats reaching the humane endpoint in the 'high-dose rifaximin' group is considerably higher than in the 'rifaximin + probiotics' group (1/9 at week 8, Chapter 2). Of note, the 'non-treated' BDL rats come from previously published studies (Simicic et al. 2019; Braissant et al. 2019) where no such assessment was performed.

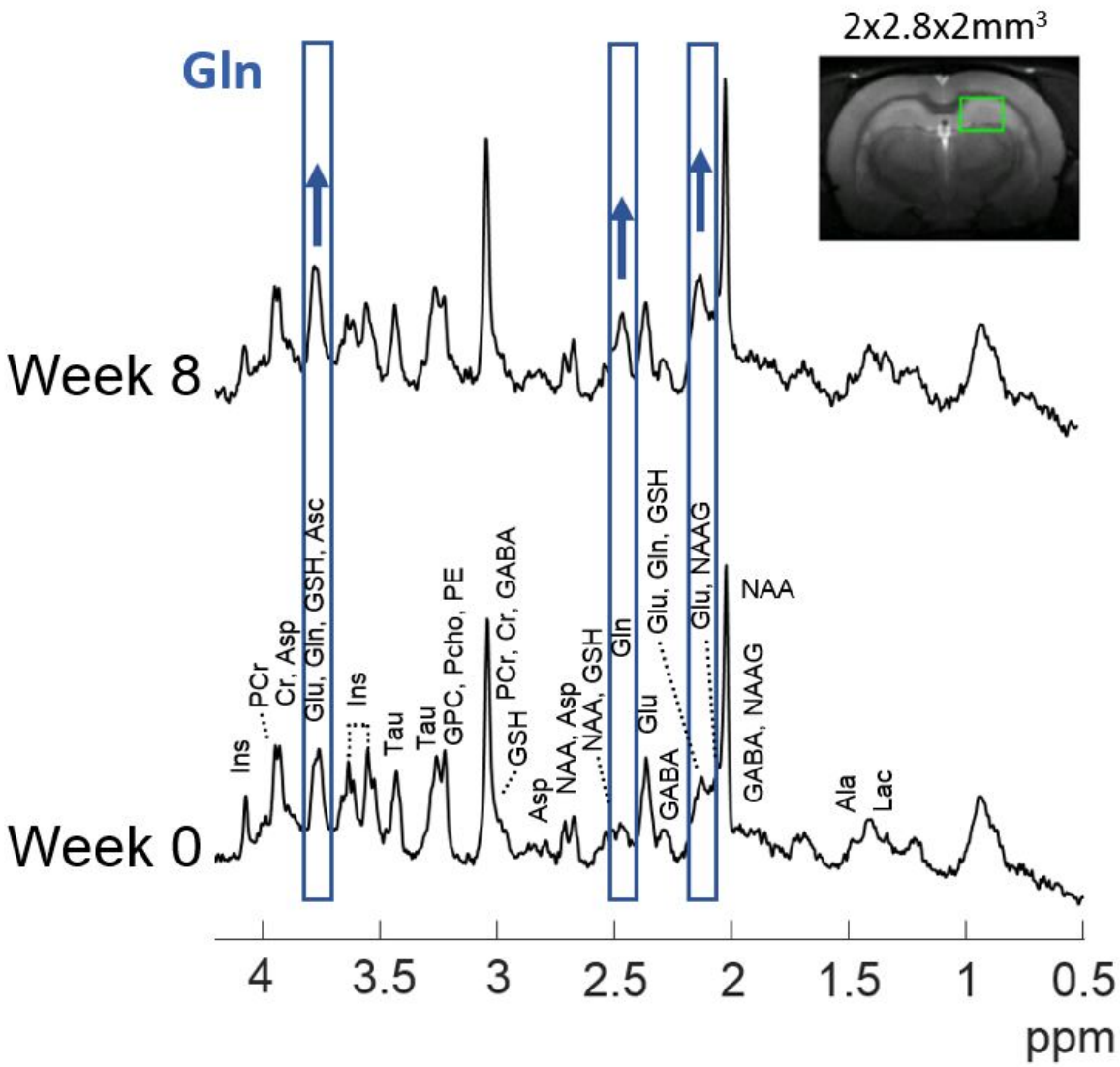


*Figure 3.2 Representative $^{1}$H MRS spectra in the hippocampus of a 'BDL + rifaximin 6x human dose' rat at week 0 and week 8 after BDL. Part of the spectra corresponding to Gln are shown in blue. Green rectangle shows the region considered in the hippocampus.*

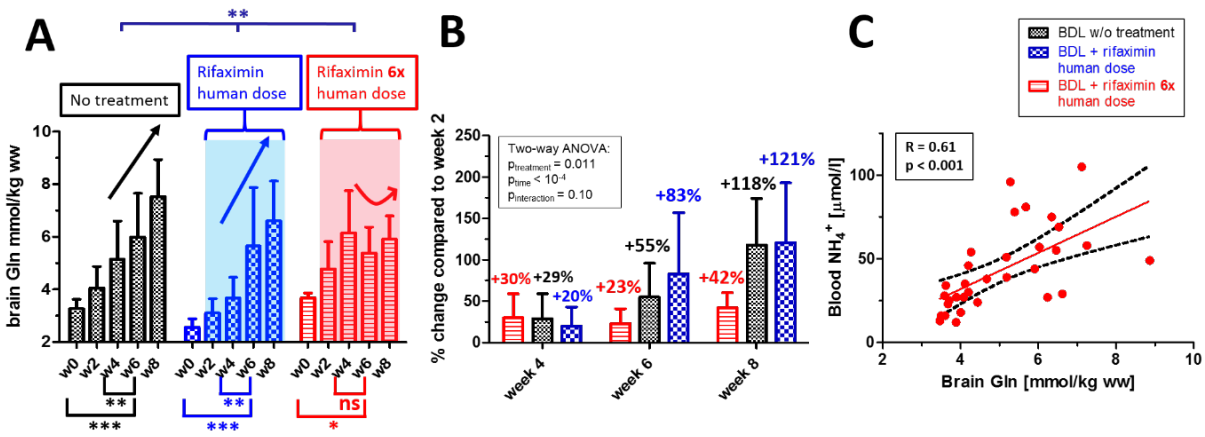


*Figure 3.3 (A) Brain Gln evolution from week 0 to week 8 in absolute value in the three groups. (B) Comparison of brain Gln evolution relative to week 2 in the three groups: BDL without treatment, BDL treated with human dose, and the BDL rats treated with 6x human dose. (C) Correlation between brain Gln and blood ammonia in rats treated with 6x human dose of rifaximin. One-way ANOVA was used to assess the significance intra-group and two-way ANOVA to assess significance between-groups. Statistical significance: * p < 0.05; ** p < 0.01; *** p < 0.001.*

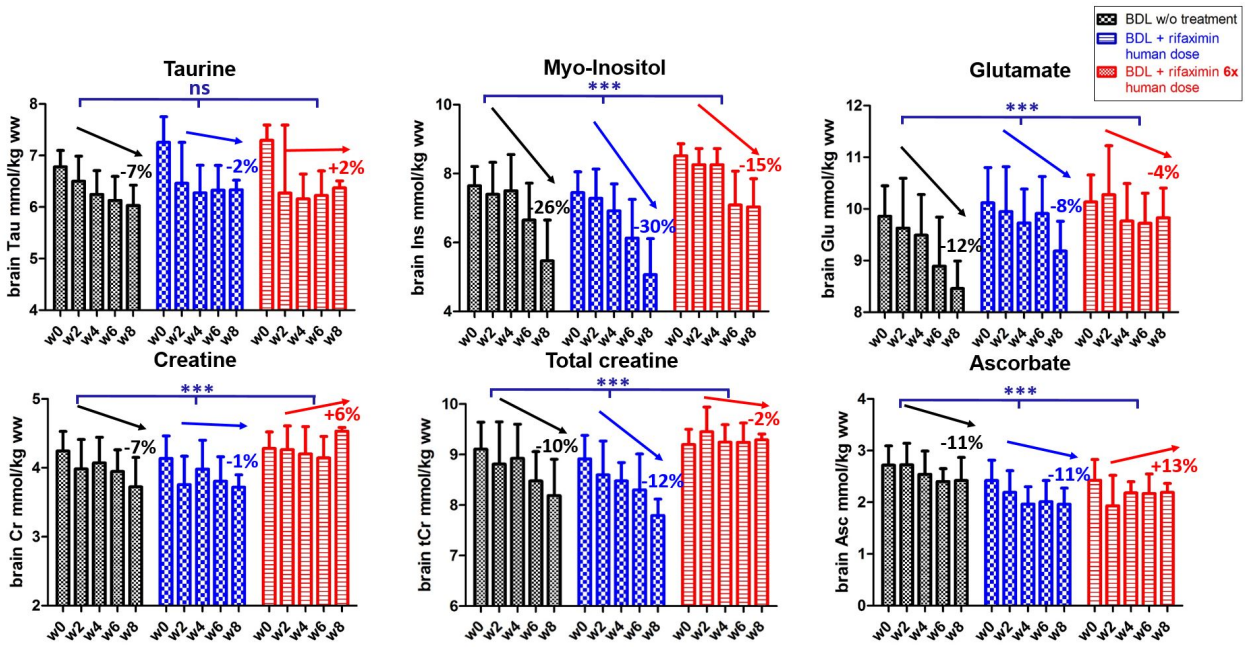


*Figure 3.4 Longitudinal evolution of some of the main brain osmolytes (Ins, Tau), metabolites involved in energy metabolism (Cr, tCr), neurotransmitter (Glu) and antioxidant (Asc) in the hippocampus of the 'high-dose rifaximin' treated group, the 'human-dose rifaximin' treated group and the group without treatment. Relative changes indicated in the graph are calculated relative to the means at week 2, corresponding to the start of the rifaximin treatment. Black, blue and red arrows show different trends in the groups from week 2. Two-way ANOVA was used to assess significance between-groups. Statistical significance: * p < 0.05; ** p < 0.01; *** p < 0.001.*

*Table 3.2 Two-way ANOVA results for each metabolite in the hippocampus. Statistical significance: * p < 0.05; ** p < 0.01; *** p < 0.001; **** p < 0.0001.*

| | Interaction $F(df_n,df_d)$; p | Treatment $F(df_n,df_d)$; p | Time $F(df_n,df_d)$; p |
|---|---|---|---|
| Gln | 2.98(8,141); * | 7.20(2,141); ** | 32.81(4,141); **** |
| Ins | 0.68(8,141); ns | 22.22(2,141); **** | 22.79(4,141); **** |
| tCho | 0.98(8,141); ns | 7.25(2,141); *** | 9.08(4,141); **** |
| Tau | 0.63(8,141); ns | 1.26(2,141); ns | 11.33(4,141); **** |
| Cr | 1.76(8,141); ns | 13.64(2,141); **** | 2.03(4,141); ns |
| PCr | 0.83(8,141); ns | 11.10(2,141); **** | 4.68(4,141); *** |
| tCr | 1.40(8,141); ns | 22.87(2,141); **** | 4.60(4,141); *** |
| Lac | 0.94(8,141); ns | 36.77(2,141); **** | 1.96(4,141); ns |
| Glu | 1.00(8,141); ns | 8.71(2,141); *** | 5.23(4,141); *** |
| Asp | 0.99(8,141); ns | 17.89(2,141); **** | 10.52(4,141); **** |
| GABA | 0.41(8,141); ns | 9.28(2,141); *** | 0.80(4,141); ns |
| Ala | 1.25(8,141); ns | 16.98(2,141); **** | 4.46(4,141); *** |
| Asc | 0.95(8,141); ns | 15.17(2,141); **** | 2.93(4,141); ** |
| GSH | 1.07(8,141); ns | 13.55(2,141); **** | 6.26(4,141); *** |
| PE | 0.81(8,141); ns | 7.98(2,141); *** | 0.84(4,141); ns |
| NAA | 0.47(8,141); ns | 5.17(2,141); ** | 0.91(4,141); ns |

## 3.4 Discussion

The present study evaluates for the first time the effect of two different doses of the antibiotic rifaximin on the neurometabolic changes both *in vivo* and longitudinally in a rat model of type C HE. The characteristic pattern of chronic HE was confirmed by our $^{1}$H MRS longitudinal measurements and was also noticeable from the spectra presented in Figure 3.2. We measured in all of the three groups the gradual increase of brain Gln. This rise was followed by a gradual decrease in the other brain osmolytes (Ins, Tau, tCho), by the decreases of Cr and the neurotransmitter Glu. These observations are in agreement with previously published studies in BDL rats and CLD patients (Córdoba et al. 2001; Rackayova et al. 2016; Braissant et al. 2019) and confirm the already well-known compensatory effect to maintain osmotic balance despite Gln accumulation.

We measured a significant increase in all groups in plasma and blood ammonium, with a high variability intra-group. No significant differences were observed between the 'non-treated' group' and the group treated with 6x human dose of rifaximin, despite the administration of rifaximin

whose alleged role is to reduce the production of gut ammonium. However, the effect of rifaximin on blood ammonium levels is still controversial. It is now generally considered that despite the indisputable and central role of ammonium in the pathogenesis of HE, its blood levels are widely dispersed in individual values, and measurement of plasma ammonia for the diagnosis and monitoring of hepatic encephalopathy is disputed and not recommended (Nicolao et al. 2003; Felipo and Butterworth 2002; Aldridge, Tranah, and Shawcross 2015; Mallet et al. 2018). In view of this and the difficulties associated with ammonium measurements, other multimodal methods should be used and combined to accurately assess the effect of different treatment options in chronic HE, as is done in this study.

Gln increase was less marked in the 'high-dose rifaximin' group at week 6 and at week 8 compared to the two other groups. In view of this fact, the non-significant decrease of brain Glu in the 'high-dose rifaximin' treated group suggests that the reduction in brain glutamate is mainly the result of ammonium detoxification through glutamine synthetase which catalyzes the formation of Gln from ammonium and Glu in astrocytes (Cooper and Plum 1987). Similarly, less pronounced decreases of Ins, Cr and PCr were measured in the 'high-dose rifaximin' group compared to the two others. This finding is consistent with the fact that Gln increase was smaller in that group and that the decreases of these different osmolytes are generally considered as compensatory mechanisms of the osmotic imbalance created by the increase of Gln. Asp also showed a similar decrease in all the groups. Even if the role of Asp as excitatory neurotransmitter is still controversial (Herring et al. 2015), it reflects the fact that even in the group of BDL rats treated with a higher dose of rifaximin, there is alteration in the neurotransmission system. Moreover, no changes in GABA concentrations were observed in any of the groups, a finding which is consistent with our previous studies (Rackayova et al. 2016; Braissant et al. 2019).

Overall, while rifaximin at human dose appeared to have no significant effect on brain metabolites profile, rifaximin treatment at higher dose was associated with some slight but significant positive effects on brain Gln, Glu and osmoregulation, with less neurometabolic alterations: the longitudinal changes in these brain metabolites concentration were less marked in the group of rats treated with a higher dose of rifaximin compared to the two other groups. The two-way ANOVA tests performed on each metabolite revealed that for many brain metabolites, both time ('week') and treatment ('non-treated', 'Rifaximin human dose' or 'Rifaximin 6x human dose') affect metabolites concentrations (Table 3.2). However, and importantly, the BDL rats treated with a higher dose of rifaximin moved significantly less than the two others groups and six out of eight rats had to be euthanized in this group before the eight weeks of the study compared to four out

of twelve rats in the 'rifaximin' group. Therefore, the few reported favourable effects of the rifaximin treatment at 6.2x human dose should be carefully valuated, bearing in mind that for several metabolites the treatment did not induce any significant effects and that the general conditions of these rats was overall worse than the two other groups. It is therefore possible that such a high dose of antibiotics also leads to some noxious effects as antibiotics imbalance the intestinal microbiota, affect intestinal permeability (Tulstrup et al. 2015) and may worsen the general condition of the rats, e.g by promoting inflammatory response (Knoop et al. 2016) which would act synergistically with the deranged nitrogen metabolism (Aldridge, Tranah, and Shawcross 2015). A limitation of this study is the lack of longitudinal measurements of inflammatory markers in the blood (TNF-α, CRP, WBC counts), and markers of neuro-inflammation. Also, immunohistochemistry or western blots of glutamine synthase levels and high-resolution *ex vivo* $^{1}$H MRS of extracted brain tissues could be performed to further validate the metabolic changes observed *in vivo* by $^{1}$H MRS. These measurements remain to be performed.

We conclude that in BDL rats, rifaximin treatment alone has limited efficacy. When administered at human dose in rats, its potential usefulness may appear only at the onset of the disease, whereas at a higher dose some neurometabolic changes associated with HE were attenuated but the general condition of the rats is worse. More generally, it illustrates the fact that finding an appropriate treatment for HE is challenging, which is why, despite years of investigation, the appropriate treatment has not yet been found. At the same time, our studies illustrate the usefulness of MR spectroscopy as a very powerful technique in pre-clinical studies for the detailed and non-invasive evaluation of the effects of drugs impacting the neurometabolic profile in particular.

# Chapter 4 Cerebral metabolism of hyperpolarized [$^{2}H_{7}$, U-$^{13}C_{6}$]-D-glucose in the healthy mouse

## Abstract

Glucose is the primary fuel for the brain and its metabolism is linked with cerebral function. Isoflurane anesthesia is commonly employed in preclinical MRS but affects cerebral hemodynamics and functional connectivity (Todd and Weeks 1996; Paasonen et al. 2018). The combination of low doses of isoflurane and medetomidine is routinely used in rodent fMRI and show similar functional connectivity as in awake animals (Paasonen et al. 2018). Given that glucose metabolism is tightly linked to neuronal activity (Sokoloff 1999), the first aim of this study (Chapter 4.1) was to compare the cerebral metabolism of hyperpolarized [$^{2}H_{7}$, U-$^{13}C_{6}$]-D-glucose under these two anesthetic conditions. Brain metabolism of hyperpolarized glucose was monitored in two groups of fasted male mice in a 9.4 T MRI system. In both anesthetic conditions, the injection of hyperpolarized [$^{2}H_{7}$,$^{13}C_{6}$]-D-glucose resulted in *de novo* synthesis of [1-$^{13}$C] lactate and the time courses were well reproducible. Changing the anesthesia from isoflurane to a combination of lower doses of isoflurane and medetomidine is known to influence brain activity and we showed in this study that it had high impact on cerebral uptake and metabolic flux of hyperpolarized [$^{2}H_{7}$,U-$^{13}C_{6}$]-D-glucose in the mouse. A larger amount of lactate was produced in the case when the functional connectivity was similar to the awake animals (+128% in lactate to glucose ratio). Also, endogenous lactate concentration was higher in the group anesthesized with isoflurane only, implying that [1-$^{13}$C] lactate production from hyperpolarized glucose is not a reflection of the steady-state pool-size but rather related to the dynamic of glucose uptake and the glycolytic flux. The second part of this study (Chapter 4.2) aims at evaluating the feasibility of quantifying cerebral glucose metabolism kinetics following infusion of hyperpolarized [$^{2}H_{7}$, U-$^{13}C_{6}$]-D-glucose in a healthy mouse by evaluating two different mathematical models, where kinetic rate constants were determined by fitting the models on $^{13}$C curves by non-linear regression using the Levenberg-Marquardt algorithm. We showed that a 3-compartment model is more stable and reliable than a 4-compartment model.

Partially adapted from:

**E.Flatt**, B.Lanz, R.Gruetter, M.Mishkovsky. Cerebral metabolism of hyperpolarized [$^{2}H_{7}$, U-$^{13}C_{6}$]-D-glucose in the healthy mouse under different anesthetic conditions, Special Issue in the journal Metabolites, manuscript in preparation.

I contributed to the design of this study, collected and processed the data, interpreted the results and wrote the paper. For the mathematical modelling part (chapter 4.2), I developed the model based on an existing model originally created by Dr. Bernard Lanz (Laboratory for Functional and Metabolic Imaging, EPFL) and performed the entire analysis.

## 4.1 Cerebral metabolism of hyperpolarized [$^{2}H_7$, U-$^{13}C_6$]-D-glucose in the healthy mouse under different anesthetic conditions

### 4.1.1 Introduction

Brain function is characterized by elevated metabolic activity and requires a continuous supply of oxygen and nutrients from the blood stream. Brain metabolism requires a complex intercellular traffic of metabolites and many processes are compartmentalized. It is well established that the mammalian brain is mainly supported by glucose as fuel to meet its high metabolic demand (Mergenthaler et al. 2013), consuming up to 25% of circulating glucose under normal conditions (L. Pellerin 2010). Under physiological conditions, glucose metabolism is tightly linked with cerebral function (Sonnay, Gruetter, and Duarte 2017; Sokoloff 1999).

Different molecular imaging techniques exist to study glucose cerebral metabolism. In particular, $^{18}$FDG-PET is a highly sensitive imaging modality very used in cancer detection and treatment because of its unique ability to measure abnormal glucose uptake. However, as this technique uses a glucose analogue, it enables only the detection of glucose uptake and the first step of glycolysis and does not detect downstream metabolic products such as lactate and TCA cycle intermediates. Besides, one of the main drawbacks of this technique is the need to use radioactive tracers and thus the exposure to ionizing radiations.

Another technique to monitor glucose uptake and that overcomes some of the limitations of $^{18}$F-FDG PET is chemical exchange saturation transfer (CEST) MRI, which makes use of simple glucose. CEST enable the indirect detection of molecules through their exchangeable protons. Glucose CEST MRI provides a significant increase in sensitivity over direct detection (Jin et al. 2012; Cai et al. 2012), with glucose uptake being detected indirectly by saturation transfer of exchangeable protons from glucose to water. This technique also has its limitations: on the one hand, due to the spectral overlap, the excitation process is not entirely specific. On the other hand, glucose uptake analysis is also complicated because of the important dependence of the exchange rate on pH (Harris et al. 2015).

A way to track the dynamic of glucose metabolism *in vivo* is based on the continuous infusion of $^{13}$C labelled glucose combined with thermally polarized $^{13}$C magnetic resonance spectroscopy ($^{13}$C MRS). Contrarily to $^{18}$FDG PET or CEST, this technique enables dynamic measurement of $^{13}$C metabolic turnover rates but has also its limitations, the main drawback being its low sensitivity, and many metabolites cannot be detected. To overcome this limitation, the signal is acquired for longer and averaged, but this decreases the temporal resolution. Thermally polarized $^{13}$C MRS

combined with $^{13}C$ labelled glucose infusion is thus able to detect only the oxidative metabolism of glucose, and not the glycolysis. For instance, it was shown using thermally polarized glucose that there is a compartmentation of the cerebral glucose metabolism between the neurons and the glia (Gruetter, Seaquist, and Ugurbil 2001).

Another method to investigate the dynamic of oxidative glucose metabolism is to use deuterium magnetic resonance spectroscopy (DMRS) combined with [6,6'-$^{2}H_2$] glucose infusion, where the dynamic labeling in the brain tissue can be monitored with well-resolved resonance signals in $^{2}H$ spectra with good sensitivity (Lu et al. 2017). An advantage of DMRS is the short longitudinal relaxation time of $^{2}H$-labeled molecules as compared to that of $^{1}H$ or $^{13}C$ spins, thus enabling more signal averaging during the same sampling time. However, contrarily to $^{13}C$ MRS the distinction between glutamine and glutamate, linked to compartmentation of brain metabolism, is not possible.

To monitor and study real-time glycolysis, hyperpolarized glucose can be used. Hyperpolarized magnetic resonance of endogenous molecules by dissolution dynamic nuclear polarization (dDNP) (Ardenkjær-Larsen et al. 2003) is able to dramatically enhance signal to noise in $^{13}C$ MRS and is a powerful method for studying cerebral intermediary metabolism in real-time (Comment and Merritt 2014). Unlike the other methods described above, this technique enables rapid dynamic imaging of $^{13}C$-labelled substrates and their metabolic products, which is not possible with conventional thermally polarized $^{13}C$ MRS. To date, very few studies reported the use of hyperpolarized glucose *in vivo*. Although glucose is central to metabolism, the short lifetime of the $^{13}C$ hyperpolarized state in glucose is challenging for real-time measurement of metabolism, partly explaining the limited studies using hyperpolarized glucose so far. It was demonstrated that hyperpolarized [$^{2}H_7$, U-$^{13}C_6$]-D-glucose can be measured *in vivo* (Allouche-Arnon et al. 2013) and employed for the real time detection of glycolytic reactions in a lymphoma mouse model (Rodrigues et al. 2014) and in the healthy mouse brain (Mishkovsky et al. 2017).

Anesthetics are commonly employed in pre-clinical MRI/MRS and have been shown to impair neural transmission and to affect other aspects of mouse physiology, such as hemodynamics and metabolism, in a dose-dependent manner (Conzen et al. 1992; Todd and Weeks 1996; Paasonen et al. 2018; Baumgart et al. 2015; Hemmings et al. 2019). In particular, isoflurane is one of the most common anesthetic drug used in preclinical MRS metabolic studies, but is known to affect cerebral hemodynamics (Todd and Weeks 1996; Conzen et al. 1992) and to influence functional connectivity (Paasonen et al. 2018). In the context of hyperpolarized $^{13}C$ MRS, isoflurane was shown to alter the cerebral metabolism of hyperpolarized pyruvate (Josan et al. 2013; Marjańska

et al. 2018; "(ISMRM 2019) Metabolism of Hyperpolarized [1-13C]Pyruvate in Awake, Isoflurane and Urethane Anesthetized Rat Brain" n.d.). Recent studies reported that combining isoflurane and medetomidine at levels of about half their mono-anesthetic dosages enables to maintain similar functional connectivity as in the awake rats, considerably better than either of the mono-anesthetic protocol alone such as isoflurane (Paasonen et al. 2018; Grandjean et al. 2014). The combination of medetomidine and isoflurane is now currently considered to be one of the most appropriate anesthetic protocols available for the evaluation of murine functional connectivity. However, the extent to which different anesthesia protocols impact cerebral metabolism is an important topic that remains to be investigated.

Therefore, given that glucose metabolism is closely linked to neuronal activity (Sonnay, Gruetter, and Duarte 2017), the aim of the present study was to compare the cerebral metabolism of hyperpolarized [$^{2}H_{7}$, U-$^{13}C_{6}$]-D-glucose in the healthy mouse under these two anesthetic conditions. As functional connectivity under combined anesthesia of medetomidine and isoflurane was found to be closer to that observed in awake animals compared to isoflurane alone (Paasonen et al. 2018; Grandjean et al. 2014), we hypothesized that glucose uptake, glycolysis and lactate production would be increased with combined anesthetics.

### 4.1.2 Material & Methods

#### *4.1.2.1 Study design*

Brain metabolism of hyperpolarized glucose was monitored in two groups of 12 hours-fasted male C57BL6/J mice (N=14, age = 17±3 weeks). In the first group (ISO; N=8), mice were kept under 1.3-1.5 % isoflurane for the entire duration of the experiment. In the second group (MED+ISO, N=6), anesthesia was switched to a combination of medetomidine (Dorbene, Graeub, Switzerland) and isoflurane at least one hour before the injection of hyperpolarized [$^{2}H_{7}$, U-$^{13}C_{6}$]-D-glucose. In this group, a first subcutaneous (SC) bolus of medetomidine 0.3 mg/kg was administered. 10 min after the bolus, isoflurane anesthesia was dropped to 0.25-0.5 % and a continuous infusion of medetomidine SC 0.6 mg/kg/h started, as described by Reynaud et al. (Reynaud et al. 2019). The time between the switch in anesthetics and the injection of hyperpolarized [$^{2}H_{7}$, U-$^{13}C_{6}$]-D-glucose was at least one hour (between 60-65 min), which has been reported to be enough time to reach a new metabolic steady-state (Sirmpilatze, Baudewig, and Boretius 2019). Single voxel $^{1}H$ MRS measurements were carried out in each mouse 10 min before the hyperpolarized [$^{2}H_{7}$, U-$^{13}C_{6}$]-D-glucose bolus and the $^{13}C$ MRS acquisition. Animal physiology was constantly monitored and complete blood analysis were performed from the eye of the mouse (retro-orbital bleeding) before

the holder was inserted inside the scanner (95 min before the glucose bolus) and immediately after the end of the $^{13}C$ MRS acquisition (~2 min post bolus) using a PocketChem™ BA analyzer. At the end of the experiment, 200µL of the solution remaining in the separator/infusion pump was collected. In order to further compute the blood fractional enrichment, $^{13}C$ glucose concentration of the injected bolus was measured in a high-resolution DRX-400 spectrometer (Bruker Biospin SA /Avancell 800MHz, TOPSPIN2) using [2-$^{13}C$] acetate 80 mM as reference. Of note, fasted male mice were used in order to compare with previously acquired data using hyerpolarised [$^{2}H_7$, U-$^{13}C_6$]-D-glucose on fasted female mice under isoflurane anesthesia (Mishkovsky et al. 2017). The outline of the experiments are summarized in Figure 4.1.

#### *4.1.2.2 Samples and liquid-state polarization*

Frozen droplets of a glycerol/water solution 50:50 (v/v) containing [$^{2}H_7$,$^{13}C_6$]D-glucose (2 M) and OX63 trityl radical (25 mM) doped with 1mM of $Gd^{3+}$ as previously described (Capozzi et al. 2019) were dynamically polarized for 120 min in a custom designed 7 T / 1 K DNP polarizer (Cheng et al. 2013). To monitor real-time *de novo* synthesis of [1-$^{13}C$]lactate, a 540 µL of 44 ± 10 mM hyperpolarized [$^{2}H_7$,$^{13}C_6$]D-glucose was dissolved in superheated $D_2O$ (12 bar, 450 K) and automatically injected through the femoral vein of the mouse using a syringe pump (Cheng et al. 2013).

The liquid-state polarization of hyperpolarized [$^{2}H_7$,$^{13}C_6$]D-glucose was measured inside a separator/infusion pump located in the bore of our adjacent 9.4 T scanner using NMR coils ($^{1}H$ and $^{13}C$) implemented on the pump after DNP and dissolution in $D_2O$, using the same protocol as *in vivo* experiment. The liquid-state polarization was calculated from the hyperpolarized signal of the $^{13}C$-glucose and its thermal equilibrium signal recorded 15 min after dissolution.

#### *4.1.2.3 In vivo MRS/MRI*

In order to evaluate the effect of the two anesthetic conditions on the endogenous concentration of brain metabolites, i*n vivo* $^{1}H$ MRS measurements were performed in the hippocampus in a voxel of interest (VOI) of 2 x 2.8 x 2 $mm^3$ using the SPECIAL (Mlynárik et al. 2006) sequence (TE=2.8ms, TR = 4000ms, 160 averages). Spectra quantification of $^{1}H$ spectra was performed using LCModel and water as internal reference (Provencher 1993). Values with Cramer–Rao lower bounds above 30% were excluded from further analyses.

To optimize signal-to-noise ratio (SNR) of the expected glucose metabolites in the carboxyl region of the $^{13}C$ spectra, we used a previously described RF excitation pulse (Mishkovsky et al. 2017): a

series of pulse-acquire sequence was triggered 5.5 s post-dissolution (2 s after the end of the injection) with 25° frequency selective Gaussian pulse (250µs/40kHz bandwidth) centered on [1-$^{13}$C] lactate resonance (183.5 ppm) and applied every 1 s for 70 s. With this RF pulse design, the glucose resonances were excited by a minimal flip angle (1.5° at 95 ppm, 0.05° at 73 ppm, Figure 4.2). The lactate-to-glucose ratio (LGR) was calculated from the summed spectra.

All measurements were performed in a 31-cm horizontal-bore actively shielded 9.4T MRI system (Varian/Magnex Scientific, Abingdon, UK) interfaced to a Varian Direct Drive console (Palo Alto, CA, USA) and using a home-built quadrature $^{1}$H-coil and a three-loop 10-mm $^{13}$C surface coil as a transceiver that was placed on top of the mouse head.

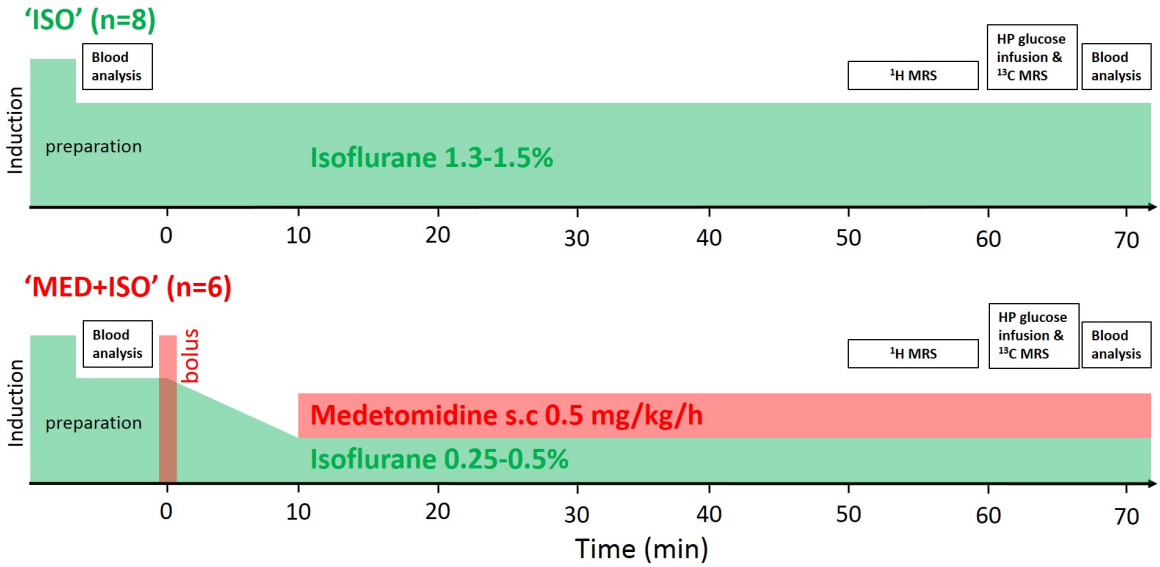


*Figure 4.1 Outline of the two anesthetic protocols in the ISO group and in the MED+ISO group.*

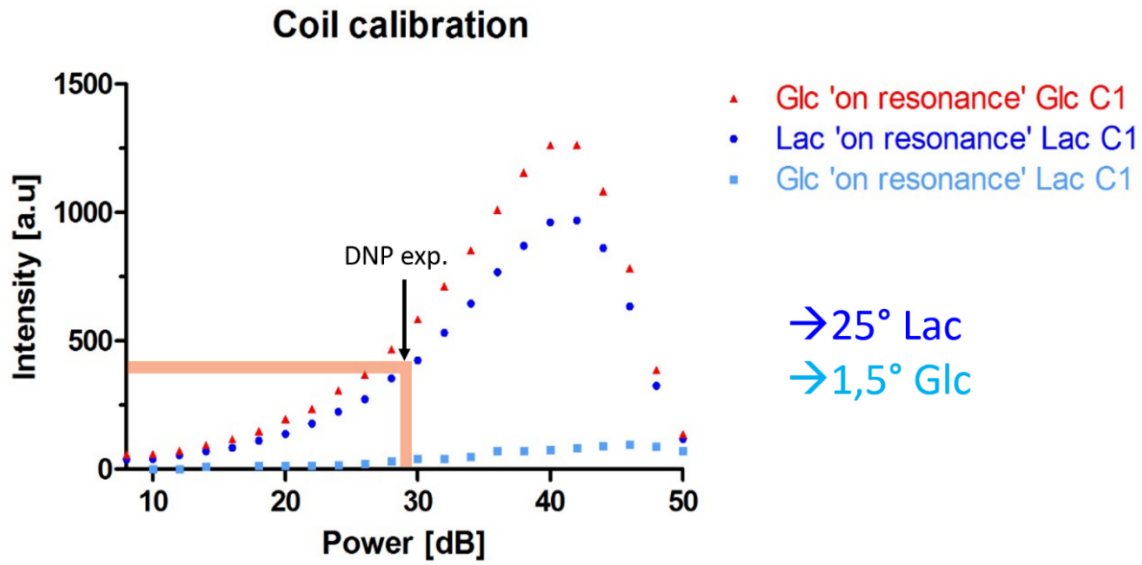


*Figure 4.2 Coil calibration. For $^{13}C$ MRS acquisition, 25° frequency selective Gaussian pulse (250 µs /40 kHz bandwidth) centered on [1-$^{13}C$] lactate resonance (183.5 ppm) were used. With this RF pulse design, the glucose resonances were excited by a minimal flip angle (1.5° at 95 ppm, 0.05° at 73 ppm).*

#### *4.1.2.4 Biochemical measurements*

Complete blood measurements (glucose, lactate, $PO_2$, $PCO_2$, electrolytes, pH, $SO_2$, tHb, Hct) were performed on a COBAS b121© analyzers (Roche Diagnostics AG, Switzerland).

#### *4.1.2.5 MRS/MRI procedures and biochemical measurements*

Animals had unrestricted access to standard mouse food and water until 12h before the experiment, where the food was removed. During all the MRS/MRI procedures, body temperature of the animals were maintained at 37-38 °C and ventilation was composed of a mixture of 30 % $O_2$ and 70 % air. Femoral vein was catheterized for glucose injection, and in the MED+ISO animals, a catheter was inserted subcutaneously on the back of the animal for medetomidine delivery. The mouse was placed on a holder together with the infusion pump and the femoral vein catheter was connected to the infusion pump. The animals were euthanized at the end of each experiment with an overdose of pentobarbital. All procedures were approved by the Committee on Animal Experimentation for the canton of Vaud, Switzerland (authorization 2353.4c).

#### *4.1.2.6 Statistical analysis*

Statistical analysis was conducted using Graphpad Prism Software (Prism 5.03, Graphpad, La Jolla CA, USA). All results are presented as mean ± SD. Unpaired, two-tailed Student's t-tests were used to compare LGR, blood measurements, age and neurometabolites concentrations between the two anesthetic conditions. Two-way ANOVA was used to compare the blood glycemia evolution

(before and after injection) between the two anesthetic conditions (* $p < 0.05$; ** $p < 0.01$; *** $p < 0.001$).

### 4.1.3 Results

Hyperpolarized [$^{2}H_{7}$, U-$^{13}C_{6}$]-D-glucose yielded a liquid-state polarization measured inside the separator/infusion pump of 29 ± 4 % (n=3).

Typical dynamic spectra show that in both anesthetic conditions, the injection of hyperpolarized [$^{2}H_{7}$, U-$^{13}C_{6}$]-D-glucose results in *de novo* synthesis of [1-$^{13}$C] lactate. Both glucose and lactate were detectable during 55 seconds following injection. The time courses of all animals in both groups were well reproducible (Figure 4.3). For the two groups, the initial blood glycemia, the post bolus blood glycemia, and $^{13}$C glucose fractional enrichment were kept similar as those may influence the metabolism of hyperpolarized [$^{2}H_{7}$, U-$^{13}C_{6}$]-D-glucose (Figure 4.4).

Interestingly, *de novo* synthesis of [1-$^{13}$C] lactate from hyperpolarized [$^{2}H_{7}$, U-$^{13}C_{6}$]-D-glucose varies with different anesthetics conditions (Figure 4.3). The total lactate-to-glucose ratio was found significantly higher in the MED+ISO group compared to ISO group (+128 %, Figure 4.5) and the [1-$^{13}$C] lactate signal was detected for a longer period of time in the MED+ISO group (Figure 4.3). Overall, the results obtained with hyperpolarized [$^{2}H_{7}$, U-$^{13}C_{6}$]-D-glucose in the mouse brain showed that medetomidine combined with a lower dose of isoflurane greatly increased the labelling of downstream lactate.

To evaluate the effect of the two anesthetic conditions on the endogenous concentration of brain metabolites, *in vivo* $^{1}$H MRS measurements were performed. Steady-state metabolites concentrations deduced from $^{1}$H MRS spectra showed significantly higher lactate pool-size and significantly lower concentration of phosophocreatine in animals anesthetized by isoflurane compared to those anesthetized by the combination of medetomidine and isoflurane (Figure 4.6). Creatine concentration was higher in the ISO group, without reaching significance. Creatine-to-phosphocreatine ratio (Cr/PCr) was found to significantly differ between the two anesthetics groups. All other metabolites in the neurochemical profile did not show any significant difference.

Regarding blood measurements, some significant differences were measured among the two anesthetics groups. In the MED+ISO group, blood lactate concentrations did not vary over the course of the study but was more than doubled in the ISO group (Figure 4.7A). Partial pressure of oxygen ($PO_2$) was found to be significantly lower in the MED+ISO group after the injection while it did not significantly vary over the course of the experiment in the ISO group (Figure 4.7B). Similarly,

partial pressure of carbon dioxide ($PCO_2$) significantly increased in MED+ISO group while it did not change in the ISO group (Figure 4.7C).

Furthermore, in order to obtain the glucose apparent $T_1$, we fitted the glucose signal to the function $S(t) = A\,(e^{-\frac{t}{T1}} - e^{-\frac{t}{Tb}})$, $T_1$ standing for the apparent $T_1$ and $T_b$ representing the signal build-up. Interestingly, the apparent $T_1$ was found significantly longer in the MED+ISO group (13.4 ± 4.6 s) compared to the ISO group (8.3 ± 0.9 s, Figure 4.8).

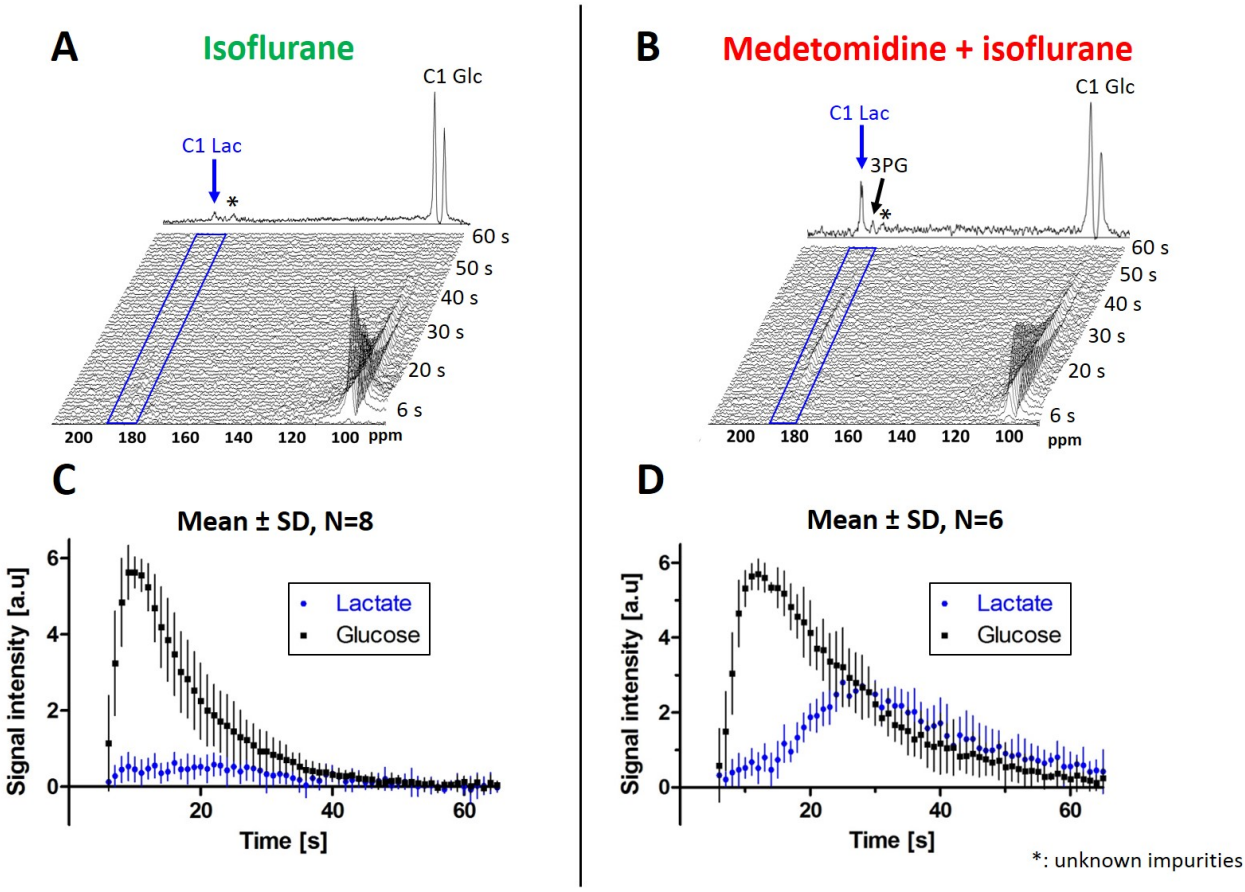


*Figure 4.3 (A, B) Characteristic spectra measured in a mouse brain under isoflurane and under medetomidine + isoflurane anesthesia following infusion of hyperpolarized [$^2H_7$,$^{13}C_6$]D-glucose. The glycolytic intermediate 3PG (179.8 ppm) can be identified in the summed spectra in addition to the lactate at 183.5 ppm. The broad peak at 175 ppm designated by (*) is an impurity in the [$^2H_7$,$^{13}C_6$]D-glucose powder. (C, D) The corresponding time courses of [1-$^{13}$C]Lactate and glucose are shown for each group (mean ± SD; glucose signal normalized to 6, arbitrary units).*

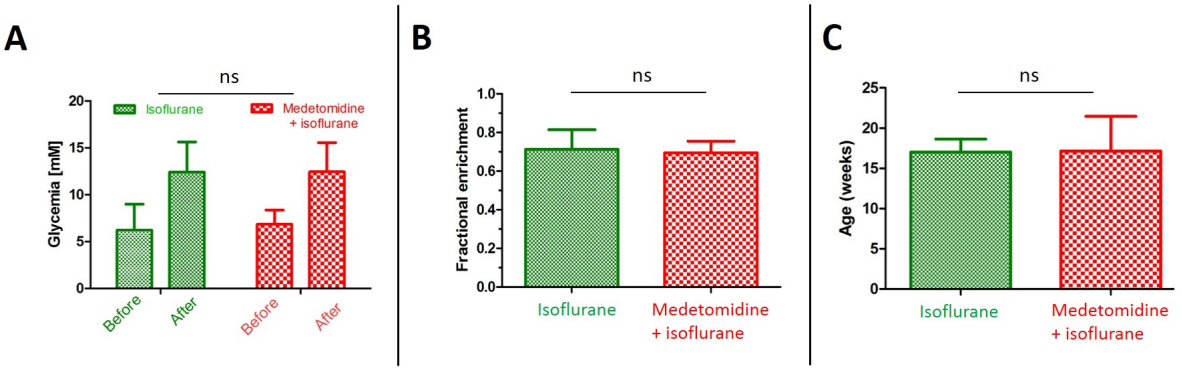


*Figure 4.4 (A) Glycemia measured when the mice enter the scanner ('before') and 2 minutes after injection of hyperpolarized [$^{2}H_{7}$,$^{13}C_{6}$]D-glucose ('after') in the two anesthesia groups. No significant differences in $^{13}C$ blood fractional enrichment (B) or age (C) between the two anesthesia groups. Unpaired, two-tailed Student's t-tests were used to compare blood fractional enrichment and age between the two anesthetic conditions. Two-way ANOVA was used to compare the blood glycemia evolution (before and after injection) between the two anesthetic conditions (* $p < 0.05$; ** $p < 0.01$; *** $p < 0.001$).*

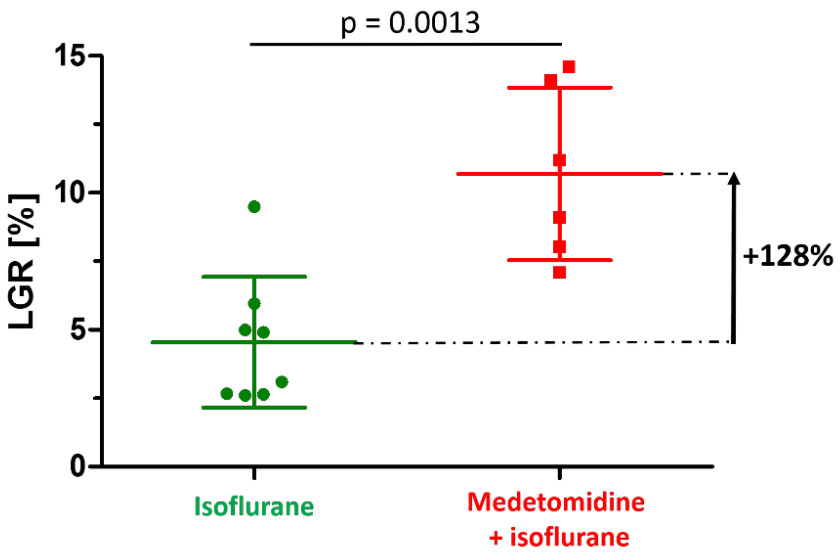


*Figure 4.5 Comparison of lactate-to-glucose ratio (LGR) between isoflurane ('ISO') and medetomidine + isoflurane ('MED+ISO') groups. Unpaired, two-tailed Student's t-tests were used to assess statistical significance.*

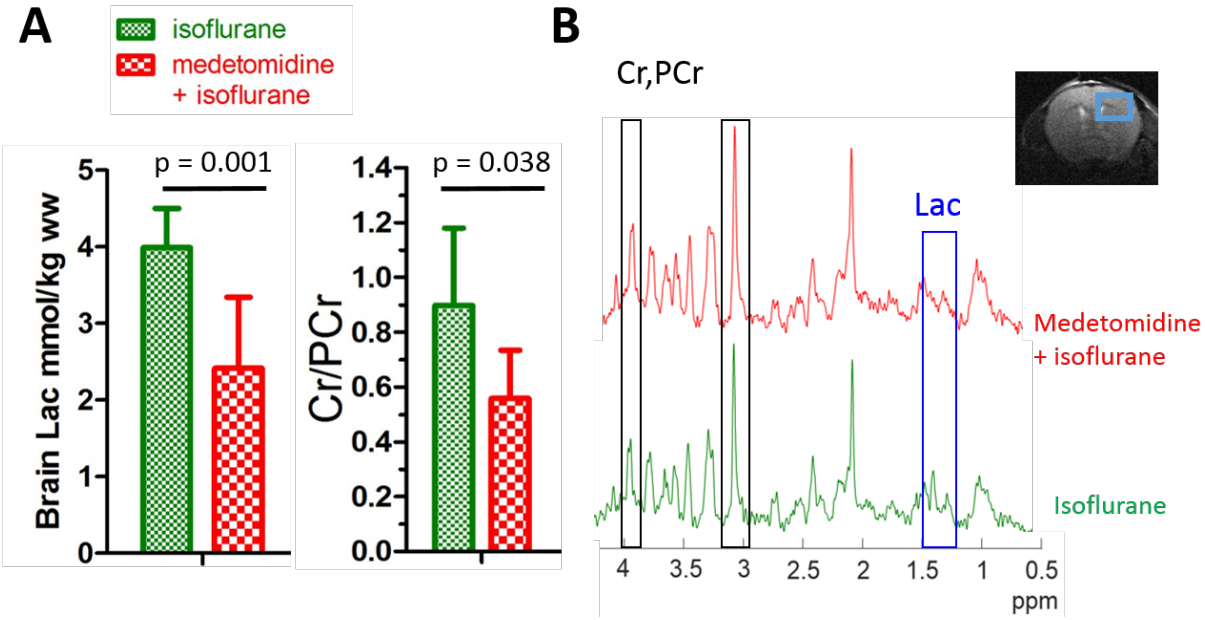


*Figure 4.6 (A) Brain lactate (Lac) concentration as well as Cr/PCr ratio in the ISO group and the MED+ISO group. (B) Representative $^{1}H$ MRS spectra in the hippocampus of an ISO mouse (green) and a MED+ISO mouse (red). Part of the spectra corresponding to Lac and Cr & PCr are shown in blue and dark, respectively. Unpaired, two-tailed Student's t-tests were used to assess statistical significance.*

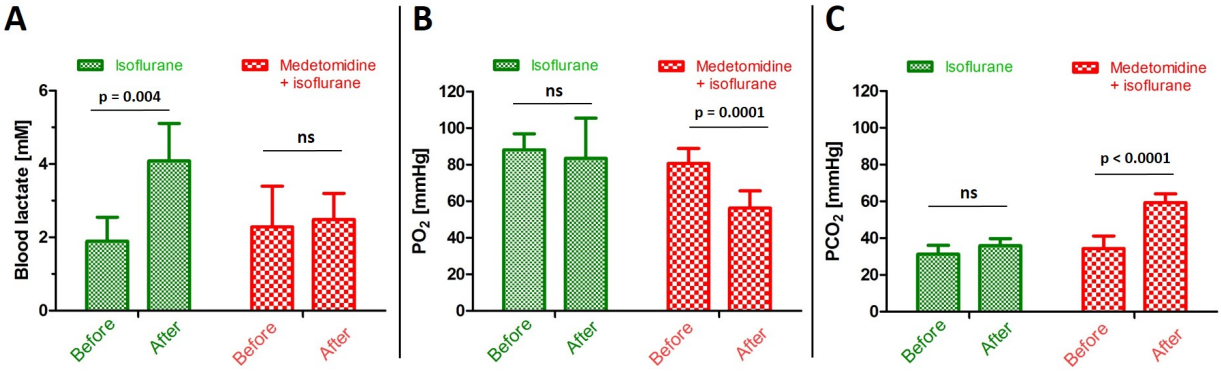


*Figure 4.7 Blood lactate (A), partial pressure of oxygen $PO_2$ (B) and partial pressure of carbon dioxide $PCO_2$ (C) measured before the mice enter the scanner ('before') and 2 minutes after injection of hyperpolarized [$^{2}H_7$,$^{13}C_6$]D-glucose ('after') in the two anesthesia groups. Unpaired, two-tailed Student's t-tests were used to assess statistical significance.*

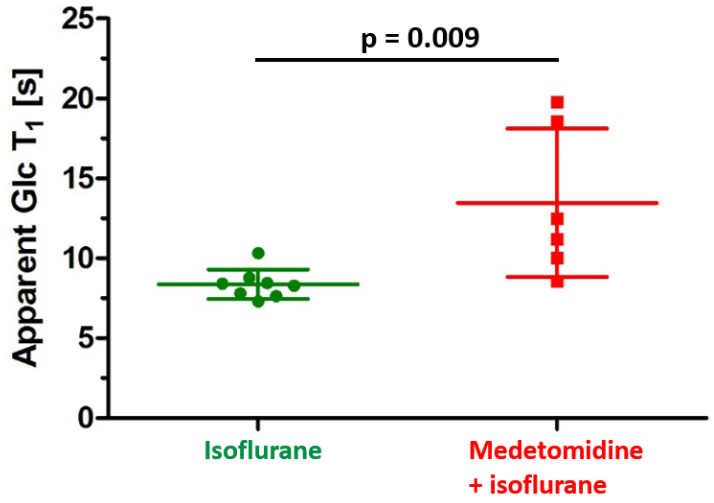


*Figure 4.8 Apparent glucose (Glc) $T_1$ in the two anesthesia groups: the glucose signal was fitted to the function $S(t) = A\,(e^{-\frac{t}{T1}} - e^{-\frac{t}{Tb}})$, $T_1$ standing for the apparent $T_1$ and $T_b$ representing the signal build-up. Unpaired, two-tailed Student's t-tests were used to assess statistical significance.*

### 4.1.4 Discussion

This study compared for the first time the cerebral metabolism of hyperpolarized glucose between animals anesthetized with isoflurane and a combination of lower doses of isoflurane and medetomidine. Our findings confirmed the initial hypothesis that the production of downstream [1-$^{13}$C] lactate would be increased when using the combination of medetomidine with a lower dose of isoflurane compared to isoflurane only, showing that the change of anesthesia had a high impact on cerebral [$^{2}H_7$,U-$^{13}C_6$]-D-glucose uptake and glycolytic flux.

#### *4.1.4.1 Increased lactate production from [$^{2}H_7$,$^{13}C_6$]-D-glucose under MED+ISO*

The glucose blood level before injection were within normal physiological concentration (6.5 ± 2 mM) and the increase of blood glucose concentration before and after injection did not exceed the typical values observed in healthy mice after glucose administration (12.5 ± 3 mM) (Nagy and Einwallner 2018).

The production of cerebral [1-$^{13}$C] lactate from [$^{2}H_7$,$^{13}C_6$]-D-glucose is a consequence of 12 enzymatic steps including glucose transport, 10 enzymatic steps of glycolysis and pyruvate conversion to lactate by lactate-dehydrogenase. Importantly, the use of medetomidine combined with isoflurane anesthesia greatly increased the labelling of downstream [1-$^{13}$C] lactate compared to isoflurane only: we found that the amount of [1-$^{13}$C] lactate and LGRs were more than doubled in animals anesthetized with the combination than with isoflurane solely. The production of

hyperpolarized [1-$^{13}$C] lactate depends on both the hyperpolarized glucose uptake and on the metabolic demands, and there are a few possible factors that may contribute to the observed differences.

First, in the literature isoflurane at clinical concentration (1.4-2.5 %) has been associated with a significantly reduced facilitated glucose transport in cells (Andersen and Amaranath 1973; Greene 1965; Greene and Cervenko 1967), a reduced local cerebral glucose utilization (LCGU) in all cortical areas (Ori et al. 1986) and a decrease in glucose metabolic rates due to the inhibition of ATP synthesis in the mitochondria in mice and rats (Kohro et al. 2001; Rottenberg 1983). Previous studies using $^{18}$F-FDG positron emission tomography also revealed a decrease of the cerebral metabolic rate of glucose under isoflurane (Toyama et al. 2004; Alkire et al. 1997). Moreover, dose-dependent anesthesia effects were reported for cerebral glucose metabolism in rats, with glucose metabolic rate decreasing up to 41–45 % in cortical regions (Ori et al. 1986; Kofke et al. 1987; Lenz et al. 1998; Stullken et al. 1977). As in our experiments the mouse cortex was well positioned under the sensitive area of the coil, the cortical areas may bring the main contribution to the measured signal and variations in LCGU between groups may explain some of the differences observed between the two groups.

Second, it is known that anesthetics such as isoflurane affect neural activity and neural processing by impacting different factors such as synaptic transmission, pre-synaptic release, post-synaptic receptors and membrane potentials (Masamoto and Kanno 2012). In the current study, we observed that a larger amount of lactate was produced in the case when the functional connectivity was similar to the awake animals (MED+ISO anesthesia) (Paasonen et al. 2018). Fox et al. were the first to show that a higher neuronal functional activity was associated with increased glucose uptake and suggesting that increased neuronal functional activity stimulates glycolysis (Fox et al. 1988; Prichard et al. 1991). It has been since claimed by several studies that an intensified neuronal activity leads to a higher release of glutamate and increases the rate of glucose uptake, glycolysis and lactate production in astrocytes, which are the preferential site for glucose uptake from the blood (P. J. Magistretti and Pellerin 1996; Pierre J. Magistretti 2006; Luc Pellerin et al. 2007). In particular, Sibson and colleagues (Sibson et al. 1998) used direct $^{13}$C NMR spectroscopy to determine the cerebral rates of the TCA cycle and glutamine synthesis simultaneously in the rat *in vivo* over a range of cerebral activity, the latter being modulated by the type of anesthesia used. Their results support a model of coupling between astrocytic glucose consumption and glutamatergic neuronal activity.

It is likely that our results are a reflection of neuronal activity, in line with these studies suggesting that glucose metabolism is linked to neuronal activity, which is decreased with isoflurane anesthesia, and that lactate production can be stimulated when neuronal activity increases (Hertz, Drejer, and Schousboe 1988; Tsacopoulos and Magistretti 1996; P. J. Magistretti et al. 1993).

#### *4.1.4.2 Differences in endogenous brain lactate and phosphocreatine assessed by $^{1}H$ MRS*

Endogenous lactate concentration was found higher in the ISO group, consistent with the known effect of isoflurane which increases lactate concentration in the brain (Valette et al. 2007; Horn and Klein 2010; Durand, Hosinking, and Jelicks 2009; Boretius et al. 2013). Particularly, Horn et al. (Horn and Klein 2010) showed that volatile anesthetics such as isoflurane cause a specific increase in extracellular lactate levels in the mouse brain and that it is not the case with intravenous nor subcutaneous anesthetics, which is coherent with our measurements. The exact mechanism of action of how volatile anesthetics increase endogenous lactate concentrations in the brain remains unknown. Importantly, Horn et al. (Horn and Klein 2010) demonstrated that lactate formation by isoflurane in the mouse brain was unrelated to neuronal impulse flow. Overall, our findings (increased downstream lactate's labelling in the MED+ISO group and higher endogenous lactate concentration in the ISO group) imply that [1-$^{13}$C] lactate production from hyperpolarized glucose is not a reflection of the steady-state pool-size but rather related to the dynamic of the glucose uptake and glycolytic flux.

Additionally, the Cr/PCr ratio, related to ATP and ADP balance, was found significantly different between the two groups. Our results suggest a difference in the energetic state between the two anesthetics groups. The shift of phosphocreatine towards creatine in the ISO group may indicate a diminished brain energy stores (ATP, PCr), similar to what has been reported on *in vivo* studies on mice under isoflurane (Boretius et al. 2013) or in post mortem studies of dogs under halothane anesthesia (Michenfelder and Theye 1975). Finally, similar to what has been reported previously (Boretius et al. 2013), we measured increases in myo-inositol, glutamate and GABA concentrations in the ISO group, without reaching significance.

#### *4.1.4.3 Liquid-state polarization*

Concerning polarization achieved, we obtained a liquid-state polarization close to 30 %, which is lower than reported by Capozzi et al. (Capozzi et al. 2019). These differences are surely due to the differences in the set-up used (polarizer, microwave source, fluid path). However, we achieved a

higher polarization than that reported by Mishkovsky et al. (Mishkovsky et al. 2017) using [$^{2}H_{7}$, U-$^{13}C_{6}$]-D-glucose without $Gd^{3+}$ doping (22 %) in the same set-up as the one used in the present study.

#### *4.1.4.4 Increased blood lactate using ISO, decreased $PO_2$ and increased $PCO_2$ using MED+ISO*

In the ISO group, blood lactate concentration was more than doubled. This significant increase is in agreement with several studies reporting that blood lactate concentration significantly increased by 2-3 fold during inhalation of volatile anesthetics such as isoflurane or halothane, probably due to the interference of volatile anesthetics with mitochondrial energy metabolism (Horn and Klein 2010; Schwarzkopf et al. 2013; Muravchick and Levy 2006). The rose of partial pressure of carbon dioxide ($PCO_2$) along with the decrease of partial pressure of oxygen ($PO_2$) measured in the MED+ISO group match the results observed in earlier studies, who also reported that isoflurane anesthetics did not induce any change in $PO_2$ and $PCO_2$ (Schwarzkopf et al. 2013).

#### *4.1.4.5 [$^{2}H_{7}$,$^{13}C_{6}$]-D-glucose apparent $T_1$*

The glucose spin-lattice relaxation time $T_{1glc}$ obtained under the two different anesthetics conditions are similar to previously reported $T_{1glc}$ in a study measuring hyperpolarized [$^{2}H_{7}$, U-$^{13}C_{6}$]-D-glucose in cells (Christensen et al. 2014) and *in vivo* in the mouse brain under isoflurane anesthesia (Mishkovsky et al. 2017). Regarding the differences in the apparent $T_1$ between the two anesthetics groups, a possible explanation is linked the difference of the cerebral glucose uptake in each group during the timeframe of the experiment. Being higher in the MED+ISO group, it contributes to a longer apparent $T_1$ in this group, similar to what has been observed with hyperpolarized compound when the uptake is increased by the transient opening of the blood-brain barrier. Another possible explanation, although less likely, might be linked to the paramagnetic property of molecular oxygen itself. Partial pressure of oxygen ($PO_2$) differed significantly between mice anaesthetized with isoflurane or the combination of isoflurane and medetomidine. Tadamura et al. (Tadamura et al. 1997) demonstrated that inhalation of 100% oxygen causes statistically significant shortening of $T_1$ relaxation times in blood and postulated that the observed $T_1$ change in the blood directly reflects the dissolved oxygen concentration, which is proportional to $PO_2$. Other previous studies also showed reduction in $T_1$ relaxation time of the blood after inhalation of oxygen (Young et al. 1981). Thus, as $PO_2$ was 50% higher in the ISO group than in the MED+ISO group, the differences in apparent $T_1$ between the anesthetics groups can be explained in part by the physical property of molecular oxygen. However, this second hypothesis should be carefully considered as it is also possible that differences in $SO_2$ (%), linked to deoxyhemoglobin which is much more paramagnetic than dissolved $O_2$, may have contributed

to the observed difference between apparent $T_1$ values. These values were however not measured in the two anesthetic groups. Further measurements remains to be performed to test these hypotheses.

In the present study, due to the experimental constraints, blood glucose was monitored only before the mice enter the scanner (70 min before injection) and immediately after injection. However, both isoflurane and medetomidine are known to increase blood glycemia, which can be a source of error. Isoflurane has been shown to increase blood glycemia up to 38-47 % in C57BL/6 mice within the first 5 minutes after anesthesia administration (Durand, Hosinking, and Jelicks 2009; Schwarzkopf et al. 2013) and up to two-fold increase in female CD-1 mice. Several reports have shown a similar effect of medetomidine on blood glycemia (Kanda and Hikasa 2008; Guedes and Rude 2013). In both cases this effect is induced by the decrease of insulin secretion. Therefore, considering the comparable effect of isoflurane and medetomidine on blood glycemia reported in the literature and that in both group anesthesia is first induced with isoflurane, we assumed that injecting a given dosage of hyperpolarized [$^{2}H_{7}$,$^{13}C_{6}$]-D-glucose would result in similar glycemia after injection in the two anesthetized groups. Our results tend to confirm this hypothesis as no differences between the two anesthetics group either in blood glycemia nor glucose fractional enrichment were observed (Figure 4.4).

Of note, in this study blood fractional enrichment was computed with a theoretical blood volume derived from the mouse body weight ("Mouse : Decision Tree for Blood Sampling | NC3Rs" n.d.), the initial blood glucose concentration, and the volume and concentration of the [$^{2}H_{7}$,$^{13}C_{6}$]-D-glucose solution injected, the latter being measured using high resolution NMR. However, a more direct method of measuring the blood [$^{2}H_{7}$,$^{13}C_{6}$]-D-glucose concentration (e.g measuring from plasma directly in high resolution NMR) would be preferable, as it would not neglect the potential effect of each anesthesia on blood volume. It is also important to point that different strains can respond differently to anesthetics and analgesics, depending partly on variations in the genetic background of experimental animals (Avsaroglu et al. 2007). Thus, the results obtained in this study should be interpreted cautiously, bearing in mind that all measurements were made in male C57BL6/J mice.

In order to evaluate in more detail how the two different types of anesthesia influence the transport of blood glucose and lactate through the BBB, we will perform $^{2}H$ MRS measurements just before and immediately after the injection of a deuterated glucose bolus under the two anesthetics conditions (ISO and MED+ISO). In the same way, we will perform $^{1}H$ MRS before and after the injection of a bolus of lactate.

Despite its few limitations, an important advantage of this study is that it is carried out under nearly physiological conditions. First, glucose is the main energy substrate in the adult brain under physiological conditions. In this sense, our study differs from many research using hyperpolarized pyruvate, for example, which is not a fuel used by the brain under normal conditions. Second, the use of hyperpolarized glucose allows us to study the cerebral metabolism of glucose at physiological concentrations, which is not possible when using thermally polarized $^{13}C$ MRS in particular, due to its low sensitivity. Finally, the choice of anesthesia reported to preserve connectivity similar to the awake state (MED+ISO) brings us a little closer to the normal physiology of the brain.

Overall, we showed for the first time the effect of anesthetics on the cerebral metabolism of hyperpolarized [$^{2}H_{7}$,U-$^{13}C_{6}$]-D-glucose. The present study revealed that the production of downstream [1-$^{13}C$] lactate were greatly increased when using the combination of medetomidine with a lower dose of isoflurane, which is a lighter anesthesia than isoflurane alone, showing that the change in anesthetics had a high impact on cerebral [$^{2}H_{7}$,U-$^{13}C_{6}$]-D-glucose uptake and glycolytic flux. It also highlights the important effect that anesthetics can create on the outcome of a pre-clinical experiment performed in animal and stresses the importance of taking this factor into account before interpreting the results and extrapolating them to humans. Also, the higher SNR reported in this work is a step toward real-time imaging of cerebral glycolysis. There are still debate about the role of non-oxidative metabolism in the brain, and hyperpolarized [$^{2}H_{7}$,U-$^{13}C_{6}$]-D-glucose can be a promising tool to give further insights and elucidate the remaining questions. Further studies need to be carried out, however, in order to better characterize the differences in non-oxidative metabolism of glucose between awake and anesthetized animals. Further research might perform similar experiment on awake animals or on animal under stimulation (visual, for example).

## 4.2 Modelling the kinetics of cerebral lactate production after hyperpolarized [$^2H_7$, U-$^{13}C_6$]-D-glucose infusion

### 4.2.1 Introduction

In the first part of the chapter (Chapter 4.1), we showed that lactate was detected shortly after injection of hyperpolarized [$^2H_7$,$^{13}C_6$]-D-glucose and the labelling of downstream lactate was greatly enhanced when using medetomidine combined with isoflurane anesthesia, with well-defined and reproducible time courses. As a second step, our goal was to explore the potential of hyperpolarized glucose as a useful complement to fluorodeoxyglucose (FDG)-PET, informing on glucose metabolism rather than glucose uptake. This part aimed thus at evaluating the feasibility of quantifying cerebral glucose metabolism kinetics following infusion of hyperpolarized [$^2H_7$, U-$^{13}C_6$]-D-glucose in a healthy mouse.

### 4.2.2 Methods

The production of cerebral [1-$^{13}$C] lactate from [$^2H_7$,$^{13}C_6$]-D-glucose is the results of 12 enzymatic steps including glucose transport, 10 enzymatic steps of glycolysis and pyruvate conversion to lactate by lactate-dehydrogenase (LDH). When injecting hyperpolarized [$^2H_7$,$^{13}C_6$]-D-glucose, the time courses of [$^2H_7$, U-$^{13}C_6$]-D-glucose and [1-$^{13}$C] lactate were measured with the tailored RF pulses design used, as described in the first part of this chapter (Chapter 4.1). A kinetic compartmental model describing the dynamic $^{13}$C labelling pattern following the metabolism of [$^2H_7$, U-$^{13}C_6$]-D-glucose was developed and is mathematically represented by a system of coupled differential equations; the labelling equations (Lanz 2012). To minimize the risk of overfitting, to keep the model as stable as possible and to obtain interpretable and informative kinetic rate constants as output, we chose to restrict ourselves to a model with 3 or 4 compartments, which can be further developped in a second step. Therefore, from a simplified schematic of glucose metabolism (Figure 4.9), two multisite kinetic models (3- and 4- compartment models, Figure 4.10) were derived and tested using the following assumptions:

(1) Each step was modelled as a first-order reaction, similar to what has been done previously when modelling hyperpolarized compound kinetics (Bastiaansen et al. 2015; Vinckenbosch 2018).

(2) A single apparent glucose to pyruvate turnover rate constant (3-compartment model) or glucose to intermediate pool (4-compartment model) turnover rate constant encompassed the combined effect of glucose transport through the blood-brain barrier, transport into cells and the intermediate steps of glycolysis.

(3) Opposite rate constants of reversible reactions are independent.

(4) Pyruvate plays a central role in the metabolism of all animal cells. Pyruvate can either be converted into alanine by alanine aminotransferase (ALT), transported into the mitochondrial matrix via mitochondrial pyruvate carriers (MPCs), or reduced to lactate by lactate dehydrogenase (LDH, Figure 4.9). Here, given the time course of our study and assuming that the exchange between pyruvate and lactate is much faster than the entry into the TCA cycle and the conversion to alanine (Quek et al. 2016), neither $V_{MPC}$ nor $V_{ALT}$ of pyruvate were included in either kinetic model.

(5) Since lactate and pyruvate resonances are close to each other (183.5 ppm and 171.1 ppm, respectively), the same flip angle was considered to be applied for both metabolites' resonances.

The measured signal decay of precursor and metabolites ($M_{13glc}$ and $M_{13Lac}$) is a combination of the effects of repeated RF excitations applied every TR seconds, longitudinal relaxation $T_1$ (included in the equations as relaxation rate $R_1 = 1/T_1$), and biochemical conversions. All were included in the differential equations of the model, resulting in:

**3-compartment model:**

$$\frac{d}{dt} M_{13Pyr} = 2k_{GlcPyr}\, IF + k_{LacPyr}\, M_{13Lac} + \left[-k_{PyrLac} - R_{1pyr} + \frac{\ln(\cos\alpha)}{TR}\right] M_{13Pyr} \qquad 4.1$$

$$\frac{d}{dt} M_{13Lac} = k_{PyrLac}\, M_{13Pyr} + \left[-k_{LacPyr} - k_{out} - R_{1Lac} + \frac{\ln(\cos\theta)}{TR}\right] M_{13Lac} \qquad 4.2$$

**4-compartment model:**

$$\frac{d}{dt} M_{13Ip} = 2k_{GlcIp}\, IF + \left[-k_{IpPyr} - R_{1Ip} + \frac{\ln(\cos\beta)}{TR}\right] M_{13Ip} \qquad 4.3$$

$$\frac{d}{dt} M_{13Pyr} = k_{IpPyr}\, M_{13Ip} + k_{LacPyr}\, M_{13Lac} + \left[-k_{PyrLac} - R_{1pyr} + \frac{\ln(\cos\alpha)}{TR}\right] M_{13Pyr} \qquad 4.4$$

$$\frac{d}{dt} M_{13Lac} = k_{PyrLac}\, M_{13Pyr} + \left[-k_{LacPyr} - k_{out} - R_{1Lac} + \frac{\ln(\cos\theta)}{TR}\right] M_{13Lac} \qquad 4.5$$

$M_{13Lac}$, $M_{13Pyr}$ and $M_{13Ip}$ denote the time-varying signal amplitude of the corresponding $^{13}C$ metabolites/pools. The glucose signal is used as input function: IF = $^{13}Glc(t)$ and the time course of lactate is fitted. k represent the different kinetic rate constants, which are free parameters. R denotes the relaxivity [$s^{-1}$], TR the repetition time of the RF pulses and α and θ are the RF nominal flip angles of pyruvate and lactate, respectively. As mentioned previously, since both resonances are close to each other the same flip angle was considered to be applied for both metabolites'

resonances. The RF excitation flip angle was 25°, applied with a repetition time TR = 1 s. [1-$^{13}$C] lactate and pyruvate spin-lattice relaxation times ($T_{1Lac}$ and $T_{1Pyr}$) were both set to be 18 s, as reported in the study from Christensen and colleagues where they measured the intracellular relaxation time $T_{1Lac}$ and $T_{1Pyr}$ in different cell lines after injection of hyperpolarized glucose (Christensen et al. 2014). Of note, they also showed in this study that $T_{1Lac}$ and $T_{1Pyr}$ were approximately doubled in extracellular space. In our case, it is assumed that pyruvate and lactate from hyperpolarized glucose are predominantly intracellular and this parameter was initially set close to the reported intracellular relaxation time value. Regarding the parameters of the intermediate pool in the 4-compartment model, as this pool does not correspond to a specific metabolite, $T_{1Ip}$ was set to vary around 25 s and the nominal flip angle between 1° and 25°. All the parameters included in the model can obviously influence the model's output, so the impact of spin-lattice relaxation time and flip angle parameters on the kinetic rates output were also evaluated.

Kinetic rate constants were determined by fitting the mathematical model to the *in vivo* measured $^{13}$C turnover curves by non-linear regression using the Levenberg-Marquardt algorithm (Marquardt 1963). The Levenberg-Marquardt algorithm is an iterative process used to solve non-linear least squares problems which often depend on several variables. In our case, the kinetic rates are the free parameters of the regression and the optimization process of the algorithm tends to minimize the sum of squared residuals (SSR):

$$\mathrm{SSR} = \sum_{i}^{N} (y(t_i)_{measured} - y(t_i)_{fitted})^2 \qquad 4.6$$

To assess the reliability of the determined free parameters (kinetic rates) and to test the stability of the model, Monte-Carlo simulations were performed: random Gaussian noise of same level as the experimental noise (whose amplitude was estimated from the difference between the best fit and the experimental data) was added to the experimental data before fitting the model and extracting the resulting parameters; the kinetic rates in the present case. The statistical distribution of each output parameter was derived by repeating this process several times, typically 100-200 times. Modelling and analysis were first performed on animal group averaged time courses. In addition to Monte Carlo simulations, the stability and robustness of the model was also assessed using different approaches:

(1) Variation of the initial conditions: the initial values of the kinetic rates were all varied in a range from 0.01 to 0.5 $s^{-1}$. Note that the minimum value was set to 0.01 $s^{-1}$ because as in the regression

the values are varied as a percentage of their initial value, they would not deviate from zero in the iterative process if they are set too low initially.

(2) Evaluation of the correlation matrices: the covariances between the estimated metabolic fluxes give indications about the extent to which free parameters influence each other. They were examined in order to assess the complexity of the model. The more correlated the fluxes are, the more it indicates an overly complex model.

(3) Modelling of individual animal (N=6): after the analysis performed on the average lactate and glucose time courses, each animal was modelled individually.

Note that all the kinetic rate constants are apparent rates, and the true reaction rates can fluctuate over time. Both models were developed in Matlab (MathWorks, Natick, MA, USA).

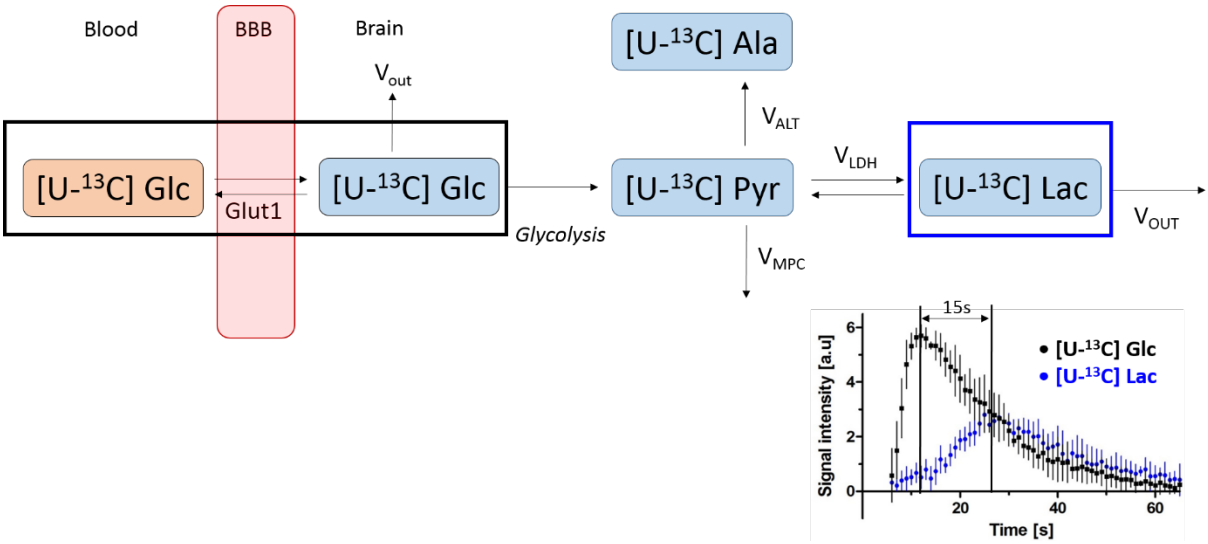


*Figure 4.9 Simplified schematic of [1-$^{13}$C] glucose metabolism. Transport of glucose across the blood-brain barrier (BBB) is accomplished by a facilitated glucose transporter, the glucose transport protein GLUT-1, which is embedded in the endothelial cell membrane. Glucose is oxidized during the 10 steps of glycolysis and the final enzyme of glycolysis yields two molecules of pyruvate. Pyruvate is either converted into alanine by alanine aminotransferase (ALT), transported into the mitochondrial matrix via mitochondrial pyruvate carriers (MPCs), or reduced to lactate by lactate dehydrogenase (LDH). In our experiments, both [U-$^{13}$C] glucose (black) and [1-$^{13}$C] lactate (blue) time courses are measured.*

*Note that for simplicity purpose, only the main glucose transporter Glut1 is depicted on the figure. Similarly, the major glucose transporters of glucose in neurons (Glut3) and in astrocytes (Glut1) are not shown.*

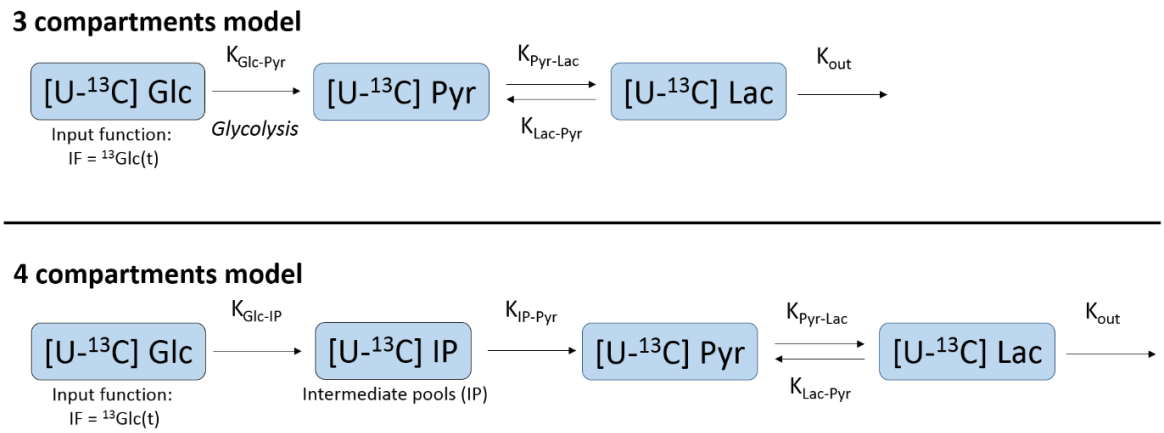


*Figure 4.10 Kinetic models. In the 3-compartment model (top), only glucose, pyruvate and lactate pools were considered. In the 4-compartment model (bottom), an intermediate pool was added. In both models [U-$^{13}$C] glucose signal was used as the input function.*

### 4.2.3 Results

As a first step, we attempted to model both the results obtained with isoflurane and with the combination of medetomidine and isoflurane in order to compare them. However, the low SNR of the lactate signal under isoflurane did not enable reliable modelling, so we first focused on the results obtained under MED+ISO to optimize the modelling approach and the model complexity.

As expected, a simple two-compartment model could not explain the experimental data obtained (data not shown). On the other hand, the fits obtained with the 3- and 4-compartment models were relatively good (Figure 4.11A). The fit was improved with the 4-compartment model, reducing the SSE by 15 % compared to the 3-compartment model. This difference between the two fits is mainly visible in the build-up of the lactate curve.

Since the exchange rate between lactate and pyruvate is much faster than the conversion of glucose to pyruvate (Quek et al. 2016), the following prior knowledge was added in each of the models: the kinetic rate constant $k_{Glc\text{-}Pyr}$ was forced to be lower than $k_{Pyr\text{-}Lac}$ (3-compartment model) and $k_{Glc\text{-}IP}$ or $k_{IP\text{-}Pyr}$ to be lower than $k_{Pyr\text{-}Lac}$ (4-compartment model).

In the 3-compartment model, both the variation of the initial conditions and the Monte Carlo simulations gave kinetic rates output in the same range, showing that the model is relatively robust (Figure 4.11B, Figure 4.11C). The variance of these parameters was slightly higher in the 4-compartment model. However, it is particularly by considering the correlations between the kinetic rate constants (Figure 4.11D) that we noticed that the increased complexity of model 3 (addition of an intermediate pool and a new kinetic rate) did not improve the modelling. Indeed, the off-diagonal covariance was increased in the 4-compartment model and the interpretation of

the kinetic rate constants is thus difficult. In model 3, the number of free parameters decreases and are therefore less dependent on each other : only the kinetic rates $k_{Glc\text{-}Pyr}$ and $k_{Pyr\text{-}Lac}$ are anti-correlated, which can be explained by the fact that the delay between the glucose and lactate signals is necessarily created by one or the other of these two steps. Thus, the rest of our analysis focused on the 3-compartment model (Figure 4.12).

The results of the individual mice were in the same range as those obtained by varying the initial conditions and by Monte Carlo simulations on the average data, confirming the good reproducibility of the data (Figure 4.12A).

As expected, the variation of the flip angle (fixed parameter) had a greater influence on the kinetic rate outputs than the spin-lattice relaxation $T_1$ value (Figure 4.12B, Figure 4.12C). Interestingly, less variability was observed in the kinetic rates output around our estimated values of $T_1$ and flip angle (18 s and 24°, respectively). Of note, setting the $T_1$ value around 30-40 s resulted in a slight reduction in $k_{Glc\text{-}Pyr}$ and a slight increase in $k_{Pyr\text{-}Lac}$ and $k_{out}$.

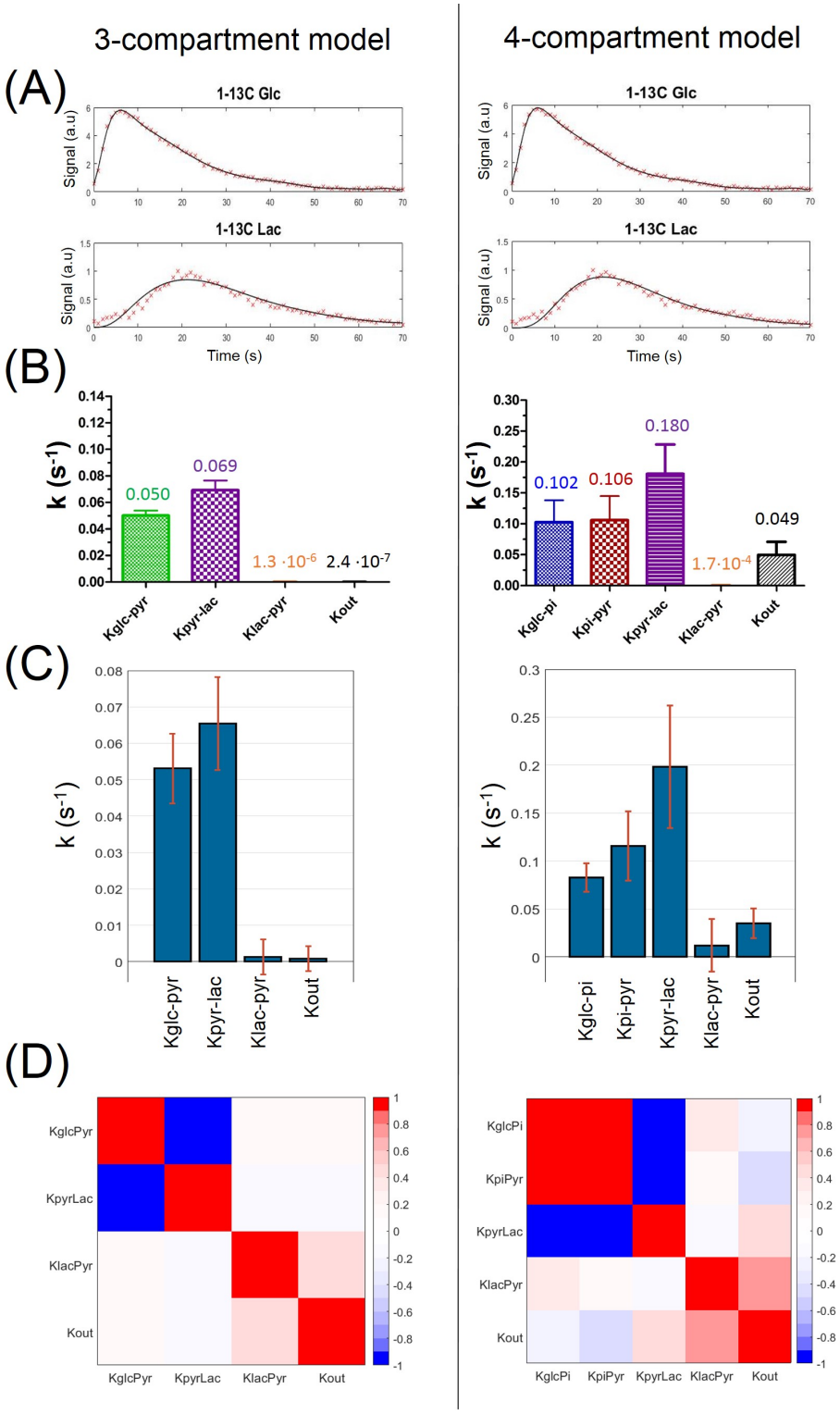


*Figure 4.11 Comparison of 3- and 4- compartment model. (A) Typical fits obtained with the two models. Glc and Lac are the average signals obtained in the MED+ISO group (n=6). (B) Kinetic rate constants deduced after fitting both models to experimental data (average Glc and Lac signals) with varying initial conditions (N=100). (C) 100 Monte-Carlo simulations were performed to evaluate the precision and accuracy of the different output kinetic rates. (D) Typical correlation matrices between estimated metabolic fluxes. These matrices are derived from the regression on the averaged Glc and Lac signals in the MED+ISO group (n=6). The off-diagonal covariance is increased in the 4-compartment model by adding an intermediate pool and a kinetic rate constant.*

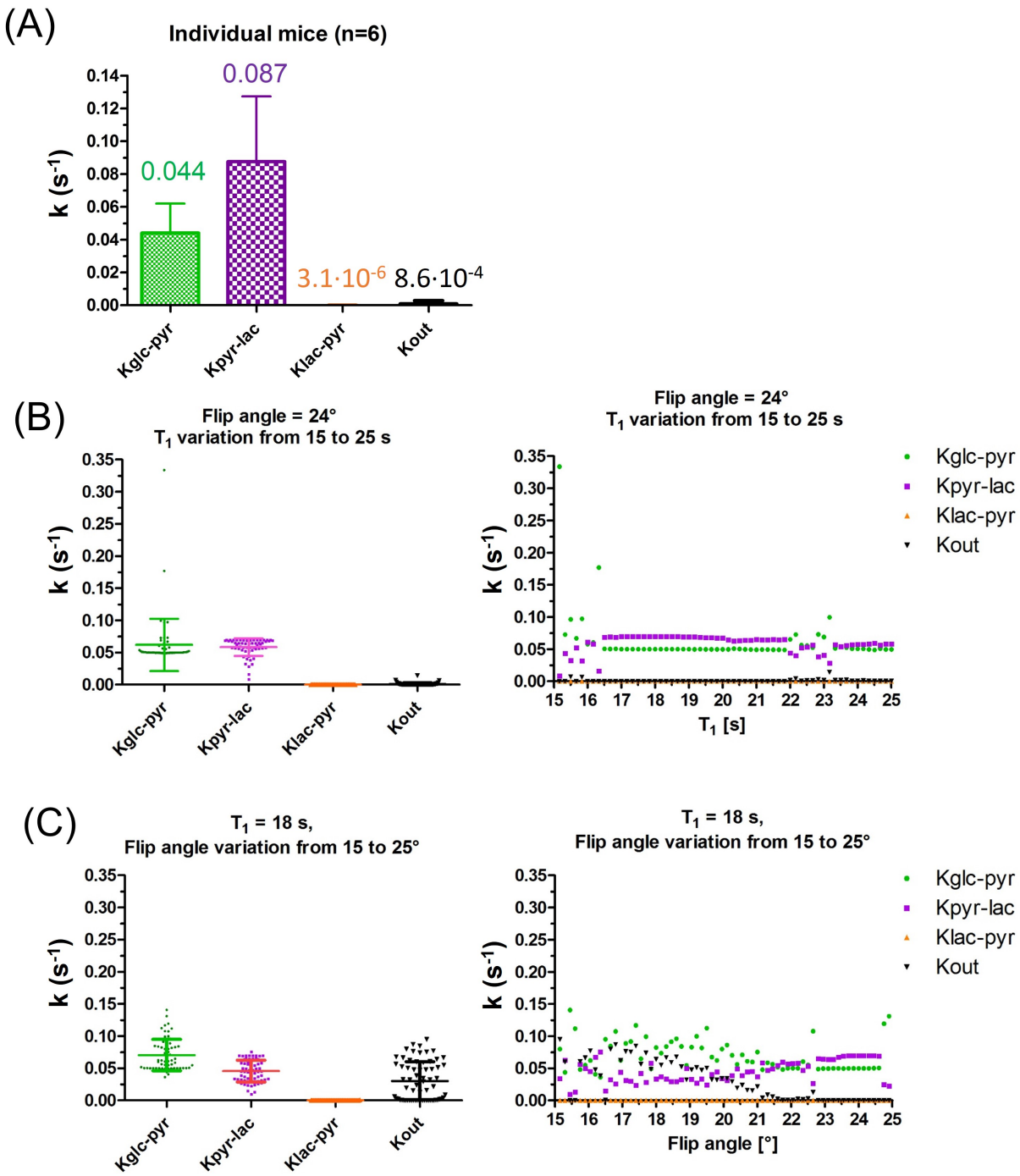


*Figure 4.12 3-compartment model. (A) Kinetic rate constants on single animals (MED+ISO, N=6). (B+C) Impact of flip angle and $T_1$ on model's kinetic rates output: flip angle fixed with varying $T_1$ of lactate and pyruvate (B) and $T_1$ fixed with varying flip angle for lactate and pyruvate (C). Of note, in these analyses no prior knowledge was added, i.e the kinetic rate constant $K_{Glc\text{-}Pyr}$ was not forced to be lower than $K_{Pyr\text{-}Lac}$.*

### 4.2.4 Discussion

Overall, the signal obtained after infusion of hyperpolarized [$^{2}H_7$, U-$^{13}C_6$]-D-glucose with the combination of medetomidine and isoflurane anesthesia is promising for obtaining quantitative information on the kinetics of cerebral glucose metabolism. Both 3- and 4- compartment model fitted overall well the data. However, unlike the 4-compartment model, the 3-compartment model appeared to be more stable and robust: both the variation of the initial conditions and the Monte Carlo simulations gave kinetic rates constants in the same range, and low variability was observed in the kinetic rates output around our estimated values of $T_1$ and flip angle.

The increased variance of the kinetic rates output and the higher covariance between the kinetic parameters indicate that the 4-compartment model is probably too complex. Indeed, the two added kinetic rates ($k_{Glc\text{-}IP}$ and $k_{iP\text{-}Pyr}$) were fully correlated and thus hardly interpretable from a biochemical point of view, indicating that the complexification of the model at this point did not make it more meaningful. Overall, the addition of a fourth compartment did not improve the model.

We noted that in both models, the error between the fit and the lactate data was mostly at the beginning. This may be in part due to the fact that the measured lactate signal is composed of both blood and brain signals. Red blood cells produce the energy carrier ATP by the glycolysis of glucose and lactic acid fermentation on the pyruvate, thus contributing to the overall signal measured. Therefore, even if the contribution of the blood signal is small overall, the lactate signal measured already 2 s after injection may contain a blood component as lactate is produced by red blood cells. Later in the time course, the error between the fit and the data is probably due to the simplification of both the cerebral glucose uptake and the 10 steps of glycolysis to only one or two steps. In spite of this, the fit remained relatively good and the kinetic rates values obtained should be compared with those of the literature.

In the 3-compartment model, we found $k_{Pyr\text{-}Lac}$ in the same range as what was reported by Marjańska et al. (Marjańska et al. 2018) with hyperpolarized [1-$^{13}$C] pyruvate in the rat brain and by Lê et al. in the mouse brain ("(ISMRM 2019) Kinetic Modeling of Hyperpolarized [1-13C]Lactate Metabolism in a Mouse Model of Ischemic Stroke" n.d.), although slightly higher. It is also similar to what was obtained by Khegai et al. (Khegai et al. 2014) where they used hyperpolarized [1-$^{13}$C] pyruvate and reported an apparent kinetic rate constant $k_{Pyr\text{-}Lac}$ between 0.05 $s^{-1}$ and 0.1 $s^{-1}$ in healthy subcutaneous tissue in rats, although this last comparison should be taken with caution as it was not measured in brain tissue. Overall, compared to the literature modelling hyperpolarised

data, our $k_{Pyr\text{-}Lac}$ seems reliable, although the comparison is a little delicate. Indeed, in the present study, the lactate measured comes mainly from brain tissue and the $k_{Pyr\text{-}Lac}$ obtained represents only the activity of the LDH enzyme. Whereas in studies using hyperpolarised pyruvate, the kinetic rate reported represents the combined effect of transport through the BBB, transport in the cell and enzyme activity. This may explain the fact that $k_{Pyr\text{-}Lac}$ obtained in the present study is slightly higher than those reported in previous studies. Regarding $k_{Lac\text{-}Pyr}$ and $k_{out}$, given that the endogenous cerebral lactate concentration is approximately 20 times higher than that of pyruvate (Ross 2014) and the duration of our experiment, the lactate fractionnal enrichment is thus low and fluxes of $^{13}C$ labelled lactate leaving the lactate pool are also limited in this timeframe. The reported values of $k_{Lac\text{-}Pyr}$ and $k_{out}$ are therefore meaningful in this context. To the best of our knowledge, no studies using hyperpolarized glucose *in vivo* reported cerebral apparent kinetic rate constants. Rather, the cerebral metabolic rate of glucose ($CMR_{glc}$) is reported together with a series of mitochondrial fluxes and apparent neurotransmission fluxes in studies using thermally polarized $^{13}C$-labelled glucose infusion. One of the challenges of modelling with hyperpolarized compounds is the conversion of the kinetic rates obtained into interpretable fluxes; thus the comparison is delicate. However, in an attempt to compare values even if the steady-state assumption is not valid in the present case, the $CMR_{glc}$ reported by different studies can be converted into an estimate of the corresponding $k_{Glc\text{-}Pyr}$. In a recent study of Lai and colleagues (Lai et al. 2018), they reported $CMR_{glc} \approx 0.38 \pm 0.02$ µmol/g/min. Using an estimated brain glucose concentration reported by Gruetter et al. (assuming that the concentration is similar in rodents and in humans ≈ 1.0 ± 0.1 µmol/ml (Gruetter et al. 1992)) and the approximate density of the mouse brain (≈ 1000 g/l (Badea, Ali-Sharief, and Johnson 2007)) one finds $k_{Glc\text{-}Pyr} \approx \frac{0.38\,\frac{\mu mol}{g \cdot min} \cdot 1000\,\frac{g}{l}}{1.0\frac{\mu mol}{ml} \cdot 60\,s} \approx 0.007\ s^{-1}$. This value is about 7 times smaller than the $k_{Glc\text{-}Pyr}$ found with our model. Overall, based on these results we believe that $k_{Pyr\text{-}Lac}$ is reliable, although slightly overestimated by the model, while $k_{Glc\text{-}Pyr}$ is more markedly overestimated. Regarding this last point, it is important to note that animal studies reporting $CMR_{glc}$ are mainly performed using isoflurane as an anesthetic, which may have a strong influence on cerebral glucose uptake and metabolism, as it has been shown in different studies (Sibson et al. 1998; Henry P-G, Ugurbil K, Gruetter R., n.d.) and in the first part of the chapter (Chapter 4.1). It has indeed been shown that the $V_{TCA}$ cycle rate in rats was approximately doubled with morphine, a mild anesthesia, compared to a deeper anesthesia such as alpha-chloralose or isoflurane (Sibson et al. 1998). It is therefore possible that the change in anesthesia results in an increased $CMR_{glc}$.

There are also other limiting factors such as the fact that the signal does not come from a localized sequence. There is hence a potential influence of the difference in metabolism in the different regions of the coil's field of view as well as the effects of flip angle difference ($B_1$ heterogeneity). It is also likely that glucose uptake is the limiting factor and that a non-negligible part of the measured glucose signal originates from the blood or the extracellular space in the timeframe of our experiment. In the study from Christensen and colleagues where they measured hyperpolarized glucose in different cell lines, they reported that only a small fraction of the hyperpolarized glucose takes part in the glycolysis and that the remaining stays extra-cellular (Christensen et al. 2014). Thus, an essential information to be added to the model would be that of glucose uptake. One possibility would be to use the information provided by a PET scan using fluorodeoxyglucose in a mouse under the same conditions (anesthetized with a combination of isoflurane and medetomidine), where the input function and tissue glucose uptake could be measured at the same time. This would add a very important information to the model and considerably improve it. Another interesting input to the model would be that of lactate dehydrogenase (LDH) activity in brain tissue. Furthermore, and more generally, when interpreting the modelling results, it is important to bear in mind that the accuracy of the results is highly dependent on the validity of the modelling assumptions.

In this section, we have paved a new way for quantifying cerebral glucose metabolism kinetics, especially of glycolysis, following infusion of hyperpolarized [$^{2}H_7$, U-$^{13}C_6$]-D-glucose in the healthy mouse. We showed that with our data, a 3-compartment model is more stable and reliable than a 4-compartment model. Despite some area for improvement, the model is promising. A robust model has the potential to improve the understanding of diseases with a disrupted cerebral energy metabolism, such as hepatic encephalopathy. It can provide a valuable tool for quantitatively comparing metabolic rates in different conditions, for example by comparing control and diseased groups. The addition of glucose uptake data obtained with PET scan would be a great improvement and we plan to conduct these experiments in the near future. In addition, a further increased SNR could provide a measurable pyruvate time course, which would also contribute to the improvement of the estimation of the kinetic rate constants.

# Chapter 5 Exploring the potential of hyperpolarized $^{6}Li$ to study lithium bio-distribution in the rat brain

## Abstract

Lithium salts are widely used for treating bipolar disorder but its mechanism of action is still not clearly understood. Dissolution DNP can be successfully applied to hyperpolarize $^{6}Li^{+}$ salts to high levels (van Heeswijk et al. 2009; Balzan et al. 2016). The goal of the present study was to evaluate the potential of hyperpolarized $^{6}Li$ injected at pharmacological doses to assess its real-time bio-distribution and pharmacokinetic in the rat brain. The dynamic of hyperpolarized $^{6}Li$ at pharmacological doses in the rat brain was assessed by performing several different *in vivo* and *ex vivo* experiments in a 9.4 T animal scanner. A dedicated coil was designed and built and consisted of a modified Alderman-Grant coil tuned to $^{6}Li$ and a $^{1}H$ surface coil. We found that the transport of lithium through the intact blood-brain barrier brain during the time of $^{6}Li$ hyperpolarization is a limiting factor. However, despite the limitations associated with the slow transport through the blood-brain barrier, we believe that hyperpolarized lithium still has the potential for promising applications given its very long intrinsic $T_1$, the good SNR obtained with our protocol, and the striking difference we found between apparent $T_1$ values in a brain with normal or disrupted blood-brain barrier.

Partially adapted from:

**E.Flatt**, A. Capozzi, R.Gruetter, M.Mishkovsky. Exploring the potential of hyperpolarized $^{6}Li$ to study lithium bio-distribution in the rat brain at 9.4T, manuscript in preparation.

I contributed to the design of this study, built the coil for *in vivo* measurements, collected and processed the data, interpreted the results and wrote the paper.

## 5.1 Introduction

Lithium carbonate is a widely used medication for the treatment of bipolar disorder, yet its mechanism of action is still not clearly understood. MRS is uniquely capable of directly and noninvasively measuring lithium in its target organ, the brain. It has been shown in animal and clinical studies that cerebral lithium concentration can be quantified by the $^{7}$Li MRS signal following lithium therapy, the latter lasting several days (Komoroski et al. 1990; S Ramaprasad 2004). However, due to the limited sensitivity of $^{7}$Li MRS, this technique does not provide real-time dynamic information (Soares et al. 2001) and the authors of these papers postulated that although MR techniques have been used to measure lithium in animal models and humans in several studies, improvements in spatial resolution and signal-to-noise ratio (SNR) are needed for detailed mapping of lithium in the brain. The advent of spin hyperpolarization techniques and in particular the dissolution DNP method (Ardenkjær-Larsen et al. 2003) enables to boost *in vivo* MRS sensitivity (Comment and Merritt 2014; Golman, Zandt, and Thaning 2006). Metabolic intermediates that were considered invisible became highlighted *in vivo* following the infusion of suitable hyperpolarized substrates (Mishkovsky, Comment, and Gruetter 2012; Rodrigues et al. 2014). Although most *in vivo* applications have focused so far on metabolic studies following the injection of hyperpolarized $^{13}$C-labeled precursors (Comment and Merritt 2014), hyperpolarization techniques can be applied to enhance the signal of small molecules for use as contrast agents for angiography and perfusion MRI (Golman and Petersson 2006; Duhamel et al. 2001; A. K. Grant et al. 2011).

Although being spin I = 1, the long $T_1$ of $^{6}$Li and its tiny quadropolar moment (Wehrli 1976; Ronconi and Sadler 2008) makes it a good candidate as a hyperpolarized bioprobe. Indeed, recent studies reported that the longitudinal relaxation times ($T_1$'s) of lithium-6 in oxygenated blood, deoxygenated blood and *in vivo* are as long as 161 ± 2 s, 144 ± 2 s, and 75 ± 5 s respectively. The slow longitudinal relaxation rate of hyperpolarized $^{6}$Li in biological systems makes it an attractive tool to study lithium pharmacokinetic in real-time.

In most of the *in vivo* applications of hyperpolarized MRS, the metabolic precursors are administered at supra-physiological concentrations. This is also the case with lithium, where it was demonstrated that hyperpolarized $^{6}$Li can be detected in the rat brain when injected at a dose much higher than the pharmacological dose (van Heeswijk et al. 2009). However, given the narrow therapeutic window of lithium (0.6-1.2 mM) and its high toxicity (>2mM in serum) (Thase and Denko 2008), any potential *in vivo* implementations should be restricted to its pharmacological doses or below. Therefore, the goal of the present study was to evaluate the potential of

hyperpolarized $^{6}$Li injected at pharmacological doses to assess its real-time bio-distribution and pharmacokinetic in the rat brain.

## 5.2 Material & Methods

### 5.2.1 Modified Alderman-Grant coil

First, a dedicated coil was designed and built and consisted of a modified $^{6}$Li Alderman-Grant coil (C. V. Grant et al. 2009) and a $^{1}$H surface coil, as this type of coil provide a much more homogeneous $B_1$ field compared to surface coils which were previously used for *in vivo* studies of $^{6}$Li in the rat brain (van Heeswijk et al. 2009).

### 5.2.2 *In vivo* measurements with modified Alderman-Grant coil

*In vivo* MRI and MRS measurements were carried out in the 9.4 T/31 cm actively shielded animal scanner (Varian/Magnex Scientific, Abingdon, UK) interfaced to a Varian Direct Drive console (Palo Alto, CA, USA) and using the modified $^{6}$Li Alderman-Grant coil combined with a $^{1}$H surface coil as transceiver. Male Sprague-Dawley rats (180-200g, n=19) were anesthetized using 1.5 % isoflurane and their physiology was monitored during the entire length of the experiments. Field inhomogeneity was corrected using the FASTMAP protocol (Gruetter and Tkáč 2000). Hyperpolarized $^{6}$Li solution was prepared by freezing droplets of glycerol:$H_2O$ (1:1, v/v) containing 3M $^{6}$LiCl and 58mM TEMPOL radical using fully protonated solvent mixture, a formulation which was found to found to provide the highest liquid state polarization (15.2 $\pm$ 1.5 %; Mishkovsky et al., data not published).

Samples were polarized for 90 min using a custom-designed DNP polarizer operating at 7T (197.14 GHz / 1.00 ± 0.05 K) (Cheng, Capozzi, et al. 2013). Sodium ascorbate was added to scavenge the radical prior to sample transfer (Miéville et al. 2010; Balzan et al. 2016). The sample was dissolved and transferred into a separator/infusion pump located inside the magnet bore. 1.2mL of hyperpolarized $^{6}$Li solution was automatically infused into the femoral vein of the rats (Cheng, Mishkovsky, et al. 2013), resulting in a $^{6}$Li blood concentration within the therapeutic window (0.98 mM ± 0.05 mM). Data acquisition was triggered at the time of injection. Arterial and venous blood gases were measured from the femoral vein and artery before the rat was inserted inside the scanner (~60 min before the lithium bolus) and immediately after the end of the MRS acquisition (~2min post bolus) using a COBAS® b 121 system (Roche Diagnostic, Mannheim, Germany).

In order to assess the dynamic of hyperpolarized $^{6}Li$ at pharmacological dose in the rat brain, different experiments were carried out:

**(1)** To evaluate the dynamic of hyperpolarized $^{6}Li$ in the rat brain, data acquisition was triggered at the time of injection and a series of $^{6}Li$ 1D spectra were acquired using 30° hard pulses every 5 s (n=4).

**(2)** In the $^{6}Li$ MRS acquisition, the $^{6}Li$ signal comes from lithium in the blood and from lithium located in the brain tissue. It is not yet clear how fast lithium enters the brain. It is generally accepted that the entry of lithium into the brain is slow (Shaw, Kellam, and Mottram 2013), however some studies using high dose of hyperpolarized $^{6}Li$ in rats suggested a predominantly cerebral localization of lithium a few minutes after its intravenous injection (van Heeswijk et al. 2009). Given these conflicting reports in the literature about the rate of lithium transport across the blood-brain barrier, our aim was to further investigate and clarify this issue. To evaluate the blood and tissue contributions on the detected $^{6}Li$ signals, the same measurements were repeated (n=4) but this time injecting $Gd^{3+}$ contrast agent 100 ± 5 s after the infusion of hyperpolarized $^{6}Li$ (Gadovist®, 1M/1mL), resulting in a $Gd^{3+}$ blood concentration of approximately 0.67 M. Gadovist® does not cross the intact blood-brain barrier in rats ("Compendium.Ch" n.d.) and dramatically reduces $^{6}Li$ $T_1$ if they are in contact: $^{6}Li$ $T_{1,blood}$ drops to ~$10^{-4}$ s at the estimated $Gd^{3+}$ blood concentration of our experiments (0.67M) (van Heeswijk et al. 2009).

**(3)** To estimate the influence of hemodynamic on the acquired signal, another set of measurements were carried out, in which a 90° saturation pulse is followed by 30° pulses every 5 s (n=3).

**(4)** To verify that the experimental parameters have only minimal effect on the dynamic of the signal, new $^{6}Li$ 1D spectra were acquired using 15° hard pulses every 5 s (n=3).

**(5)** Finally, to evaluate the effect of the permeabilization of the blood-brain barrier on the acquired $^{6}Li$ cerebral time course, anesthetized rats were infused with mannitol to osmotically disrupt the blood-brain barrier in one brain hemisphere. A solution of 25 % d-Mannitol (Sigma-Aldrich, Switzerland) was prepared and manually injected through the loop catheter inserted in the internal carotid artery (3ml/300g) as previously described (Auffret et al. 2016). 20 min after mannitol infusion, hyperpolarized $^{6}Li$ was infused and the signal was acquired using slab-selective excitations in the two brain hemispheres every 5 s (n=2). 30 min after mannitol infusion, $Gd^{3+}$ (Gadovist®, 1M/1mL) was injected in the femoral vein and $T_1$-weighted images were acquired.

All animal experiments were performed according to the guidelines of the local ethical committee and the protocols were approved by the local regulatory body of the Canton Vaud, Switzerland (Service de la Consommation et des Affaires Vétérinaires, Affaires Vétérinaires, Canton de Vaud, Switzerland).

### 5.2.3 Measuring $^6$Li $T_1$ in arterial and venous blood *ex vivo*

To evaluate the difference in $^6$Li $T_1$ in arterial and venous blood, *ex vivo* measurements on fresh rat blood samples were performed as previously described by Balzan et al. (Balzan et al. 2016): 300µl of hyperpolarized $^6$Li solution was injected manually and sequentially into each tube through PTFE capillary within 10 s after dissolution, reaching a $^6$Li concentration of 0.65 mM. The signal was acquired during 20 min (hard pulse, $\alpha$ = 20°, TR = 10 s).

In addition, in order to estimate the blood gases values in both arterial and venous blood at the time of our *ex vivo* measurements with hyperpolarized $^6$Li, blood gases of rat's arterial and venous blood samples were measured every 5 min (n=2) using a COBAS® b 121 system (Roche Diagnostic, Mannheim, Germany).

## 5.3 Results

$B_1$ map of the built modified Alderman-Grant coil showed good $B_1$ homogeneity at the rat head area (Figure 5.1B-C). The sample optimization together with the volume coil allowed us to detect $^6$Li *in vivo* in the rat head more than 6 min following injection and the excellent SNR (ranging from 860 to 8.9) achieved with our protocol can be appreciated from the *in vivo* spectra in Figure 5.2A. The time courses of all animals were well reproducible (Figure 5.2A) and we found that the apparent $T_1$ = 53.6 $\pm$ 2.9 s (mean $\pm$ SD, N=4).

To differentiate the signal from the blood and tissue compartments, the same measurements were repeated but this time injecting $Gd^{3+}$ contrast agent ~100 s after the $^6$Li infusion. In each experiment (n=4), the $^6$Li signal rapidly decayed upon Gadovist injection, indicating that $^6$Li is mostly located in the vascular system during the timeframe of our experiments (Figure 5.2B).

Then, we sought to estimate the influence of hemodynamic on the acquired signal. Another set of measurements were thus performed, in which a 90° saturation pulse was followed by 30° pulses every 5 s. After the 90° saturation pulse, a build-up was observed for approximately 15 s followed by the typical $^6$Li signal decay with apparent $T_1$ = 55.2 $\pm$ 1.6 s (Figure 5.2D), similar to what we found in acquisitions using 30° hard pulse only. The build-up after the 90°pulse was attributed to

the inflow $^6$Li spins through blood circulation, showing that in successive acquisitions different $^6$Li spins were detected.

Concerning the impact of the flip angle on the signal dynamics, as expected *in vivo* acquisition with a smaller flip angle (15°) resulted in an only slightly larger apparent $T_1$ (60.2 $\pm$ 5.9 s) than with a flip angle of 30° (Figure 5.2C), and confirmed that the correction for RF excitation is not straightforward in this type of *in vivo* experiment.

As it appeared from these different experiments that $^6$Li remains mainly in the vascular compartment during the first 2 min after injection, we then sought to evaluate the effect of the permeabilization of the blood-brain barrier on the acquired $^6$Li cerebral time course. In these experiments in which the blood-brain barrier was disrupted in one hemisphere, interestingly we observed a striking difference in the $^6$Li apparent $T_1$ between the two hemispheres (normal or disrupted). $^6$Li apparent $T_1$ measured on the hemisphere with the normal blood-brain barrier was found to be ~57 s (Figure 5.3), similar to what was found in our first sets of experiments (Figure 5.2A) while the $^6$Li apparent $T_1$ was tripled (~177 s) within the mannitol-permeabilized hemisphere (Figure 5.3).

Our next goal was to further investigate the $^6$Li characteristic decay measured. For this purpose, both mono- and bi-exponential fit were tested on our data acquired with 30° hard pulse every 5 s. As expected, bi-exponential decay better represents our measurements, as reflected by the sum of squared errors (SSE) values (Figure 5.2E). Given the very high sensitivity of $^6$Li to deoxyhemoglobin oxygenation levels *in vitro* (1.5 % difference in $SO_2$ has been shown to induce between 7-10 % difference in $^6$Li $T_1$ (Balzan et al. 2016)) and the approximately 10 % difference in $SO_2$ measured in our rats between arterial and venous blood (Figure 5.2E), we hypothesized that the two decays may correspond to venous blood (fast decay, $T_{1,a}$ in Figure 5.4) and arterial blood (slow decay, $T_{1,b}$ in Figure 5.4). To test this hypothesis, we performed *ex vivo* experiments to measure $^6$Li $T_1$ in both fresh arterial and venous blood and in $D_2O$ as described previously (Balzan et al. 2016). We found that despite the difference in deoxyhemoglobin between the two samples, as reflected by $SO_2$ (%) value, there were no significant difference between apparent or corrected $T_1$ relaxation times in venous or arterial blood (Figure 5.5C, Figure 5.5D). At the time of the *ex vivo* measurements (~60 min after blood collection), the difference in $SO_2$ (%) between the venous and arterial blood samples was approximately 15 % (Figure 5.6), similar to the difference measured *in vivo*. We therefore concluded that the two decays obtained from the bi-exponential fitting cannot be attributed to venous and arterial blood.

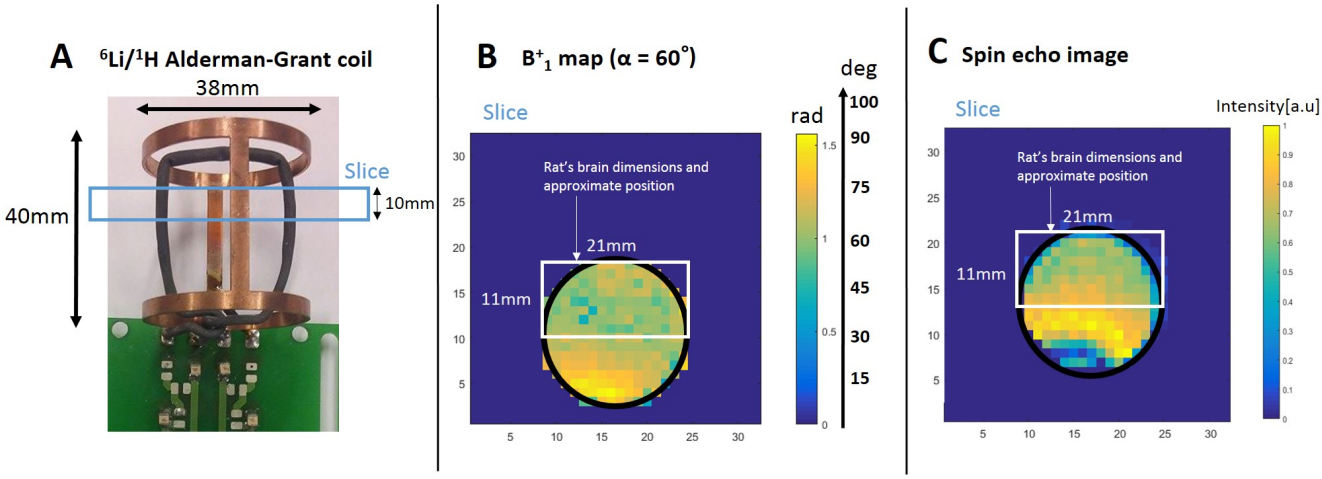


*Figure 5.1 (A) A photo of the $^6$Li modified Alderman-Grant coil (38 mm inner diameter, 40 mm length)/$^1$H surface coil and (B) its corresponding angle map that was calculated using the double flip angle method (Insko and Bolinger 1993) from two gradient echo images acquired on a phantom containing 250 mM $^6$LiCl; 16 µM Gadovist in $H_2O$ with 60°/120° flip angles (TR=65 s, FOV=42x42 mm, Data Matrix=32X32 mm, 4 averages). The spin echo image corresponds well to the angle map. (C) White rectangle represents the volume taken by the rat brain in our setting, showing good $B_1$ homogeneity in the area of interest (mean±SD=57°± 7°).*

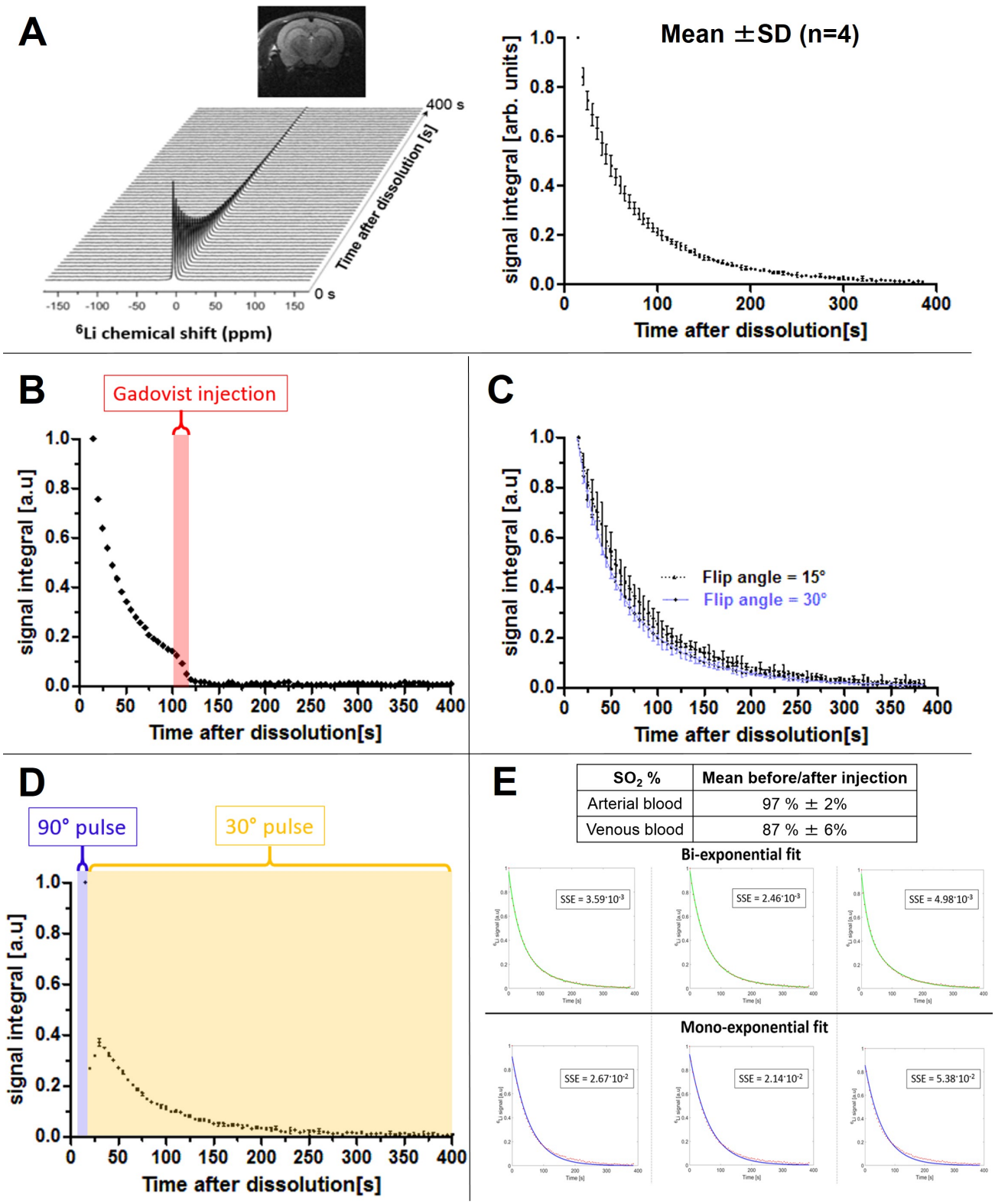


| $SO_2$ % | Mean before/after injection |
|---|---|
| Arterial blood | 97 % ± 2% |
| Venous blood | 87 % ± 6% |

*Figure 5.2 (A) On the left, a typical dynamic spectra of hyperpolarized $^6$Li signal acquired in the rat head with modified Alderman-Grant coil demonstrates the excellent SNR achieved in the experiments (SNR ranging from 860 to 8.9). The estimated $^6$Li concentration in blood at the time of injection was 0.98 mM. On the right, $^6$Li signal profile obtained with non-localized MRS, mean ± SD, n=4. (B) Evaluation of blood and tissue compartment: a typical normalized time course of hyperpolarized $^6$Li obtained in the rat head in upon Gadovist injection. The injection of the contrast agent (1 M/ 1 mL) started at 95 s and lasted 30 s (red bar), leading to the rapid decay of the $^6$Li signal. (C) Mean ± SD of $^6$Li signal profiles obtained with*

*non-localized MRS (30° hard pulses: n=4; 15° hard pulses: n=3). (D) Influence of hemodynamic on the acquired signal: mean ± SD of $^{6}Li$ signal profiles obtained with non-localized MRS (n=3): a 90° hard pulse is followed by a series of 30° hard pulses. The build-up after the 90° pulse corresponds to the inflow $^{6}Li$ spins through blood circulation. (E) Average $SO_2$ (%) measured before and after $^{6}Li$ injection (n=3) and time courses of hyperpolarized $^{6}Li$ detected in the rat head of three different rats, each of which was normalized to its maximal $^{6}Li$ signal. In the upper panel, data was fitted to bi-exponential decay and in the lower panel to mono-exponential decay. Sum of squared errors (SSE) is shown, indicating that bi-exponential decay better represents our measurements.*

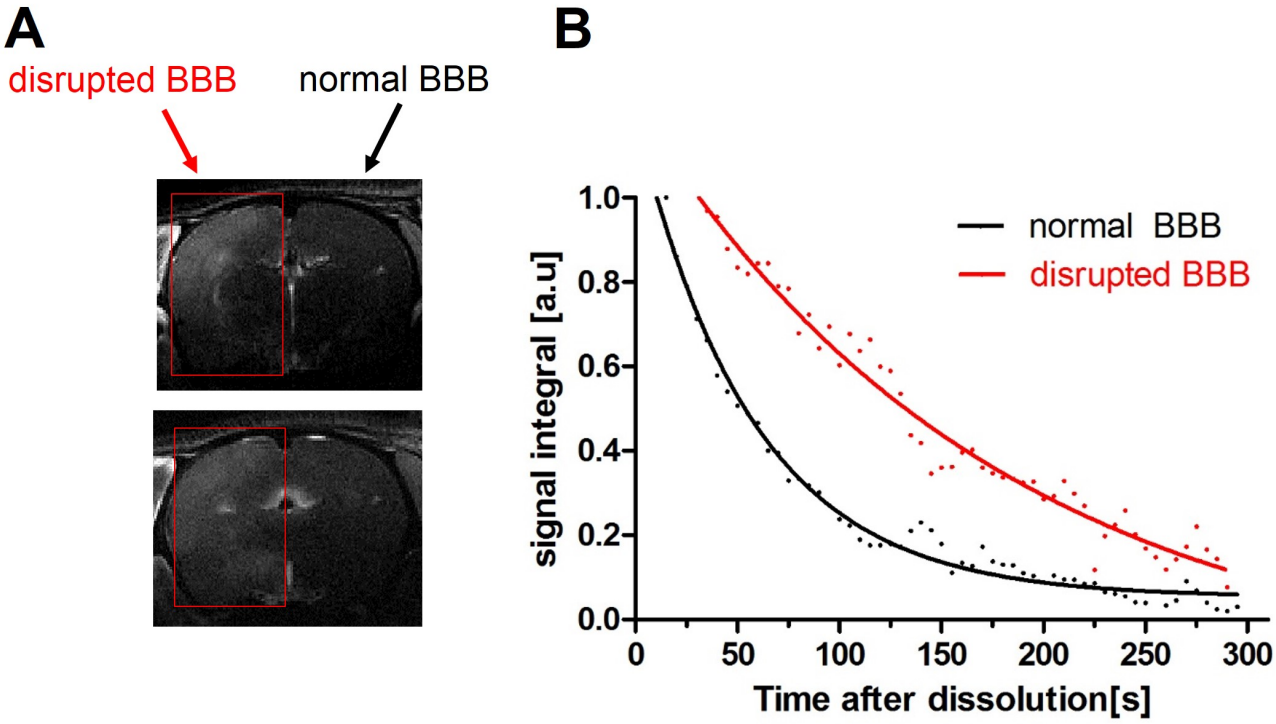


*Figure 5.3 (A) 30 min after mannitol infusion, the presence of blood-brain barrier disruption is visible via gadolinium enhanced $T_1$-weighted images (B) 20 min after mannitol infusion, hyperpolarized $^{6}Li$ signal acquired in the two brain hemispheres using slab-selective excitations every 5 s. Note that for simplicity purpose, only the decay of the signal is shown for each hemisphere.*

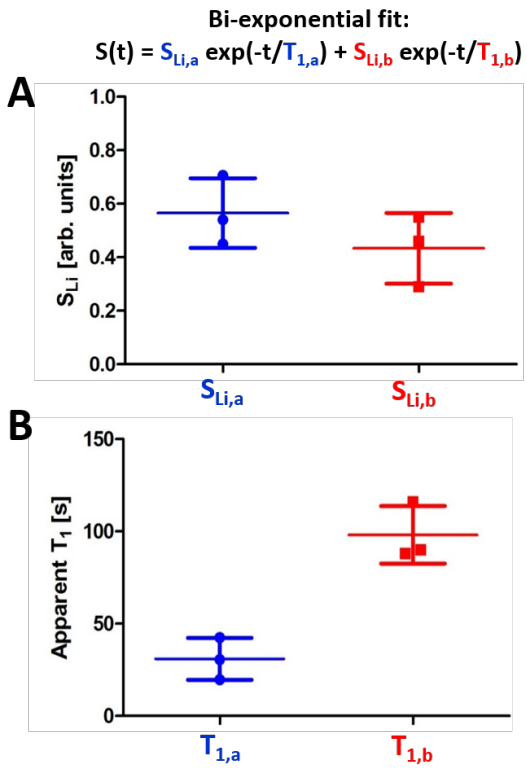


*Figure 5.4 Parameters obtained from the bi-exponential fitting of three different in vivo non-localized MRS acquisition following $^{6}$Li infusion.*

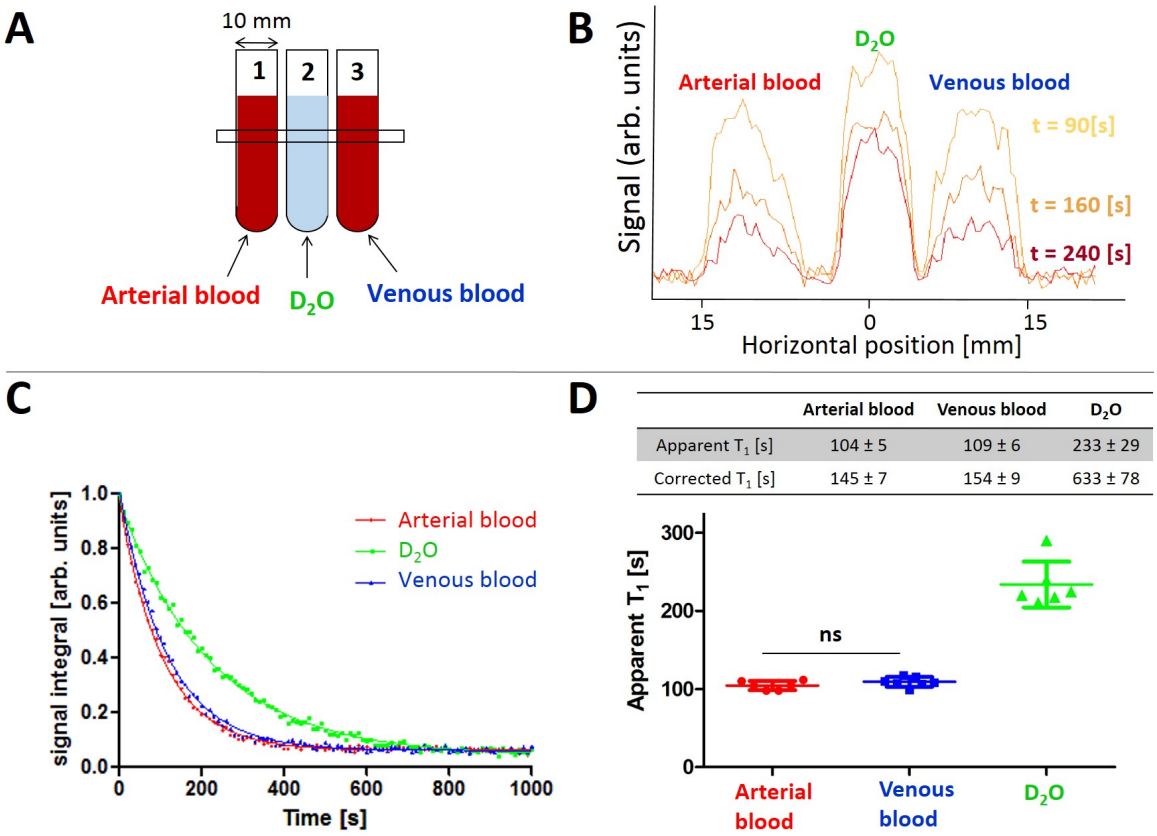


| | Arterial blood | Venous blood | $D_2O$ |
|---|---|---|---|
| Apparent $T_1$ [s] | 104 ± 5 | 109 ± 6 | 233 ± 29 |
| Corrected $T_1$ [s] | 145 ± 7 | 154 ± 9 | 633 ± 78 |

*Figure 5.5 (A) Schematic cross section of the three 10 mm glass tubes inside the tube holder and the surrounding coils (40 mm inner diameter). Tube 2 was used as a reference to assess the relaxation time of each hyperpolarized $^6$Li solution. Tubes 1 and 3 were used for the measurements of arterial and venous blood. (B) Time evolution of the tomographic projection of the $^6$Li signal acquired after the injection of a hyperpolarized $^6$Li solution into the three tubes. The projections were measured along the horizontal axis perpendicular to the static magnetic field as described previously (Balzan et al. 2016). (C) Integral of the projected $^6$Li signal measured in the three tubes as a function of time and their mono-exponential fit. (D) Apparent $T_1$ and corrected $T_1$ (deduced after correcting for the effect of the pulses on the signal decay) obtained from the mono-exponential fit in arterial blood, venous blood and $D_2O$ (n=6). Results are presented as mean ± SD. Unpaired, two-tailed Student's t-tests were used to assess statistical significance ($p<0.05$). Apparent $T_1$ and corrected $T_1$ significantly differed between $D_2O$ and arterial and venous blood ($p<0.0001$) (data not shown for simplicity).*

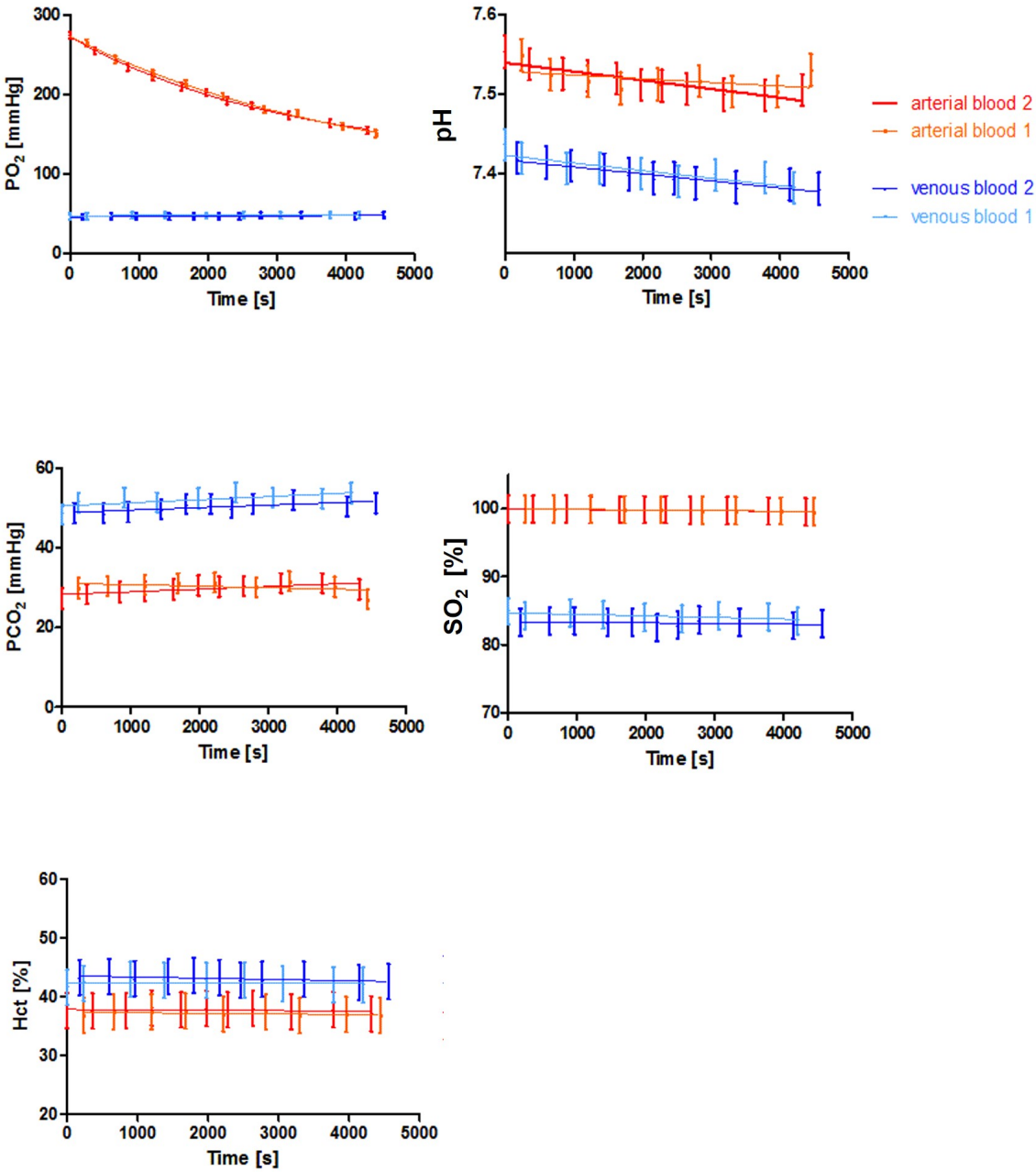


*Figure 5.6 Blood gases evolution of rat's arterial and venous blood samples (n=2) measured in the same 10 mm-glass tubes used in the ex vivo experiments with hyperpolarized $^{6}Li$. Measurements were performed approximately every 5 min from the time of the withdrawal (t = 0 s) and 80 min thereafter. Values were obtained using a COBAS® b 121 system (Roche Diagnostic, Mannheim, Germany). The error bar represents the error on the measurements as specified by COBAS®.*

## 5.4 Discussion

In the present study, we demonstrated that hyperpolarized $^{6}$Li can be detected at pharmacological concentration (<1.2 mM) in the rat head with high SNR. The use of our custom-built modified Alderman-Grant coil allowed us to obtain a much more homogeneous $B_1$ field than surface coil used in previous studies with hyperpolarized $^{6}$Li (van Heeswijk et al. 2009), and the polarization achieved with our protocol also substantially exceeded the liquid state polarization reported in previous studies (Balzan et al. 2016).

In order to better understand the mechanisms of action of lithium therapy, knowledge about lithium traversing membranes and especially the blood-brain barrier is of utmost importance (Birch 2012). Absorption of lithium in the brain is generally considered to be very slow (Shaw, Kellam, and Mottram 2013), however some studies measuring lithium absorption have suggested that after intravenous administration, a certain amount of lithium already enters the brain within the first few hours (Ebadi et al. 1974; Subbaraya Ramaprasad et al. 2005) or the first few minutes (van Heeswijk et al. 2009). In our experiments, we demonstrated that upon injection of Gadovist, the $^{6}$Li signal decreased very rapidly, showing that the majority of $^{6}$Li signal remained mainly confined to the vascular compartment and that its uptake in the rat brain during the length of our measurements was low. These results provide new insights to a question that remains to be further investigated.

It takes ~17 s for the blood to circulate around the body in the anesthetized rat (Sweet et al. 1987). Given that the $^{6}$Li is mostly located in blood and that the volume of blood in the head excited by the coil is small, we hypothesized that in successive acquisitions different $^{6}$Li spins were detected. The build-up measured after the 90° pulse (Figure 5.2D) supports this hypothesis and confirmed that the effect of the RF excitation cannot be corrected as previously stated (van Heeswijk et al. 2009; Day et al. 2007), and thus the characteristic decays of the $^{6}$Li signal acquired *in vivo* that we report were not adjusted for the effect of the RF pulse. We noted that the apparent relaxation constant $T_1$ reported in the present study is slightly lower than what was previously reported *in vivo* (van Heeswijk et al. 2009). The main reason probably accounting for this difference is that the $T_1$ value reported in the mentioned study was corrected for the magnetization decrease due to the repetitive excitations and did not consider the inflow into the sensitive volume of the coil, thus providing only an upper estimate of the *in vivo* relaxation time. Another difference is the type of coil used: they used a surface coil whereas in the present study we used a volume coil, providing a more homogeneous $B_1$ and exciting more spins with each RF pulse.

We also demonstrated that it is possible to enhance the transient uptake of lithium in the brain by temporarily opening the blood-brain barrier using mannitol. By introducing mannitol to osmotically disrupt the blood-brain barrier in one brain hemisphere, we observed that the $^{6}Li$ apparent $T_1$ was more than tripled in the disrupted hemisphere compared to the normal hemisphere, most probably reflecting a greater transport of lithium into the brain.

Overall, these different results confirm that without any blood-brain barrier disruption, $^{6}Li$ uptake in the rat brain during the length of our measurements is low, and the majority of $^{6}Li$ signal is intravascular.

Regarding our *ex vivo* measurements performed on arterial blood, venous blood and $D_2O$, we found corrected $^{6}Li$ $T_1$ values in the similar range as what reported by Balzan et al. (Balzan et al. 2016) for both venous blood and $D_2O$. In their study, they reported that paramagnetic deoxyhemoglobin dominates $^{6}Li$ relaxation in blood, and the shorter $T_1$ measured in deoxygenated blood ($SO_2$=75.4 $\pm$ 0.7 %) compared to whole blood ($SO_2$=76.9 $\pm$ 0.3 %), was attributed to paramagnetic deoxyhemoglobin (Balzan et al. 2016). In our experiments, since hemoglobin oxygenation levels were higher in arterial blood ($SO_2$=97 $\pm$ 2 %), compared to venous blood ($SO_2$=87 $\pm$ 6 %), we expected $T_{1,artery}$ to be higher than $T_{1,venous}$. However, unexpectedly we found no significant differences in the $T_1$ (neither apparent nor corrected) between the venous and arterial blood despite the large difference in deoxyhemoglobin. Arterial $T_1$ was even found to be slightly lower than venous $T_1$, which was surprising given its low deoxyhemoglobin level. This leads us to conclude that the fast decay component and the slow decay component of apparent $^{6}Li$ $T_1$ relaxation do not correspond to arterial and venous blood as we initially hypothesized, and it could also be that $^{6}Li$ uptake in other tissues or organs such as liver or kidney also account for some of the fast decay component. Therefore, contrary to what has been reported (Balzan et al. 2016), it appeared in our experiments that deoxyhemoglobin was not a key factor accounting for $T_1$ relaxation of $^{6}Li$ in blood, and these apparent discrepancies remain to be investigated.

Overall, we conclude that the transport of lithium through the intact blood-brain barrier during the time of $^{6}Li$ hyperpolarization is a limiting factor and thus that the usefulness of hyperpolarized lithium as a tool to evaluate its pharmacokinetic in real time or its distribution in the brain is limited. However, despite the limitations associated with the slow transport through the blood-brain barrier, we believe that hyperpolarized lithium still has the potential for promising applications given its very long intrinsic $T_1$, the good SNR obtained with our protocol, and the

striking difference we found between apparent $T_1$ values in a brain with normal or disrupted blood-brain barrier.

# Chapter 6 Conclusion and perspectives

The present thesis first aimed to assess *in vivo* and longitudinally the effects of different treatments for hepatic encephalopathy (HE) on the neurometabolic changes associated with chronic HE using a rat model of type C HE and a multimodal approach including $^{1}$H MRS. We demonstrated for the first time the positive effects of the combined rifaximin and the probiotic Vivomixx® on brain metabolic changes during CLD and CHE. It appears that the progression of CHE can be slowed by administering the antibiotic rifaximin combined with probiotic treatment that modulates the intestinal flora. We also concluded that in BDL rats, rifaximin treatment alone had limited efficacy. When administered at human dose in rats, its effects appeared only at the early stages of the disease, whereas at a higher dose some neurometabolic changes associated with HE were attenuated but the general condition of the rats was worse. The clinical implications of these two studies are essential given that both rifaximin and some probiotics are currently used in the treatment of HE. Since both rifaximin and probiotics influence systemic inflammation, it would be of interest to also evaluate inflammatory markers in the blood (TNF-α, CRP, WBC count) and markers of neuroinflammation, which could be an improvement for future treatment studies in BDL rats. Given the current burden of liver disease worldwide, understanding the mechanisms of action of these treatments may have a significant impact on public health in the long term. More generally, our studies also illustrate the fact that finding an appropriate treatment for HE is challenging, which is why, despite years of investigation, the appropriate treatment has not yet been found. At the same time, our studies illustrate the usefulness of high-resolution MR spectroscopy as a very powerful technique in pre-clinical studies for the detailed and non-invasive evaluation of the effects of drugs impacting the neurometabolic profile in particular.

The second part of this thesis was dedicated to the development and application of DNP techniques for *in vivo* studies in rodents. Since glucose is the main energy substrate in the brain, our goal was to study the real-time cerebral metabolism of glucose in mice after infusion of $^{13}$C-labelled hyperpolarized glucose and especially to investigate how the change in anesthesia impacts the cerebral metabolism of hyperpolarized glucose. We showed for the first time that switching from isoflurane anesthesia to a combination of lower doses of isoflurane and medetomidine had a high impact on cerebral glucose uptake and glycolytic flux. An important advantage of our study is that it was carried out under nearly physiological conditions. First, glucose is the main energy substrate in the brain under physiological conditions, in contrast for example to pyruvate which is mainly used in metabolic studies using hyperpolarized substrates. Also, the use of hyperpolarized glucose allowed us to study the cerebral metabolism of glucose at physiological concentrations. Finally, the choice of anesthesia reported to preserve connectivity similar to the awake state

brought us a little closer to the normal physiology of the brain. Our results also highlighted the important effect that anesthetics can create on the outcome of a pre-clinical experiment performed in animal and stresses the importance of taking this factor into account before interpreting the results and extrapolating them to humans. In addition, the higher SNR reported in this work offer new perspectives for better characterizing the energetic deficiencies in neuropsychiatric diseases such as HE. The extent and characterization of brain energetic disorders in HE is still debated, and hyperpolarized glucose can be a promising tool to give further insights and elucidate the remaining questions.

We also paved a new way for quantifying cerebral glucose metabolism kinetics, especially of glycolysis. Different mathematical model of metabolism were evaluated and we showed that a 3-compartment model is more stable and reliable than a 4-compartment model. As is often the case when modelling using hyperpolarized substrates, the determination of kinetic rate constants was challenging. The normalization of DNP spectra and the lack of measured input function and cerebral glucose uptake were the main limiting aspects. The addition of glucose uptake data obtained with PET scan would be a great improvement and we plan to conduct these experiments in the near future. In addition, a further increased SNR could provide a measurable pyruvate time course, which would also contribute to the improvement of the estimation of the kinetic rate constants. A robust model has the potential to improve the understanding of diseases with a disrupted cerebral energy metabolism such as hepatic encephalopathy. It can provide a valuable tool for quantitatively comparing metabolic rates in different conditions, for example by comparing control and diseased groups.

We finally investigated the potential of hyperpolarized lithium to enhance the understanding of the mechanism of action of lithium salts in the treatment of bipolar disorders. Overall, we concluded that the transport of lithium through the intact blood-brain barrier during the time of $^{6}$Li hyperpolarization is a limiting factor and thus that the usefulness of hyperpolarized lithium as a tool to evaluate its pharmacokinetic in real time or its distribution in the brain is limited. However, despite the limitations associated with the slow transport through the blood-brain barrier, we believe that hyperpolarized lithium still has the potential for promising applications given its very long intrinsic $T_1$, the good SNR obtained with our protocol, and the striking difference we found between apparent $T_1$ values in a brain with normal or disrupted blood-brain barrier.

# Appendix 1 Setting up dDNP experiments using a 5 T polarizer connected to a 14 T animal scanner

The work presented in this part was carried out in collaboration with three PhD students from the LIFMET (T.P. Lê, A. Radaelli, C. Zanella). All four of us contributed equally to this work.

## Introduction

This section presents work carried out at the LIFMET, consisting of restarting dissolution DNP (dDNP) experiments using a 5 T /1.5 K custom-designed polarizer connected to a 14.1 T animal scanner as well as the optimisation of the protocol. At the time this work started, the 5 T polarizer was working but was only used for solid state polarization measurements. Our goal was thus multiple: first, the aim was to make the 5 T polarizer connected to the 14.1 T scanner functional again to (1) allow liquid state polarization measurements on this set-up and (2) to be able to perform *in vivo* metabolic measurements on rodents after injection of hyperpolarized solution. At the same time, the different parameters were characterized and optimized.

## Method & Results

First, the transfer line was put back in place as well as the automatic triggering of the measurement 5 seconds after dissolution. The optimal length of the transfer line was found to be 7.5 m. 2, 3 and 4 seconds pushing time under a pressure of 6 bar were tested. 3 seconds pushing time gave rise to a volume transferred of 2.15 ml, which is optimal for *in vivo* applications.

Before determining the optimal path for the transfer line, we evaluated which sample (sodium pyruvate or pyruvic acid with different radicals) provides the highest liquid state polarization. The sample composed of 2.7 M [1-$^{13}$C] Na-Pyr + 45 mM TEMPOL + 65 µl Na-Asc 1M gave the highest polarization (Figure 7.1) and the next measurements were pursued with this sample composition.

| **Sample** | **Polarization (%)** | **$T_1$ (s)** |
|---|---|---|
| 2.7M NaPyr + 45mM TEMPOL | 6.7 | 26.2 |
| 2.7M NaPyr + 45mM TEMPOL + NaAsc | 10.7 | 41.3 |
| 2.7M NaPyr + 15mM OX63 | 7.6 | 36.7 |
| 7M PA + UV radicals (1h irradiation) | 8.3 | 36.6 |

*Figure 7.1 Liquid state polarization and build-up time achieved with different sample composition. NaPyr stands for sodium pyruvate and PA stands for pyruvic acid.*

As the distribution of the magnetic field (amplitude and direction) influences the polarization loss during the transfer from the polarizer to the scanner, we tried to determine if the path had an influence in the present case, and if so what was the optimal path for the transfer line. Three different holes in the panel were tested (Figure 7.2). No significant difference between the three

holes was found either in the liquid state polarization or in the polarization built-up time. For the following measurements, hole 2 was selected in order to minimize the length of the transfer line.

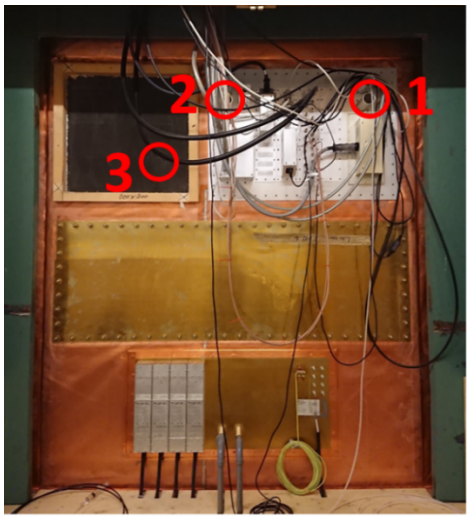


| Hole | P (%) | $T_1$ (s) | n |
|---|---|---|---|
| 1 | 11.5 ± 3.6 | 33.3 ± 1.3 | 3 |
| 2 | 15.3 ± 6.8 | 29.3 ± 3.7 | 3 |
| 3 | 12.7 ± 1.8 | 32.8 ± 1.9 | 3 |

*Figure 7.2 Transfer path optimization. The different holes tested are labelled as 1, 2 and 3. For each hole, measurements were pereformed 3 times. Polarization (P) and longitudinal relaxation time ($T_1$) were measured. No significant difference was found between the three holes.*

As a next step, our goal was to reduce the time of polarization by using microwave modulations. By modulating around the frequency of interest (10 kHz around 140.25 GHz), we found that the built-up time polarization was reduced by about six times, from $T_1$ = 5000 s to $T_1$ = 770 s (Figure 7.3), without however significantly improved the total polarization achieved.

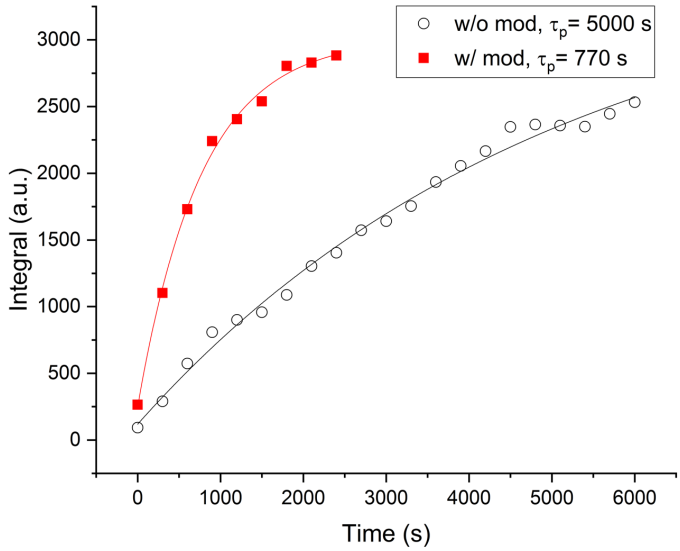


*Figure 7.3 Effect of microwave modulation (10 kHz around 140.25 GHz) on polarization built-up time of a sample composed of 2.7 M [1-$^{13}$C]Na-pyr + 45 mM TEMPOL.*

In order to determine the polarization loss during the transfer, we also performed solid state polarization measurements. Due to some problems encountered with the polarizer (notably the

difficulty to maintain a temperature of 4 K for several hours), the success rate of these experiments was low. We tried 12 times and succeeded 3 times. We obtained a solid state polarization of $P_{SS}$ = 14.56 ± 1.55 % (n=3), meaning that there is only small polarization loss during transfer ($P_{LS}$ = 12.7 ± 1.8 %, n=3).

As a next step, we performed an *in vivo* experiment**.** All measurements were performed in a 14.1 T MRI system and using a home-built quadrature $^{1}$H-coil and a $^{13}$C surface coil as a transceiver that was placed on top of the rat's abdomen at the location of the liver (Figure 7.4A).

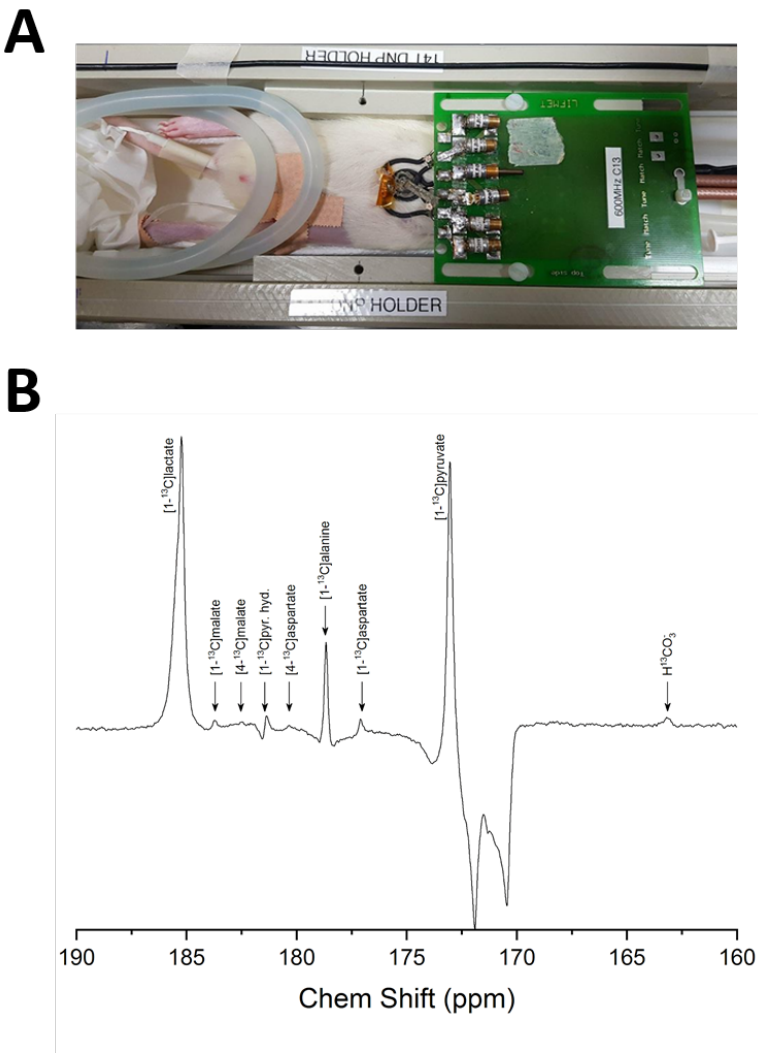


*Figure 7.4* In vivo *measurements. (A) Male Sprague Dawley rat placed in the holder with the home-built quadrature $^{1}$H-coil and $^{13}$C surface coil placed on the abdomen. (B) Resulting summed spectra (n=13 scans added) and the corresponding metabolites. [1-$^{13}$C] lactate was visible until 60 s after injection.*

A male Sprague-Dawley rat (180 g) was anesthetized using 1.5% isoflurane and its physiology was monitored during the entire length of the experiments. Field inhomogeneity was corrected using the FASTMAP protocol (Gruetter and Tkáč 2000). Hyperpolarized sodium [1-$^{13}$C] pyruvate sample

was prepared by freezing droplets of glycerol:$H_2O$ (1:3, v/v) containing 2.7 M Na-Pyr and 45 mM TEMPOL radical. Samples were polarized for 100 min using the 5 T DNP polarizer (140.25 GHz / 1.2 ± 0.05 K). Sodium ascorbate was added to scavenge the radical prior to sample transfer (Miéville et al. 2010; Balzan et al. 2016). The sample was dissolved and transferred into the separator/infusion pump located inside the magnet bore. 1.2 mL of hyperpolarized solution was automatically infused into the femoral vein of the rat. Data acquisition was triggered at the time of injection and data were acquired using non localized 30° adiabatic pulses (BIR4.30) with a repetition time (TR) of 3 s. This first *in vivo* experiment was a success and several metabolites could be observed in real time in rat liver with good SNR (Figure 7.4). [1-$^{13}$C] lactate was visible until 60 s after injection.

Finally, we performed another set of liquid state polarization measurements on a sample composed of pyruvic acid + 15mM OX63 radical. We obtained a higher liquid state polarization than the one obtained so far with the different sample composition (Figure 7.1), with $P_{LS}$ = 23.3 ± 1.7 % (n=3), which is high enough for *in vivo* measurements in the brain.

## Discussion & Conclusion

During this project, we were able to re-establish dissolution DNP experiments using a custom designed 5 T /1.5 K polarizer connected to a 14.1 T animal scanner. This enabled us to perform *in vivo* experiments and to optimize the protocol. The results obtained show that the different filter panel holes do not significantly influence the liquid state polarization and that little polarization is lost during the transfer. The microwave sweep resulted in a reduction of the polarization time, reducing it by a factor of about 6, as shown by various recent studies (Bornet et al., 2014). In conclusion, these preliminary results are encouraging for the continuation of *in vivo* and *in vitro* dDNP experiments with this set-up, and other refinements are currently in progress such as the improvement of the set-up to minimize the amount of helium required for solid state measurement.

# Acknowledgments

Now that I have come to the end of this journey, I would like to thank all the people who made this thesis work possible.

First of all, I would like to thank my thesis supervisor, Professor Rolf Gruetter, for giving me the opportunity to do my PhD in your laboratory, the LIFMET. I very much enjoyed working in this stimulating interdisciplinary environment. I am grateful for the trust you gave me as well as for your valuable and judicious advice throughout these years, which helped me to guide my research and improve it considerably. Your deep knowledge in the MR field inspired me throughout my thesis. Thank you also for making LIFMET such a great example of gender equality in science.

Cristina, thank you for all that you have taught me throughout these years, starting with the use of the scanner when I arrived or the sharing of your great expertise in proton spectroscopy. I greatly appreciated your rigor and your structured scientific approach, your great work force and your availability. The BDL team has a bright future!

Mor, thank you so much for introducing me to the fascinating world of dDNP! Thank you for all that you have taught me over the years and for the great projects that I have had the opportunity to carry out with you. I admire your scientific creativity, your unfailing enthusiasm for your research and for all these new ideas that you have and are constantly implementing!

Bernard, thank you very much for your availability, for all the interesting and stimulating discussions, and for taking the time to answer all my questions before my thesis defence: it helped me a lot.

I also want to deeply thank Professors M. Dal Peraro, S. R. Williams, M. Chaumeil and M. Rudin for accepting to be members of my thesis committee.

Thanks to the BDL team, Cristina, Veronika, Dunja, Kasia, Jessie, Dario, Stefan, Valérie, Olivier for all the stimulating exchanges we had, and which enabled us to advance our research.

To the whole DNP team: Mor, Hikari, Andrea, Thanh, Alice, Claudia, Jean-Noël, thank you for the projects that I had the opportunity to work on with you, for the always very interesting discussions during our meetings and for your availability.

Thanks to all the external collaborators I had the chance to work with: Jocelyn Grosse, Sharon de Morrow, Claudio de Simone, Paola Mastromarino, and finally Romain Gosselin for his valuable expertise with the statistics.

Thank you to all the PhD students with whom I have had the pleasure of sharing my office these past few years. Whether it was with you Jeremie, Fred, Joao, Yohan, Claudia or Radek, I have good memories of these moments shared in the office with you. I will miss our discussions about the world, about gourmet restaurants, our coffee/beer breaks or our bodyattack sessions at Let's Go or football in Dorigny! Thanks to all the other PhD students, Antoine, Alice, Thanh, Dunja, Jessie, Song-I, Yujian, Elise, Masoumeh, Guillaume, Veronika, for the good times.

Many thanks also to the whole veterinary team, Stefan, Mario and Analina. Your know-how and expertise in this field are essential to the success of our experiments.

A big thank you to Yves for all your help in building coils and solving technical problems. Thanks also to Lillian and Tanja for all the administrative work, the trips organisation for our conferences and for your precious availability.

And thank you to all the people at LIFMET/CIBM for the nice moments spent in the laboratory, scientific or recreational!

Clémence, ma “EPFL-partner“ depuis maintenant 10 ans - merci pour tous ces beaux moments passés dans l’enceinte et hors de l’EPFL, pour ta précieuse amitié.

Adrien, un immense merci pour ton précieux soutien, tes encouragements et tes conseils tout au long de ma thèse et particulièrement lors de la rédaction de celle-ci dans notre salon ! Tu as toujours été là quand j’en avais besoin. Merci d’être à mes côtés et d’être là pour moi, tu es une personne formidable et j’ai tellement de chance de t’avoir.

Finalement, j’aimerais remercier ma famille. Solange, tu sais que je pourrais écrire un roman, mais je vais faire l’effort de me restreindre à quelques lignes. Ces années ont été belles grâce à toi et je ne peux les imaginer sans nos flarca, flunch et autres fiestaflaques ! Merci pour ton soutien indéfectible si précieux, merci tout simplement pour tout ce que tu m’apportes depuis maintenant 26 ans. Merci à vous Papa et Maman, vous qui m’avez encouragée et soutenue depuis toute petite et qui m’avez fourni un environnement idéal pour la réussite de mes études. Je n’aurais pas pu arriver là sans vous. Merci à vous trois pour votre amour, merci pour tout. Vous êtes les meilleurs et j’aimerais vous dédier cette thèse.

# References

Aamann, Luise, Rafael Ochoa-Sanchez, Mariana Oliveira, Mélanie Tremblay, Chantal Bémeur, Gitte Dam, Hendrik Vilstrup, Niels Kristian Aagaard, and Christopher F. Rose. 2019. "Progressive Resistance Training Prevents Loss of Muscle Mass and Strength in Bile Duct-Ligated Rats." *Liver International: Official Journal of the International Association for the Study of the Liver* 39 (4): 676–83. https://doi.org/10.1111/liv.13997.

Abdo, Ayman A. 2006. "An Evidence-Based Update on Hepatic Encephalopathy." *Saudi Journal of Gastroenterology* 12 (1): 8. https://doi.org/10.4103/1319-3767.27738.

Abraham, M., M. A. H. McCausland, and F. N. H. Robinson. 1959. "Dynamic Nuclear Polarization." *Physical Review Letters* 2 (11): 449–51. https://doi.org/10.1103/PhysRevLett.2.449.

Aldridge, Dominic R., Edward J. Tranah, and Debbie L. Shawcross. 2015. "Pathogenesis of Hepatic Encephalopathy: Role of Ammonia and Systemic Inflammation." *Journal of Clinical and Experimental Hepatology* 5 (Suppl 1): S7–20. https://doi.org/10.1016/j.jceh.2014.06.004.

Alkire, M. T., R. J. Haier, N. K. Shah, and C. T. Anderson. 1997. "Positron Emission Tomography Study of Regional Cerebral Metabolism in Humans during Isoflurane Anesthesia." *Anesthesiology* 86 (3): 549–57. https://doi.org/10.1097/00000542-199703000-00006.

Allouche-Arnon, Hyla, Trevor Wade, Lanette Friesen Waldner, Valentina N. Miller, J. Moshe Gomori, Rachel Katz-Brull, and Charles A. McKenzie. 2013. "In Vivo Magnetic Resonance Imaging of Glucose – Initial Experience." *Contrast Media & Molecular Imaging* 8 (1): 72–82. https://doi.org/10.1002/cmmi.1497.

Als-Nielsen, Bodil, Lise L. Gluud, and Christian Gluud. 2004. "Non-Absorbable Disaccharides for Hepatic Encephalopathy: Systematic Review of Randomised Trials." *BMJ (Clinical Research Ed.)* 328 (7447): 1046. https://doi.org/10.1136/bmj.38048.506134.EE.

Amodio, P., F. Del Piccolo, E. Pettenò, D. Mapelli, P. Angeli, R. Iemmolo, M. Muraca, et al. 2001. "Prevalence and Prognostic Value of Quantified Electroencephalogram (EEG) Alterations in Cirrhotic Patients." *Journal of Hepatology* 35 (1): 37–45. https://doi.org/10.1016/s0168-8278(01)00129-5.

Andersen, N. B., and L. Amaranath. 1973. "Anesthetic Effects on Transport across Cell Membranes." *Anesthesiology* 39 (2): 126–52. https://doi.org/10.1097/00000542-197308000-00005.

Ardenkjær-Larsen, Jan H., Björn Fridlund, Andreas Gram, Georg Hansson, Lennart Hansson, Mathilde H. Lerche, Rolf Servin, Mikkel Thaning, and Klaes Golman. 2003. "Increase in Signal-to-Noise Ratio of > 10,000 Times in Liquid-State NMR." *Proceedings of the National Academy of Sciences* 100 (18): 10158–63. https://doi.org/10.1073/pnas.1733835100.

Auffret, Matthieu, Idrees Samim, Mario Lepore, Rolf Gruetter, and Nathalie Just. 2016. "Quantitative Activity-Induced Manganese-Dependent MRI for Characterizing Cortical Layers in the Primary Somatosensory Cortex of the Rat." *Brain Structure and Function* 221 (2): 695–707. https://doi.org/10.1007/s00429-014-0933-3.

Avsaroglu, H., A. S. van der Sar, H. A. van Lith, L. F. M. van Zutphen, and L. J. Hellebrekers. 2007. "Differences in Response to Anaesthetics and Analgesics between Inbred Rat Strains." *Laboratory Animals* 41 (3): 337–44. https://doi.org/10.1258/002367707781282811.

Azhari, Hassan, and Mark G. Swain. 2018. “Role of Peripheral Inflammation in Hepatic Encephalopathy.” *Journal of Clinical and Experimental Hepatology* 8 (3): 281–85. https://doi.org/10.1016/j.jceh.2018.06.008.

Badea, A., A.A. Ali-Sharief, and G.A. Johnson. 2007. “Morphometric Analysis of the C57BL/6J Mouse Brain.” *NeuroImage* 37 (3): 683–93. https://doi.org/10.1016/j.neuroimage.2007.05.046.

Bahceci, Funda, Bulent Yildirim, Melih Karincaoglu, Ibrahim Dogan, and Birsen Sipahi. 2005. “Memory Impairment in Patients with Cirrhosis.” *Journal of the National Medical Association* 97 (2): 213–16.

Bajaj, J. S. 2016. “Review Article: Potential Mechanisms of Action of Rifaximin in the Management of Hepatic Encephalopathy and Other Complications of Cirrhosis.” *Alimentary Pharmacology & Therapeutics* 43 Suppl 1 (January): 11–26. https://doi.org/10.1111/apt.13435.

Bajaj, Jasmohan S., ed. 2018. *Diagnosis and Management of Hepatic Encephalopathy: A Case-Based Guide*. Springer International Publishing. https://doi.org/10.1007/978-3-319-76798-7.

Bajaj, Jasmohan S., Muhammad Hafeezullah, Jose Franco, Rajiv R. Varma, Raymond G. Hoffmann, Joshua F. Knox, Darrell Hischke, Thomas A. Hammeke, Steven D. Pinkerton, and Kia Saeian. 2008. “Inhibitory Control Test for the Diagnosis of Minimal Hepatic Encephalopathy.” *Gastroenterology* 135 (5): 1591-1600.e1. https://doi.org/10.1053/j.gastro.2008.07.021.

Bajaj, Jasmohan S., Douglas M. Heuman, Arun J. Sanyal, Phillip B. Hylemon, Richard K. Sterling, R. Todd Stravitz, Michael Fuchs, et al. 2013. “Modulation of the Metabiome by Rifaximin in Patients with Cirrhosis and Minimal Hepatic Encephalopathy.” *PloS One* 8 (4): e60042. https://doi.org/10.1371/journal.pone.0060042.

Bajaj, Jasmohan S., Douglas M. Heuman, James B. Wade, Douglas P. Gibson, Kia Saeian, Jacob A. Wegelin, Muhammad Hafeezullah, et al. 2011. “Rifaximin Improves Driving Simulator Performance in a Randomized Trial of Patients with Minimal Hepatic Encephalopathy.” *Gastroenterology* 140 (2): 478-487.e1. https://doi.org/10.1053/j.gastro.2010.08.061.

Bajaj, Jasmohan S., Zain Kassam, Andrew Fagan, Edith A. Gavis, Eric Liu, I. Jane Cox, Raffi Kheradman, et al. 2017. “Fecal Microbiota Transplant from a Rational Stool Donor Improves Hepatic Encephalopathy: A Randomized Clinical Trial.” *Hepatology (Baltimore, Md.)* 66 (6): 1727–38. https://doi.org/10.1002/hep.29306.

Bajaj, Jasmohan S., Jason M. Ridlon, Phillip B. Hylemon, Leroy R. Thacker, Douglas M. Heuman, Sean Smith, Masoumeh Sikaroodi, and Patrick M. Gillevet. 2012. “Linkage of Gut Microbiome with Cognition in Hepatic Encephalopathy.” *American Journal of Physiology. Gastrointestinal and Liver Physiology* 302 (1): G168-175. https://doi.org/10.1152/ajpgi.00190.2011.

Balzan, Riccardo, Mor Mishkovsky, Yana Simonenko, Ruud B. van Heeswijk, Rolf Gruetter, Uzi Eliav, Gil Navon, and Arnaud Comment. 2016. “Hyperpolarized 6Li as a Probe for Hemoglobin Oxygenation Level.” *Contrast Media & Molecular Imaging* 11 (1): 41–46. https://doi.org/10.1002/cmmi.1656.

Bass, Nathan M., Kevin D. Mullen, Arun Sanyal, Fred Poordad, Guy Neff, Carroll B. Leevy, Samuel Sigal, et al. 2010. “Rifaximin Treatment in Hepatic Encephalopathy.” *New England Journal of Medicine* 362 (12): 1071–81. https://doi.org/10.1056/NEJMoa0907893.

Bastiaansen, Jessica A. M., Tian Cheng, Hongxia Lei, Rolf Gruetter, and Arnaud Comment. 2015. "Direct Noninvasive Estimation of Myocardial Tricarboxylic Acid Cycle Flux in Vivo Using Hyperpolarized $^{13}$C Magnetic Resonance." *Journal of Molecular and Cellular Cardiology* 87 (October): 129–37. https://doi.org/10.1016/j.yjmcc.2015.08.012.

Baumgart, Joel P., Zhen-Yu Zhou, Masato Hara, Daniel C. Cook, Michael B. Hoppa, Timothy A. Ryan, and Hugh C. Hemmings. 2015. "Isoflurane Inhibits Synaptic Vesicle Exocytosis through Reduced Ca2+ Influx, Not Ca2+-Exocytosis Coupling." *Proceedings of the National Academy of Sciences of the United States of America* 112 (38): 11959–64. https://doi.org/10.1073/pnas.1500525112.

Bémeur, Chantal, and Roger F. Butterworth. 2013. "Liver-Brain Proinflammatory Signalling in Acute Liver Failure: Role in the Pathogenesis of Hepatic Encephalopathy and Brain Edema." *Metabolic Brain Disease* 28 (2): 145–50. https://doi.org/10.1007/s11011-012-9361-3.

Bender, Alex S, and Michael D Norenberg. 2000. "Effect of Ammonia on GABA Uptake and Release in Cultured Astrocytes." *Neurochemistry International* 36 (4): 389–95. https://doi.org/10.1016/S0197-0186(99)00130-8.

Bessman, Samuel P., and Alice N. Bessman. 1955. "THE CEREBRAL AND PERIPHERAL UPTAKE OF AMMONIA IN LIVER DISEASE WITH AN HYPOTHESIS FOR THE MECHANISM OF HEPATIC COMA." *The Journal of Clinical Investigation* 34 (4): 622–28. https://doi.org/10.1172/JCI103111.

Birch, Nicholas J. 2012. *Lithium and the Cell: Pharmacology and Biochemistry*. Academic Press.

Blei, A. T., J. Córdoba, and Practice Parameters Committee of the American College of Gastroenterology. 2001. "Hepatic Encephalopathy." *The American Journal of Gastroenterology* 96 (7): 1968–76. https://doi.org/10.1111/j.1572-0241.2001.03964.x.

Blüml, S., K. J. Seymour, and B. D. Ross. 1999. "Developmental Changes in Choline- and Ethanolamine-Containing Compounds Measured with Proton-Decoupled (31)P MRS in in Vivo Human Brain." *Magnetic Resonance in Medicine* 42 (4): 643–54. https://doi.org/10.1002/(sici)1522-2594(199910)42:4<643::aid-mrm5>3.0.co;2-n.

Boretius, Susann, Roland Tammer, Thomas Michaelis, Jürgen Brockmöller, and Jens Frahm. 2013. "Halogenated Volatile Anesthetics Alter Brain Metabolism as Revealed by Proton Magnetic Resonance Spectroscopy of Mice in Vivo." *NeuroImage* 69 (April): 244–55. https://doi.org/10.1016/j.neuroimage.2012.12.020.

Bornet, Aurélien, Jonas Milani, Basile Vuichoud, Angel J. Perez Linde, Geoffrey Bodenhausen, and Sami Jannin. 2014. "Microwave Frequency Modulation to Enhance Dissolution Dynamic Nuclear Polarization." *Chemical Physics Letters* 602 (May): 63–67. https://doi.org/10.1016/j.cplett.2014.04.013.

Bosoi, Cristina R., and Christopher F. Rose. 2009. "Identifying the Direct Effects of Ammonia on the Brain." *Metabolic Brain Disease* 24 (1): 95–102. https://doi.org/10.1007/s11011-008-9112-7.

Boyanova, Lyudmila, and Ivan Mitov. 2012. "Coadministration of Probiotics with Antibiotics: Why, When and for How Long?" *Expert Review of Anti-Infective Therapy* 10 (4): 407–9. https://doi.org/10.1586/eri.12.24.

Braissant, Olivier. 2010. “Ammonia Toxicity to the Brain: Effects on Creatine Metabolism and Transport and Protective Roles of Creatine.” *Molecular Genetics and Metabolism* 100 Suppl 1: S53-58. https://doi.org/10.1016/j.ymgme.2010.02.011.

Braissant, Olivier, Valérie A. McLin, and Cristina Cudalbu. 2013. “Ammonia Toxicity to the Brain.” *Journal of Inherited Metabolic Disease* 36 (4): 595–612. https://doi.org/10.1007/s10545-012-9546-2.

Braissant, Olivier, Veronika Rackayová, Katarzyna Pierzchala, Jocelyn Grosse, Valérie A. McLin, and Cristina Cudalbu. 2019. “Longitudinal Neurometabolic Changes in the Hippocampus of a Rat Model of Chronic Hepatic Encephalopathy.” *Journal of Hepatology* 71 (3): 505–15. https://doi.org/10.1016/j.jhep.2019.05.022.

Brand, A., C. Richter-Landsberg, and D. Leibfritz. 1993. “Multinuclear NMR Studies on the Energy Metabolism of Glial and Neuronal Cells.” *Developmental Neuroscience* 15 (3–5): 289–98. https://doi.org/10.1159/000111347.

Bröer, Stefan, Angelika Bröer, Jonas T. Hansen, William A. Bubb, Vladimir J. Balcar, Fatima A. Nasrallah, Brett Garner, and Caroline Rae. 2007. “Alanine Metabolism, Transport, and Cycling in the Brain.” *Journal of Neurochemistry* 102 (6): 1758–70. https://doi.org/10.1111/j.1471-4159.2007.04654.x.

Bromberg, Philip A., Eugene D. Robin, and Claude E. Forkner. 1960. “THE EXISTENCE OF AMMONIA IN BLOOD IN VIVO WITH OBSERVATIONS ON THE SIGNIFICANCE OF THE NH4+–NH3 SYSTEM *.” *Journal of Clinical Investigation* 39 (2): 332–41.

Brulatout, S., P. Méric, I. Loubinoux, J. Borredon, J. L. Corrèze, P. Roucher, B. Gillet, et al. 1996. “A One-Dimensional (Proton and Phosphorus) and Two-Dimensional (Proton) in Vivo NMR Spectroscopic Study of Reversible Global Cerebral Ischemia.” *Journal of Neurochemistry* 66 (6): 2491–99. https://doi.org/10.1046/j.1471-4159.1996.66062491.x.

Brusilow, Saul W., Raymond C. Koehler, Richard J. Traystman, and Arthur J. L. Cooper. 2010. “Astrocyte Glutamine Synthetase: Importance in Hyperammonemic Syndromes and Potential Target for Therapy.” *Neurotherapeutics: The Journal of the American Society for Experimental NeuroTherapeutics* 7 (4): 452–70. https://doi.org/10.1016/j.nurt.2010.05.015.

Busa, W. B., and R. Nuccitelli. 1984. “Metabolic Regulation via Intracellular PH.” *The American Journal of Physiology* 246 (4 Pt 2): R409-438. https://doi.org/10.1152/ajpregu.1984.246.4.R409.

Butterworth, Roger F. 2003. “Pathogenesis of Hepatic Encephalopathy: New Insights from Neuroimaging and Molecular Studies.” *Journal of Hepatology* 39 (2): 278–85. https://doi.org/10.1016/S0168-8278(03)00267-8.

Butterworth, Roger F., Michael D. Norenberg, Vicente Felipo, Peter Ferenci, Jan Albrecht, Andres T. Blei, and Members of the ISHEN Commission on Experimental Models of HE. 2009. “Experimental Models of Hepatic Encephalopathy: ISHEN Guidelines.” *Liver International: Official Journal of the International Association for the Study of the Liver* 29 (6): 783–88. https://doi.org/10.1111/j.1478-3231.2009.02034.x.

Cai, Kejia, Mohammad Haris, Anup Singh, Feliks Kogan, Joel H. Greenberg, Hari Hariharan, John A. Detre, and Ravinder Reddy. 2012. “Magnetic Resonance Imaging of Glutamate.” *Nature Medicine* 18 (2): 302–6. https://doi.org/10.1038/nm.2615.

Capozzi, Andrea, Saket Patel, W. Thomas Wenckebach, Magnus Karlsson, Mathilde H. Lerche, and Jan Henrik Ardenkjær-Larsen. 2019. “Gadolinium Effect at High-Magnetic-Field DNP: 70% 13C Polarization of [U-13C] Glucose Using Trityl.” *The Journal of Physical Chemistry Letters* 10 (12): 3420–25. https://doi.org/10.1021/acs.jpclett.9b01306.

Cash, W. J., P. McConville, E. McDermott, P. A. McCormick, M. E. Callender, and N. I. McDougall. 2010. “Current Concepts in the Assessment and Treatment of Hepatic Encephalopathy.” *QJM: Monthly Journal of the Association of Physicians* 103 (1): 9–16. https://doi.org/10.1093/qjmed/hcp152.

Chan, C.-Y., S.-W. Huang, T.-F. Wang, R.-H. Lu, F.-Y. Lee, F.-Y. Chang, C.-J. Chu, et al. 2004. “Lack of Detrimental Effects of Nitric Oxide Inhibition in Bile Duct-Ligated Rats with Hepatic Encephalopathy.” *European Journal of Clinical Investigation* 34 (2): 122–28. https://doi.org/10.1111/j.1365-2362.2004.01295.x.

Chavarria, Laia, and Juan Cordoba. 2015. “Magnetic Resonance Imaging and Spectroscopy in Hepatic Encephalopathy.” *Journal of Clinical and Experimental Hepatology* 5 (Suppl 1): S69–74. https://doi.org/10.1016/j.jceh.2013.10.001.

Cheng, Tian, Andrea Capozzi, Yuhei Takado, Riccardo Balzan, and Arnaud Comment. 2013. “Over 35% Liquid-State 13C Polarization Obtained via Dissolution Dynamic Nuclear Polarization at 7 T and 1 K Using Ubiquitous Nitroxyl Radicals.” *Physical Chemistry Chemical Physics* 15 (48): 20819–22. https://doi.org/10.1039/C3CP53022A.

Cheng, Tian, Mor Mishkovsky, Jessica A. M. Bastiaansen, Olivier Ouari, Patrick Hautle, Paul Tordo, Ben van den Brandt, and Arnaud Comment. 2013. “Automated Transfer and Injection of Hyperpolarized Molecules with Polarization Measurement Prior to in Vivo NMR.” *NMR in Biomedicine* 26 (11): 1582–88. https://doi.org/10.1002/nbm.2993.

Chih, Ching-Ping, and Eugene L. Roberts. 2003. “Energy Substrates for Neurons during Neural Activity: A Critical Review of the Astrocyte-Neuron Lactate Shuttle Hypothesis.” *Journal of Cerebral Blood Flow and Metabolism: Official Journal of the International Society of Cerebral Blood Flow and Metabolism* 23 (11): 1263–81. https://doi.org/10.1097/01.WCB.0000081369.51727.6F.

Christensen, Caspar Elo, Magnus Karlsson, Jakob R. Winther, Pernille Rose Jensen, and Mathilde H. Lerche. 2014. “Non-Invasive in-Cell Determination of Free Cytosolic [NAD+]/[NADH] Ratios Using Hyperpolarized Glucose Show Large Variations in Metabolic Phenotypes.” *The Journal of Biological Chemistry* 289 (4): 2344–52. https://doi.org/10.1074/jbc.M113.498626.

Coltart, Iona, Thomas H. Tranah, and Debbie L. Shawcross. 2013. “Inflammation and Hepatic Encephalopathy.” *Archives of Biochemistry and Biophysics* 536 (2): 189–96. https://doi.org/10.1016/j.abb.2013.03.016.

Comment, Arnaud, and Matthew E. Merritt. 2014a. “Hyperpolarized Magnetic Resonance as a Sensitive Detector of Metabolic Function.” *Biochemistry* 53 (47): 7333–57. https://doi.org/10.1021/bi501225t.

———. 2014b. “Hyperpolarized Magnetic Resonance as a Sensitive Detector of Metabolic Function.” *Biochemistry* 53 (47): 7333–57. https://doi.org/10.1021/bi501225t.

“Compendium.” n.d. Accessed January 8, 2020. https://compendium.ch/fr/product/1292134-xifaxan-filmtabl-550-mg.

"Compendium.Ch." n.d. Accessed June 22, 2020. https://compendium.ch/fr/product/121134-gadovist-1-0-inj-los/mpro#MPro7600.

Conzen, P. F., B. Vollmar, H. Habazettl, E. J. Frink, K. Peter, and K. Messmer. 1992. "Systemic and Regional Hemodynamics of Isoflurane and Sevoflurane in Rats." *Anesthesia and Analgesia* 74 (1): 79–88. https://doi.org/10.1213/00000539-199201000-00014.

Cooper, A. J., and B. S. Kristal. 1997. "Multiple Roles of Glutathione in the Central Nervous System." *Biological Chemistry* 378 (8): 793–802.

Cooper, A. J., and F. Plum. 1987. "Biochemistry and Physiology of Brain Ammonia." *Physiological Reviews* 67 (2): 440–519. https://doi.org/10.1152/physrev.1987.67.2.440.

Córdoba, J., J. Alonso, A. Rovira, C. Jacas, F. Sanpedro, L. Castells, V. Vargas, et al. 2001. "The Development of Low-Grade Cerebral Edema in Cirrhosis Is Supported by the Evolution of (1)H-Magnetic Resonance Abnormalities after Liver Transplantation." *Journal of Hepatology* 35 (5): 598–604. https://doi.org/10.1016/s0168-8278(01)00181-7.

Cudalbu, Cristina. 2013. "In Vivo Studies of Brain Metabolism in Animal Models of Hepatic Encephalopathy Using $^{1}$H Magnetic Resonance Spectroscopy." *Metabolic Brain Disease* 28 (2): 167–74. https://doi.org/10.1007/s11011-012-9368-9.

D'Adamo, A. F., L. I. Gidez, and F. M. Yatsu. 1968. "Acetyl Transport Mechanisms. Involvement of N-Acetyl Aspartic Acid in de Novo Fatty Acid Biosynthesis in the Developing Rat Brain." *Experimental Brain Research* 5 (4): 267–73. https://doi.org/10.1007/BF00235902.

D'Adamo, A. F., and F. M. Yatsu. 1966. "Acetate Metabolism in the Nervous System. N-Acetyl-L-Aspartic Acid and the Biosynthesis of Brain Lipids." *Journal of Neurochemistry* 13 (10): 961–65. https://doi.org/10.1111/j.1471-4159.1966.tb10292.x.

Day, Iain J., John C. Mitchell, Martin J. Snowden, and Adrian L. Davis. 2007. "Applications of DNP-NMR for the Measurement of Heteronuclear T1 Relaxation Times." *Journal of Magnetic Resonance (San Diego, Calif.: 1997)* 187 (2): 216–24. https://doi.org/10.1016/j.jmr.2007.04.015.

Dienel, Gerald A. 2012. "Brain Lactate Metabolism: The Discoveries and the Controversies." *Journal of Cerebral Blood Flow & Metabolism* 32 (7): 1107–38. https://doi.org/10.1038/jcbfm.2011.175.

Ding, X., F. Zhang, and Y. Wang. 2014. "Letter: Probiotics vs. Lactulose for Minimal Hepatic Encephalopathy Therapy." *Alimentary Pharmacology & Therapeutics* 39 (9): 1000. https://doi.org/10.1111/apt.12661.

D'Mello, Charlotte, Natalie Ronaghan, Raza Zaheer, Michael Dicay, Tai Le, Wallace K. MacNaughton, Michael G. Surrette, and Mark G. Swain. 2015. "Probiotics Improve Inflammation-Associated Sickness Behavior by Altering Communication between the Peripheral Immune System and the Brain." *The Journal of Neuroscience: The Official Journal of the Society for Neuroscience* 35 (30): 10821–30. https://doi.org/10.1523/JNEUROSCI.0575-15.2015.

Duhamel, G., P. Choquet, E. Grillon, L. Lamalle, J. L. Leviel, A. Ziegler, and A. Constantinesco. 2001. "Xenon-129 MR Imaging and Spectroscopy of Rat Brain Using Arterial Delivery of Hyperpolarized Xenon in a Lipid Emulsion." *Magnetic Resonance in Medicine* 46 (2): 208–12. https://doi.org/10.1002/mrm.1180.

DuPont, Herbert L., Zhi-Dong Jiang, Pablo C. Okhuysen, Charles D. Ericsson, Francisco Javier de la Cabada, Shi Ke, Margaret W. DuPont, and Francisco Martinez-Sandoval. 2005. "A

Randomized, Double-Blind, Placebo-Controlled Trial of Rifaximin to Prevent Travelers' Diarrhea." *Annals of Internal Medicine* 142 (10): 805–12. https://doi.org/10.7326/0003-4819-142-10-200505170-00005.

Durand, J. L., W. Hosinking, and L. A. Jelicks. 2009. "Time Course of Effects of Inhalation Anesthesia on Blood Glucose Level in Male and Female C57BL/6 Mice." *Hormone and Metabolic Research = Hormon- Und Stoffwechselforschung = Hormones Et Metabolisme* 41 (4): 339–41. https://doi.org/10.1055/s-0028-1112114.

Ebadi, Manuchair S., Vickie J. Simmons, Merrill J. Hendrickson, and Priti S. Lacy. 1974. "Pharmacokinetics of Lithium and Its Regional Distribution in Rat Brain." *European Journal of Pharmacology* 27 (3): 324–29. https://doi.org/10.1016/0014-2999(74)90007-7.

Erecińska, M., and I. A. Silver. 1990. "Metabolism and Role of Glutamate in Mammalian Brain." *Progress in Neurobiology* 35 (4): 245–96. https://doi.org/10.1016/0301-0082(90)90013-7.

Felipo, Vicente. 2013. "Hepatic Encephalopathy: Effects of Liver Failure on Brain Function." *Nature Reviews. Neuroscience* 14 (12): 851–58. https://doi.org/10.1038/nrn3587.

Felipo, Vicente, and Roger F. Butterworth. 2002. "Neurobiology of Ammonia." *Progress in Neurobiology* 67 (4): 259–79. https://doi.org/10.1016/s0301-0082(02)00019-9.

Festi, D., G. Mazzella, M. Orsini, S. Sottili, A. Sangermano, S. Li Bassi, P. Parini, et al. 1993. "Rifaximin in the Treatment of Chronic Hepatic Encephalopathy; Results of a Multicenter Study of Efficacy and Safety." *Current Therapeutic Research* 54 (5): 598–609. https://doi.org/10.1016/S0011-393X(05)80681-2.

Firbank, M. J., R. M. Harrison, and J. T. O'Brien. 2002. "A Comprehensive Review of Proton Magnetic Resonance Spectroscopy Studies in Dementia and Parkinson's Disease." *Dementia and Geriatric Cognitive Disorders* 14 (2): 64–76. https://doi.org/10.1159/000064927.

Flatt, Emmanuelle, Olivier Braissant, Stefanita Mitrea, Dario Sessa, Paola Mastromarino, Rolf Gruetter, Valérie A. McLin, and Cristina Cudalbu. 2019. "P: 37 Probiotics Combined With Rifaximin for the Treatment of Chronic Hepatic Encephalopathy: A Longitudinal In Vivo 1H-MRS Study of Brain Metabolism Using BDL Rats." *American Journal of Gastroenterology* 114 (September): S19. https://doi.org/10.14309/01.ajg.0000582124.67482.93.

Flatt, Emmanuelle, Cristina Cudalbu, Olivier Braissant, Stefan Mitrea, Dario Sessa, Rolf Gruetter, and Valérie McLin. 2017. "Rifaximin in Chronic Liver Disease-Induced Hepatic Encephalopathy: An In Vivo Longitudinal Study of Brain Metabolism on BDL Rats." *Journal of Clinical and Experimental Hepatology* 7 (February): S55–56. https://doi.org/10.1016/j.jceh.2017.01.072.

Fox, P. T., M. E. Raichle, M. A. Mintun, and C. Dence. 1988. "Nonoxidative Glucose Consumption during Focal Physiologic Neural Activity." *Science (New York, N.Y.)* 241 (4864): 462–64. https://doi.org/10.1126/science.3260686.

Fukuzawa, Takeshi, Shoichi Matsutani, Hitoshi Maruyama, Taro Akiike, Hiromitsu Saisho, and Takamichi Hattori. 2006. "Magnetic Resonance Images of the Globus Pallidus in Patients with Idiopathic Portal Hypertension: A Quantitative Analysis of the Relationship between Signal Intensity and the Grade of Portosystemic Shunt." *Journal of Gastroenterology and Hepatology* 21 (5): 902–7. https://doi.org/10.1111/j.1440-1746.2006.04226.x.

Gitlin, Norman. 2011. “Treatment of Hepatic Encephalopathy with Rifaximin: More to Think About.” *Hepatology (Baltimore, Md.)* 53 (3): 1059; author reply 1059-1060. https://doi.org/10.1002/hep.24112.

Golman, Klaes, and J. Stefan Petersson. 2006. “Metabolic Imaging and Other Applications of Hyperpolarized 13C1.” *Academic Radiology* 13 (8): 932–42. https://doi.org/10.1016/j.acra.2006.06.001.

Golman, Klaes, René in ‘t Zandt, and Mikkel Thaning. 2006. “Real-Time Metabolic Imaging.” *Proceedings of the National Academy of Sciences* 103 (30): 11270–75. https://doi.org/10.1073/pnas.0601319103.

Gonzalez-Toledo, Eduardo, Roger E. Kelley, and Alireza Minagar. 2006. “Role of Magnetic Resonance Spectroscopy in Diagnosis and Management of Multiple Sclerosis.” *Neurological Research* 28 (3): 280–83. https://doi.org/10.1179/016164106X98161.

Govindaraju, V., K. Young, and A. A. Maudsley. 2000. “Proton NMR Chemical Shifts and Coupling Constants for Brain Metabolites.” *NMR in Biomedicine* 13 (3): 129–53. https://doi.org/10.1002/1099-1492(200005)13:3<129::aid-nbm619>3.0.co;2-v.

Graaf, Robin A. de. 2019. *In Vivo NMR Spectroscopy: Principles and Techniques*. John Wiley & Sons.

Grandjean, Joanes, Aileen Schroeter, Imene Batata, and Markus Rudin. 2014. “Optimization of Anesthesia Protocol for Resting-State FMRI in Mice Based on Differential Effects of Anesthetics on Functional Connectivity Patterns.” *NeuroImage* 102 Pt 2 (November): 838–47. https://doi.org/10.1016/j.neuroimage.2014.08.043.

Grant, Aaron K., Elena Vinogradov, Xiaoen Wang, Robert E. Lenkinski, and David C. Alsop. 2011. “Perfusion Imaging with a Freely Diffusible Hyperpolarized Contrast Agent.” *Magnetic Resonance in Medicine* 66 (3): 746–55. https://doi.org/10.1002/mrm.22860.

Grant, Christopher V., Yuan Yang, Mira Glibowicka, Chin H. Wu, Sang Ho Park, Charles M. Deber, and Stanley J. Opella. 2009. “A Modified Alderman-Grant Coil Makes Possible an Efficient Cross-Coil Probe for High Field Solid-State NMR of Lossy Biological Samples.” *Journal of Magnetic Resonance (San Diego, Calif. : 1997)* 201 (1): 87–92. https://doi.org/10.1016/j.jmr.2009.08.009.

Greene, N. M. 1965. “Inhalation Anesthetics and Permeability of Human Erythrocytes to Monosaccharides.” *Anesthesiology* 26 (6): 731–42. https://doi.org/10.1097/00000542-196511000-00007.

Greene, N. M., and F. W. Cervenko. 1967. “Inhalation Anesthetics, Carbon Dioxide and Glucose Transport across Red Cell Membranes.” *Acta Anaesthesiologica Scandinavica*, 1–18.

Gruetter, R, E J Novotny, S D Boulware, D L Rothman, G F Mason, G I Shulman, R G Shulman, and W V Tamborlane. 1992. “Direct Measurement of Brain Glucose Concentrations in Humans by 13C NMR Spectroscopy.” *Proceedings of the National Academy of Sciences of the United States of America* 89 (3): 1109–12.

Gruetter, R., E. R. Seaquist, and K. Ugurbil. 2001. “A Mathematical Model of Compartmentalized Neurotransmitter Metabolism in the Human Brain.” *American Journal of Physiology. Endocrinology and Metabolism* 281 (1): E100-112. https://doi.org/10.1152/ajpendo.2001.281.1.E100.

Gruetter, Rolf, and Ivan Tkáč. 2000. “Field Mapping without Reference Scan Using Asymmetric Echo-Planar Techniques.” *Magnetic Resonance in Medicine* 43 (2): 319–23. https://doi.org/10.1002/(SICI)1522-2594(200002)43:2<319::AID-MRM22>3.0.CO;2-1.

Guedes, Alonso G. P., and Elaine P. Rude. 2013. “Effects of Pre-Operative Administration of Medetomidine on Plasma Insulin and Glucose Concentrations in Healthy Dogs and Dogs with Insulinoma.” *Veterinary Anaesthesia and Analgesia* 40 (5): 472–81. https://doi.org/10.1111/vaa.12047.

Haase, A., J. Frahm, W. Hänicke, and D. Matthaei. 1985. “1H NMR Chemical Shift Selective (CHESS) Imaging.” *Physics in Medicine and Biology* 30 (4): 341–44. https://doi.org/10.1088/0031-9155/30/4/008.

Hadjihambi, Anna, Natalia Arias, Mohammed Sheikh, and Rajiv Jalan. 2017. “Hepatic Encephalopathy: A Critical Current Review.” *Hepatology International* 12 (Suppl 1): 135–47. https://doi.org/10.1007/s12072-017-9812-3.

Hammes, Thais Ortiz, Renata Leke, Thayssa Dalla Costa Escobar, Laisa Beduschi Fracasso, Fabiola Schons Meyer, Michael Éverton Andrades, and Themis Reverbel da Silveira. 2017. “Lactobacillus RhamnosusGG Reduces Hepatic Fibrosis in a Model of Chronic Liver Disease in Rats.” *Nutricion Hospitalaria* 34 (3): 702–9. https://doi.org/10.20960/nh.626.

Hanson, Lars G. 2008. “Is Quantum Mechanics Necessary for Understanding Magnetic Resonance?” *Concepts in Magnetic Resonance Part A* 32A (5): 329–40. https://doi.org/10.1002/cmr.a.20123.

Harris, Robert J., Timothy F. Cloughesy, Linda M. Liau, Robert M. Prins, Joseph P. Antonios, Debiao Li, William H. Yong, et al. 2015. “PH-Weighted Molecular Imaging of Gliomas Using Amine Chemical Exchange Saturation Transfer MRI.” *Neuro-Oncology* 17 (11): 1514–24. https://doi.org/10.1093/neuonc/nov106.

Häussinger, Dieter. 2006. “Low Grade Cerebral Edema and the Pathogenesis of Hepatic Encephalopathy in Cirrhosis.” *Hepatology (Baltimore, Md.)* 43 (6): 1187–90. https://doi.org/10.1002/hep.21235.

Heeswijk, Ruud B. van, Kai Uffmann, Arnaud Comment, Fiodar Kurdzesau, Chiara Perazzolo, Cristina Cudalbu, Sami Jannin, et al. 2009. “Hyperpolarized Lithium-6 as a Sensor of Nanomolar Contrast Agents.” *Magnetic Resonance in Medicine : Official Journal of the Society of Magnetic Resonance in Medicine / Society of Magnetic Resonance in Medicine* 61 (6): 1489–93. https://doi.org/10.1002/mrm.21952.

Hemmings, Hugh C., Paul M. Riegelhaupt, Max B. Kelz, Ken Solt, Roderic G. Eckenhoff, Beverley A. Orser, and Peter A. Goldstein. 2019. “Towards a Comprehensive Understanding of Anesthetic Mechanisms of Action: A Decade of Discovery.” *Trends in Pharmacological Sciences* 40 (7): 464–81. https://doi.org/10.1016/j.tips.2019.05.001.

Henry P-G, Ugurbil K, Gruetter R. n.d. “In Vivo 13C NMR Measurement of Activity-dependent Malate-aspartate Shuttle Flux in the Brain.” In . ISMRM 2004, Kyoto, Japan.

Hermann, B., A. Santiago, S. Mouri, D. Thabut, and N. Weiss. 2018. “Nouveautés dans l’encéphalopathie hépatique : de l’encéphalopathie hépatique minimale à l’encéphalopathie hépatique clinique.” *Pratique Neurologique - FMC* 9 (1): 1–12. https://doi.org/10.1016/j.praneu.2018.01.001.

Herring, Bruce E., Katlin Silm, Robert H. Edwards, and Roger A. Nicoll. 2015. "Is Aspartate an Excitatory Neurotransmitter?" *The Journal of Neuroscience* 35 (28): 10168–71. https://doi.org/10.1523/JNEUROSCI.0524-15.2015.

Hertz, Leif, Jørgen Drejer, and Arne Schousboe. 1988. "Energy Metabolism in Glutamatergic Neurons, GABAergic Neurons and Astrocytes in Primary Cultures." *Neurochemical Research* 13 (7): 605–10. https://doi.org/10.1007/BF00973275.

Hore, P. J. 1999. "NMR Principles." In *Encyclopedia of Spectroscopy and Spectrometry*, edited by John C. Lindon, 1545–53. Oxford: Elsevier. https://doi.org/10.1006/rwsp.2000.0206.

Horn, Tobias, and Jochen Klein. 2010. "Lactate Levels in the Brain Are Elevated upon Exposure to Volatile Anesthetics: A Microdialysis Study." *Neurochemistry International* 57 (8): 940–47. https://doi.org/10.1016/j.neuint.2010.09.014.

Hoult, D. I. 1989. "The Magnetic Resonance Myth of Radio Waves." *Concepts in Magnetic Resonance* 1 (1): 1–5. https://doi.org/10.1002/cmr.1820010104.

Insko, E. K., and L. Bolinger. 1993. "Mapping of the Radiofrequency Field." *Journal of Magnetic Resonance, Series A* 103 (1): 82–85. https://doi.org/10.1006/jmra.1993.1133.

"(ISMRM 2019) Kinetic Modeling of Hyperpolarized [1-13C]Lactate Metabolism in a Mouse Model of Ischemic Stroke." n.d. Accessed July 15, 2020. http://archive.ismrm.org/2019/0259.html.

"(ISMRM 2019) Metabolism of Hyperpolarized [1-13C]Pyruvate in Awake, Isoflurane and Urethane Anesthetized Rat Brain." n.d. Accessed February 12, 2020. http://archive.ismrm.org/2019/0722.html.

Ivanov, Anton I., Anton E. Malkov, Tatsiana Waseem, Marat Mukhtarov, Svetlana Buldakova, Olena Gubkina, Misha Zilberter, and Yuri Zilberter. 2014. "Glycolysis and Oxidative Phosphorylation in Neurons and Astrocytes during Network Activity in Hippocampal Slices." *Journal of Cerebral Blood Flow and Metabolism: Official Journal of the International Society of Cerebral Blood Flow and Metabolism* 34 (3): 397–407. https://doi.org/10.1038/jcbfm.2013.222.

Jin, Tao, Ping Wang, Xiaopeng Zong, and Seong-Gi Kim. 2012. "Magnetic Resonance Imaging of the Amine-Proton EXchange (APEX) Dependent Contrast." *NeuroImage* 59 (2): 1218–27. https://doi.org/10.1016/j.neuroimage.2011.08.014.

Josan, Sonal, Ralph Hurd, Kelvin Billingsley, Lasitha Senadheera, Jae Mo Park, Yi-Fen Yen, Adolf Pfefferbaum, Daniel Spielman, and Dirk Mayer. 2013. "Effects of Isoflurane Anesthesia on Hyperpolarized 13C Metabolic Measurements in Rat Brain." *Magnetic Resonance in Medicine : Official Journal of the Society of Magnetic Resonance in Medicine / Society of Magnetic Resonance in Medicine* 70 (4): 1117–24. https://doi.org/10.1002/mrm.24532.

Kalambokis, Georgios N., Athanasia Mouzaki, Maria Rodi, Konstantinos Pappas, Andreas Fotopoulos, Xanthi Xourgia, and Epameinondas V. Tsianos. 2012. "Rifaximin Improves Systemic Hemodynamics and Renal Function in Patients with Alcohol-Related Cirrhosis and Ascites." *Clinical Gastroenterology and Hepatology: The Official Clinical Practice Journal of the American Gastroenterological Association* 10 (7): 815–18. https://doi.org/10.1016/j.cgh.2012.02.025.

Kalambokis, Georgios N., and Epameinondas V. Tsianos. 2012. “Rifaximin Reduces Endotoxemia and Improves Liver Function and Disease Severity in Patients with Decompensated Cirrhosis.” *Hepatology* 55 (2): 655–56. https://doi.org/10.1002/hep.24751.

Kanda, Teppei, and Yoshiaki Hikasa. 2008. “Neurohormonal and Metabolic Effects of Medetomidine Compared with Xylazine in Healthy Cats.” *Canadian Journal of Veterinary Research* 72 (3): 278.

Kao, Dina, Brandi Roach, Heekuk Park, Naomi Hotte, Karen Madsen, Vince Bain, and Puneeta Tandon. 2016. “Fecal Microbiota Transplantation in the Management of Hepatic Encephalopathy.” *Hepatology (Baltimore, Md.)* 63 (1): 339–40. https://doi.org/10.1002/hep.28121.

Kharbanda, Parampreet S., Vivek A. Saraswat, and Radha K. Dhiman. 2003. “Minimal Hepatic Encephalopathy: Diagnosis by Neuropsychological and Neurophysiologic Methods.” *Indian Journal of Gastroenterology: Official Journal of the Indian Society of Gastroenterology* 22 Suppl 2 (December): S37-41.

Khegai, O., R. F. Schulte, M. A. Janich, M. I. Menzel, E. Farrell, A. M. Otto, J. H. Ardenkjaer-Larsen, et al. 2014. “Apparent Rate Constant Mapping Using Hyperpolarized [1-(13)C]Pyruvate.” *NMR in Biomedicine* 27 (10): 1256–65. https://doi.org/10.1002/nbm.3174.

Knoop, Kathryn A., Keely G. McDonald, Devesha H. Kulkarni, and Rodney D. Newberry. 2016. “Antibiotics Promote Inflammation through the Translocation of Native Commensal Colonic Bacteria.” *Gut* 65 (7): 1100–1109. https://doi.org/10.1136/gutjnl-2014-309059.

Kofke, W. A., R. A. Hawkins, D. W. Davis, and J. F. Biebuyck. 1987. “Comparison of the Effects of Volatile Anesthetics on Brain Glucose Metabolism in Rats.” *Anesthesiology* 66 (6): 810–13. https://doi.org/10.1097/00000542-198706000-00016.

Kohro, S., Q. H. Hogan, Y. Nakae, M. Yamakage, and Z. J. Bosnjak. 2001. “Anesthetic Effects on Mitochondrial ATP-Sensitive K Channel.” *Anesthesiology* 95 (6): 1435–1340. https://doi.org/10.1097/00000542-200112000-00024.

Koller, K. J., R. Zaczek, and J. T. Coyle. 1984. “N-Acetyl-Aspartyl-Glutamate: Regional Levels in Rat Brain and the Effects of Brain Lesions as Determined by a New HPLC Method.” *Journal of Neurochemistry* 43 (4): 1136–42. https://doi.org/10.1111/j.1471-4159.1984.tb12854.x.

Komoroski, R. A., J. E. O. Newton, E. Walker, D. Cardwell, N. R. Jagannathan, S. Ramaprasad, and J. Sprig. 1990. “In Vivo NMR Spectroscopy of Lithium-7 in Humans.” *Magnetic Resonance in Medicine* 15 (3): 347–56. https://doi.org/10.1002/mrm.1910150302.

Kreis, R. 1997. “Quantitative Localized 1H MR Spectroscopy for Clinical Use.” *Progress in Nuclear Magnetic Resonance Spectroscopy* 31 (2): 155–95. https://doi.org/10.1016/S0079-6565(97)00014-9.

Lai, J. C., and A. J. Cooper. 1986. “Brain Alpha-Ketoglutarate Dehydrogenase Complex: Kinetic Properties, Regional Distribution, and Effects of Inhibitors.” *Journal of Neurochemistry* 47 (5): 1376–86. https://doi.org/10.1111/j.1471-4159.1986.tb00768.x.

Lai, Marta, Bernard Lanz, Carole Poitry-Yamate, Jackeline F Romero, Corina M Berset, Cristina Cudalbu, and Rolf Gruetter. 2018. “In Vivo 13C MRS in the Mouse Brain at 14.1 Tesla and Metabolic Flux Quantification under Infusion of [1,6-13C2]Glucose.” *Journal of Cerebral Blood Flow & Metabolism* 38 (10): 1701–14. https://doi.org/10.1177/0271678X17734101.

Lanz, Bernard. 2012. “Mathematical Modeling of Brain Energy Metabolism, Measured with PET and MRS in Rodents.” Infoscience. EPFL. 2012. https://doi.org/10.5075/epfl-thesis-5468.

Lehmann, A., H. Hagberg, I. Jacobson, and A. Hamberger. 1985. “Effects of Status Epilepticus on Extracellular Amino Acids in the Hippocampus.” *Brain Research* 359 (1–2): 147–51. https://doi.org/10.1016/0006-8993(85)91422-2.

Lenz, Christian, Annette Rebel, Klaus van Ackern, Wolfgang Kuschinsky, and Klaus F. Waschke. 1998. “Local Cerebral Blood Flow, Local Cerebral Glucose Utilization, and Flow-Metabolism Coupling during Sevoflurane versus Isoflurane Anesthesia in Rats.” *Anesthesiology: The Journal of the American Society of Anesthesiologists* 89 (6): 1480–88.

Lockwood, Alan H., Karin Weissenborn, Martin Bokemeyer, U. Tietge, and Wolfgang Burchert. 2002. “Correlations Between Cerebral Glucose Metabolism and Neuropsychological Test Performance in Nonalcoholic Cirrhotics.” *Metabolic Brain Disease* 17 (1): 29–40. https://doi.org/10.1023/A:1014000313824.

Lu, Ming, Xiao-Hong Zhu, Yi Zhang, Gheorghe Mateescu, and Wei Chen. 2017. “Quantitative Assessment of Brain Glucose Metabolic Rates Using in Vivo Deuterium Magnetic Resonance Spectroscopy.” *Journal of Cerebral Blood Flow and Metabolism: Official Journal of the International Society of Cerebral Blood Flow and Metabolism* 37 (11): 3518–30. https://doi.org/10.1177/0271678X17706444.

Lunia, Manish Kumar, Barjesh Chander Sharma, Praveen Sharma, Sanjeev Sachdeva, and Siddharth Srivastava. 2014. “Probiotics Prevent Hepatic Encephalopathy in Patients with Cirrhosis: A Randomized Controlled Trial.” *Clinical Gastroenterology and Hepatology: The Official Clinical Practice Journal of the American Gastroenterological Association* 12 (6): 1003-1008.e1. https://doi.org/10.1016/j.cgh.2013.11.006.

Luo, Ming, Lei Li, Chen-Zheng Lu, and Wu-Kui Cao. 2011. “Clinical Efficacy and Safety of Lactulose for Minimal Hepatic Encephalopathy: A Meta-Analysis.” *European Journal of Gastroenterology & Hepatology* 23 (12): 1250–57. https://doi.org/10.1097/MEG.0b013e32834d1938.

Magistretti, P. J., and L. Pellerin. 1996. “Cellular Bases of Brain Energy Metabolism and Their Relevance to Functional Brain Imaging: Evidence for a Prominent Role of Astrocytes.” *Cerebral Cortex (New York, N.Y.: 1991)* 6 (1): 50–61. https://doi.org/10.1093/cercor/6.1.50.

Magistretti, P. J., O. Sorg, N. Yu, J. L. Martin, and L. Pellerin. 1993. “Neurotransmitters Regulate Energy Metabolism in Astrocytes: Implications for the Metabolic Trafficking between Neural Cells.” *Developmental Neuroscience* 15 (3–5): 306–12. https://doi.org/10.1159/000111349.

Magistretti, Pierre J. 2006. “Neuron–Glia Metabolic Coupling and Plasticity.” *Journal of Experimental Biology* 209 (12): 2304–11. https://doi.org/10.1242/jeb.02208.

Malisza, K. L., P. Kozlowski, and J. Peeling. 1998. “A Review of in Vivo 1H Magnetic Resonance Spectroscopy of Cerebral Ischemia in Rats.” *Biochemistry and Cell Biology = Biochimie Et Biologie Cellulaire* 76 (2–3): 487–96. https://doi.org/10.1139/bcb-76-2-3-487.

Mallet, Maxime, Nicolas Weiss, Dominique Thabut, and Marika Rudler. 2018. “Why and When to Measure Ammonemia in Cirrhosis?” *Clinics and Research in Hepatology and Gastroenterology* 42 (6): 505–11. https://doi.org/10.1016/j.clinre.2018.01.004.

Manto, Mario, James M. Bower, Adriana Bastos Conforto, José M. Delgado-García, Suzete Nascimento Farias da Guarda, Marcus Gerwig, Christophe Habas, et al. 2012. "Consensus Paper: Roles of the Cerebellum in Motor Control--the Diversity of Ideas on Cerebellar Involvement in Movement." *Cerebellum (London, England)* 11 (2): 457–87. https://doi.org/10.1007/s12311-011-0331-9.

Marjańska, Małgorzata, Alexander A. Shestov, Dinesh K. Deelchand, Emily Kittelson, and Pierre-Gilles Henry. 2018. "Brain Metabolism under Different Anesthetic Conditions Using Hyperpolarized [1-13C]Pyruvate and [2-13C]Pyruvate." *NMR in Biomedicine* 31 (12): e4012. https://doi.org/10.1002/nbm.4012.

Marquardt, Donald W. 1963. "An Algorithm for Least-Squares Estimation of Nonlinear Parameters." *Journal of the Society for Industrial and Applied Mathematics* 11 (2): 431–41.

Martinez-Hernandez, A., K. P. Bell, and M. D. Norenberg. 1977. "Glutamine Synthetase: Glial Localization in Brain." *Science* 195 (4284): 1356–58. https://doi.org/10.1126/science.14400.

Masamoto, Kazuto, and Iwao Kanno. 2012. "Anesthesia and the Quantitative Evaluation of Neurovascular Coupling." *Journal of Cerebral Blood Flow and Metabolism: Official Journal of the International Society of Cerebral Blood Flow and Metabolism* 32 (7): 1233–47. https://doi.org/10.1038/jcbfm.2012.50.

Mastromarino, Paola, Daniela Capobianco, Giuseppe Campagna, Nicola Laforgia, Pietro Drimaco, Alessandra Dileone, and Maria E. Baldassarre. 2014. "Correlation between Lactoferrin and Beneficial Microbiota in Breast Milk and Infant's Feces." *Biometals: An International Journal on the Role of Metal Ions in Biology, Biochemistry, and Medicine* 27 (5): 1077–86. https://doi.org/10.1007/s10534-014-9762-3.

Mergenthaler, Philipp, Ute Lindauer, Gerald A. Dienel, and Andreas Meisel. 2013. "Sugar for the Brain: The Role of Glucose in Physiological and Pathological Brain Function." *Trends in Neurosciences* 36 (10): 587–97. https://doi.org/10.1016/j.tins.2013.07.001.

Merli, Manuela, Cristina Lucidi, Ilaria Pentassuglio, Valerio Giannelli, Michela Giusto, Vincenza Di Gregorio, Chiara Pasquale, et al. 2013. "Increased Risk of Cognitive Impairment in Cirrhotic Patients with Bacterial Infections." *Journal of Hepatology* 59 (2): 243–50. https://doi.org/10.1016/j.jhep.2013.03.012.

Michenfelder, J. D., and R. A. Theye. 1975. "In Vivo Toxic Effects of Halothane on Canine Cerebral Metabolic Pathways." *The American Journal of Physiology* 229 (4): 1050–55. https://doi.org/10.1152/ajplegacy.1975.229.4.1050.

Miéville, Pascal, Puneet Ahuja, Riddhiman Sarkar, Sami Jannin, Paul R. Vasos, Sandrine Gerber-Lemaire, Mor Mishkovsky, et al. 2010. "Scavenging Free Radicals To Preserve Enhancement and Extend Relaxation Times in NMR Using Dynamic Nuclear Polarization." *Angewandte Chemie International Edition* 49 (35): 6182–85. https://doi.org/10.1002/anie.201000934.

Miller, Jack J., James T. Grist, Sébastien Serres, James R. Larkin, Angus Z. Lau, Kevin Ray, Katherine R. Fisher, et al. 2018. "13 C Pyruvate Transport Across the Blood-Brain Barrier in Preclinical Hyperpolarised MRI." *Scientific Reports* 8 (1): 15082. https://doi.org/10.1038/s41598-018-33363-5.

Mishkovsky, Mor, Brian Anderson, Magnus Karlsson, Mathilde H. Lerche, A. Dean Sherry, Rolf Gruetter, Zoltan Kovacs, and Arnaud Comment. 2017. "Measuring Glucose Cerebral

Metabolism in the Healthy Mouse Using Hyperpolarized 13 C Magnetic Resonance." *Scientific Reports* 7 (1): 1–8. https://doi.org/10.1038/s41598-017-12086-z.

Mishkovsky, Mor, Arnaud Comment, and Rolf Gruetter. 2012. "In Vivo Detection of Brain Krebs Cycle Intermediate by Hyperpolarized Magnetic Resonance." *Journal of Cerebral Blood Flow and Metabolism: Official Journal of the International Society of Cerebral Blood Flow and Metabolism* 32 (12): 2108–13. https://doi.org/10.1038/jcbfm.2012.136.

Mittal, Vibhu Vibhas, Barjesh Chander Sharma, Praveen Sharma, and Shiv Kumar Sarin. 2011. "A Randomized Controlled Trial Comparing Lactulose, Probiotics, and L-Ornithine L-Aspartate in Treatment of Minimal Hepatic Encephalopathy." *European Journal of Gastroenterology & Hepatology* 23 (8): 725–32. https://doi.org/10.1097/MEG.0b013e32834696f5.

Mlynárik, Vladimír, Giulio Gambarota, Hanne Frenkel, and Rolf Gruetter. 2006. "Localized Short-Echo-Time Proton MR Spectroscopy with Full Signal-Intensity Acquisition." *Magnetic Resonance in Medicine* 56 (5): 965–70. https://doi.org/10.1002/mrm.21043.

"Mouse : Decision Tree for Blood Sampling | NC3Rs." n.d. Accessed February 12, 2020. https://www.nc3rs.org.uk/mouse-decision-tree-blood-sampling.

Mullen, Kevin D., Arun J. Sanyal, Nathan M. Bass, Fred F. Poordad, Muhammad Y. Sheikh, R. Todd Frederick, Enoch Bortey, and William P. Forbes. 2014. "Rifaximin Is Safe and Well Tolerated for Long-Term Maintenance of Remission from Overt Hepatic Encephalopathy." *Clinical Gastroenterology and Hepatology: The Official Clinical Practice Journal of the American Gastroenterological Association* 12 (8): 1390-1397.e2. https://doi.org/10.1016/j.cgh.2013.12.021.

Muravchick, Stanley, and Richard J. Levy. 2006. "Clinical Implications of Mitochondrial Dysfunction." *Anesthesiology: The Journal of the American Society of Anesthesiologists* 105 (4): 819–37.

Nagy, Csörsz, and Elisa Einwallner. 2018. "Study of In Vivo Glucose Metabolism in High-Fat Diet-Fed Mice Using Oral Glucose Tolerance Test (OGTT) and Insulin Tolerance Test (ITT)." *Journal of Visualized Experiments: JoVE*, no. 131 (07). https://doi.org/10.3791/56672.

Nair, Anroop B., and Shery Jacob. 2016. "A Simple Practice Guide for Dose Conversion between Animals and Human." *Journal of Basic and Clinical Pharmacy* 7 (2): 27–31. https://doi.org/10.4103/0976-0105.177703.

Narayana, Ponnada A. 2005. "Magnetic Resonance Spectroscopy in the Monitoring of Multiple Sclerosis." *Journal of Neuroimaging : Official Journal of the American Society of Neuroimaging* 15 (4 Suppl): 46S-57S. https://doi.org/10.1177/1051228405284200.

Nava, Gerardo M., and Thaddeus S. Stappenbeck. 2011. "Diversity of the Autochthonous Colonic Microbiota." *Gut Microbes* 2 (2): 99–104. https://doi.org/10.4161/gmic.2.2.15416.

Nguyen, Justin H., Satoshi Yamamoto, Jeffery Steers, Daniel Sevlever, Wenlang Lin, Naoki Shimojima, Monica Castanedes-Casey, et al. 2006. "Matrix Metalloproteinase-9 Contributes to Brain Extravasation and Edema in Fulminant Hepatic Failure Mice." *Journal of Hepatology* 44 (6): 1105–14. https://doi.org/10.1016/j.jhep.2005.09.019.

Nicolao, Francesca, Cesare Efrati, Andrea Masini, Manuela Merli, Adolfo Francesco Attili, and Oliviero Riggio. 2003. "Role of Determination of Partial Pressure of Ammonia in Cirrhotic Patients

with and without Hepatic Encephalopathy." *Journal of Hepatology* 38 (4): 441–46. https://doi.org/10.1016/s0168-8278(02)00436-1.

Norenberg, M. D. 1998. "Astroglial Dysfunction in Hepatic Encephalopathy." *Metabolic Brain Disease* 13 (4): 319–35. https://doi.org/10.1023/a:1020688925901.

Ochoa-Sanchez, Rafael, and Christopher F. Rose. 2018. "Pathogenesis of Hepatic Encephalopathy in Chronic Liver Disease." *Journal of Clinical and Experimental Hepatology* 8 (3): 262–71. https://doi.org/10.1016/j.jceh.2018.08.001.

Ordidge, R. J, A Connelly, and J. A. B Lohman. 1986. "Image-Selected in Vivo Spectroscopy (ISIS). A New Technique for Spatially Selective Nmr Spectroscopy." *Journal of Magnetic Resonance (1969)* 66 (2): 283–94. https://doi.org/10.1016/0022-2364(86)90031-4.

Ori, C., M. Dam, G. Pizzolato, L. Battistin, and G. Giron. 1986. "Effects of Isoflurane Anesthesia on Local Cerebral Glucose Utilization in the Rat." *Anesthesiology* 65 (2): 152–56. https://doi.org/10.1097/00000542-198608000-00004.

Paasonen, Jaakko, Petteri Stenroos, Raimo A. Salo, Vesa Kiviniemi, and Olli Gröhn. 2018. "Functional Connectivity under Six Anesthesia Protocols and the Awake Condition in Rat Brain." *NeuroImage* 172: 9–20. https://doi.org/10.1016/j.neuroimage.2018.01.014.

Paik, Yong Han, Kwan Sik Lee, Kwang Hyub Han, Kun Hoon Song, Myoung Hwan Kim, Byung Soo Moon, Sang Hoon Ahn, et al. 2005. "Comparison of Rifaximin and Lactulose for the Treatment of Hepatic Encephalopathy: A Prospective Randomized Study." *Yonsei Medical Journal* 46 (3): 399–407. https://doi.org/10.3349/ymj.2005.46.3.399.

Palomero-Gallagher, Nicola, and Karl Zilles. 2013. "Neurotransmitter Receptor Alterations in Hepatic Encephalopathy: A Review." *Archives of Biochemistry and Biophysics* 536 (2): 109–21. https://doi.org/10.1016/j.abb.2013.02.010.

Pan, J. W., D. B. Twieg, and H. P. Hetherington. 1998. "Quantitative Spectroscopic Imaging of the Human Brain." *Magnetic Resonance in Medicine* 40 (3): 363–69. https://doi.org/10.1002/mrm.1910400305.

Papa, S., V. Petruzzella, and S. Scacco. 2007. "1.5 Electron Transport. Structure, Redox-Coupled Protonmotive Activity, and Pathological Disorders of Respiratory Chain Complexes." In *Handbook of Neurochemistry and Molecular Neurobiology: Brain Energetics. Integration of Molecular and Cellular Processes*, edited by Abel Lajtha, Gary E. Gibson, and Gerald A. Dienel, 93–118. Boston, MA: Springer US. https://doi.org/10.1007/978-0-387-30411-3_5.

Patching, Simon G. 2017. "Glucose Transporters at the Blood-Brain Barrier: Function, Regulation and Gateways for Drug Delivery." *Molecular Neurobiology* 54 (2): 1046–77. https://doi.org/10.1007/s12035-015-9672-6.

Pedretti, G., C. Calzetti, G. Missale, and F. Fiaccadori. 1991. "Rifaximin versus Neomycin on Hyperammoniemia in Chronic Portal Systemic Encephalopathy of Cirrhotics. A Double-Blind, Randomized Trial." *The Italian Journal of Gastroenterology* 23 (4): 175–78.

Pellerin, L. 2010. "Food for Thought: The Importance of Glucose and Other Energy Substrates for Sustaining Brain Function under Varying Levels of Activity." *Diabetes & Metabolism* 36 Suppl 3 (October): S59-63. https://doi.org/10.1016/S1262-3636(10)70469-9.

Pellerin, L., G. Pellegri, P. G. Bittar, Y. Charnay, C. Bouras, J. L. Martin, N. Stella, and P. J. Magistretti. 1998. "Evidence Supporting the Existence of an Activity-Dependent Astrocyte-Neuron Lactate Shuttle." *Developmental Neuroscience* 20 (4–5): 291–99. https://doi.org/10.1159/000017324.

Pellerin, Luc, Anne-Karine Bouzier-Sore, Agnès Aubert, Sébastien Serres, Michel Merle, Robert Costalat, and Pierre J. Magistretti. 2007. "Activity-Dependent Regulation of Energy Metabolism by Astrocytes: An Update." *Glia* 55 (12): 1251–62. https://doi.org/10.1002/glia.20528.

Pellerin, Luc, and Pierre J. Magistretti. 2004. "Neuroenergetics: Calling upon Astrocytes to Satisfy Hungry Neurons." *The Neuroscientist: A Review Journal Bringing Neurobiology, Neurology and Psychiatry* 10 (1): 53–62. https://doi.org/10.1177/1073858403260159.

———. 2012. "Sweet Sixteen for ANLS." *Journal of Cerebral Blood Flow and Metabolism: Official Journal of the International Society of Cerebral Blood Flow and Metabolism* 32 (7): 1152–66. https://doi.org/10.1038/jcbfm.2011.149.

Pereg, David, Andy Kotliroff, Natan Gadoth, Ruth Hadary, Michael Lishner, and Yona Kitay-Cohen. 2011. "Probiotics for Patients with Compensated Liver Cirrhosis: A Double-Blind Placebo-Controlled Study." *Nutrition (Burbank, Los Angeles County, Calif.)* 27 (2): 177–81. https://doi.org/10.1016/j.nut.2010.01.006.

Petrazzo, Grégory. 2020. "Cibler Le Système Digestif Pour Protéger Le Foie : Évaluation de l'efficacité Prophylactique et Thérapeutique de Traitements de l'encéphalopathie Hépatique Dans Un Modèle Murin de Cholestase Hépatique Par Ligature de La Voie Biliaire," March. https://papyrus.bib.umontreal.ca/xmlui/handle/1866/23673.

Pfeuffer, J., I. Tkác, S. W. Provencher, and R. Gruetter. 1999. "Toward an in Vivo Neurochemical Profile: Quantification of 18 Metabolites in Short-Echo-Time (1)H NMR Spectra of the Rat Brain." *Journal of Magnetic Resonance (San Diego, Calif.: 1997)* 141 (1): 104–20. https://doi.org/10.1006/jmre.1999.1895.

Ponziani, Francesca Romana, Viviana Gerardi, Silvia Pecere, Francesca D'Aversa, Loris Lopetuso, Maria Assunta Zocco, Maurizio Pompili, and Antonio Gasbarrini. 2015. "Effect of Rifaximin on Gut Microbiota Composition in Advanced Liver Disease and Its Complications." *World Journal of Gastroenterology* 21 (43): 12322–33. https://doi.org/10.3748/wjg.v21.i43.12322.

Poptani, H., R. K. Gupta, R. Roy, R. Pandey, V. K. Jain, and D. K. Chhabra. 1995. "Characterization of Intracranial Mass Lesions with in Vivo Proton MR Spectroscopy." *AJNR. American Journal of Neuroradiology* 16 (8): 1593–1603.

Pouwels, P. J., and J. Frahm. 1997. "Differential Distribution of NAA and NAAG in Human Brain as Determined by Quantitative Localized Proton MRS." *NMR in Biomedicine* 10 (2): 73–78. https://doi.org/10.1002/(sici)1099-1492(199704)10:2<73::aid-nbm448>3.0.co;2-4.

———. 1998. "Regional Metabolite Concentrations in Human Brain as Determined by Quantitative Localized Proton MRS." *Magnetic Resonance in Medicine* 39 (1): 53–60. https://doi.org/10.1002/mrm.1910390110.

"PowerSampleSize < Main < Vanderbilt Biostatistics Wiki." n.d. Accessed July 1, 2020. http://biostat.mc.vanderbilt.edu/wiki/Main/PowerSampleSize.

Prakash, Ravi, and Kevin D. Mullen. 2010. “Mechanisms, Diagnosis and Management of Hepatic Encephalopathy.” *Nature Reviews. Gastroenterology & Hepatology* 7 (9): 515–25. https://doi.org/10.1038/nrgastro.2010.116.

Prasad, Srinivasa, Radha K. Dhiman, Ajay Duseja, Yogesh K. Chawla, Arpita Sharma, and Ritesh Agarwal. 2007. “Lactulose Improves Cognitive Functions and Health-Related Quality of Life in Patients with Cirrhosis Who Have Minimal Hepatic Encephalopathy.” *Hepatology (Baltimore, Md.)* 45 (3): 549–59. https://doi.org/10.1002/hep.21533.

Pratap Mouli, Venigalla, Jaya Benjamin, Mamta Bhushan Singh, Kalaivani Mani, Sushil Kumar Garg, Anoop Saraya, and Yogendra Kumar Joshi. 2015. “Effect of Probiotic VSL#3 in the Treatment of Minimal Hepatic Encephalopathy: A Non-Inferiority Randomized Controlled Trial.” *Hepatology Research: The Official Journal of the Japan Society of Hepatology* 45 (8): 880–89. https://doi.org/10.1111/hepr.12429.

Prichard, J., D. Rothman, E. Novotny, O. Petroff, T. Kuwabara, M. Avison, A. Howseman, C. Hanstock, and R. Shulman. 1991. “Lactate Rise Detected by 1H NMR in Human Visual Cortex during Physiologic Stimulation.” *Proceedings of the National Academy of Sciences of the United States of America* 88 (13): 5829–31. https://doi.org/10.1073/pnas.88.13.5829.

Provencher, S. W. 1993. “Estimation of Metabolite Concentrations from Localized in Vivo Proton NMR Spectra.” *Magnetic Resonance in Medicine* 30 (6): 672–79. https://doi.org/10.1002/mrm.1910300604.

Pujol, A., J. Pujol, F. Graus, A. Rimola, J. Peri, J. M. Mercader, J. C. García-Pagan, J. Bosch, J. Rodés, and E. Tolosa. 1993. “Hyperintense Globus Pallidus on T1-Weighted MRI in Cirrhotic Patients Is Associated with Severity of Liver Failure.” *Neurology* 43 (1): 65–69. https://doi.org/10.1212/wnl.43.1_part_1.65.

Quek, Lake-Ee, Menghan Liu, Sanket Joshi, and Nigel Turner. 2016. “Fast Exchange Fluxes around the Pyruvate Node: A Leaky Cell Model to Explain the Gain and Loss of Unlabelled and Labelled Metabolites in a Tracer Experiment.” *Cancer & Metabolism* 4 (July). https://doi.org/10.1186/s40170-016-0153-9.

Rackayova, Veronika, Olivier Braissant, Corina Berset, Jocelyn Grosse, Daniela Capobianco, Paola Mastromarino, Valerie A. McLin, and Cristina Cudalbu. 2017. “Probiotic Treatment Improves Outcome of Chronic Hepatic Encephalopathy in BDL Rats, an In Vivo Longitudinal 1H MRS Study.” *Journal of Clinical and Experimental Hepatology* 7 (February): S8–9. https://doi.org/10.1016/j.jceh.2017.01.012.

Rackayova, Veronika, Olivier Braissant, Valérie A. McLin, Corina Berset, Bernard Lanz, and Cristina Cudalbu. 2016. “1H and 31P Magnetic Resonance Spectroscopy in a Rat Model of Chronic Hepatic Encephalopathy: In Vivo Longitudinal Measurements of Brain Energy Metabolism.” *Metabolic Brain Disease* 31 (6): 1303–14. https://doi.org/10.1007/s11011-015-9715-8.

Rae, Caroline D. 2014. “A Guide to the Metabolic Pathways and Function of Metabolites Observed in Human Brain 1H Magnetic Resonance Spectra.” *Neurochemical Research* 39 (1): 1–36. https://doi.org/10.1007/s11064-013-1199-5.

Ramaprasad, S. 2004. “Lithium Spectroscopic Imaging of Rat Brain at Therapeutic Doses.” *Magnetic Resonance Imaging* 22 (5): 727–34. https://doi.org/10.1016/j.mri.2004.01.063.

Ramaprasad, Subbaraya, Elzbieta Ripp, Jiaxiong Pi, and Melvin Lyon. 2005. “Pharmacokinetics of Lithium in Rat Brain Regions by Spectroscopic Imaging.” *Magnetic Resonance Imaging* 23 (8): 859–63. https://doi.org/10.1016/j.mri.2005.07.007.

Reid, Gregor. 2006. “Probiotics to Prevent the Need For, and Augment the Use Of, Antibiotics.” *The Canadian Journal of Infectious Diseases & Medical Microbiology* 17 (5): 291–95.

Reynaud, Olivier, Analina R. da Silva, Rolf Gruetter, and Ileana O. Jelescu. 2019. “Multi-Slice Passband BSSFP for Human and Rodent FMRI at Ultra-High Field.” *Journal of Magnetic Resonance* 305 (August): 31–40. https://doi.org/10.1016/j.jmr.2019.05.010.

Ridlon, Jason M., Joao Marcelo Alves, Phillip B. Hylemon, and Jasmohan S. Bajaj. 2013. “Cirrhosis, Bile Acids and Gut Microbiota: Unraveling a Complex Relationship.” *Gut Microbes* 4 (5): 382–87. https://doi.org/10.4161/gmic.25723.

Rockey, Don C., John M. Vierling, Parvez Mantry, Marwan Ghabril, Robert S. Brown, Olga Alexeeva, Igor A. Zupanets, et al. 2014. “Randomized, Double-Blind, Controlled Study of Glycerol Phenylbutyrate in Hepatic Encephalopathy.” *Hepatology (Baltimore, Md.)* 59 (3): 1073–83. https://doi.org/10.1002/hep.26611.

Rodrigues, Tiago B., Eva M. Serrao, Brett W. C. Kennedy, De-En Hu, Mikko I. Kettunen, and Kevin M. Brindle. 2014. “Magnetic Resonance Imaging of Tumor Glycolysis Using Hyperpolarized 13C-Labeled Glucose.” *Nature Medicine* 20 (1): 93–97. https://doi.org/10.1038/nm.3416.

Román, Eva, Juan Camilo Nieto, Cristina Gely, Sílvia Vidal, Marta Pozuelo, Maria Poca, Cándido Juárez, Carlos Guarner, Chaysavanh Manichanh, and Germán Soriano. 2019. “Effect of a Multistrain Probiotic on Cognitive Function and Risk of Falls in Patients With Cirrhosis: A Randomized Trial.” *Hepatology Communications* 3 (5): 632–45. https://doi.org/10.1002/hep4.1325.

Ronconi, Luca, and Peter J. Sadler. 2008. “Applications of Heteronuclear NMR Spectroscopy in Biological and Medicinal Inorganic Chemistry.” *Coordination Chemistry Reviews*, Applications of NMR to Inorganic and Organometallic Chemistry, 252 (21): 2239–77. https://doi.org/10.1016/j.ccr.2008.01.016.

Rose, Christopher F., Piero Amodio, Jasmohan S. Bajaj, Radha Krishan Dhiman, Sara Montagnese, Simon D. Taylor-Robinson, Hendrik Vilstrup, and Rajiv Jalan. 2020. “Hepatic Encephalopathy: Novel Insights into Classification, Pathophysiology and Therapy.” *Journal of Hepatology* 73 (6): 1526–47. https://doi.org/10.1016/j.jhep.2020.07.013.

Ross, Brian. 2014. “Chapter 4.3 - Hyperpolarized Magnetic Resonance Imaging and Spectroscopy of the Brain.” In Magnetic Resonance Spectroscopy, edited by Charlotte Stagg and Douglas Rothman, 331–49. San Diego: Academic Press. https://doi.org/10.1016/B978-0-12-401688-0.00024-0.

Rottenberg, H. 1983. “Uncoupling of Oxidative Phosphorylation in Rat Liver Mitochondria by General Anesthetics.” *Proceedings of the National Academy of Sciences of the United States of America* 80 (11): 3313–17. https://doi.org/10.1073/pnas.80.11.3313.

Rowland, Ian, Lucio Capurso, Kevin Collins, John Cummings, Nathalie Delzenne, Olivier Goulet, Francisco Guarner, Philippe Marteau, and Rémy Meier. 2010. “Current Level of Consensus on Probiotic Science--Report of an Expert Meeting--London, 23 November 2009.” *Gut Microbes* 1 (6): 436–39. https://doi.org/10.4161/gmic.1.6.13610.

Saab, Sammy, Duminda Suraweera, Jennifer Au, Elena G. Saab, Tori S. Alper, and Myron J. Tong. 2016. "Probiotics Are Helpful in Hepatic Encephalopathy: A Meta-Analysis of Randomized Trials." *Liver International: Official Journal of the International Association for the Study of the Liver* 36 (7): 986–93. https://doi.org/10.1111/liv.13005.

Schousboe, Arne, Helle S. Waagepetersen, Renata Leke, and Lasse K. Bak. 2014. "Effects of Hyperammonemia on Brain Energy Metabolism: Controversial Findings in Vivo and in Vitro." *Metabolic Brain Disease* 29 (4): 913–17. https://doi.org/10.1007/s11011-014-9513-8.

Schurr, Avital, James J. Miller, Ralphiel S. Payne, and Benjamin M. Rigor. 1999. "An Increase in Lactate Output by Brain Tissue Serves to Meet the Energy Needs of Glutamate-Activated Neurons." *Journal of Neuroscience* 19 (1): 34–39. https://doi.org/10.1523/JNEUROSCI.19-01-00034.1999.

Schwarzkopf, Tina M., Tobias Horn, Dorothee Lang, and Jochen Klein. 2013. "Blood Gases and Energy Metabolites in Mouse Blood before and after Cerebral Ischemia: The Effects of Anesthetics." *Experimental Biology and Medicine (Maywood, N.J.)* 238 (1): 84–89. https://doi.org/10.1258/ebm.2012.012261.

Sestili, Piero, Chiara Martinelli, Giorgio Bravi, Giovanni Piccoli, Rosa Curci, Michela Battistelli, Elisabetta Falcieri, Deborah Agostini, Anna Maria Gioacchini, and Vilberto Stocchi. 2006. "Creatine Supplementation Affords Cytoprotection in Oxidatively Injured Cultured Mammalian Cells via Direct Antioxidant Activity." *Free Radical Biology & Medicine* 40 (5): 837–49. https://doi.org/10.1016/j.freeradbiomed.2005.10.035.

Sharma, Praveen, Amit Agrawal, Barjesh C. Sharma, and Shiv K. Sarin. 2011. "Prophylaxis of Hepatic Encephalopathy in Acute Variceal Bleed: A Randomized Controlled Trial of Lactulose versus No Lactulose." *Journal of Gastroenterology and Hepatology* 26 (6): 996–1003. https://doi.org/10.1111/j.1440-1746.2010.06596.x.

Sharma, Praveen, Barjesh C. Sharma, Vinod Puri, and Shiv Kumar Sarin. 2008. "An Open-Label Randomized Controlled Trial of Lactulose and Probiotics in the Treatment of Minimal Hepatic Encephalopathy." *European Journal of Gastroenterology & Hepatology* 20 (6): 506–11. https://doi.org/10.1097/MEG.0b013e3282f3e6f5.

Shaw, David M., A. M. P. Kellam, and R. F. Mottram. 2013. *Brain Sciences in Psychiatry*. Butterworth-Heinemann.

Shawcross, Debbie L., Nathan A. Davies, Roger Williams, and Rajiv Jalan. 2004. "Systemic Inflammatory Response Exacerbates the Neuropsychological Effects of Induced Hyperammonemia in Cirrhosis." *Journal of Hepatology* 40 (2): 247–54. https://doi.org/10.1016/j.jhep.2003.10.016.

Shin, Seung Kak, Oh Sang Kwon, Jong Joon Lee, Yeon Ho Park, Cheol Soo Choi, Sung Hwan Jeong, Duck Joo Choi, Yun Soo Kim, and Ju Hyun Kim. 2017. "Effect of Rifaximin on Hepatic Fibrosis in Bile Duct-Ligated Rat Model." *The Korean Journal of Gastroenterology = Taehan Sohwagi Hakhoe Chi* 70 (5): 239–46. https://doi.org/10.4166/kjg.2017.70.5.239.

Sian, J., D. T. Dexter, A. J. Lees, S. Daniel, Y. Agid, F. Javoy-Agid, P. Jenner, and C. D. Marsden. 1994. "Alterations in Glutathione Levels in Parkinson's Disease and Other Neurodegenerative Disorders Affecting Basal Ganglia." *Annals of Neurology* 36 (3): 348–55. https://doi.org/10.1002/ana.410360305.

Sibson, Nicola R., Ajay Dhankhar, Graeme F. Mason, Douglas L. Rothman, Kevin L. Behar, and Robert G. Shulman. 1998. “Stoichiometric Coupling of Brain Glucose Metabolism and Glutamatergic Neuronal Activity.” *Proceedings of the National Academy of Sciences* 95 (1): 316–21. https://doi.org/10.1073/pnas.95.1.316.

Simicic, Dunja, Katarzyna Pierzchala, Veronika Rackayová, Olivier Braissant, Stefanita-Octavian Mitrea, Dario Sessa, Valérie A. McLin, and Cristina Cudalbu. 2019. “P: 33 In Vivo Longitudinal 1H MRS Study of Hippocampal, Cereberal and Striatal Metabolic Changes in the Adult Brain Using an Animal Model of Chronic Hepatic Encephalopathy.” *American Journal of Gastroenterology* 114 (September): S17. https://doi.org/10.14309/01.ajg.0000582108.29364.13.

Sirmpilatze, Nikoloz, Jürgen Baudewig, and Susann Boretius. 2019. “Temporal Stability of FMRI in Medetomidine-Anesthetized Rats.” *Scientific Reports* 9 (1): 1–13. https://doi.org/10.1038/s41598-019-53144-y.

Soares, J. C., F. Boada, S. Spencer, A. G. Mallinger, C. S. Dippold, K. F. Wells, E. Frank, M. S. Keshavan, S. Gershon, and D. J. Kupfer. 2001. “Brain Lithium Concentrations in Bipolar Disorder Patients: Preliminary (7)Li Magnetic Resonance Studies at 3 T.” *Biological Psychiatry* 49 (5): 437–43. https://doi.org/10.1016/s0006-3223(00)00985-9.

Sogni, P. n.d. “Rifaximine et encéphalopathie hépatique,” 2.

Sokoloff, L. 1999. “Energetics of Functional Activation in Neural Tissues.” *Neurochemical Research* 24 (2): 321–29. https://doi.org/10.1023/a:1022534709672.

Solís, J. M., A. S. Herranz, O. Herreras, J. Lerma, and R. Martín del Río. 1988. “Does Taurine Act as an Osmoregulatory Substance in the Rat Brain?” *Neuroscience Letters* 91 (1): 53–58. https://doi.org/10.1016/0304-3940(88)90248-0.

Sonnay, Sarah, Rolf Gruetter, and João M. N. Duarte. 2017. “How Energy Metabolism Supports Cerebral Function: Insights from 13C Magnetic Resonance Studies In Vivo.” *Frontiers in Neuroscience* 11: 288. https://doi.org/10.3389/fnins.2017.00288.

Stadlbauer, Vanessa, Rajeshwar P. Mookerjee, Stephen Hodges, Gavin A. K. Wright, Nathan A. Davies, and Rajiv Jalan. 2008. “Effect of Probiotic Treatment on Deranged Neutrophil Function and Cytokine Responses in Patients with Compensated Alcoholic Cirrhosis.” *Journal of Hepatology* 48 (6): 945–51. https://doi.org/10.1016/j.jhep.2008.02.015.

Stullken, E. H., J. H. Milde, J. D. Michenfelder, and J. H. Tinker. 1977. “The Nonlinear Responses of Cerebral Metabolism to Low Concentrations of Halothane, Enflurane, Isoflurane, and Thiopental.” *Anesthesiology* 46 (1): 28–34. https://doi.org/10.1097/00000542-197701000-00007.

Swaminathan, Mirashini, Mark Alexander Ellul, and Timothy JS Cross. 2018. “Hepatic Encephalopathy: Current Challenges and Future Prospects.” *Hepatic Medicine : Evidence and Research* 10 (March): 1–11. https://doi.org/10.2147/HMER.S118964.

Sweet, C. S., S. E. Emmert, A. A. Seymour, I. I. Stabilito, and L. Oppenheimer. 1987. “Measurement of Cardiac Output in Anesthetized Rats by Dye Dilution Using a Fiberoptic Catheter.” *Journal of Pharmacological Methods* 17 (3): 189–203. https://doi.org/10.1016/0160-5402(87)90050-7.

Tadamura, E., H. Hatabu, W. Li, P. V. Prasad, and R. R. Edelman. 1997. “Effect of Oxygen Inhalation on Relaxation Times in Various Tissues.” *Journal of Magnetic Resonance Imaging: JMRI* 7 (1): 220–25. https://doi.org/10.1002/jmri.1880070134.

Takahashi, Kazuyoshi, Hiroyuki Kameda, Mikiko Kataoka, Kenshou Sanjou, Nobutoshi Harata, and Norio Akaike. 1993. “Ammonia Potentiates GABAA Response in Dissociated Rat Cortical Neurons.” *Neuroscience Letters* 151 (1): 51–54. https://doi.org/10.1016/0304-3940(93)90043-K.

Taylor, D. L., S. E. Davies, T. P. Obrenovitch, M. H. Doheny, P. N. Patsalos, J. B. Clark, and L. Symon. 1995. “Investigation into the Role of N-Acetylaspartate in Cerebral Osmoregulation.” *Journal of Neurochemistry* 65 (1): 275–81. https://doi.org/10.1046/j.1471-4159.1995.65010275.x.

Thabut, D, S Mouri, H El Mourabit, R Morichon, D Wandum, E Lasnier, C Housset, and N Weiss. 2015. “Sodium Benzoate and Rifaximin Are Able to Restore Blood-Brain Barrier Integrity in He Cirrhotic Rats.” *Intensive Care Medicine Experimental* 3 (Suppl 1). https://doi.org/10.1186/2197-425X-3-S1-A691.

Thase, Michael E., and Timothey Denko. 2008. “Pharmacotherapy of Mood Disorders.” *Annual Review of Clinical Psychology* 4: 53–91. https://doi.org/10.1146/annurev.clinpsy.2.022305.095301.

Tkác, I., Z. Starcuk, I. Y. Choi, and R. Gruetter. 1999. “In Vivo 1H NMR Spectroscopy of Rat Brain at 1 Ms Echo Time.” *Magnetic Resonance in Medicine* 41 (4): 649–56. https://doi.org/10.1002/(sici)1522-2594(199904)41:4<649::aid-mrm2>3.0.co;2-g.

Tkác, Ivan, Raghavendra Rao, Michael K. Georgieff, and Rolf Gruetter. 2003. “Developmental and Regional Changes in the Neurochemical Profile of the Rat Brain Determined by in Vivo 1H NMR Spectroscopy.” *Magnetic Resonance in Medicine* 50 (1): 24–32. https://doi.org/10.1002/mrm.10497.

Todd, M. M., and J. Weeks. 1996. “Comparative Effects of Propofol, Pentobarbital, and Isoflurane on Cerebral Blood Flow and Blood Volume.” *Journal of Neurosurgical Anesthesiology* 8 (4): 296–303. https://doi.org/10.1097/00008506-199610000-00007.

Toyama, Hiroshi, Masanori Ichise, Jeih-San Liow, Douglass C. Vines, Nicholas M. Seneca, Kendra J. Modell, Jurgen Seidel, Michael V. Green, and Robert B. Innis. 2004. “Evaluation of Anesthesia Effects on [18F]FDG Uptake in Mouse Brain and Heart Using Small Animal PET.” *Nuclear Medicine and Biology* 31 (2): 251–56. https://doi.org/10.1016/S0969-8051(03)00124-0.

Trabesinger, A. H., O. M. Weber, C. O. Duc, and P. Boesiger. 1999. “Detection of Glutathione in the Human Brain in Vivo by Means of Double Quantum Coherence Filtering.” *Magnetic Resonance in Medicine* 42 (2): 283–89. https://doi.org/10.1002/(sici)1522-2594(199908)42:2<283::aid-mrm10>3.0.co;2-q.

Tsacopoulos, M., and P. J. Magistretti. 1996. “Metabolic Coupling between Glia and Neurons.” *The Journal of Neuroscience: The Official Journal of the Society for Neuroscience* 16 (3): 877–85.

Tulstrup, Monica Vera-Lise, Ellen Gerd Christensen, Vera Carvalho, Caroline Linninge, Siv Ahrné, Ole Højberg, Tine Rask Licht, and Martin Iain Bahl. 2015. “Antibiotic Treatment Affects Intestinal Permeability and Gut Microbial Composition in Wistar Rats Dependent on Antibiotic Class.” *PLOS ONE* 10 (12): e0144854. https://doi.org/10.1371/journal.pone.0144854.

"Understanding NMR Spectroscopy, 2nd Edition | Wiley." n.d. Wiley.Com. Accessed September 11, 2020. https://www.wiley.com/en-us/Understanding+NMR+Spectroscopy%2C+2nd+Edition-p-9780470746080.

Valette, Julien, Martine Guillermier, Laurent Besret, Philippe Hantraye, Gilles Bloch, and Vincent Lebon. 2007. "Isoflurane Strongly Affects the Diffusion of Intracellular Metabolites, as Shown by 1H Nuclear Magnetic Resonance Spectroscopy of the Monkey Brain." *Journal of Cerebral Blood Flow and Metabolism: Official Journal of the International Society of Cerebral Blood Flow and Metabolism* 27 (3): 588–96. https://doi.org/10.1038/sj.jcbfm.9600353.

Vinckenbosch, Elise Marie Catherine. 2018. "Ultra high magnetic field for glial contribution into brain metabolism studied by MR spectroscopy and CEST methods for molecular imaging of glycogen." Infoscience. EPFL. 2018. https://doi.org/10.5075/epfl-thesis-8125.

Wallimann, T, M Wyss, D Brdiczka, K Nicolay, and H M Eppenberger. 1992. "Intracellular Compartmentation, Structure and Function of Creatine Kinase Isoenzymes in Tissues with High and Fluctuating Energy Demands: The 'phosphocreatine Circuit' for Cellular Energy Homeostasis." *Biochemical Journal* 281 (Pt 1): 21–40.

Wang, Y., and S. J. Li. 1998. "Differentiation of Metabolic Concentrations between Gray Matter and White Matter of Human Brain by in Vivo 1H Magnetic Resonance Spectroscopy." *Magnetic Resonance in Medicine* 39 (1): 28–33. https://doi.org/10.1002/mrm.1910390107.

Wehrli, Felix W. 1976. "Temperature-Dependent Spin-Lattice Relaxation of 6Li in Aqueous Lithium Chloride." *Journal of Magnetic Resonance (1969)* 23 (3): 527–32. https://doi.org/10.1016/0022-2364(76)90289-4.

Weiss, Nicolas, Rajiv Jalan, and Dominique Thabut. 2018. "Understanding Hepatic Encephalopathy." *Intensive Care Medicine* 44 (2): 231–34. https://doi.org/10.1007/s00134-017-4845-6.

Weissenborn, K., J. C. Ennen, H. Schomerus, N. Rückert, and H. Hecker. 2001. "Neuropsychological Characterization of Hepatic Encephalopathy." *Journal of Hepatology* 34 (5): 768–73. https://doi.org/10.1016/s0168-8278(01)00026-5.

Wright, Gavin, Debbie Shawcross, Steven W. M. Olde Damink, and Rajiv Jalan. 2007. "Brain Cytokine Flux in Acute Liver Failure and Its Relationship with Intracranial Hypertension." *Metabolic Brain Disease* 22 (3–4): 375–88. https://doi.org/10.1007/s11011-007-9071-4.

Young, I. R., G. J. Clarke, D. R. Bailes, J. M. Pennock, F. H. Doyle, and G. M. Bydder. 1981. "Enhancement of Relaxation Rate with Paramagnetic Contrast Agents in NMR Imaging." *The Journal of Computed Tomography* 5 (6): 543–47. https://doi.org/10.1016/0149-936x(81)90089-8.

# Publications and Resume

## 9.1 Journal articles

Veronika Rackayová, **Emmanuelle Flatt**, Olivier Braissant, Jocelyn Grosse, Daniela Capobianco, Paola Mastromarino, Matthew McMillin, Sharon DeMorrow, Valérie A. McLin and Cristina Cudalbu. Probiotics improve the neurometabolic profile of rats with chronic cholestatic liver disease, *Sci Rep 11, 2269 (2021).*

**Emmanuelle Flatt**, Valérie A. McLin, Olivier Braissant, Paola Mastromarino, Rolf Gruetter and Cristina Cudalbu. Do probiotics combined with rifaximin influence the neurometabolic changes in a rat model of type C HE?, Clinical and Translational Gastroenterology, *submitted*.

**Emmanuelle Flatt**, Valérie A. McLin, Olivier Braissant, Rolf Gruetter and Cristina Cudalbu. Antibiotic rifaximin at different doses for treatment of chronic liver disease-induced HE: a longitudinal in vivo $^{1}$H MRS study of brain metabolism in bile duct-ligated rat model. *Manuscript in preparation*.

**Emmanuelle Flatt**, Bernard Lanz, Rolf Gruetter, Mor Mishkovsky. Cerebral metabolism of hyperpolarized [$^{2}H_7$, U-$^{13}C_6$]D-glucose in the healthy mouse under different anesthetic conditions, Special Issue in the journal Metabolites, *manuscript in preparation*.

**Emmanuelle Flatt**, Andrea Capozzi, Rolf Gruetter, Mor Mishkovsky. Exploring the potential of hyperpolarized $^{6}$Li to study lithium bio-distribution in the rat brain at 9.4 T. *Manuscript in preparation*.

## 9.2 Conference Proceedings

**Emmanuelle Flatt**, Cristina Cudalbu, Olivier Braissant, Stefan Mitrea, Dario Sessa, Valérie McLin, Rolf Gruetter. Antibiotic rifaximin for treatment of chronic liver disease-induced HE: a longitudinal in vivo $^{1}$H-MRS study of brain metabolism.
ISMRM (International Society for Magnetic Resonance in Medicine) 2019, Montreal, Canada.
Oral presentation

**Emmanuelle Flatt**, Bernard Lanz, Andrea Capozzi, Rolf Gruetter, Mor Mishkovsky. Cerebral metabolism of hyperpolarized [$^{2}H_7$, U-$^{13}C_6$]D-glucose in the healthy mouse under different anesthetic conditions.
ISMRM 2020, Virtual conference.
Oral presentation

**Emmanuelle Flatt**, Bernard Lanz, Andrea Capozzi, Rolf Gruetter, Mor Mishkovsky. Cerebral metabolism of hyperpolarized [$^{2}H_7$, U-$^{13}C_6$]D-glucose in the healthy mouse under different anesthetic conditions.
EMIM (European Molecular Imaging Meeting) 2020, Virtual conference.
Oral presentation

**Emmanuelle Flatt**, Cristina Cudalbu, Olivier Braissant, Stefanita Mitrea, Dario Sessa, Rolf Gruetter, and Valérie McLin. 2017. "Rifaximin in Chronic Liver Disease-Induced Hepatic Encephalopathy: An In Vivo Longitudinal Study of Brain Metabolism on BDL Rats." Journal of Clinical and Experimental Hepatology 7 (February): S55–59. https://doi.org/10.1016/j.jceh.2017.01.072.
Presented at the 17th ISHEN (International Society for Hepatic Encephalopathy and Nitrogen Metabolism) Symposium in Gurgaon, India, 2017.
Poster presentation

**Emmanuelle Flatt**, Cristina Cudalbu, Olivier Braissant, Stefanita Mitrea, Dario Sessa, Valerie A.

McLin and Rolf Gruetter. Treatments in chronic liver disease induced hepatic encephalopathy: a longitudinal in vivo $^{1}$H-MRS study of brain metabolism using rifaximin.
ISMRM 2017, Hawai, USA.
Poster presentation

**Emmanuelle Flatt**, Cristina Cudalbu, Olivier Braissant, Stefanita Mitrea, Dario Sessa, Valerie A. McLin and Rolf Gruetter. Synergy between probiotics and antibiotics for the treatment of chronic hepatic encephalopathy: a longitudinal in vivo $^{1}$H MRS study of brain metabolism.
ISMRM 2018, Paris, France.
Poster presentation

**Emmanuelle Flatt**, Alice Radaelli, Andrea Capozzi, J-N Hyacinthe, Hikari A I Yoshihara, Rolf Gruetter, Mor Mishkovsky. Differentiating between venous and arterial blood in the rat head: a study using hyperpolarized $^{6}$Li MRS.
HYP18 (International Conference on Nuclear Hyperpolarization), Southampton, UK, 2018.
Poster presentation

**Emmanuelle Flatt**, Olivier Braissant, Stefanita Mitrea, Dario Sessa, Rolf Gruetter, Valérie McLin, Cristina Cudalbu. Effects of probiotics and antibiotics for the treatment of chronic hepatic encephalopathy in different brain regions: a longitudinal in vivo $^{1}$H-MRS study.
ISMRM MRS Workshop, Utrecht, the Netherlands, 2018.
Poster presentation

**Emmanuelle Flatt**, Olivier Braissant, Stefanita Mitrea, Dario Sessa, Paola Mastromarino, Rolf Gruetter, Valérie A. McLin, and Cristina Cudalbu. 2019. "P: 37 Probiotics Combined With Rifaximin for the Treatment of Chronic Hepatic Encephalopathy: A Longitudinal In Vivo $^{1}$H-MRS Study of Brain Metabolism Using BDL Rats." American Journal of Gastroenterology 114 (September): S19. https://doi.org/10.14309/01.ajg.0000582124.67482.93.
Presented at the 18th ISHEN Symposium in Williamsburg, USA, 2019.
Poster presentation

**Emmanuelle Flatt**, Olivier Braissant, Stefanita Mitrea, Dario Sessa, Rolf Gruetter, Valérie A. McLin, and Cristina Cudalbu. 2019. "P: 36 Antibiotic Rifaximin for Treatment of Chronic Liver Disease-Induced HE: A Longitudinal In Vivo $^{1}$H-MRS Study of Brain Metabolism on BDL Rats." Official Journal of the American College of Gastroenterology | ACG 114 (September): S18. https://doi.org/10.14309/01.ajg.0000582120.59858.08.
Presented at the 18th ISHEN Symposium in Williamsburg, USA, 2019.
Poster presentation

## Awards

**Summa cum laude merit award** for abstract "Antibiotic rifaximin for treatment of chronic liver disease-induced HE: a longitudinal in vivo $^{1}$H-MRS study of brain metabolism" rated by the five reviewers to be among the 3 % in its category at the Joint Annual Meeting ISMRM-ESMRMB, Montréal, 2019.

**MR in Drug Research Award (3$^{rd}$ place)** for abstract "Antibiotic rifaximin for treatment of chronic liver disease-induced HE: a longitudinal in vivo $^{1}$H-MRS study of brain metabolism" at the MR in Drug Research Study Group, ISMRM-ESMRMB, Montréal, 2019.

**Magna cum laude merit award** for abstract "Cerebral metabolism of hyperpolarized [$^{2}H_{7}$, U-$^{13}C_{6}$]D-glucose in the healthy mouse under different anesthetic conditions" rated by the five reviewers to

be among the 10 % in its category at the Joint Annual Meeting ISMRM-ESMRMB, Virtual conference, 2020.

## 9.3 Resume


# Emmanuelle Flatt

Av. du Rond-Point 1B
1006 Lausanne
+41 78 627 49 99
emmanuelle.flatt@protonmail.ch


View my profile on LinkedIn

## Education

| | |
|---|---|
| 2016 – 2021 | **Swiss Federal Institute of Technology Lausanne (EPFL),** Lausanne, CH<br>PhD candidate in Biotechnology and Bioengineering. |
| 2014 – 2015 | **Imperial College London, London, UK**<br>Master thesis in the Department for Bioengineering. |
| 2010 – 2015 | **Swiss Federal Institute of Technology Lausanne (EPFL),** Lausanne, CH<br>Master in Bioengineering (GPA 5.22/6).<br>Bachelor in Life Sciences and Technologies (GPA 5.12/6). |
| 2007 – 2010 | **Gymnase du Bugnon,** Lausanne, CH<br>Swiss Maturity Certificate (GPA 5.28/6).<br>▪ Major in Physics and Applied Mathematics, Chemistry award. |

## Professional experience

| | |
|---|---|
| 2016 – 2019 | **Laboratory for Functional and Metabolic Imaging (LIFMET), Institute of Physics, EPFL**<br>*Research assistant*<br>▪ Setting up the two first Massive Open Online Courses (MOOCs) on Biomedical Imaging at EPFL.<br>▪ Teaching assistant for General Physics and Biomedical Imaging courses. |
| 2013 | **Institute of Radiophysics (IRA),** Lausanne, CH (3-months internship)<br>*Intern in the Radiopharmaceutical Chemistry group*<br>▪ Detailed analysis of the influence of different parameters on the quality controls of radiopharmaceutical agents.<br>▪ Formulation of specific recommendations for improving the accuracy of quality controls. |

## Academic projects

**PhD thesis, Laboratory for Functional and Metabolic Imaging, Institute of Physics, EPFL**

- Development of technical and computational tools for studying kinetic of different substrates and drugs in the brain using magnetic resonance spectroscopy.
  - Improved detection of substrates in the brain: SNR more than doubled.
  - Elaboration of a more accurate protocol for evaluating the efficacy of a novel therapeutic approach in chronic liver disease.
  - *Summa cum laude* award (top 3%) & MR in drug research award (3rd place) at the ISMRM 2019 conference. *Magna cum laude* award (top 10%) at the ISMRM 2020 conference.
- Implementation of a project consisting of repairing existing experimental facilities and setting them up for new operations purpose.

**Master Thesis, Department for Bioengineering, Imperial College London**

- Development of a new mathematical model of retinal detachment progression.
- Validation of the model in collaboration with physicians at St Thomas' Hospital, London.
- 2nd prize at the MEIbioeng15 conference, Medical and Bioengineering category.

## Technical Skills

- Multinuclear Magnetic Resonance Spectroscopy (MRS) and Imaging (MRI).
- Numerical modeling: kinetic modeling of cerebral metabolism, Monte Carlo approach.
- Statistical analysis (GraphPad Prism, Origin).
- Programming languages (C, C++, Matlab), Image processing (ImageJ), Finite element analysis (Multiphysics COMSOL 4.1), specific software (VnmrJ, jMRUI), MS Office, LaTeX.
- Animal experimentation (Module 1 RESAL).

## Extra-curricular activities

| | |
|---|---|
| 2018 – current | **First aid volunteer, EPFL**<br>▪ Events and assistance during emergencies on campus. IAS 1 certified. |

## Languages

| | |
|---|---|
| **French** | Native language |
| **English** | Fluent (C1)<br>▪ Master program and PhD thesis mainly in English.<br>▪ Academic exchange at Imperial College, London (9 months). |
| **German** | High school level (B2) |

## Interests

Football, tennis, ski-touring, guitar

## Personal information

28 years old (10.06.1992), single, Swiss nationality.